



**PRELIMINARY STUDY OF FATIGUE BEHAVIOUR
OF TIMBER MOMENT RESISTING JOINT**

by

Daniel S. C. Lee

B.E. (Civil)

Thesis presented for the degree of
Master of Engineering Science
at the University of Adelaide
Australia

-August 1995-

ABSTRACT

There is an increasing popularity of timber portal frame as a cost-effective structure in NZ, USA and Australia. Moment resisting joints are essential to this type of structure, and nail plywood gusset joints with LVL members are commonly used for their superior strength quality and efficiency. However, there is inadequate existing design knowledge on the fatigue behaviour of this specific joint. Such loads are induced by wind or cranes.

To provide such knowledge, seven half-scale specimens were tested in the laboratory. This is a preliminary study of the fatigue effect on this type of joint by applying a constant load to represent the dead load and live load while a sinusoidal cyclic loading was superimposed to represent wind load.

Two tests were performed to confirm the joint static strength. These tests gave ultimate static strengths of 96kN-m and 79kN-m compared with the theoretical value was 65kN-m for the upper nail group by thin tube analogy. Three specimens were subjected to a base load of 44kN-m (68% of the theoretical ultimate strength) with cyclic loading of ± 16 kN-m (24% of the theoretical ultimate strength) with varying number of cycles before a static test to failure. The remaining two specimens were tested with a larger cyclic loading amplitude of ± 35 kN-m and ± 26 kN-m (54% & 41% of the theoretical ultimate strength) and were failed by cyclic loading. Joint rotation, applied moment, strain across LVL members and ram displacement were recorded throughout each test.

From the investigation, the results showed no drastic change in joint properties under the influence of large number of cyclic loading of low amplitude. This type of moment resisting timber joints behaved very well under fatigue loading. Variation in timber material seemed to be a **more** prominent factor when determining the joint properties.

Nail loosening and nail slip were not dominant factors in the joints' failure mode. Material tension failure was observed in six specimens (all but the last specimen) either across the rafter LVL or across the plywood gusset plate. Therefore, the ultimate moment capacities were dependent on the remaining timber strength rather than the nail groups.

The residual strength after the cyclic tests ranged from 79kN-m to 88kN-m (122% & 135% of the theoretical ultimate strength) which was within the tested static strength range of 79kN-m to 96kN-m (122% & 148% of the theoretical ultimate strength). Since the residual

strength of identical specimens after enduring a set number of cycles should not be bigger than its original static strength, the results suggested that timber material variation played an important role in ultimate strength.

There was a gradual increase in the average rotation with increased number of cycles. This suggested a typical timber creeping effect where there was permanent bending induced into the LVL members and minor nail slip. This could also explain the gradual decrease in stiffness of the joint as the number of cycles increased.

There was no particular trend for changes in stiffness for the initial few thousand cycles. Afterwards, the stiffness plots showed a linear decrease to demonstrate the fatigue effect. There were slightly steeper stiffness plots for specimens with higher cyclic loading amplitude. However, due to material variability as suggested by the stiffness slope for specimens with identical cyclic amplitude, no definite conclusion could be made on the relationship between cyclic amplitude and stiffness.

The strain across the LVL members in four specimens was linear as expected by the applied axial and bending stresses along the members. The other three specimens with non-linear strain profiles across the rafters which had failure across the LVL members.

For future research, it is recommended to have a nail pattern design that is less conservative than the one in this project which was adopted from an existing timber portal frame structure. In this way, the jointing system can be investigated for its efficiency and thus improvement on joint design can be made. Theoretical study on the remaining life and the practical ways for strengthening the weak points in a joint would be valuable for designers. Moreover, as we are more confident on the fatigue behaviour of this type of joint, this jointing technique can be employed in other areas apart from the timber portal frame, e.g. bridges.

Declaration

I declare that this thesis does not contain any material which has been accepted for the award of any degree in any university and, to the best of my knowledge and belief, it does not contain any material previously published or written by another person except where due reference has been made in the text of the thesis. I also declare that I have no objection to the thesis being made available for photocopying and loan, if accepted for the award of the degree.

Daniel Lee

Acknowledgments

The author would very much like to express his deep gratitude to the research supervisors Dr. M.C. Griffith and Dr. M.J.S. Hirst for their experienced advice and heart-felt encouragement. A full tribute to their keen interest to the project and practical assistance throughout the research which have greatly motivated the author and made this project possible.

This project was supported by the grant from the Australian Research Council. Special thanks is given to International Panel and Lumber and Stanley Bostitch Pty. Ltd. for their generous supply of materials and to Mr. Bruce Hutchings of Timberbuilt Pty. Ltd., Mr. Peter Yttrup of Yttrup & Associates and Mr. Rob Rundle of Signature Joinery for their invaluable assistance and advice.

The author wishes to thank the fellow post graduate students, the staffs of Civil Engineering Department for their genuine help. Preparation and monitoring of experimental testing have called for an unusually large amount of time and effort, praise should be given to Mr. Werner Eidam, Mr. Colin Haese, Mr. Robert Kelman, Mr. Greg Atkins and Mr. Robert Marcussen. Special thanks to Mr. Bruce Lucas for his assistance in instrumentation and Dr. George Sved for his advice on mounting of strain gauges.

Finally, the author wish to acknowledge the encouragement and help from Dr. Karen Woo and my father, Mr. Bernard Lee.

Content

Abstract	i
Declaration	iii
Acknowledgments	iv
Table of Contents	v
List of Figures & Tables	viii
Chapter 1 Introduction	
1.1 Background	1
1.2 Scope and Objectives	2
1.3 General Introduction	3
Chapter 2 Literature Review	
2.1 Introduction	5
2.2 Overview of behaviour of the joint and its components	6
2.2.1 Laminated veneer lumbar as an engineering material for the members	9
2.2.2 Gusset plates	10
2.2.3 Dimensions of joint components	11
2.3 Simple nail joints	18
2.3.1 Nail head restraint	18
2.3.2 Grain direction and cyclic loading characteristic	21
2.3.3 Single vs multi-nails	24
2.4 Multi- nail joints	26

2.4.1	Nail pattern	26
2.4.2	Experimental testing of moment resisting joints	27
2.4.3	Static strength and failure mode	31
2.5	Summary	36
Chapter 3	Theoretical Study of actual joint & test specimen	
3.1	Introduction	38
3.2	Field experiment	40
3.3	Wind loads on the Wingfield building joint	43
3.4	Specimen design	46
3.4.1	Joint form and scale effects	46
3.4.2	Loading on specimen	53
3.5	Joint strength	56
3.5.1	Nail group strength	56
3.5.2	LVL member strength	58
3.5.3	Plywood gusset strength	59
3.5.4	Summary	59
Chapter 4	Experimental Research	
4.1	Introduction	61
4.2	Testing program	63
4.3	Testing apparatus	65
4.3.1	Fabrication	65
4.3.2	Experimental arrangement	69
4.3.3	Instrumentation and data acquisition	78
4.4	Testing Procedure	98

Chapter 5	Results and Discussion	
5.1	Introduction	103
5.2	Presentation of results	104
5.3	Comparison of results	144
5.3.1	Static behaviour	146
5.3.2	Fatigue behaviour	153
Chapter 6	Conclusion	
6.1	Summary and general conclusions	168
6.2	Recommendations and suggestions for future work	171
Appendix A	Preliminary study on mounting strain gauges	175
Appendix B	DCDT method	179
Appendix C	Basic Program for controlling the data logger through the laptop computer	180
Appendix D	Calculations of joint strengths	184
Bibliography		189

List of Figures & Tables

(a) Figures:

Figure 2.1 Types of joints

Figure 2.2 Typical effect of timber density

Figure 2.3 Headside of nail fixed from rotation

Figure 2.4 Graphical relationship between nailed joint capacity and the t/d ratio

Figure 2.5 Deformed nail shapes for various headside plywood thickness

Figure 2.6 Typical effect of nail head restraint

Figure 2.7 Two types of nail head shape

Figure 2.8 Modelling of a nail with nonlinear material properties

Figure 2.9 Typical load displacement behaviour for nail loaded parallel and perpendicular to wood grain

Figure 2.10 Effect of load magnitude and assembly condition on viscous damping

Figure 2.11 Some typical failure modes for two-member joints

Figure 2.12 Test set-up in New Zealand researches

Figure 2.13 Test set-up in the full-scale testing of prefabricated timber frame

Figure 3.1 Moment resisting joint in the actual timber portal frame at Wingfield

Figure 3.2 Different load cases on the timber portal frame

Figure 3.3 The actual joint in the timber portal frame & the test specimen

Figure 3.4 Layout of the whole specimen

Figure 3.5 Details of the specimen design

Figure 3.6 Actions along the LVL members

Figure 4.1 Template for marking the nail pattern onto the gusset plywood

Figure 4.2 Plywood strut

Figure 4.3 Nailing by the pneumatic nail gun

Figure 4.4 Stack of assembled specimens before testing

Figure 4.5 Layout of the specimen

Figure 4.6 LVL base connection

Figure 4.7 Hydraulic ram which provides both static & dynamic loads
Figure 4.8 Connection at the column end
Figure 4.9 Middle support at the gusset plate
Figure 4.10 Pivot connection that connects to the rafter end & truss system
Figure 4.11 Top view of the set up of the specimen
Figure 4.12 Control unit of the Instron machine
Figure 4.13 Specimen testing set up
Figure 4.14 LVDT method by forming an imaginary triangle
Figure 4.15 LVDT method
Figure 4.16 Rotary Variable Differential Transformer
Figure 4.17 Mounting boards for the RVDT
Figure 4.18 RVDT and the mounting system
Figure 4.19 Locations of the RVDT
Figure 4.20 Arrangement of the DCDT method
Figure 4.21 Geometry of the DCDT method
Figure 4.22 Moment vs rotation for specimen 1
Figure 4.23 Moment vs rotation during the failure loading for specimen 2
Figure 4.24 Gauge positions in the Batchelar and Cavanagh experiment
Figure 4.25 Gauge positions in the Batchelar and Hunt experiment
Figure 4.26 Locations of the strain gauges across the LVL members
Figure 4.27 Flow chart for the data logging system
Figure 4.28 Data logger and the laptop computer as the controller
Figure 4.29 Load vector diagram for the specimen
Figure 4.30 Points chosen for data logging within a complete load cycle

Figure 5.1 Moment vs rotation for specimen 1
Figure 5.2 Strain across column for specimen 1
Figure 5.3 Strain across rafter for specimen 1
Figure 5.4 Failure mode of specimen 1
Figure 5.5 Rotation at 44kN-m vs number of cycles for specimen 2
Figure 5.6 Difference in rotation vs number of cycles for specimen 2
Figure 5.7 Stiffness vs number of cycles for specimen 2
Figure 5.8 Moment vs rotation for specimen 2
Figure 5.9 strain across rafter after 250000 cycles for specimen 2
Figure 5.10 strain across column after 250000 cycles for specimen 2

Figure 5.11 Failure mode of the specimen 2

Figure 5.12 Rotation at 44kN-m vs number of cycles for specimen 3

Figure 5.13 Difference in rotation vs number of cycles for specimen 3

Figure 5.14 stiffness vs number of cycles for specimen 3

Figure 5.15 Moment vs rotation after 1,000,000 cycles for specimen 3

Figure 5.16 Strain across rafter during initial loading for specimen 3

Figure 5.17 Strain across rafter at N=1009752 for specimen 3

Figure 5.18 Strain across rafter during the final static test for specimen 3

Figure 5.19 Strain across column at initial loading for specimen 3

Figure 5.20 Strain across column at n=1009752 for specimen 3

Figure 5.21 Failure mode for specimen 3

Figure 5.22 Rotation at 44kN-m vs number of cycles for specimen 4

Figure 5.23 Difference in rotation vs number of cycles for specimen 4

Figure 5.24 Stiffness vs number of cycles for specimen 4

Figure 5.25 Moment vs rotation at failure loading for specimen 4

Figure 5.26 Strain across rafter at N=206 for specimen 4

Figure 5.27 Strain across rafter at N=483389 for specimen 4

Figure 5.28 Strain across column at N=206 for specimen 4

Figure 5.29 Strain across column at N=483389 for specimen 4

Figure 5.30 Failure mode of specimen 4

Figure 5.31 Moment vs rotation for specimen 5

Figure 5.32 Strain across rafter for specimen 5

Figure 5.33 Strain across column for specimen 5

Figure 5.34 Failure mode for specimen 5

Figure 5.35 Rotation at 44kN-m vs number of cycles for specimen 6

Figure 5.36 Difference in rotation vs number of cycles for specimen 6

Figure 5.37 Stiffness vs number of cycles for specimen 6

Figure 5.38 Strain across rafter at N=10 for specimen 6

Figure 5.39 Strain across rafter at N=6182 for specimen 6

Figure 5.40 Strain across column at N=10 for specimen 6

Figure 5.41 strain across column at N=6182 for specimen 6

Figure 5.42 Failure mode of specimen 6

Figure 5.43 Rotation at 44kN-m vs number of cycles for specimen 7

Figure 5.44 Difference in rotation vs number of cycles for specimen 7

Figure 5.45 stiffness vs number of cycles for specimen 7

Figure 5.46 strain across rafter at N=157028 for specimen 7

Figure 5.47 strain across column at N=157028 for specimen 7
 Figure 5.48 Failure mode of specimen 7
 Figure 5.49 Residual strength vs number of cycles
 Figure 5.50 Moment vs rotation for all specimens
 Figure 5.51 Endurance limit at different loading magnitude
 Figure 5.52 Stiffness vs number of cycles for all specimens
 Figure 5.53 Moment vs rotation at initial cycles
 Figure 5.54 Moment vs rotation at certain number of cycles
 Figure 5.55 Diagram for calculating rotation as a function of ram displacement
 Figure 5.56 Rotation vs ram displacement for specimen 1
 Figure 5.57 Rotation vs ram displacement for all specimens
 Figure 5.58 Strain vs number of cycles for all specimens
 Figure 5.59 Strain vs number of cycles for specimens 6 & 7

Figure A.1 10mm strain gauge bonded onto a plastic sheet covering the timber surface
 Figure A.2 68mm strain gauge mounted directly onto the timber surface
 Figure A.3 Experimental set-up for strain gauge test
 Figure A.4 Comparison between different strain gauge settings
 Figure B.1 DCDT method
 Figure D.1 Nail rings in actual joint
 Figure D.2 Nail rings in test specimen

(b) Tables:

Table 2.1 Properties comparison of LVL and radiata pine
 Table 2.2 Summary of previous moment resisting joint experimental research
 Table 3.1 Theoretical analysis by Images 3D of Moment shear ratio
 Table 3.2 Moment capacity of the actual joint and specime
 Table 4.1 Details of the seven specimens
 Table 4.2 Measurement methods for rotation
 Table 5.1 Key features of the experimental results
 Table 5.2 Axial load and bending moment derived from strain profiles
 Table A.1 Summary of the six strain gauge settings
 Table A.2 Results of the preliminary test on different strain gauge settings



CHAPTER 1

INTRODUCTION

1.1 BACKGROUND

The popularity of timber portal frame structures in Europe and America is increasing. This is also true in Australia and New Zealand. Up to 50m clear span structures have been found to be cost-effective alternatives to steel portal frames (10). Moderate sized timber framed industrial buildings have been erected recently for about 90% of the cost of an equivalent steel framed structure. As a result, the engineering profession is becoming aware of the timber alternative to steel industrial buildings with a corresponding increase in the use of structural timber. Some reasons for its growing popularity are:

- i) Improvements in producing reliable timber as an engineering material with increased static strength (10)(23);
- ii) Improvements in timber technology from research and experience in design and construction;
- iii) Increasing confidence in this type of structure; and

- iv) Ease of construction.

In a timber portal frame, loads imposed on the structure are transmitted to the foundation through moment resisting joints. However, the present design knowledge only gives designer guidance on the static and earthquake performance (37) for timber moment resisting joints. There is no information on the long term dynamic performance and fatigue strength of moment resisting joints where dynamic load is superimposed on a static component in a particular direction and there is no true load reversal.

Vibration induced by wind or machinery such as cranes commonly occurs in timber portal frame structures. In order to properly account for these effects, a better understanding of the dynamic response of plywood gusset joints is required. Even under service load where the nails are probably loaded to about 40% of their ultimate load capacity, plastic deformation of at least some of the nails occurs. This is especially true in the corners of the nail pattern, whereby the flexibility of the joint is considerably increased due to load-slip deformations (13). Moreover, the wood-bearing behaviour near the nail sites and fracture propagation are not completely understood in the study of multi-nail timber joints.

1.2 SCOPE AND OBJECTIVES

The long-term strength of timber moment resisting joints is crucial to the survival of the structure since they maintain the stability of the structure and provide resistance against lateral loads. Considering the lack of knowledge in the area of long-term dynamic performance, the aim of this research is to study the effect of dynamic loading on the long term strength of timber moment resisting joints. Some of the

different joint configurations, gusset materials and nail patterns used in the family of timber moment resisting joints are briefly reported in the next chapter. In order to give special reference to Australian structures, a typical joint type which was used in a recently constructed industrial building in the District of Wingfield in South Australia was adopted for experimental investigation (52). A concurrent research project was performed by Stevens to determine the likely magnitude of dynamic loads applied to this particular structure (see Chapter 3). The particular joint studied is a plywood gusset plate joint connecting LVL (Laminated Veneer Lumber) beam and column members. The joint consists of many nails evenly distributed around the gusset, thereby distributing the stress in the timber and avoiding large stress concentrations associated with the traditional bolted connection. Seven half-scale replicas of the joint were constructed and tested in the University of Adelaide (Chapman laboratory). The behaviour of each specimen, such as the joint rotation and strain across the LVL members, under cyclic loading was monitored. While classic fatigue studies have concentrated on the number of loading cycles to failure, this research also investigated the reduction in static strength due to fatigue and the performance of the joint during loading. This is especially relevant in determining the reduction in strength of existing structures and aiding the understanding of the dynamic performance during loading. The results are expected to be applicable to other similar multi-nailed plywood gusseted joints.

1.3 GENERAL INTRODUCTION

Keeping in mind the scope and objectives in Section 1.2, this thesis presents the dynamic behaviour of the joint under different stress levels and compares the fatigue strength with the results of static tests. A survey of the current literature relating to the subject of timber joints is presented in Chapter 2 which sets out the background

information to timber engineering and in particular, multi-nail moment resisting joints. Reports on single nail joints provide information on the interaction of nail and timber plus timber as an engineering material. Previous researches on multi-nail joints helped in designing the experimental joint used here and gave an insight to the laboratory testing.

Chapter 3 presents findings of the field study on the moment resisting joint in Wingfield by Stevens (52) and a theoretical comparison between the actual joint and the experimental joint is carried out in order to relate the experimental results to the actual joint in the timber portal frame. A detailed appraisal of the experimental research in chapter 4 gives an account of the testing program, the testing apparatus and the testing procedure. The design of the experimental work is based on the findings of Chapters 2 and 3.

Chapter 5 presents a comparison between the test results and findings from the literature survey. Static behaviour, namely the joint strength and the creep effect, is dealt with separately from the dynamic behaviour. Finally, Chapter 6 summarizes the main findings and further investigations are suggested to supplement this study.

CHAPTER 2

LITERATURE REVIEW

2.1 INTRODUCTION

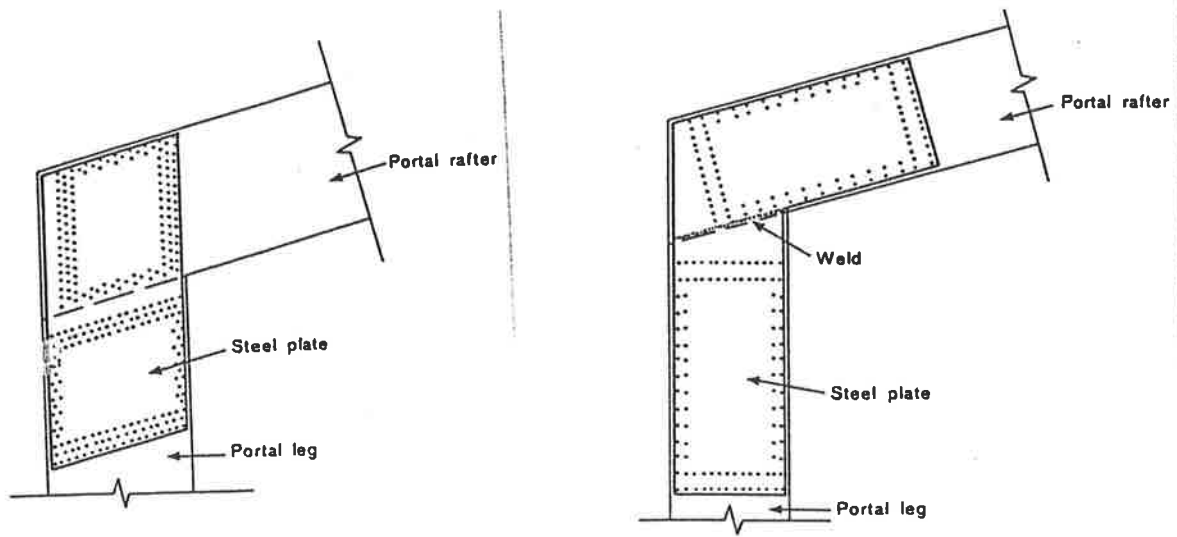
This chapter provides the relevant theoretical support to the development of arguments in later chapters. Hence, a comprehensive survey of technical reports on the subject of structural timber joints is carefully presented. In order to obtain a broad understanding of timber joints, special references are given to the increasing popularity of timber portal frames and the progress of research on moment resisting timber joints. In this way, it is easier to appreciate how this research is related to previous timber joint research and actual timber joints. The portal frame members and gusset are dealt with early in **this chapter**. Not only are the material properties of the individual portal frame members discussed, but different gusset types are also considered. Moreover, the importance of member thickness on the stiffness and failure mode are highlighted. Previous research has been categorised into simple nail joints (less than eight nails) and multi-nail joints (more than eight nails). Comprehensive studies have been carried out on simple nail joints and their results provide relevant data on the effects of nail head restraint, grain orientation and cyclic characteristics. However, special considerations

are required when these results are applied to multi-nail joints. In such joints, nail patterns also influence the performance of the joint. Wherever possible, the results of previous prototype testing is reported. However, comparisons are limited because of the emphasis of this experimental study on residual static strength, and fatigue type loading.

2.2 OVERVIEW OF BEHAVIOUR OF THE JOINT AND ITS COMPONENTS

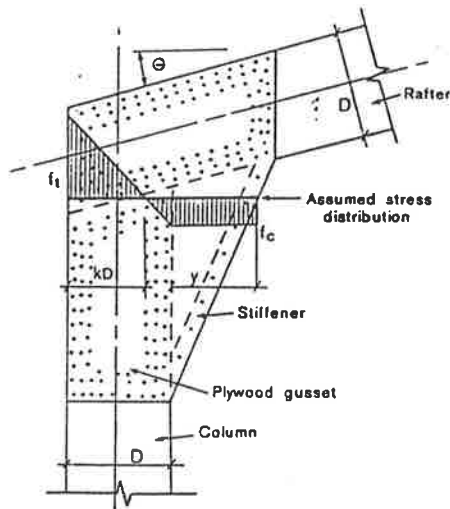
For the past three to four decades, many researchers have performed tests to investigate the properties of timber joints and modelled them mathematically in order to predict their characteristics. The advantages of timber structures are more readily recognised by engineers nowadays. Hence it is not surprising to see that timber has grown in popularity as an engineering material, especially in New Zealand, the United States, Japan and Australia. Timber portal frame structures are claimed in some instances to be less costly than steel portal frame structures by as much as 10-30% (38). The construction of timber structures is faster as the material has a good strength to weight ratio and is easier to handle (38). In addition, it has the added advantage of easily accommodating alterations for fittings such as lighting.

Gibson (16), in his paper on "timber moment frames and their use", listed five types of moment resisting joints with their advantages. Three common commercially used joints are shown in Figure 2.1 (55).



① - Gibson type joint

② - Timbertec type joint



③ - Batchelar type joint

Figure 2.1 Types of joints

The joint under investigation in this study is the Batchelar type and has been used in an existing building north of Adelaide in Wingfield, S.A. (see Chapter 3). The laminated veneer lumber (LVL) members of the portal frames in this particular building were connected by a pair of plywood plates by means of nailing. The technologically advanced product, LVL, brings about cost effectiveness of large timber portal frames and details of this material are given in 2.2.1.

Since the 1960's, Mack has investigated the behaviour of single nailed joints under dynamic loading (35). He concluded that a nailed joint is subjected to adverse effects of fatigue. Following the introduction of steel side plates in the 1970's, more experimental work was conducted on single nail joints to study the effects of loading frequency, load magnitude, interlayer friction, material type, creep and damping.

Hensen and Mortensen (19), and Hunt and Bryant (23) have observed the behaviour of multi-nail joints under dynamic loading. More recently, Boulton (10) has tested moment resisting joints under static conditions. The accumulated findings from research and experience are the basis of the present design practice. AS 1720 (3) accounts for static loading and seismic performance, however, it does not explicitly consider fatigue loading and its effects. Combined with the results of previous findings and this research into the fatigue characteristics and potential loss of long term strength, it is **expected** to establish the effect of fatigue on multi nail joints as used in timber portal frames.

2.2.1 Laminated veneer lumber (LVL) as an engineering material for the members

In order to meet the demands of efficiency and effectiveness in building products and systems, manufacturers are utilizing modern technology to develop new building materials. As well, there remain overriding requirements that they have demonstrable long term performance expectations. LVL has gained wide acceptance as one of these new generation materials and an Australian company International Panel and Lumber Pty Ltd. is continuing the process by successfully marketing prefabricated portal frame building systems.

The main structural members used in this study were laminated veneer lumber (LVL) which is manufactured in Australia entirely from *Pinus Radiata* Veneers. The veneers are rotary-peeled, dried and laminated together under heat and pressure. The 3.2 mm thick veneers are then glued with phenol formaldehyde adhesive. The grain direction of all veneers is oriented in the direction of the long dimension of the beam. An introduction to the material LVL is given by Rowley and Kroonenberg (48). In terms of consistency and reliability, LVL is excellent, as the laminations eliminate strength limiting natural timber defects such as knots and voids. Because LVL is gang sawn from larger width pieces, it is expected to have uniform cross sections and can be width sawn to the required dimension without affecting the design properties. In addition, LVL has superior strength properties to solid timber and its strength/weight ratio is high compared to other structural beam materials. Moreover, LVL has good stability for it does not twist or warp easily. Also, apart from the above, LVL is good for handling, installation and is quality assured by accurate design specification. The availability of large sections of LVL for design, combined with very cost effective connection systems, have made timber industrial buildings economically competitive for spans of 15m to 40m (57). The

material and section properties of LVL listed alongside those of radiata pine are shown in Table 2.1:

	LVL	Plain Radiata Pine
Modules of elasticity E	13,200MPa	7,900MPa
Basic working bending stress F'_b	16MPa	6.9MPa
Basic working shear stress F'_v	1.7 MPa	0.70MPa
Basic working density	620 kg/m ³	550kg/m ³

Table 2.1 Properties comparison of LVL and radiata pine

2.2.2 Gusset plates

(A) Timber side plates

The most commonly used materials for gussets in timber joints are plywood and solid woods. Due to the differences in density and stiffness of these timber materials, the gusset dimensions may vary which will alter the properties of the joints.

In the Australian Timber Code, AS 1720, a wide range of timber materials are listed to aid the user in designing timber structures. Several researchers have conducted experimental studies using different locally available timber types to investigate their characteristics in more depth so as to supplement the present code. Mack (35) has studied the behaviour of nailed timber joints under repetitive loading with many cycles (1000 or 10000 cycles) using three popular types of solid wood (Radiata

pine, Jarrah and Karri) for the main members. In this research, he observed that the three species gave no significant differences in slip behaviour but the increase in slip of dry joints was approximately equal to half that of green joints. Therefore, when designing experiments, a fixed moisture content was used so that the drying effect could be ignored when comparing the results from different tests. Polensek (46) also reported that wood drying would influence the experimental results. The consequence of wood drying is to induce a gap between the main member and the side plates. This would reduce the damping modulus and the interlayer friction resulting in a less stiff joint. The LVL used in this research had a moisture content of approximately 12% and was kiln dried.

Apart from considering the main member, side plates have also been investigated as they transmit loads (shear and moment) from the rafter to the column. Hence, different combinations of timber main members and timber side plates have been researched. When investigating creep of timber joints, Atherton et al (5) discovered that gypsum plasterboard has both a higher energy absorption and slip modulus than plywood which suggested different mechanical properties and thus different slip characteristics should be expected. The average energy absorption was about 9 times greater for gypsum board than for a plywood joint at 60 pounds (27kg) load. This observation suggested that joint displacement at equal load was higher for a gypsum sided joint than for a plywood sided joint. Polensek (46) commented on the failure mechanism of the **lumber-gypsum** joint. He noted that when the joint failed, the gypsum side plate was crushed around the nails and that the crushing was quite prominent at high loads. The wood shear failure mode in the gypsum would contribute to the less stiff and high slip characteristics of this type of joints. In addition, he claimed that the interlayer friction was less significant in this joint.

Lhuede (29) studied different joint arrangements with different combinations of material. He explained that a 10% higher than expected embedment strength (material strength to withstand tension stress transferred by nails) in plywood was due to its higher density in relation to the solid wood. However, even with the same density, the joint capacity was higher with plywood side plates than that of solid wood. This proved that the embedment strength of the plywood is higher than solid wood. Generally, plywood is superior to solid wood in this respect. In the research by Soltis & Mtenga (50), joint resistance due to load cycling was very similar when 1.5" (38mm) Douglas fir and 0.5" (13mm) plywood were used as side plates. Moreover, apart from embedment strength, the characteristics of different timber joints using different timber species were suggested to be related to their density (22) as shown in Figure 2.2.

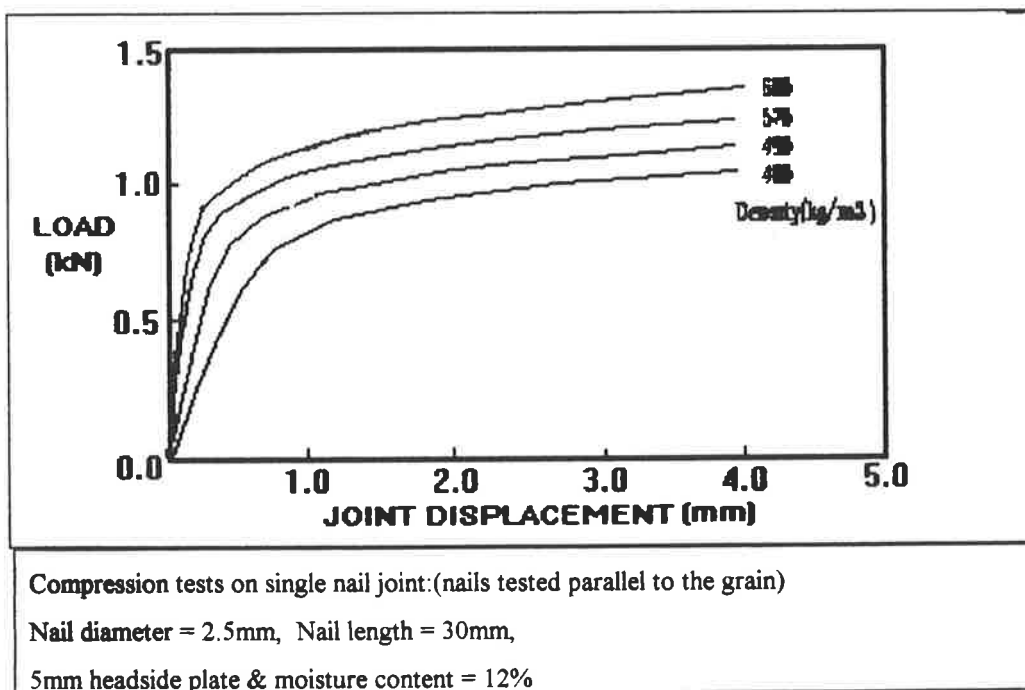


Figure 2.2 Typical effect of timber density on joint strength

Plywood was proved to be a more sound structural timber material than solid wood and solid ash even with higher density and thickness due to its superior embedment strength.

(B) Metal side plates

In 1970, some timber structural joints in New Zealand were found to have inadequate stiffness and strength. Subsequent investigation revealed that they were mostly designed for resisting one directional moment and compression perpendicular to the grain at points where the rafter rested on the column. The joints lacked strength because the lagscrews and shear plates introduced stress-raising discontinuities and had end distances that were too small. Walford (55) recommended a steel side plate as a remedy. He constructed and tested a portal frame with nailed joints using steel side plates and demonstrated that it had a similar stiffness to the all timber joint. Afterwards, Gibson (16) commercially applied this design and further investigations were carried out by Boulton (10). In New Zealand, a 3mm steel side plate was bonded with epoxy to 18mm plywood which served to join glulam members 90mm thick. The plywood stabilized the steel against buckling and enabled hardened nails to be driven with a pneumatic nail gun (55). Apart from New Zealand, researchers in other countries have also looked into this type of joint. The Canadian researchers Karacabeyli and Foschi (25) investigated a Glulam rivet connection under eccentric loading and Japanese researchers, Komatsu et al (26) studied a multi-nail timber joint with 9mm thick steel side plates. Although the Japanese joint required predrilling of the plates, it offered a stiffer and stronger joint to the traditional all timber joint. This was explained by the fixity of the nail's headside which only allowed deformation in the wood member. This created a point of contraflexure in the pointside end of the nail unlike the situation in an ordinary joint

where the point of contraflexure in the nail was on the headside (21) as shown in Figure 2.3.

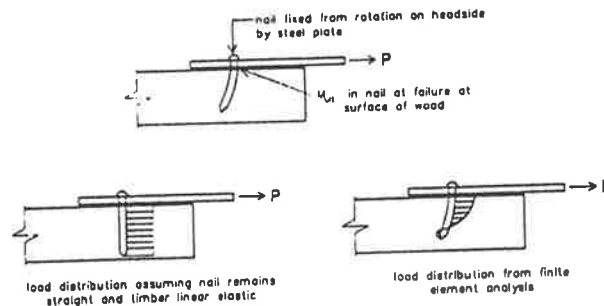


Figure 2.3 Headside of nail fixed from rotation

In 1990, Lheude (29) showed that the yield load F_u for joints with thick timber side plates shared the same equation as for joints with steel side plate of minimal head restraint:

$$F_u = \sqrt{2M_y F_e d}$$

where M_y = yield moment for nail

F_e = embedding stress for nail in wood

d = nail diameter

This is because in both cases, the side plate provides an almost rigid support where the failure mode is by yielding of the nail itself. However, if there is head restraint in the steel side plate case, the yield load will have a 1.44 increase as the steel

plate would effectively limit the lateral displacement of the nail head. Therefore, the k_{16} =1.2 factor for steel plated joint in AS 1720 underestimates its effect. Moreover, Lhuede suggested that even a relatively thin steel side plate can provide a high degree of constraint to the nail (see 2.3.1).

Lowe & Edwards (33) stated that the improved stiffness caused by steel side plates was due to the fixity of nail head by the steel side plate. Thus, they suggested that square shoulders nails should be used to ensure better nail head restraint in the steel plates. In their report, plywood and steel were claimed to have good energy absorption properties, thus they were both considered sound engineering materials for this type of joint. However, the steel plated joint has a greater difference in residual stiffness when loaded along the grain of the timber member than across it. Moreover, for steel plated joints, the contribution of friction between member and side plate to joint residual stiffness was only significant at low amplitude slip (say 0.5mm) whereas the contribution of friction was low (10% or less) for plywood joints at all amplitudes. Steel plated joints have been shown to be stiffer than plywood joints at low strain amplitude but the difference in residual stiffness was insignificant at high strain amplitudes.

2.2.3 Dimensions of joint components

Apart from the effect of different materials on the strength of a joint, dimensions also play a vital role in determining the stiffness and slip characteristics of the whole joint. Lhuede (29) has conducted a series of experimental studies to investigate the effect of side plate thickness and nail dimension ratio (t/d , where t is the timber thickness and d is the diameter of the nail) on the joint capacity. Comparing

plywood sided joints with solid/solid wood joints, the results show that the load capacity varies with the t/d ratio (see Figure 2.4).

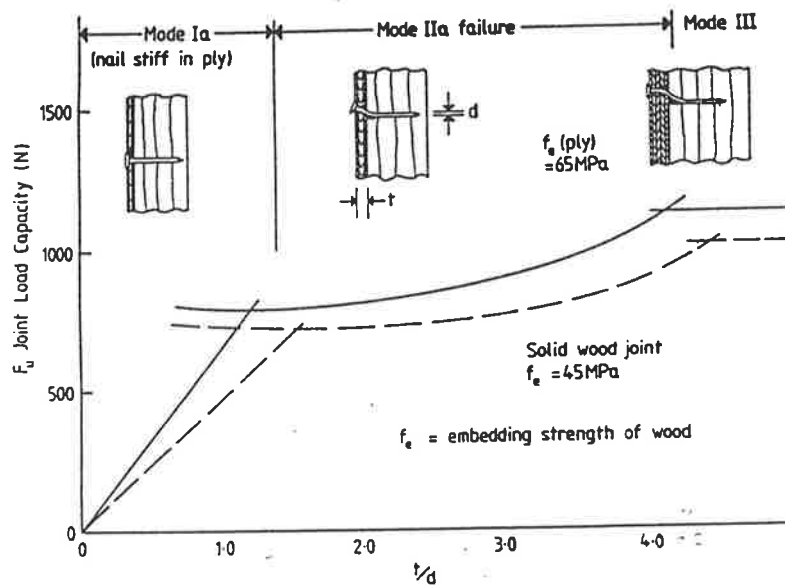


Figure 2.4 Graphical relationship between nailed joint capacity and the t/d ratio

A 5% to 17% excess of load capacity for plywood sided joints for $t/d > 1.7$ is seen in Figure 2.4. However, when the t/d ratio was unity, the load capacity of the plywood sided joint dropped to only 60-70% of that for the solid/solid wood joint. Lowering the t/d ratio has a more adverse effect on the load capacity of the plywood sided joint. Moreover, splitting of the side plate along the grain was likely when the t/d ratio was dropped to a lower bound value for the t/d ratio. In this research, where the t/d ratio for the joints as tested was $19/2.87 = 6.6$, the plywood side plates were regarded as

thick side plates (see Figure 2.5) and this ratio suggested a mode III failure mechanism should be expected (Figure 2.4).

Effects of the thickness of both plates are significant. Polensek (46) found that 3/8in.(9.5mm) thick plywood absorbed more energy than 5/8in.(15.9mm) plywood and that the thicker plywood had a higher slip modulus when there was joint friction. In addition, residual slip was greater in the case of the 3/8in.(9.5mm) thick plywood. Hunt & Bryant (21) performed tests to investigate the nail penetration and headside thickness effects. For pointside penetration of $6d$ to $22d$ (where d is the diameter of the nail), there were small differences in loads at 0.4mm joint displacement, but the ultimate load increased with penetration of the nails. For a penetration of $4d$, there was compression of nail-to-wood bearing down one side of the whole length of the nail and there was insufficient penetration to ensure yielding of the nail at the joint interface. When studying the effect of thickness of headside plate, there were noticeable nail head rotations at small displacements when the plywood thickness was 7.5mm and that, even at large displacements, head rotation was small when the plywood thickness was 20mm or more. In this test, with plywood thickness of 19mm, minimal nail head rotation was expected. The thickness of the side plate would influence the shape of the deformed nail and thus the location of the point of contraflexure. Stiffness at lower loads as well as ultimate strength increased with the plywood thickness up to a certain limit (in the experiment the limit was 18mm) as shown in Figure 2.5.

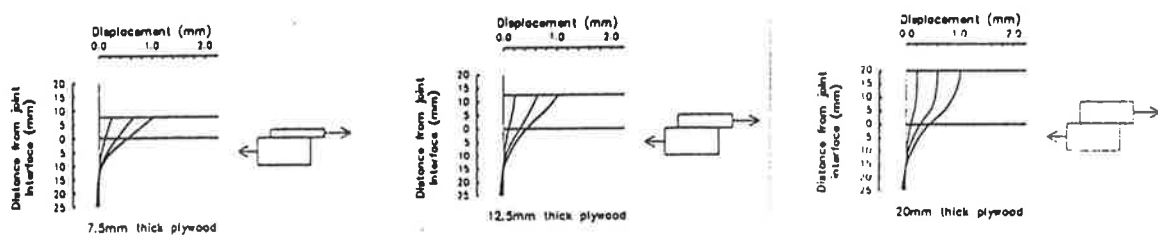


Figure 2.5 Deformed nail shapes for various headside plywood thickness

In a report by Lhuede (29), yield load equations were assigned to three different configurations of 100% timber joints. If the side plate was thin, its thickness controlled the ultimate load by failing in wood shear mode. On the other hand, if the thickness of the side plate was large (compared to the main member), the ultimate load capacity was controlled by the yield moment of the nails. The failure of a single nail joint with t/d ratio of 6.6, as in this study, was expected to be caused by nail yielding.

2.3 SIMPLE NAIL JOINTS

Interaction of nails and wood in timber joints has been studied so as to investigate the properties of the joint performance under static and dynamic loading. An enormous amount of research work has been conducted on the topic of simple nailed joints with one to four nails.

2.3.1 Nail head restraint

It was reported by Hunt & Bryant (22) (see Figure 2.6) and Lowe & Edwards (33) that nail head restraint plays an important part in determining the strength and stiffness of the entire timber nailed joint. In another report by Hunt & Bryant (21), a theoretical description of loaded nail behaviour was given which described a no restraint nail with the point of contraflexure of the deformed shape at the ends of the nail. However, if the nail head was fully fixed, the point of contraflexure would be in the pointside with yielding at the joint interface and such an arrangement produced a stiffer and stronger joint. This conclusion was supported by Foschi & Longworth (15) who found experimentally that the increase in strength due to head fixity was 45%. This is in

good agreement with the value of 40% claimed by Lheude (29) for both steel and plywood side plates.

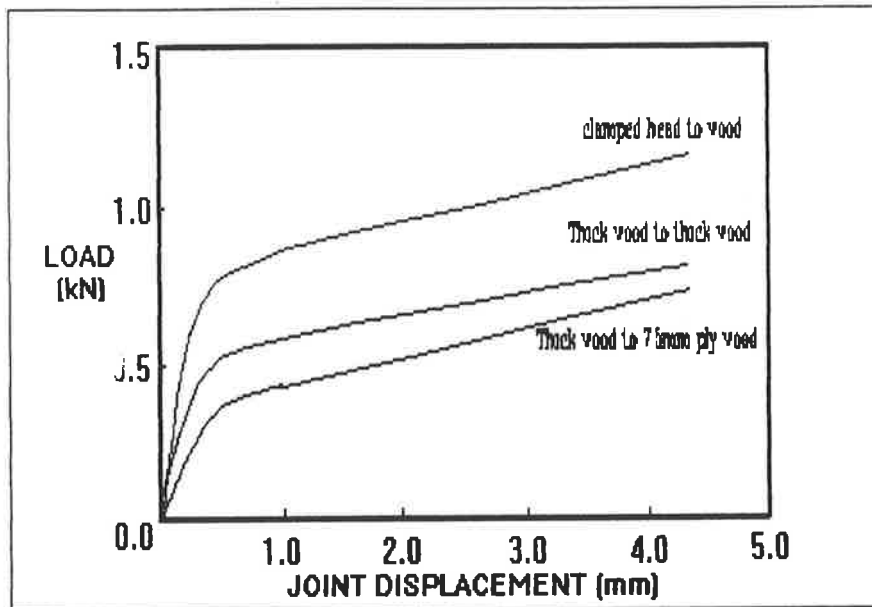


Figure 2.6 Typical effect of nail head restraint

One of the most commonly agreed factors influencing nail fixity was nail plate material. Greater nail head restraint is possible with steel side plates. Even with relatively thin steel plates, a high degree of constraint to the nail head can be achieved. This is because the steel plate provides a rigid support to the portion of the nail near the head and severely limits the displacement of the nail head. As the thickness of the side plate increases, the nail rotational restraint is improved. Moreover, stiffness increases with the thickness at lower loads as well as at ultimate strength.

Nail head shape is also a factor to be considered, especially when thin steel side plates are used. Nails with square shoulders as shown in Figure 2.7 give stiffer and stronger joints than those with sloping shoulders because head restraint effects are present at all loads.

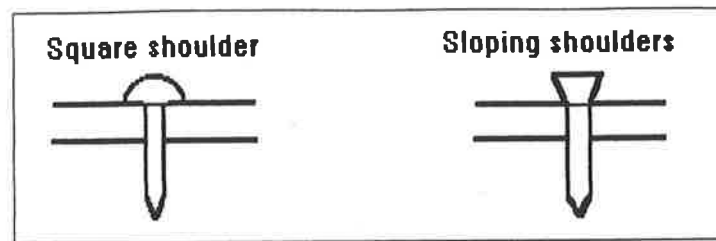


Figure 2.7 Two types of nail head shape

Nicholls (39) modelled the degree of nail head restraint in his investigations in which fully-fixed, partially-fixed and pinned nail head fixity conditions were considered as shown in Figure 2.8. As in the Hunt & Bryant research (21), Nicholls took the fully restrained case as nails were driven through thick metal side plates (c.f. Lheude (29) also assumed high strength nails were fully-fixed when using gun-driven nails in steel side plates). For the partially-fixed condition, a 2mm plate with no preformed holes was utilised. Finally, Nicholls simulated the pinned head fixity using a 2mm plate with oversize preformed holes. He then used a finite element model with non linear material properties to model the nail in each of the conditions:

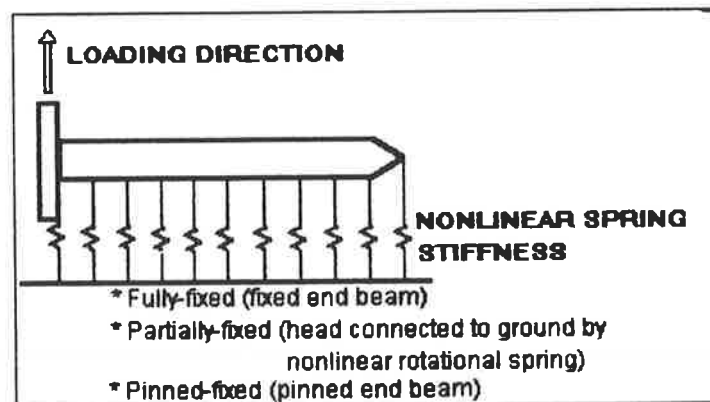


Figure 2.8 Modelling of a nail with nonlinear material properties

The theoretical analysis was confirmed by testing several multi-nail joints. From both the experimental and theoretical results, Nicholls concluded that at high loads

the joint behaved as though the nails were in the pinned condition, while at working loads the joint behaved as though the nail heads were effectively fully-fixed. This was expected to represent the nail head restraint for the test specimens in this research.

2.3.2 Grain direction & cyclic loading characteristic

In 1990, Hunt & Bryant (21) investigated, in particular, the effects of the angle of loading, nail head restraint and nail penetration on the strength of single nail joints. In their experiment, when the loading direction was perpendicular to the direction of the grain, the initial nail stiffness was only 60%-70% of the stiffness for loading parallel to the grain direction (see Figure 2.9). However, nails loaded perpendicular to grain have higher ultimate strengths than nails loaded parallel to the grain. This result is applicable to LVL and plywood members of the test specimens.

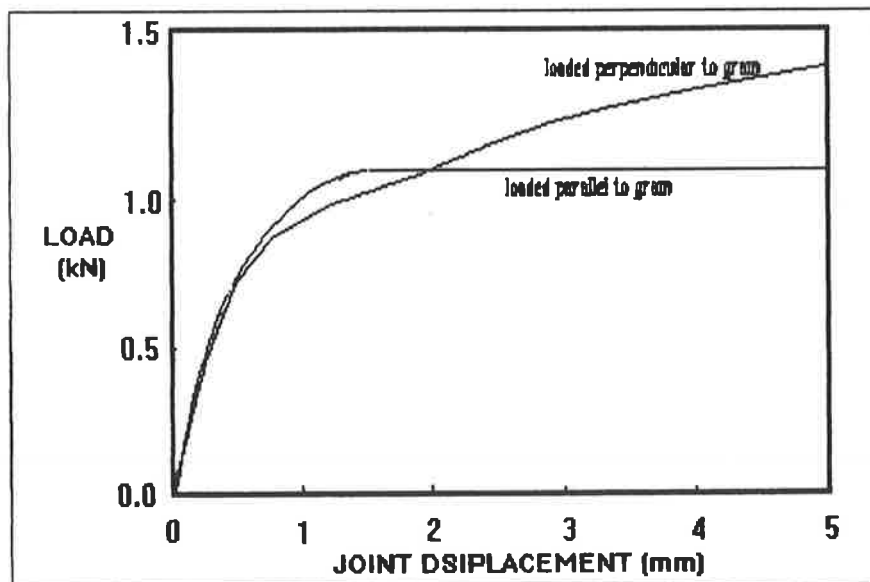


Figure 2.9 Typical load displacement behaviour for nail loaded parallel and perpendicular to wood grain

Soltis and Mtenga (50) investigated the topic of dynamic loading for single nailed joints; some findings are of particular interest here. When comparing the results of static tests to the results of tests conducted using 1 and 10 Hz cyclic loading, they found that at small deformations the increase in joint capacity due to higher rate of loading was offset by decreased joint capacity due to load cycling. At large deformations and number of load cycles, joint resistance decreased. As in this research, the specimen underwent large deformation and many cycles of load which produced decreasing joint capacity as shown in Chapter 5. On the other hand, the loading history of joints had little effect when the previous load cycles resulted in relatively small deformations. A study by Girhammar and Andersson (17) addressed the loading or deformation rate effect on the yield loads of nailed timber joints. They found that the increase in the ultimate strength of the simple nailed joints was linearly dependent on the logarithmic deformation rate and the influence of the deformation rate was much greater for wood than for the nails.

A standard timber joint testing method was suggested by Polensek (46), as he realized that testing conditions (e.g. assembling techniques, loading patterns and assumption of linearity of slip) would significantly affect the test results. By generating two types of cyclic loading, namely ramp and sinusoidal loading, he modelled the joint slip and damping mathematically in terms of loading frequency and amplitude. Generally, high rate of loading and low amplitude load and slip would enhance the effect of damping and the stiffness of the joint. Polensek (46) also addressed the effect of gaps in the joint by: (a) wood drying and (b) pushing the final 16mm of the nails into place rather than hammering. Both techniques gave insufficient pressure to bring the joints into enough contact to engage interlayer friction. The joints without gap had high stiffness and damping at low loads. In contrast, the opposite was experienced by joints with gaps (see Figure 2.10). In Chapter 4, a testing method for this research was derived

to suit the specimens and the testing conditions which resulted in a unique assembling technique and loading patterns.

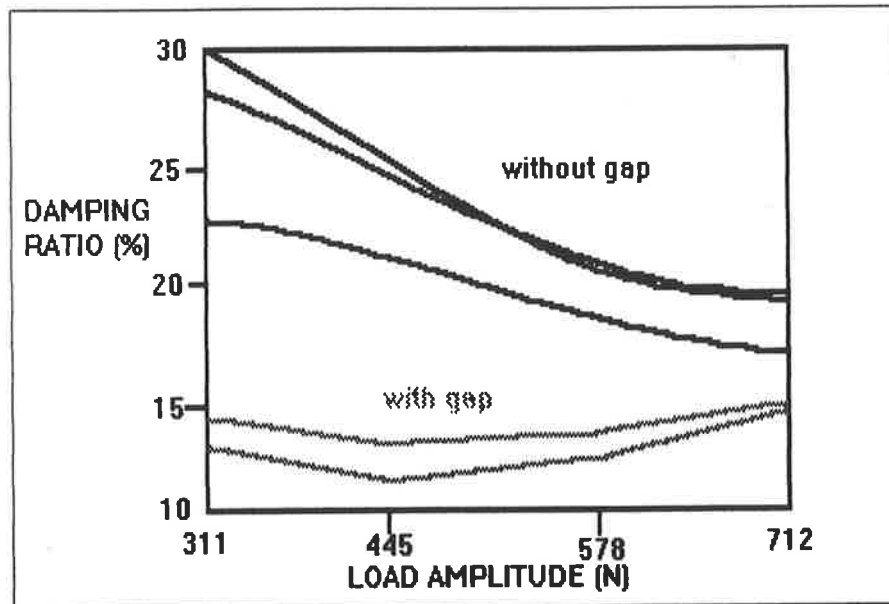
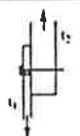



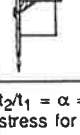


Figure 2.10 Effect of load magnitude and assembly condition on viscous damping

Figure 2.10 shows that damping decreased when the load was increased in tight (without gap) joints. This was due to partial gaps forming in the contact interlayer because the increasing shear load loosened and pulled the nails out. The reduction of joint tightness lessens interlayer friction and damping. On the other hand, joints with gaps have relatively constant damping for most of the loading range and a small increase at high loads as the gap partially disappears thereby increasing the interlayer friction. This explanation was applied to the behaviour of the various test specimens under certain loading conditions (see Chapter 5).

2.3.3 Single vs multi-nails

Lheude (29) has written a comprehensive reappraisal of nailed timber joint behaviour and summarised some of the more important factors for single nailed joints which include a table of yield loads, F_u , for some typical failure modes for two member joints as shown in Figure 2.11. In addition, he concluded that the load capacities would be improved if hardened nails were used.

Failure geometry condition	Yield load F_u
 1 All wood	$F_u = t_1 \cdot f_e \cdot d$
 2 All wood	$F_u = \frac{t_1 \cdot f_e \cdot d}{2} \left[\sqrt{3\alpha^2 + 2\alpha} - (1 + \alpha) \right]$
 3 All wood	$F_u = \sqrt{2M_y \cdot f_e \cdot d}$
 4 Steel side t_1	$F_u = \sqrt{2M_y \cdot f_e \cdot d}$
 5 Steel side t_1	$F_u = \sqrt{2} \cdot \sqrt{2M_y \cdot f_e \cdot d}$

$t_2/t_1 = \alpha$ = ratio of thicker/thinner member; f_e = embedding stress for nail in wood (MPa); d = nail diameter; M_y = yield moment for nail = $d^3/6 \cdot f_s$; f_s = yield stress of nail.

Figure 2.11 Some typical failure modes for two-member joints

Hunt & Bryant (21) showed that for thin headside members, head restraining effects can be significant and that they increase with the nail head size of the nail.

These qualitative findings were valuable when considering multi-nailed joints and set the directions for further investigations. However, it has been shown that the distribution of laterally applied load on the nails in a joint are not uniform. For example, the end nails in a nail group were found to carry more load than the central nails.

In tests performed on multi-nail joints with steel side plates, Foschi & Longworth (15) found that as the load was increased, the end nails would begin to yield first, while the wood under the shanks started to fail in bearing. Any subsequent load increase, after the end nails' maximum carrying capacity was reached, was then shared by other un-yielded nails. Eventually, the load reached an ultimate value corresponding to a situation in which every nail in the connection had reached its ultimate capacity.

$$\text{Therefore, } P_n = n \times P_1 \dots \dots \dots [1]$$

where P_n = load capacity of the joint;

P_1 = load capacity of a single nailed joint ; and

n = number of nails.

Equation [1] applies only to nails in shear and is valid only when every nail has yielded and without premature failure of the wood. Thomas & Malhotra (53) supported this view with experimental evidence and introduced a coefficient for multi-nail effects, C_n . In their investigation, an attempt was made to study the effects of the number of nails on the stiffness of laterally loaded timber joints with interface friction, fabricated with 2 to 8 nails in a row. The coefficient varied with the values of joint slip for a particular configuration. In the experiment, it was found that C_n attained a nearly constant value of 0.9 for a joint with eight nails in a row and that the reduction for one to three nails was negligible. It was suggested that $P_n = C_n \times n \times P_1$ correlates better with the real situation. For design purposes, C_n was assigned to be unity if 1 to 3 nails were used and $C_n = 0.9$, otherwise. Thomas & Malhotra (53) successfully employed the theory used in predicting the behaviour of single nail joints to multi-nail joints using energy principles. Boulton (10) has, on the other hand, looked at multi-nail moment resisting joints. He investigated the significance of the pattern of nailing and the grain direction in these joints. Therefore, the behaviour of multi-nail joints under static load

can be predicted with reasonable accuracy applying the results from tests of single nail joints.

2.4 MULTI-NAIL JOINTS

2.4.1 Nail pattern

A number of researchers have reported on the influence of nail pattern on the overall joint performance. Nail distribution within the joint was also reported to be significant. Foschi and Longworth (15) suggested that nail spacing determined the mode of failure. For the case of large nail spacing in a rectangular pattern, the nail yielding mode dominated which was desirable as this achieved the ultimate capacity of the joint. However, if the nail spacing was small, wood shear failure could occur around the group of nails at relatively low loads. In the case of shear failure, increasing the end distance from the edge was found to increase the load capacity. AS 1720 specifies minimum edge distances and spacings as a result of their work. The joint test specimen was designed following AS1720 guidelines (see section 3.4).

In order to design a joint to best suit its performance requirements, Karacabeyli (25) found that it was advisable to minimize the possibility of high tension in the **direction** perpendicular to the grain of timber in a steel side plated joint. Thus, in a rectangular nail pattern, the longest side should be positioned perpendicular to the grain so as to increase the joint's load capacity. Since the stress is not uniformly distributed amongst the nails, stress concentration will occur but should be minimised. Boulton (10) has described in his report that a larger portion of the total moment was resisted by the outer laminates of the timber. Thus, the mechanical properties of the timber, particularly

the outer laminates where the bending stresses and nail loads are both at a maximum, play a significant part in the behaviour of the joint. Hunt and Bryant (23) agreed, stating that stress concentrations within a few of the laminates for certain nail patterns could lead to failure at loads smaller than the design load capacity. Moreover, nail point loads create a significant stress concentration in the timber at its point of application which can initiate crack propagation at relatively low timber stresses. This phenomenon is less likely in the case of LVL (as opposed to solid timber) which has superior uniformity and strength properties as stated in section 2.2.1.

To further the analysis, Boulton (10) adopted a computer model to test various nailing patterns with a view to reducing peak nail loads (stress concentration). Adequate joint stiffness and timber stresses in the vicinity of the joint were other factors used to gauge the effectiveness of different joint geometries. Six corner nails were removed from the outer nail group which lowered the peak nail forces significantly without aggravating the timber stresses. However, such changes to the nail group reduced the stability of the plate with regards to buckling when the joint was loaded in the closing mode.

2.4.2 Experimental testing of moment resisting joints

Experiments have been conducted on timber moment resisting joints for the past two decades, especially by New Zealand researchers. From 1987 onwards, researchers such as Hunt and Bryant, by testing moment resisting nailed joints, established a new era in timber engineering for this type of technically satisfying and cost effective joint for commercial use. Batchelor (8)(9) investigated plywood side plated joints and later steel/ply composite plated joints, in place of steel sheet side plates.

Tearing of the plywood gusset at the ultimate strength limit state was observed in most of his tests while the theoretically predicted ductile failure by nail yielding was uncommon. That triggered a series of comprehensive experimental programs in parallel with computer modelling of nail failure mechanisms. Boulton continued the investigation into joint ductility and found that stress concentrations were probable along the extreme nail locations. In his steel plated experiment, he commented that reduced nail numbers could bring improvement in joint ductility without sacrificing strength (32).

Table 2.2 lists some of the experiments conducted by New Zealand researchers in the last two decades on multi-nail timber moment resisting joints with different nail patterns, gusset materials, member configurations and methods of testing. Batchelar (7), as a pioneer in this field of prototype joint testing, has designed a unique procedure for testing joint specimens both statically and dynamically in the laboratory. Subsequent investigations in New Zealand utilised his experimental set-up for testing different joints at different load levels and displacements. The experimental arrangement was a vertical loaded equal-leg specimen secured by lateral restraints to prevent side sway when the specimens were loaded in compression (see Figure 2.12). One end of the specimen was connected to a stationary anchorage on the ground by a metal hinge joint that would permit load transfer with no moment. The other end of the specimen was linked to a servo actuator through a similar hinge system. In contrast, joint specimens in this study were tested horizontally and loaded in tension (see section 4.3.2).

RESEARCHER(S)	GUSSET PLATE	NAIL PATTERN	TESTING METHOD	FINDINGS
BATCHELAR (7)	6 types, e.g. specimen 6 18.0DD Radiata Pine 6 ply, reinforcing strip	3 rows, 60mm spacing, 2.8x50mm nails	vertical testing with 2790mm legs, load reversal	strain within the gusset, Pu=34kN, Pdesign=17.5kN
BATCHELAR & CAVANAGH (8)	7 types, e.g. specimen 2: 9mm plywood	5 rows, 2.8x50mm nails	vertical testing with 3118mm legs, load reversal	strain within the gusset, Peak ram load=80kN, ram displacement=30mm
BATCHELAR & HUNT (9)	14 types, 2 composite steel/plywood: 2x12.5mm and 1x18mm plywood and 0.75mm G550 galvanized steel sheet between each plywood, reinforcing strip	10 rows, 3.33x89mm nails, 50mm centres, 25mm between rows	vertical testing with 5962mm legs, load reversal	Peak ram cyclic load=135kN and ram displacement=110mm
BOULT (10)	5mm steel sheet	2 rows of 3.55mm diameter nails	vertical testing with 2600mm legs, load reversal	Ultimate stress=15.27MPa and peak ram load=15kN
HANSEN & MORTENSEN (19)	3 types, e.g. series 2: 2mm steel gusset =160mmx400mm	annular grooved nails 40/40, 2x32pcs	Full scale timber frame testing at 3Hz	fatigue test up to 1 million cycles
HUNT & BRYANT (23)	2 types, e.g. Type 2: 4mm steel plate = 320mmx735mm	4 rows, 332 of 3.55x40mm nails	vertical testing	stress in joint region

Table 2.2 Summary of previous moment resisting joint experimental research

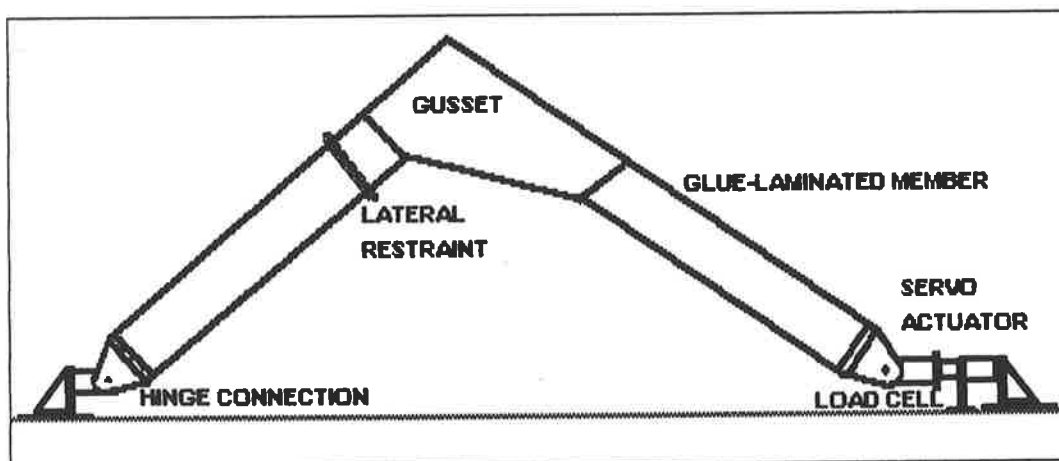


Figure 2.12 Test set-up in New Zealand researches

A typical V-frame specimen loaded vertically is shown in Figure 2.12. These specimen were tested in isolation to the rest of the portal frame structure and the behaviour of the joint was singled out for analysis. A variation of moment resisting joint testing was conducted on a full-scale timber frame by Hansen and Mortensen (19). The load was imposed at four points on one of the rafters and the bending moment at the knee

joint opposite the loaded rafter varied between a value corresponding to the moment from the dead load of a roof and a value corresponding to the moment from the dead load of a roof plus the characteristic wind load acting on the roof (see Figure 2.13). Due to the large load required and complexity of construction, only small moment resisting joints could be tested using this full-scale frame method where the actual response of the joint in a portal frame loaded dynamically under the influence of surrounding features (like bracing and walls) could be realised directly. On the other hand, Batchelar's vertical testing method with the V-frame provided an easier set-up and more realistic load magnitude, even for large joints. By comparing the ultimate loads of the tested specimens with similar configurations to those of the test specimens in this research, the ultimate load capacity of the test joints could be approximated.

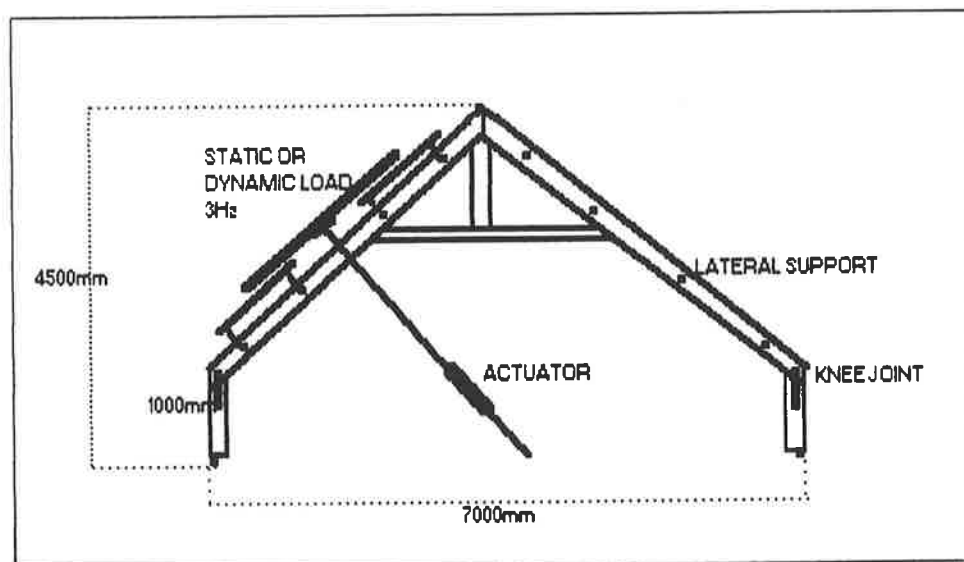


Figure 2.13 Test set-up in the full-scale testing of prefabricated timber frame

2.4.3 Static strength and failure mode

It is generally agreed (19) that the strength and stiffness of a timber portal frame are strongly dependent on the strength and stiffness of the knee joint. Therefore, it is important to realise the ultimate moment capacity required for a joint to provide adequate structural support to the portal frame in order to withstand the axial and bending moment. This is also why the static strength of the moment resisting joint is the main consideration in design. This section presents a brief discussion of the characteristics of this strength and methods of calculating the static strength and the corresponding failure modes.

In the 1990 Gottstein report by Crews (13), the author summarised the factors which influence strength and deformation characteristics of timber joints as follows:

- specific gravities of timber members;
- direction of grain in timber members;
- orientation of growth rings and grade effects in timber members;
- moisture content of timber members prior to and after loading;
- connector materials and geometry;
- joint member geometry;
- arrangement of joint members with multiple shear planes;
- number and position of the connectors;
- the method of joint fabrication;
- the previous loading history (cumulative load effects);
- the rate at which load is applied; and
- the regime of loading (e.g.: repetitive, long or short duration).

It is interesting to note that among the twelve points, there are seven factors related to the areas of timber material properties and loading. The remaining

factors are concerned with the nails and the gusset plates. Clearly, consistency in timber quality and careful selection of loading pattern are very important considerations in the testing to ensure reliable and applicable results. Actually, most of the factors that affect joint static strength are incorporated in design codes as coefficients (k-factors in AS1720) or in parts of the design calculations. Researchers in New Zealand and Japan (22)(26)(27)(29) have suggested that their design codes are too conservative. In particular, Walford concluded in his analysis of timber portal gusset joints that current research supported much higher allowable nail loads than those permissible under the New Zealand design code NZS3603. Crews (13) explained that this conservatism was due to:

1. The large number of nails used in these joints reduces the variability.
2. In cases where steel side plates are used, fixity of nail head results in stiffer joints. Increased head rigidity results in significantly less (greater than 50%) slip for a given load, as well as an increase in maximum capacity of the connection.
3. Large numbers of nails generate pressure between the gusset and member resulting in significant moment capacity due to friction. Seasonal moisture changes may alter the pressure in time as the wood shrinks and swells. This factor is not considered in the design process and it is difficult to quantify the frictional component as a part of the design procedure.

Apart from comments on the high loads that were assigned to individual nails, Walford (55) compared different ways of calculating the moment capacity of a moment resisting joint from the nailing pattern and the allowable nail loads. The thin walled tube analogy assumes that the nailed area is a cross section of a tube subjected to torsional loading and that the stress is uniform. This method was considered the least accurate. The shared rivet group analogy states that the stress at any point in the nailed area is proportional to the joint moment and the distance of the point from the centroid

and is considered to be an improvement over the thin walled tube analogy method. In the discrete rivet group analogy, it is assumed that the force on each nail acts individually and the joint has a linear load/slip relationship while the nonlinear rivet group analogy assumes the load is proportional to (slip)^m where m ranges from 0.5 to 1. Theoretically, the last method gives an exact prediction of the nail group strength, however, the m value is an unknown factor in most cases. This is because in the case of moment resisting joints, for the majority of nails in the group, the resultant load would be at some angle (which controls the m-value) to the grain between the extremes of parallel and perpendicular and insignificant load/slip data for these unique directions exists. The thin walled tube analogy and the shared rivet group analogy methods were used to predict the strength of the full-scale and half-scale joints in Chapter 3.

Boult (10) found that a significant number of previously tested moment resisting joints failed at the corner nails. However, wherever timber failure occurred, the ultimate moment capacity was calculated for maximum centreline moment and not for the moment at the position of failure. This could greatly reduce the "true moment" at the failure spot as the lap length could be considerably large. Moreover, the definition of the specific point of failure was not totally consistent in different studies. If only the elastic phase was considered in the failure mechanism, this implied that failure occurred when the first nail started to yield which was the onset of its plastic behaviour. This could largely underestimate the true moment capacity of the joint and limit the application of the failure mechanism only to small joint rotation. On the other hand, if the failure was noted by the rapid increase of joint rotation as in the study of Karacabeyli and Foschi (25), the full joint strength was then realised at the point where all nails were at uniform load when yielding occurred. This state of joint failure matched closely the thin walled tube analogy prediction which assumes uniform nail load at large joint rotations.

Joint slip was used to determine the failure for single nail joints. Atherton et al (5) investigated the slip and damping characteristics of wood-plywood joints with respect to load-cycling, specific gravity, tension-compression loading, plywood thickness and interface friction where the latter effects were found to be more significant. The failure mode as commonly observed in other laboratory tests of moment resisting joints, especially those in New Zealand, was tension failure in the timber material rather than nail slip. Nails being pulled out of the plywood gusset plate was observed in the failure of simple nailed timber joints (5)(6)(14)(21).

Therefore, the potential for premature or brittle wood splitting failures could not be ignored in this project. A review of nail plate moment resisting joint experiments at Auckland University showed that a significant number of timber moment resisting joints failed as a result of brittle tension fracture of the outer timber laminates at loads that were below those that engineers might expect from rules in New Zealand design codes(24). Some joints failed at embarrassingly low nominal timber stresses in Boulton's experiment (10). This was thought to be due to (13):

1. Stresses in joint region significantly higher than prediction;
2. Nails or nail holes triggered failure in clear grain glulam laminates at average values of stress that might be one third of the standard modulus of rupture test values; and
3. Nail pattern that concentrated moment resistance in outer laminates could cause higher stress than patterns that distributed resistance over many laminates.

In a test conducted by Batchelar (7), he put a reinforcing strip at the outer edge of the plywood gusset plate in order to prevent timber rupture by bending at that position. However, the specimens failed by timber fracture rather than nail yielding and thus the moment capacity was not fully realised. Some joint designs have proved to give

timber stresses that were significantly higher than those given by usual calculations. Tension tests of the outer laminates, in particular showed that brittle tensile failures (perpendicular to the grain) could occur at stresses close to permissible design levels. This result suggested that nails could trigger tension failures at average stresses of similar magnitude to the allowable design failure stresses which occurred in the timber of moment resisting joints (13). Hunt and Bryant (22A), in 1993, attempted to model nail holes and other interruptions to the grains of wood when analysing timber stress. They suggested that stress concentration effects initiate fracture in some wood fibres. The stress concentration factors for holes in *Pinus radiata* wood members loaded in axial tension are about twice the corresponding values for a member made from an isotropic material. The stress concentration factor, C , is found by dividing the maximum axial stress around the hole by the average axial stress. Brittle, perpendicular to the grain fracture is being controlled by fracture mechanics rules, such as the stress intensity factor, K . Hunt and Bryant found that stress intensity factors for a member made from an orthotropic material such as wood are effectively the same as those for a corresponding member made from an isotropic material, where K is defined as:

$$K = F_1 \sigma (a)^{1/2}$$

where a = crack or flaw size,

σ = stress that would exist if there was no crack,

F_1 = constant that depends on the geometry, loading situation and perhaps the material.

If the crack or flaw size (a) is doubled, the stress intensity factor (K) is increased by 1.4 times given the stress is constant. As the loading increases, brittle fracture occurs when the stress intensity factor reaches a critical value which is based on experimental tests.

Hunt and Bryant (24) concluded that the nail pattern should be such that the nails do not cause increases in nominal stresses in higher stressed outer laminates and the nails should be spread over a reasonably large proportion of the joint area. Given the possibility of brittle failure, it was important to watch for such failure in the experimental work reported in Chapter 5.

2.5 SUMMARY

The key findings of the literature survey, which relate directly to the type of joint tested in this study, are summarised in this section.

In terms of the timber materials used in the test specimen, LVL provides good strength and reliability while the plywood gusset plates have superior embedment strength and stiffness qualities. Since $t/d = 6.6$, the test specimens were classified as thick plate with mode III failure and nail yielding mechanisms were expected based on the results of simple joint tests.

In the literature review for simple nail joints, it was confirmed that head restraint, provided by thick gusset plates, improves joint strength. In addition, square shoulder nails (as in the test specimen) were found to improve nail fixity. At low deformation, the effect of increasing loading rate for improving joint capacity offsets the opposite effect of cyclic loading. At high deformation, joint resistance is lowered by cyclic loading. It was interesting to find that increases in ultimate strength are proportional to logarithmic increases in deformation rate and the influence of deformations is higher in wood than nails.

Generally, high loading rate and low amplitude load and slip enhance the stiffness of the joint. It was pointed out that joints without gap had high stiffness at low loads. In contrast, the opposite was experienced by joints with gaps. Furthermore, the distribution of laterally applied load on a joint was not uniform. The end nails in a nail group were found to carry more load than the central nails. In an axially loaded tensile test, it was suggested that $P_n = C_n \times n \times P_1$, for design purposes, C_n was assigned to be unity if 1 to 3 nails were used and 0.9 otherwise

In multi-nail joint investigations, a larger portion of the total moment was resisted by the outer laminates of the timber and stress concentrations within a few of the laminates for certain nail patterns could lead to failure at loads smaller than the design load capacity. Moreover, tearing of the plywood gusset at the ultimate strength limit state was observed in many tests while the theoretically predicted ductile failure by nail yielding was uncommon. Thin walled tube analogy and the shared rivet group analogy were suggested for calculating the moment capacity of a moment resisting joint from the nailing pattern. However, brittle tensile failures (perpendicular to the grain) could occur at stresses close to permissible design levels where nails could trigger tension failures at average stresses of similar magnitude to the allowable design failure stresses which occurred in the timber of moment resisting joints.

CHAPTER 3

THEORETICAL STUDY OF ACTUAL JOINT & TEST SPECIMEN

3.1 INTRODUCTION

This chapter discusses the properties of the plywood gusseted moment resisting joint in a timber portal frame building at Wingfield and the half scale replica of this joint which was used for testing. Joints are commonly designed only for static loading in Australia. As such, limited information is provided by AS 1720 for the design of moment resisting joints, in particular those of plywood gusset plates and hardened nails design standards. With respect to dynamic/fatigue loads, calculations are largely based on empirical formulae although theoretical calculations on the actual joint and test specimen assist in the interpretation of the experimental results. Different loading on the portal frame building that affect the joint are considered (sections 3.2, 3.3), resulting in realistic applied loads for the test specimens. The test specimen design is discussed in section 3.4. Theoretical predictions of joint strength and individual member strengths are presented in sections 3.5, 3.6, and are used for comparison with the experimental results in Chapter 5. The existing structure is a light industrial timber portal frame

structure situated at Dundee Street in the suburb of Wingfield in Adelaide, South Australia. It was constructed in 1989 and was designed by P.J. Yttrup & Associates. The building is located in an area that is open and is categorised as "Terrain Category 2" as defined by AS 1170 (2). The prevailing wind for Adelaide is South-West in winter and North-West in summer which produces high wind gust speeds at the building site.

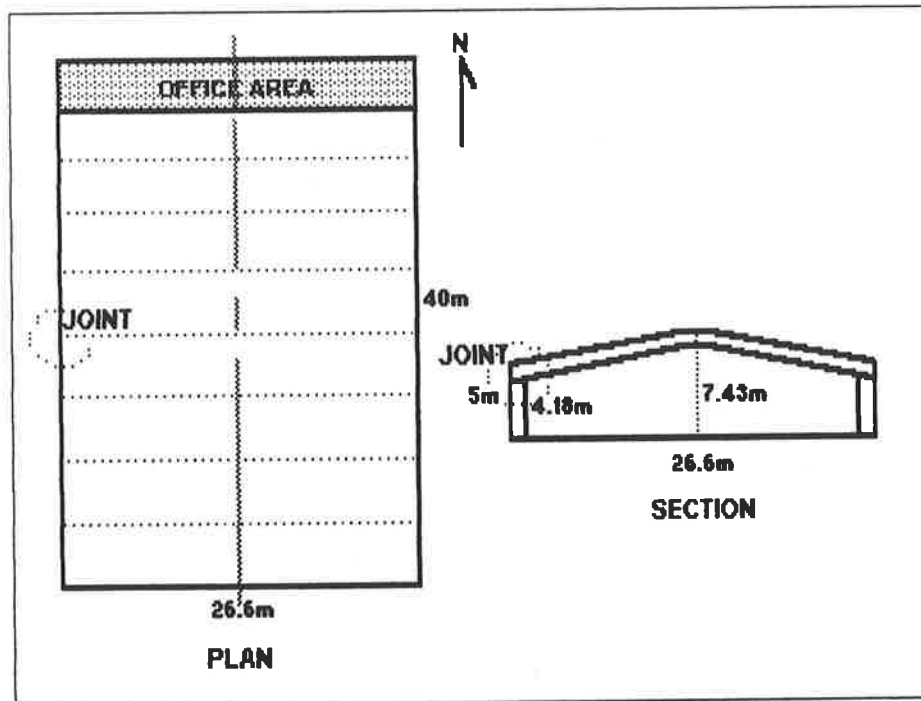


Figure 3.1 Moment resisting joint in the actual timber portal frame at Wingfield

The building is symmetrical about the North-South axis with the reception and offices on the northern side. The eaves height is 5m, the column is 4.18m high and the ridge height is 7.43m. The total dimension of the structure in plan view is 40m by 26.6m where 26.6m is the span of the portal frame (see Figure 3.1). The joint is composed of LVL limbs with plywood gusset plates nailed onto both sides of the column-rafter connection. The LVL and plywood thicknesses are 63mm and 19mm respectively. Two nail groups are located on the joint with the upper group nailed onto the rafter and the lower group nailed onto the column. The upper group contains 410 nails as shown in

Figure 3.3. The nails used are 2.87×50mm made from hardened steel with flat heads, and the penetration is the full length of the nail as a pneumatic nail gun was used to drive the nails. This gives a t/d ratio of 6.62 (19mm divided by 2.87mm) and nail penetration of the LVL of $10.8d$ ((50mm-19mm)÷2.87mm). Hence, a nail yielding mode was anticipated for this joint given the t/d value and the high nail head restraint (see section 2.2.3). Furthermore, friction effects were expected to be more prominent due to the large number of nails ($\cong 800$ nails on each side). Recall that in a moment resisting joint, a large number of nails tend to clamp the plywood gusset plates onto the member and enhance the frictional effect due to pressure between the gusset plates and LVL members (refer to section 2.3.2).

3.2 FIELD EXPERIMENT

In the research reported in this thesis, experiments were conducted on $1/2$ -scale models of the prototype joint in the Wingfield building to study the fatigue behaviour of the joint. Factors such as static strength, residual strength after enduring a set number of cycles, failure mode, strain and stiffness were investigated. However, at the same time a colleague, Mr. Wade Stevens(52), undertook field research of the actual joint of the portal frame structure at Wingfield. This concurrent study concentrated mainly on investigating the performance of an actual joint. His instrumentation was designed to measure the actual joint response to ambient wind loading. Apart from the difference in the level of loading (loading in the field test and ultimate loading in the experimental tests), the actual joint was in a somewhat "softened" state as it was constructed more than three years before Stevens' tests while the $1/2$ -scale specimens were tested within six months of their fabrication (without any preloading). The Stevens study provided some insight into how the joint behaves in the real portal frame building and

served as a comparison to this research. Initially, measured wind loading from the field experiment was intended to give actual inputs for dynamic loads to the laboratory testing. However, due to the small magnitude of loads measured in the field and complications due to temperature effects, the moment used in the experiments was based on theoretical calculations. Instruments (similar to those used in the laboratory tests) were used to record the joint performance under wind loading. Joint rotation, bending strain, lateral frame side sway and frequency of response were recorded. The speed of wind, which served as a trigger for recording, was measured by an anemometer at the top of a post erected in the parking area to the west of the building near the actual joint.

In the actual portal frame building, the joint responded to a wind gust of 36km/hr by a change in moment of approximately 6.5kN-m, or 7% of the joint's calculated moment capacity. When the moment in the joint due to the average wind load was superimposed on this gust response, the total moment was estimated to be about double, or 14% of, the joint's calculated capacity (18). The result showed that the joint is likely to be loaded with $\approx 10\%$ of its calculated capacity most of the time by the average wind pressure and the occasional wind gust.

In the field test, as in the laboratory test, the moment-rotation relationship was the prime interest and only the most significant events, as defined by Stevens, were measured. Continuous output (strain and rotation) was collected by a data logging system with internal trigger from the period of June to September 1992. Only events with a change in strain $\geq 20\mu\epsilon$ in the bottom side of the rafter were taken as significant events of 10 seconds duration. From all the 477 significant occasions presented in a moment vs rotation plot by Stevens, an envelope band was drawn to sufficiently represent the response of 1 to 10kN-m moment and 2×10^{-4} to 4×10^{-3} rad rotation induced by the Westerly winds of 30 to 70km/hr. A Rotary Variable Differential Transformer, or

RVDT, (see section 4.3.3) was utilised to detect the change in rotation of the joint 170mm from the vertical edge of the gusset plate, i.e. location 2 in Figure 4.18. A conversion method was devised by Stevens to correlate the measured value to the intersection of the centrelines of the LVL members, i.e. location 1 in Figure 4.18. Of all the events taken, the maximum response gave a moment of 9.28kN-m at closing mode and 4.1×10^{-3} rad of rotation while for joint opening, the maximum moment was 5.94kN-m and maximum rotation was 2.3×10^{-3} rad. These values were smaller than the laboratory test inputs, since they were loads at serviceability levels. Even so, the moment-rotation relationships for the Wingfield building joints were non-linear at this level of loading. Such behaviour also occurred in the $\frac{1}{2}$ -scale test specimens (see Chapter 5).

From the non-linear curves of moment versus rotation, the stiffness of the real joint was calculated by dividing the change in moment by the change in rotation. Stevens(52) estimated the initial tangent stiffness for a chosen population of 23 events, and it ranged from 1000 to 10200kN-m/rad (average=3930kN-m/rad). On the other hand, the secant stiffness was 779kN-m/rad to 6324kN-m/rad and the average was 3033kN-m/rad. Interestingly, the results for the closing mode differed very little from those for the opening mode. The average secant stiffness for all recorded events was 4000kN-m/rad. Apart from rotation and strain, another measured parameter was side sway of the frame which was obtained by mounting an accelerometer horizontally on the joint and then **integrating** the measurements. From 67 events, the maximum displacement was 10.7mm.

3.3 WIND LOADS ON THE WINGFIELD BUILDING JOINT

Wind load was investigated in this research to establish whether it might cause fatigue strength problems in the joint. Wind loading is considered prominent in these lightweight timber structures due to their large surface area. It applies loads on the joint almost continuously at different intensities over the life of the structure by putting pressure on the walls which is transferred to the ground via the portal frame and the joint. This dynamic lateral load is generally small in magnitude but the number and duration of load applications can be significant. Such loading could soften the joint and cause local deformations of the wood and nail slippage. Hence, the overall joint strength and stiffness may be gradually reduced over time.

Images 3D™, a structural computer analysis program, was used to calculate the moment and shear in the portal frame due to different sets of external loading on the structure. The loadings are taken from the loading code AS 1170(2) and are tabulated below:

<u>Live Load</u>	§4.8.3:	For Industrial and commercial buildings, portal frames 4.5kN load applies to whichever point will produce the most adverse effect
	§4.8.1.1:	0.25kPa i.e. 1.25kN/m (for 5m centres)
<u>Dead Load</u>	♦	Timber has self weight of $\cong 1000\text{kg/m}^3$,
	∴	D.L.(timber rafter at joint end) = $0.8\text{m} \times 0.06\text{m} \times 1000\text{kg/m}^3 \times 9.81\text{m/s}^2$ = 471N/m $\cong 0.5\text{kN/m}$ (including purlin)
	∴	D.L.(timber rafter at ridge end) = $0.4\text{m} \times 0.06\text{m} \times 1000\text{kg/m}^3 \times 9.81\text{m/s}^2$ = 235N/m $\cong 0.25\text{kN/m}$ (including purlin)
	♦	Roof has self weight of $\cong 12.2\text{kg/m}^2$, for a width of 5m;
	∴	D.L.(roof) = $5\text{m} \times 12.2\text{kg/m}^2 \times 9.81\text{m/s}^2 \cong 0.6\text{kN/m}$
<u>Wind Load</u>	§3.4.3:	External pressure $P_e = K_a \times C_{p,e}$ for Westerly wind (see Figure 3.2(B)) and q_z is assumed 1. (Stevens (52) found a value of 1.239kPa for q_z if V_u is used)

The two main loading cases are shown in Figure 3.2. These loadings represented the loads on one portal frame are working (unfactored) loads as given by AS 1170.2. The LVL rafter and column properties used for analysis were those specified in section 2.2.1. The computer program calculated the moment and shear at all the nodal points. The point of contraflexure (point of zero moment) was located from the dead loading case and was found to be 6.1m from the eaves along the rafter section. Apart from analysing the original timber portal frame, the dimensions of the frame were altered to investigate the sensitivity of the moment-shear ratio of the joint to changes in frame dimensions. The column height was shortened and lengthened by 1m and the span changed by 5m. The results are tabulated in Table 3.1.

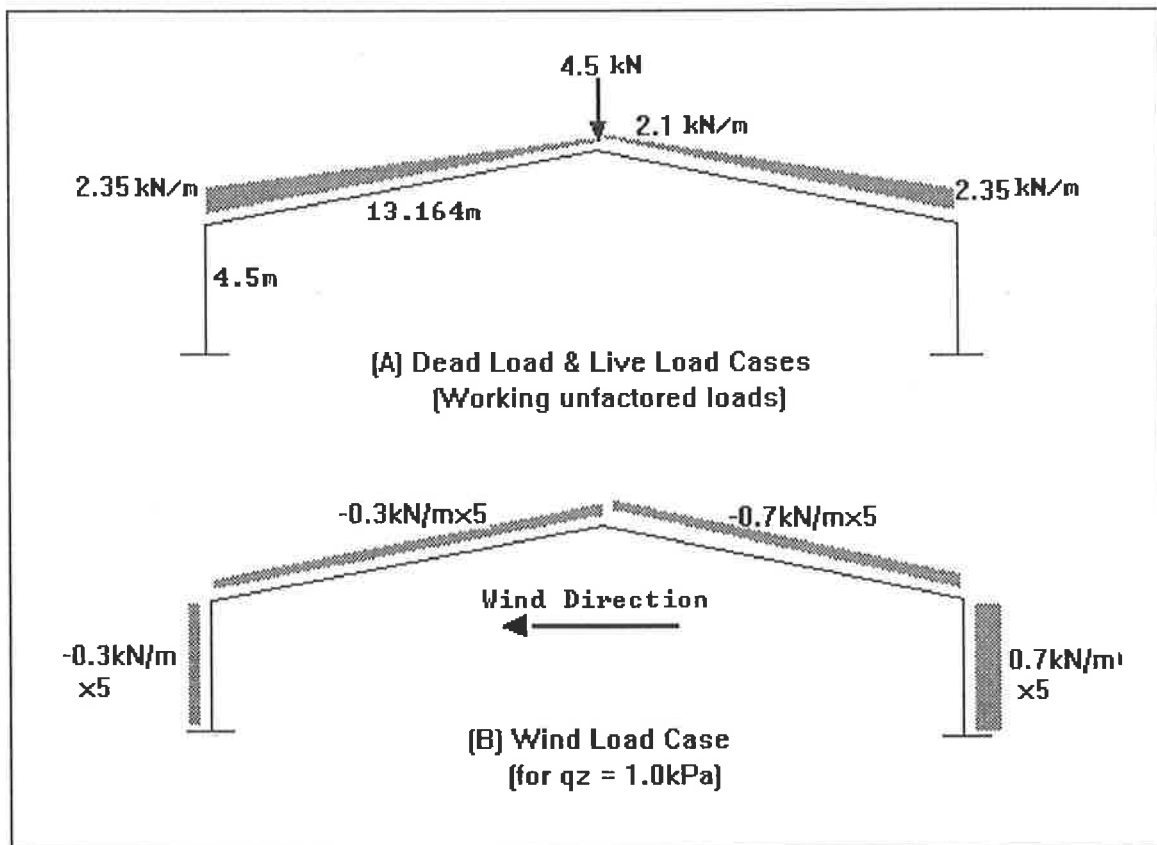


Figure 3.2 Different load cases on the timber portal frame

From Table 3.1, the moment and the shear ratio with respect to the dimensions of the portal frame were derived by altering the column height and the span length. In the table, the total load case refers to the summation of all three load cases, and the moment/shear values were calculated by dividing the moment by the shear. There are significant changes in these ratios reflecting a sensitive behaviour between moment/shear ratio and the portal frame dimensions for both joints on the western side and the eastern side. Suffice it to say that significant alterations to the portal frame dimension can change the moment to shear ratio remarkably. Since different portal frame configurations resulted in different moment to shear ratios at the joint, results from a typical portal frame structure, as in this study, might only be applied to similar joints with approximately the same column and rafter lengths.

For the Wingfield building location, ultimate wind speed (V_u) was used to find the ultimate wind load which corresponded to 50m/s. The probability that V_u will occur at least once in a year is approximately 1 in 975, that is, it has a return period of 975 years. On the other hand, the serviceability state wind speed V_s is 38m/s and has a return period of 20 years. The corresponding external wind pressure (q_z) was arbitrarily chosen as 1kPa/m in the analysis for ease of subsequent calculations (as in Table 3.1). The external wind pressure q_z is related to wind speed V_z at height z by $q_z = 0.6V_z^2 \times 10^{-3}$ (2). Hence, q_z was multiplied by the calculated results (where $q_z=1$) before the corrected results corresponding to a particular wind speed were obtained (see section 3.4.2).

	WIND LOAD CASE	DEAD LOAD CASE	LIVE LOAD CASE	TOTAL LOAD CASE	MOMENT/ SHEAR (kN-m/kN)
<i>Joint on western side</i>	shear/moment	shear/moment	shear/moment	shear/moment	
Original case	23.50/90.60	-8.530/-38.37	-13.14/-59.13	1.83/-6.9	-3.770
-1m to Column	29.35/93.50	-7.110/-39.09	-10.95/-60.23	11.29/-5.82	-0.516
+1m to Column	19.20/83.00	-10.530/-36.86	-16.23/-56.81	-7.56/-10.67	1.411
-5m to span	15.15/53.10	-12.370/-55.64	-18.60/-83.71	-15.82/-86.25	5.452
+5m to span	33.70/136.45	-5.390/-24.26	-8.610/-38.74	19.70/73.45	3.728
<i>Joint on eastern side</i>					
Original case	-18.25/-117.6	-8.530/38.37	-13.14/59.13	-39.92/-20.10	0.504
-1m to Column	-24.1/-105.75	-7.110/39.09	-10.95/60.23	-42.16/-6.43	0.153
+1m to Column	-13.95/-129.75	-10.530/36.86	-16.23/56.81	-40.71/-36.08	0.886
-5m to span	-9.950/-80.10	-12.370/55.64	-18.60/83.71	-40.92/59.25	-1.448
+5m to span	-28.45/-160.65	-5.390/24.26	-8.610/38.74	-42.45/-97.65	2.300

Table 3.1 Theoretical analysis by Images 3D of Moment shear ratio

3.4 SPECIMEN DESIGN

3.4.1 Joint form and scale effects

Three different joint configurations (7) were discussed earlier in section 2.2. In each case, the rafter rested on top of the column member with plywood gusset plates positioned on each side to act as a moment / load transferring mechanism. In addition to the form of the gusset, nail pattern also plays an important role in the performance of the joint (see section 2.4.1). A nail pattern that concentrates joint forces

into a few laminates will cause larger stress concentrations which will contribute to a lower joint capacity. In order to make sensible comparisons with the actual moment-resisting joint in the timber portal frame structure at Wingfield (Figure 3.3), the joint pattern (Figure 3.4) and joint types used in this research were the same as those in the Wingfield building, namely the Batchelar type.

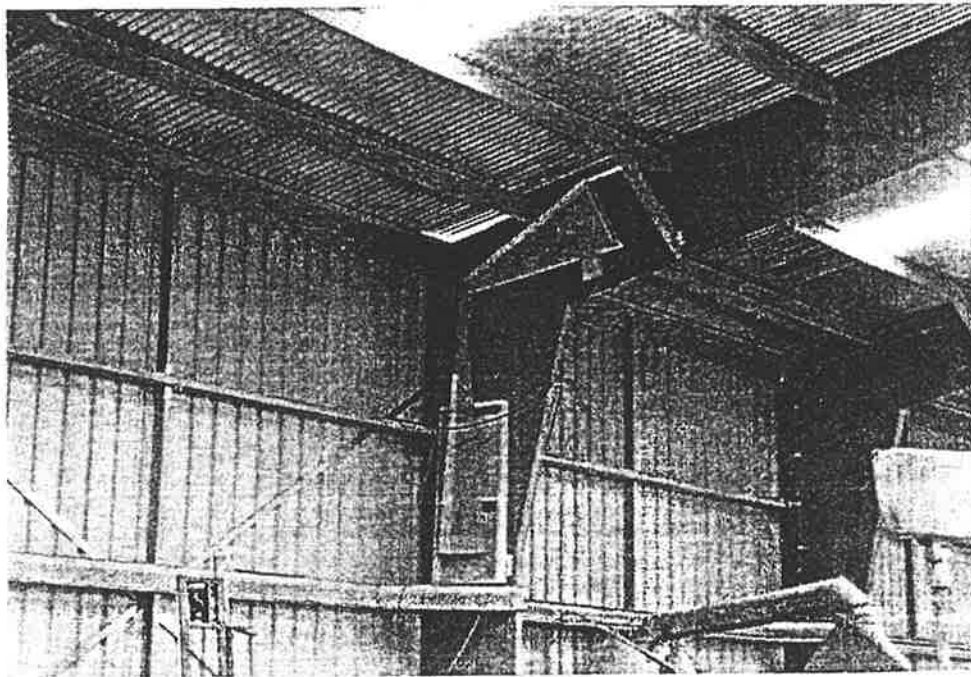


Figure 3.3 The actual joint in the timber portal frame & the test specimen

It should be noted that the timber leg representing the rafter in the test specimen (Figure 3.4) was untapered with a length corresponding to the distance to the point of contraflexure in the Wingfield building (see Figure 3.2, section 3.3). Tapering was used in the actual rafter in the timber portal frame (Figure 3.3). The width of this LVL member was reduced from the joint end to the apex in order to minimise the cost of material and reduce the self weight of the structure since maximum moment is usually found near the eaves. However, for laboratory testing, self weight was not important and pure joint failure was desirable. Consequently, a constant width LVL of 400mm was used for the test specimens.

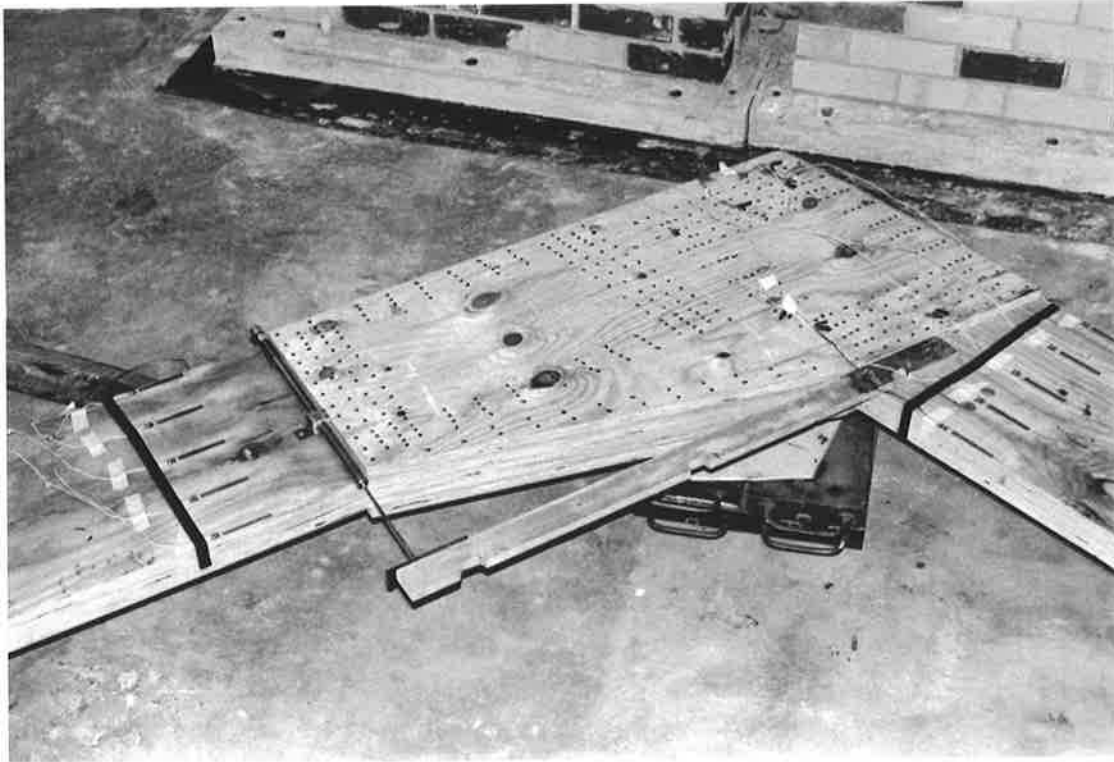


Figure 3.4 Layout of the whole specimen

Details of the test joint are shown in Figure 3.4. This type of timber joint is common, with the nailed plywood gusseted joint located at the intersection of the LVL column and rafter members. Each test specimen was considered to be a section of a portal frame between a pinned base and the point of contraflexure of the rafter. Those two parts of the portal frame were assumed to have zero moment which was represented by the pinned connections between the test specimen ends and the metal anchorages (see section 4.3.2). The location of the point of contraflexure along the rafter was found by applying the dead load (see section 3.3). Therefore, with unequal lengths of LVL legs, a better correlation to shear and moment to the actual frame was achieved. The moment shear ratio is discussed later in this section.

The next step in designing the specimen was to consider the resources available to test a joint in the laboratory. There were two logical options for specimen size:

- a) *Full-scale joint*: The exact version of the actual timber joint could be tested. Without making many theoretical calculations and assumptions, a "true joint" can be tested directly. In this case, a full scale model would give good correlation to the field testing and have a close resemblance to the actual joint in the building.
- b) *Reduced scale joint*: Due to space limitations in the laboratory, a scale model version of the joint was preferred. Even if the size of the joint was maintained but with shortened LVL members, this would require loads beyond the capacity of the testing load jack (250kN and 125mm displacement). On the other hand, a scale model made handling and fabrication much easier and had a capacity which was compatible with the testing equipment. Furthermore, a reduced scale joint had the advantage of ease of construction, a reduction in cost for materials and transportation.

Hence, $\frac{1}{2}$ -scale specimens were selected as being the most feasible way to accomplish the experimental work. The main aim was to investigate the fatigue behaviour of the joint as a whole and so it was important that the individual nail stresses were **consistent** with the nail stresses in the actual joint. To do this, the following variables were considered:

- a) Number of nails;
- b) Size of nails;
- c) Penetration of the nails (head restraint & t/d effects);
- d) Thickness of plywood gusset; and
- e) Size of LVL members.

For various reasons, each parameter could not simply be halved in the test specimens. The size of the nails was fixed by the use of nail gun so that 2.87x50mm nails were used, the same as in the portal frame at Wingfield. The degree of nail penetration would affect the head restraint, but full penetration was possible with the use of a nail gun. Furthermore, it was advisable to ensure that the size of nails and grain were consistent to prevent wood crushing.

The LVL and plywood thicknesses were chosen to be the same as in the real timber portal frame joint, as they are available only in standard thickness (63mm and 19mm respectively were used in the Wingfield building). However, all other dimensions were halved.

The nail spacing and nail pitch were kept the same. In this case, the number of the nail rows was unaltered so that the number of nails were approximately halved in each row. Therefore, the load per nail and thus the shear stress per nail would be approximately equal to the full-scale values if the applied load was halved.

For P = load, N = number of nails, V = shear of the actual joint, and P_s = load, N_s = number of nails and V_s = shear of the test specimen.

$$P_s/N_s = (P/2)/(N/2) = P/N \text{ \&}$$

$$V_s/N_s = (V/2)/(N/2) = V/N$$

Therefore, the test specimen nails carried the same load and shear as the nails in the full-scale joint.

Since the length of the limbs was halved for practical reasons and the load was halved, the moment on the joint was one quarter of the full-scale joint. The limbs had the same width but only half the depth so the section modulus was also one quarter.

$$M_s = (P/2) \times (L/2) = P \times L / 4 = M/4$$

$$Z_s = B(D/2)^2/6 = 0.25 \times (BD^2/6) = Z/4$$

where M = moment, L = moment arm, Z = section modulus, B & D = dimensions of the actual joint; M_s = moment, Z_s = section modulus of the test specimen.

This means that the bending stress σ_b was unchanged ($\sigma_b = M/Z = M_s/Z_s$) from the full-scale values since both moment and section modulus for the scale-model was a quarter of the full-scale value. The shear force was halved since the load was halved and the cross-sectional area was also halved. Hence, the average shear stress was similar to the full-scale value.

$$\tau_s = P_s/A_s = (P/2)/(A/2) = P/A = \tau$$

where τ = average shear stress, A = cross-sectional area of the actual joint; and τ_s = average shear stress, A_s = cross-sectional area of the specimen.

However, the moment / shear ratio in the test specimen was reduced to half the value with the actual joint since:

$$M_s/V_s = (M/4)/(V/2) = 0.5 \times (M/V)$$

In section 3.3, a sensitivity analysis on the moment-shear ratio was carried out in order to study the influence of portal frame configuration. Nevertheless, the change in this ratio between the actual joint and the test specimen was due to its specific design and the halved applied load. Therefore, it was expected that shear might have more effect on the test specimen than might be expected to occur in a similar full-scale specimen. However, this was felt to be acceptable since the nails and wood surrounding the nails in the specimens would experience the same stress as in the actual joint.

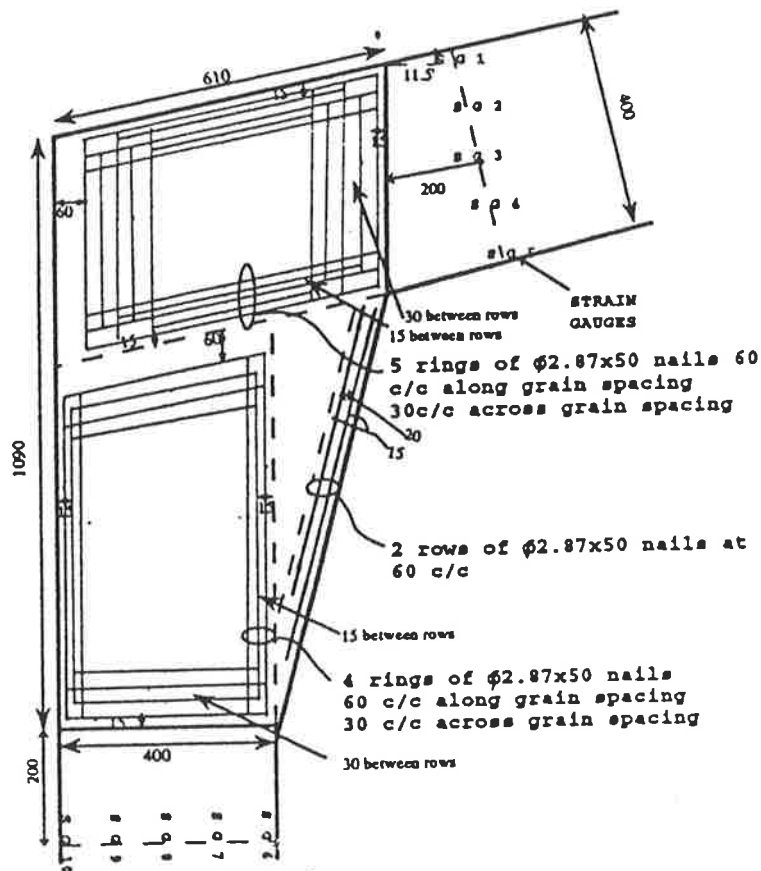


Figure 3.5 Details of the specimen design

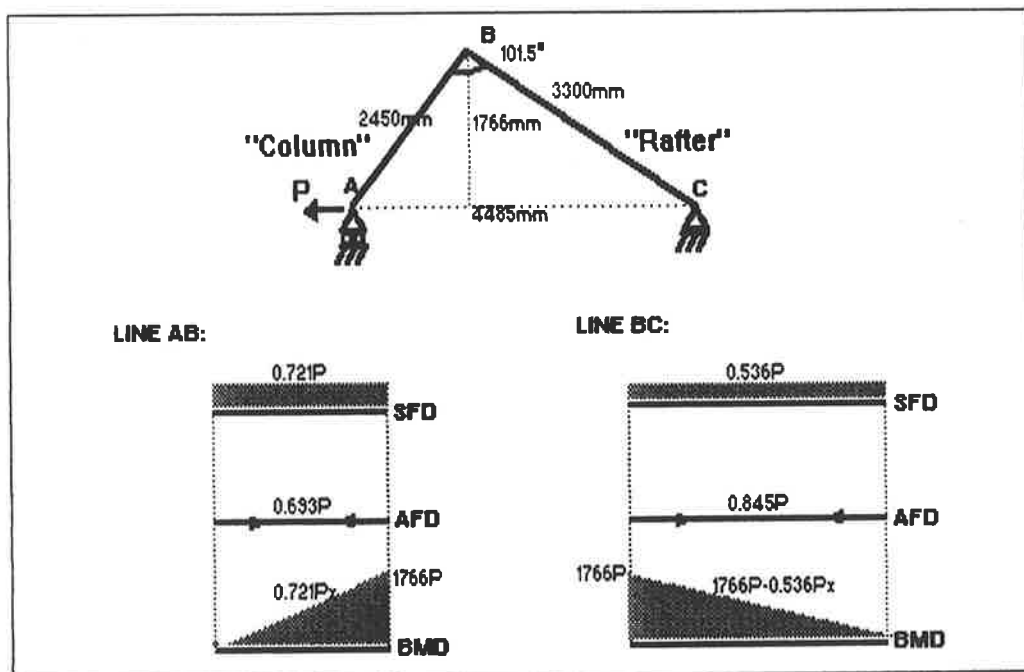
The nail pattern geometry for the test specimens is shown in Figure 3.5. Sufficient nail edge distances were allowed to prevent wood fibre crushing.

By adopting the $\frac{1}{2}$ -scale test specimen design, there were some unavoidable deviations of the $\frac{1}{2}$ -scale joint from the actual joint. Apart from the scaling difference of the key dimensions (i.e. the length and depth of the timber members), the number of nails was halved accordingly. The physical modifications of the test specimen brought about a reduction in both moment and section modulus to a quarter of the original values in the actual joint. Similarly, the moment to shear ratio was halved. Therefore, allowance should be given when interpreting the experimental results. On the other hand, nail size, timber thickness, nail spacing, nail pitch and number of nail rows

were kept the same which ensured nail stresses (bending and shear) were unaltered. This was important since one of the prime targets was to observe the interaction between the nails and timber in the joint.

3.4.2 Loading on specimen

The load P was applied at the column base of the test specimen which created a moment in the joint. The actions in the $\frac{1}{2}$ -scale model are shown in Figure 3.6.



where P = load, M = Moment & x = distance along the LVL member

Figure 3.6 Actions along the LVL members

It was clear that with uneven lengths of LVL legs in the joint specimen, there would be lower shear force and higher axial force along the longer limbs which represented the rafter section of the joint. Triangular bending moment distribution would

be experienced by both members, in contrast to the constant force of shear and axial, and the maximum moment would occur at the joint. If the stiffening effect of the gusset plate at this location is considered, the critical bending stresses were located off the gusset in the LVL sections. The rafter section was more critical because the moment drop along the longer limb was more gentle and the extension of gusset plate to the rafter section was shorter.

From Figure 3.4, which shows the layout of the 1/2-scale test specimens, the working load of the 1/2-scale joint was obtained using AS1720 (3) based on the basic nail load capacity as follows:

$$Q' \cong 239.3\text{N}$$

§ 4.2.1.2: $Q = k_1 k_{13} k_{14} k_{16} k_{17} Q'$

$$= 2 \times 1 \times 1 \times 1.1 \times 1.18 \times 239.3 = 621.2\text{N}$$

$$M_n = Q r_{\max} \sum_{i=1}^n (r_i / r_{\max})^{1.5}$$

$$= 621.2 \times 355 \times (355)^{-1.5} \times \sum (r_i)^{1.5}$$

$$= 19.4\text{kNm}$$

for two sides: $M_n = 38.8\text{kNm}$

Working load = $P = 38.8 / 1.766 = 22\text{kN}$

where Q' = basic nail load capacity
 Q = permissible nail load capacity
 $k_1 k_{13} k_{14} k_{16} k_{17}$ = modification factors
 M_n = permissible joint moment
 r = distance from joint centroid to nail

This method was based primarily on static strength and this result gives the static loading to the test specimens. A load of 25kN (instead of 22kN) was chosen to

be the static load for the tests. This load represented the scaled dead plus live loads of the actual joint as described in section 3.3. The working load calculated from the design code was taken as a continuous static load on the ½-scale model during the fatigue test where an additional cyclic load was superimposed onto the static load level to create a dynamic loading pattern which opened the joint by pulling the ends of the LVL limbs in opposite directions. The dynamic component of loading simulated the wind loading measured in the Wingfield joint using a sinusoidal form of loading. From computer analyses (Images 3D™), the induced moment at the joint by a wind load of 1kPa external pressure per metre length of the building was 18.12kN-m (see table 3.1). Since $M_{\text{specimen}} = (P/2) \times (L/2) = P \times L/4 = M_{\text{actual joint}}/4$ (see previous section), the moment calculated for the actual joint was divided by four to find an equivalent moment for the test specimen. A service wind speed V_s of 38m/s was chosen for the wind load level on the specimen and its return period was 20 years calculated from §3.2.2 of AS1170 (2) ($V = 29.2 + 7 \log_e R$; where V is the wind speed and R is the return period).

From AS1170.2 §3.6.3 - Interpolated method for Westerly:

Distance for developing inner layer for 6.21m roof height = x_i

$$x_i = z_{O,r}(h/0.3z_{O,r})^{1.5} = 0.2(6.21/0.3 \times 0.2)^{1.5} = 210\text{m}$$

(Assuming $x=900\text{m}$; $M_{(z,cat3)}$ for North=0.955 and

$M_{(z,cat2)}$ for South=0.79)

$$\text{Terrain category multiplier} = M_x = M_o + (x-x_i)(M_{(z,cat)} - M_o)/2500$$

...Eq.3.2.6(3)

$$M_x = 0.955 + (900 - 210)(0.79 - 0.955)/2500 = 0.909$$

$$\therefore V_z = V \times M_x = 38 \times 0.909 = 34.5\text{m/s}$$

(Service wind speed V_s was used as V , c.f. section 3.3 where V_u was used)

§3.3 Dynamic wind pressure = $q_z = 0.6V_z^2 \times 10^{-3} = 0.6 \times (34.5)^2 \times 10^{-3}$

$$\therefore q_z = 0.714\text{kPa}$$

Since the induced moment at the joint was 18.12kN-m for every 1m of building by 1kPa of wind pressure and every portal frame supports a 5m length of the

building, the applied dynamic moment on the actual joint has a magnitude of $18,12\text{kN-m/m/kPa} \times 5\text{m} \times 0.714\text{kPa} = 64.7\text{kN-m}$. The equivalent dynamic moment on the specimen was $64.7 \div 4 = 16.2\text{kN-m}$ and the applied load was $16.2\text{kN-m} \div 1.766\text{m} \cong 9\text{kN}$ since the moment arm was 1.766m . Hence to simulate the dead plus wind load case, a cyclic load with a magnitude of $\pm 9\text{kN}$ was superimposed on the static load of 25kN .

3.5 JOINT STRENGTH

The theoretical strength of the specimen was the key consideration when designing the experimental set up. It also formed a basis for predictions of joint performance. Thus, in this section, the basic mechanics and various methods for determining joint strength are discussed. To ensure that the test specimens could be loaded to failure, the possible failure modes were considered: failure of the nail group, LVL timber fracture, or plywood gusset failure.

3.5.1 Nail group strength

The nail group strength was estimated by the thin walled tube analogy and the shared rivet group analogy (55). (see section 2.4.3) The thin walled tube analogy method would generally give the upper bound design moment capacity as it assumed all nails would bear the same ultimate load. Since both upper and lower nail groups were expected to carry the same moment, the design capacity of each group was the same despite the difference in shape due to the geometric limitations of the gusset. In this theoretical investigation of strength capacity of the nail group, only the upper nail group, which consisted of five rings, was considered.

Appendix D gives the detailed calculations of the nail yield load, working load of the joint and the upper nail group moment capacity of both the actual joint and test specimen by two different methods. The ultimate load of a single 2.87x50mm nail was 798.4N by the yield theory as in mode 1.3 (6). The working moment of the test specimen was 38.8kN-m by AS1720 (3) (see section 3.4.2). Other theoretical results (ultimate load capacities) are summarised in Table 3.2.

	ACTUAL JOINT	SPECIMEN
AS 1720 (working moment capacity)	67.2kN-m (52)	38.8kN-m
THIN WALLED TUBE ANALOGY	370kN-m	65kN-m
SHARED RIVET GROUP ANALOGY	328kN-m	58.1kN-m

Table 3.2 Moment capacity of the actual joint and specimen

It was interesting to note that the thin walled tube analogy always gave a higher moment capacity estimation (by about 12%) compared to the shared rivet group analogy. This was due to the assumption of equal load bearing of each nail. There was a ratio of 5.7 between the nail group strength for the full-scale and ½-scale joint. The difference was due to slight differences in the nailing patterns, since all materials and the nail spacings were identical. The spacing used in test joint was designed to follow the actual joint, in order to satisfy the requirements of the design code and the limitations of the size of the plywood gusset plate. The only difference was the dimensions of the timber members. From section 3.4, the moment capacity of the actual joint was expected to be four times that of the test specimen due to the decrease of load and moment arm by a half each. However, the nail pattern dimensions were not actually halved (see Appendix D).

Thus the calculated moment capacity for the test specimen was 1/5.7 instead of 1/4 of the full-scale joint when moment capacity was determined by the nail capacity method.

This study of the specimen assumes that all the loadings would be resisted by portal frames with wind load distributed evenly upon each of them and that the joints would provide the stability of the frames. However, load capacity of this isolated joint specimen were expected to give a lower bound to the actual strength of the building since the effects of the bracing, the end wall and the roof were ignored.

3.5.2 LVL member strength

Two possible failure modes, apart from nail slip, were considered. These were bending tension fracture of the LVL members and plywood gusset plate failure. In case of LVL failure, the location was most likely to be at the most stressed point, ie, where the applied loads induced the highest bending stress. The likely site was along the rafter section next to the gusset plate (section 3.5). The likely point of failure in the plywood would be along the line perpendicular to the column centreline between the two nail groups and passing through RVDT2 in Figure 4.19. This was the shortest distance across the plywood gusset (7).

LVL, as a material, has been discussed in section 2.2.1 (see Table 2.1). By AS1720 (3), the working moment capacity of the rafter section was calculated as follows:

$$M = k_1 k_{11} F_b Z = 1 \times 0.952 \times 16 \times (63 \times 400^2 \div 6)$$

$$= 25.6 \text{ kN-m}$$

where F_b is the allowable bending stress of LVL

3.5.3 Plywood gusset strength

Plywood gusset plates were cut from 2400mm by 1200mm 19-32-7 (F17) plywood sheet. Plywood has a higher embedment strength than solid wood and k_{16} was 1.1(3). It has Young's Modulus of 14,000MPa, allowable bending stress of 17MPa and effective thickness of 11mm. The critical section has a width of about 580mm. Hence, the working moment capacity of the plywood was calculated as:

$$\begin{aligned} M &= k_1 k_{11} F_b' Z = 1 \times 0.9008 \times 17 \times (2 \times 19 \times 580^2 \div 6) \\ &= 32.62 \text{ kN-m} \end{aligned}$$

3.5.4 Summary

Based on the calculations in sections 3.5.1 to 3.5.3, the critical allowable joint capacity was estimated to be 25.6kN-m. The corresponding failure mode was expected to be LVL failure. The working moment of LVL and Plywood gusset was 66% and 84% that of nail group's. From this simple theoretical calculation, LVL was expected to be the weakest link of the joint system and its strength would probably give the ultimate static strength of the whole joint.

In other timber moment resisting joints studies, particularly those done in New Zealand, material failure was very common. This type of failure was found either across the LVL limb near the gusset plate or in the plywood gusset itself. Timber governed the joint failure instead of the nails. As a result, a revision of the present design

code was suggested by Batchelar and Cavanagh. It seemed that the adoption of a constant value per nail was not adequate in order to get optimum solutions (49). Discussions concerning improvements in nail pattern design are presented in Chapter 6. The complete system composed of LVL, plywood gusset and nail groups should be considered simultaneously.

In this chapter, many of the theoretical predictions and relationships between the actual joint and the «-scale test joint have been mentioned. The next chapter will report on the experiments.

CHAPTER 4

EXPERIMENTAL RESEARCH

4.1 INTRODUCTION

The strength and stiffness of multi-nail joints governs the transfer of forces due to wind pressure on the walls and roof into the portal frame and to the foundation. Therefore, it is essential to understand the dynamic behaviour of this type of joint in order to conduct any theoretical evaluation of the building performance in a wind storm.

In other investigations(7)(8)(9)(10)(23), the strength reduction due to cyclic loading **has been** investigated. However, in this research, the joint was opened up by a static load and a relatively small cyclic load component added onto the static service load to simulate wind loads in the Wingfield building. This is important as the wood might suffer from significant permanent deformations due to long term cyclic loading. Moreover, the fixity of nails and the friction between members could well be reduced, resulting in loss of stiffness and ultimate strength.

In order to investigate the fatigue strength of a moment-resisting joint, an experimental testing programme was established to test seven knee joint specimens under laboratory conditions. The experimental study focused on quantifying performance characteristics for this type of connection. This was undertaken by a combination of specimen testing and analytical modelling techniques which were verified against the experimental data.

Angular displacement (joint rotation), ram displacement and the applied load were measured simultaneously throughout the tests at appropriate time intervals. From this data, joint rotation and moment relationships were derived for each specimen. Furthermore, the effect of fatigue on the residual strength and joint stiffness was studied by looking at the subsequent static response of joints subjected to varying amounts of fatigue loading. Finally, the design code prediction of the static load capacity of the joint was compared to the dynamic test results. As the present design philosophy is based predominantly on static analysis considerations, the static and dynamic results were compared to see if the present design methods need to be improved in order to account for long term deterioration of the joint due to fatigue loading.

In this chapter, the experimental programme is first discussed, including aspects of theoretical planning and design as well as the practical side of the experiments. A detailed description of the testing apparatus, specimen fabrication, and the testing program follows. The chapter concludes with discussions of the measurement and data logging methods and the manner in which the specimens were tested.

4.2 TESTING PROGRAM

Seven specimens were tested, covering a range of conditions which moment resisting joints in the real structure might be expected to experience. A constant level of static load was applied to the joint in the experiment. The working stress magnitude of the load and its relation to the forces on the real building have been discussed in section 3.4.2. A continuous sinusoidal loading was then added to represent the effects of serviceability wind load. Because the amplitude of the sinusoidal loading component was smaller than the static load component, there was no true load reversal during these fatigue tests (see Table 4.1).

SPECIMEN	NATURE OF TEST	APPLIED LOAD (kN)	APPLIED MOMENT (kN-m)	NUMBER OF CYCLES	CYCLING FREQUENCY (Hz)
1	STATIC			0	0
2	FATIGUE	25±9	44±16	250,000	0.6
3	FATIGUE	25±9	44±16	1,000,000	0.6
4	FATIGUE	25±9	44±16	500,000	0.6
5	STATIC			0	0
6	FATIGUE	25±20	44±35	6200	0.3
7	FATIGUE	25±15	44±26	180290	0.45

Table 4.1 Details of the seven specimens

In order to obtain a "feel" for the performance of the joint and the data recording system, a simple static test was performed first to establish the joint's ultimate moment capacity for comparison with the theoretical predictions. The first specimen was

loaded at 8.8kN-m (equivalent to 5kN of ram load) increments and readings were taken at each increment until the specimen failed at an ultimate joint moment of 96kN-m.

Subsequently, the second test specimen was confidently loaded with a static moment of 44kN-m (equivalent to a load of 25kN where the moment arm was 1.766m) plus a 0.6 Hz sinusoidal load of ± 16 kN-m. The test was closely monitored and the best way of measuring joint rotation was finalized during this first dynamic test. The second test specimen was subjected to (and survived) 250,000 cycles of loading at which time the load was removed. In order to find the residual strength, the specimen was then loaded statically to failure. The third specimen was tested with a million cycles of sinusoidal loading after which the loading was removed and the specimen then tested statically to failure. The fourth specimen was similarly tested and survived 500,000 cycles of loading before it was unloaded and tested statically to failure. At this stage, the data was analysed closely. The joints seemed to be very stiff and relatively insensitive to fatigue, thus the last two specimens were planned to have a much higher dynamic loading component. However, before these tests, it was decided to conduct only a static load test on the fifth specimen in order to investigate the variability of the joint strength and to give a more reliable value for the unfatigued static strength for comparison with the residual strength of the fatigue tested specimens. The sixth specimen was loaded statically to 44kN-m and ± 35 kN-m loading was superimposed. The peak of this loading was in the region of ultimate capacity of the joints. Frequent readings at regular intervals were taken within the first few thousand cycles to study the early behaviour of the joint during dynamic loading. The seventh, and last, test specimen was loaded with 44 ± 26 kN-m loading where the dynamic component was lowered by 25% from specimen 6. The dynamic load magnitude of ± 20 kN and ± 15 kN corresponded to 58m/s and 50m/s of wind speed respectively (see section 3.4.2) which exceeded the ultimate wind speed. Although the applied dynamic loads for specimens 6 & 7 were extremely high and not

expected to occur regularly in real timber structures, the results did provide insights into the joint performance during the initial few thousand cycles and its endurance of the joint to these high levels of dynamic loading. Each of the last two test specimens failed during fatigue loading and a major depreciation of the strength and stiffness of the joint was observed.

4.3 TESTING APPARATUS

4.3.1 Fabrication

The technique of constructing joint specimens profoundly affects test results (46). The assembling technique and nailing method control friction between contact surfaces which in turn control joint strength and stiffness as a whole. In the same way, the sequence of construction for a portal frame building has a significant influence on its structural behaviour. Three construction methods for common industrial portal frame structures have been reported by Yttrup(57): (1) stick-by-stick, (2) roof lift, and (3) roof lift with folding columns (Method 3 was used for the construction of the timber portal frame structure in Wingfield).

The laboratory fabrication of the moment-resisting joint test specimens was conducted in an efficient manner resulting in minimal initial stresses. This was because identical specimens in term of the stress level were desirable and significant initial stress could alter the test results. Additional factors affecting test results include wood drying after assemblage, lack of consistency in nail penetration (angle & depth), and amplitude of cyclic loading. All of these factors could introduce gaps in the contact

surface between the elements of the nailed joints which would in turn reduce friction and effective joint stiffness.

LVL with a cross section of 400 x 63mm, and 2400 x 1200 x 20mm plywood sheets were transported to the University laboratory. It was decided to manufacture and assemble the moment resisting joints in the laboratory because of the difficulties associated with moving the assembled test specimen. Once the timber had arrived, the LVL was sawn to give the required lengths and the plywood sheets were cut into gusset plate shapes. As is normally done in practice, a template for the nailing pattern was made and used to mark the gussets with the appropriate nailing locations.

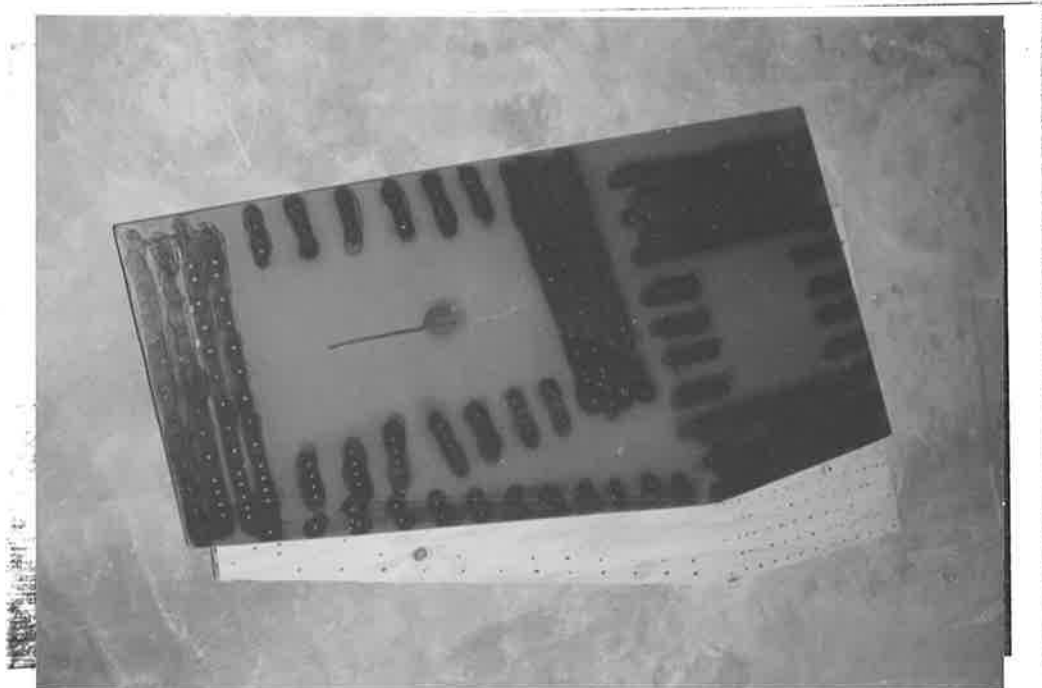


Figure 4.1 Template for marking the nail pattern onto the gusset plywood

Struts, the LVL bars that were located at the edge of the joint between the plywood plates, were cut from the remaining LVL into desirable sizes. In Batchelar & Cavanagh's experiment(8), strain measurements taken on the ends of the gusset strut showed that the strut was not effective in end bearing on the leg-rafter members, despite

particular care having been taken to ensure that contact was made at these points during assembly. In this study, the joints were tested in an opening direction, and the members acted as a tie. Strut nailing was therefore only required to stabilize the inside edge of the plywood gusset against buckling in case of compression and was not needed for the purpose of retaining the strut in position as a result of applied end loads (see Figure 4.2).



Figure 4.2 Plywood strut

In order to assemble the joint, the LVL column and rafter members were first laid out on the ground in the correct position before the plywood gusset was positioned. Special care was taken to ensure that the rafter and column touched each other without leaving any visible gap since they touched in the Wingfield joint. Next, 2.87 x 50mm nails were used to attach the gusset plate by following the marked nailing pattern. All nails were driven into the timber with a pneumatic nail gun as was done during construction of the full size structure (see Figure 4.3).

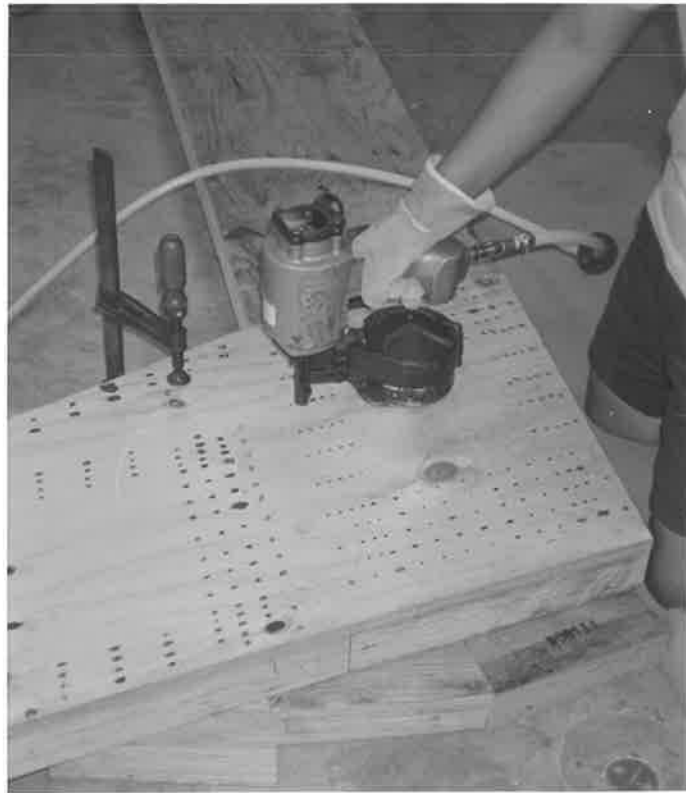


Figure 4.3 Nailing by the pneumatic nail gun

Nail head restraint and penetration angle are known to have a significant effect on the strength and stiffness of nailed joints (22)(33). The nail gun, with its consistency, provided good quality nailing, head restraint and a 90 degree angle of penetration. The other side plate and strut were put in place before nailing the second side. The completed specimen was then taken to an empty space in the laboratory for storage. All specimens were made one after the other over a one month period. The specimens were then stacked up ready for testing (see Figure 4.4).

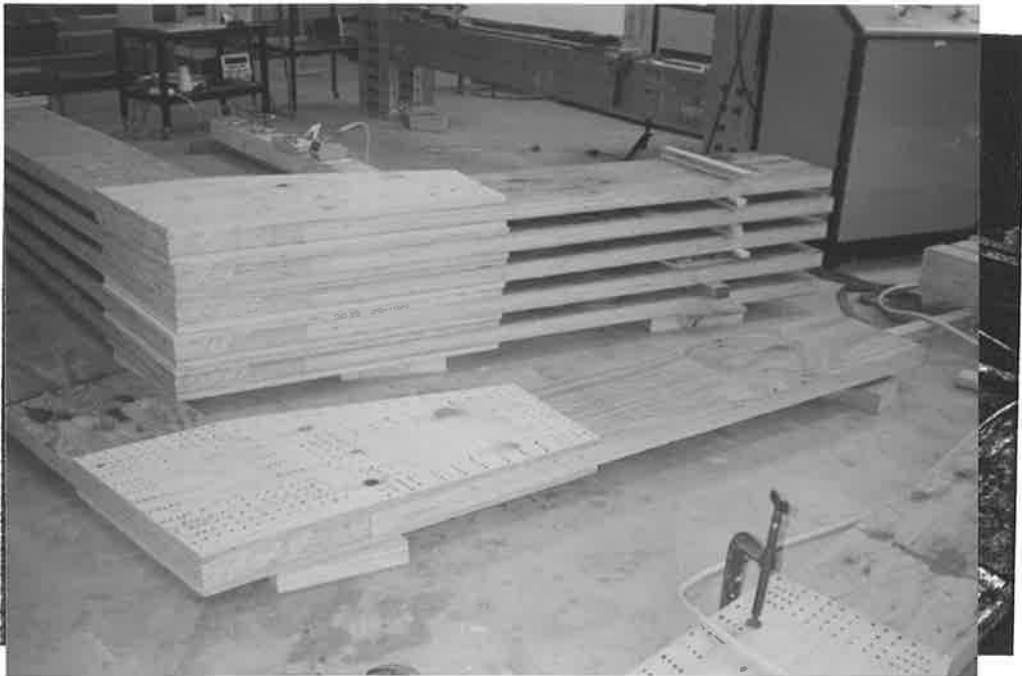


Figure 4.4 Stack of assembled specimens before testing

4.3.2 Experimental arrangement

The aim of this experiment was to study the fatigue behaviour of moment resisting joints by applying a pair of loads acting in opposite direction to each other at each end of the LVL members (see Figure 4.29). This tension testing method eliminated the possibility of buckling. Moreover, to eliminate any torsional and bending stresses out of the plane of the specimen, leveling of the joint was necessary. That is, the joint was set "perfectly" on a horizontal plane. With a density of 620kg/m^3 for LVL, the dead weight of the specimen was approximately 1000kg.



Figure 4.5 Layout of the specimen

Figure 4.5 shows the details for the specimen which allowed for the **maximum displacement** of 125mm in the ram. The connections for both ends of the LVL members were similar to the connections used in the Wingfield building. A metal plate was nailed onto both sides of the LVL while a metal angle was fixed to each side of this plate. One side of metal angle was fixed to the metal plate and the other side was bolted onto the anchorage (see Figure 4.6). The function of this system was to allow load transfer from the LVL member to the anchor in a similar way to that in the actual

building. It was not only used for tension and compression loads transfer but to provide shear resistance. In the experimental set-up, the connections served the same purposes, but they were fixed to the ram and pivot joint instead of to the ground. Careful consideration was also given when selecting the location for testing since a plan area of 5m x 2m was necessary. Existing floor studs at 1200mm intervals were used to form the anchorage for supporting the hydraulic ram and the pivot end (see Figure 4.5). The arrangement is shown below in Figure 4.6.

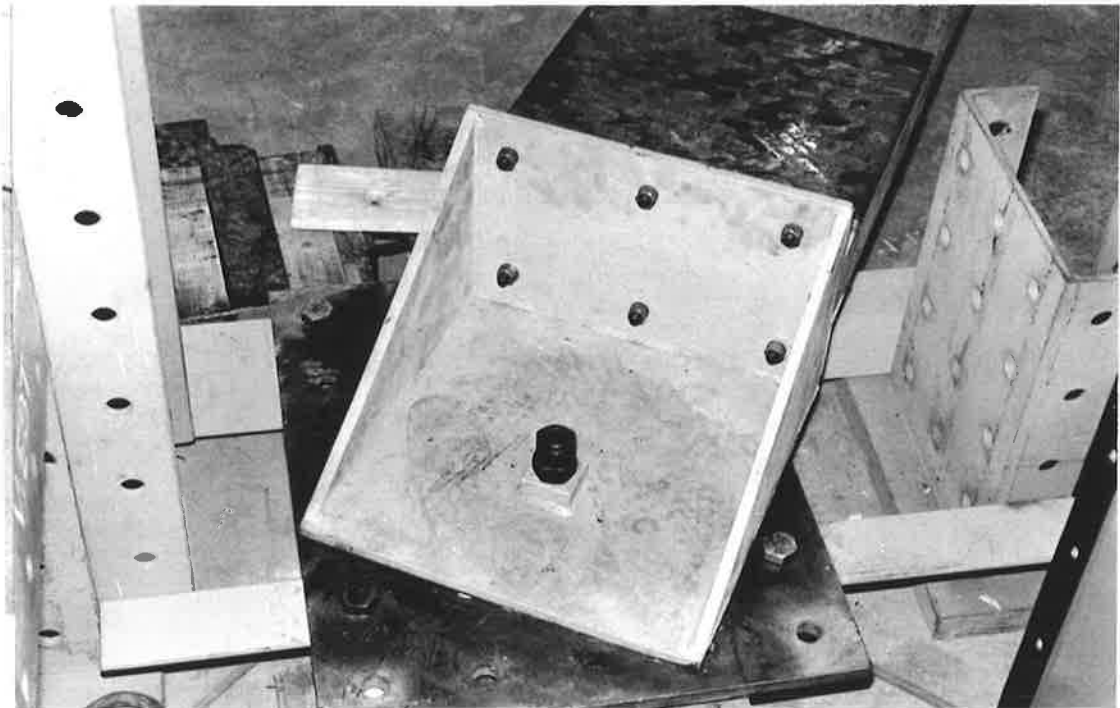


Figure 4.6 LVL base connection

The base connections (see Figure 4.6) were over-designed so they would not fail before the joint. In addition, the base plate connections were designed for easy mounting and dismounting from the LVL members. The four connections (one on each side for each end) were reused for each of the specimens. The load from the LVL members was transferred to the base by means of 12 rows by 8 columns of 2.87mmx50mm nails. Nailing was preferred to bolting because the stress distribution of

many small nails as compared to a few large bolts renders wood crushing less likely. The welding of the base plate to the angle was very reliable and the angle provided an excellent linkage to the anchorage where bolts were utilized effectively in the steel-to-steel connections.

The column base of the specimen was connected to the hydraulic jack which was secured to the laboratory strong floor by a steel truss system (see Figure 4.7).

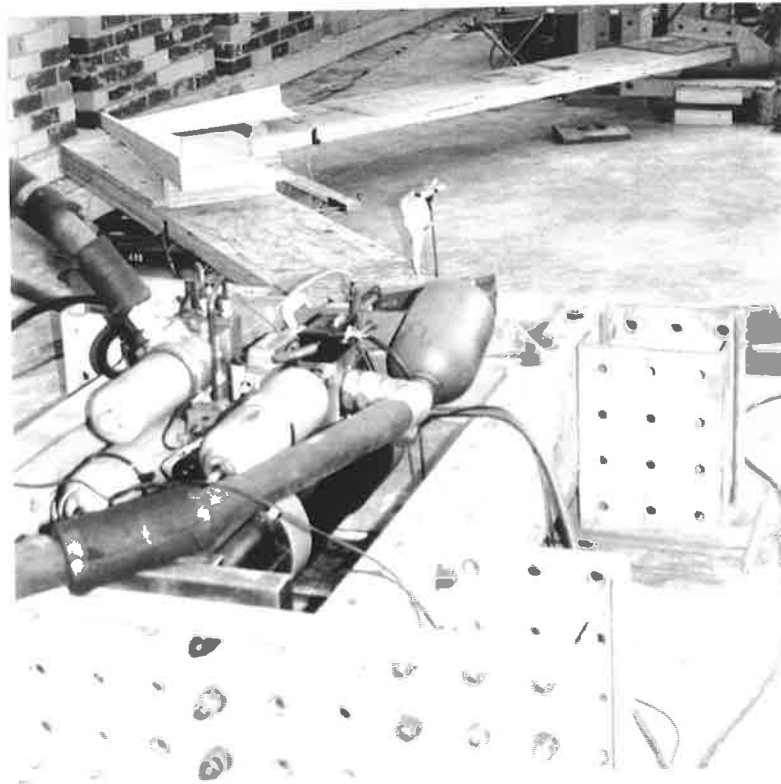


Figure 4.7 Hydraulic ram which provides both static & dynamic loads

In order to ensure a moment-free connection at the base of the column member, the column base connection was joined to a knuckle joint which in turn was bolted to the loading ram through a steel tube (see Figure 4.8). This provided unidirectional loading to the timber joint. The 60mm diameter pin in the knuckle joint ensured that no moment was applied to the end of the test specimen.

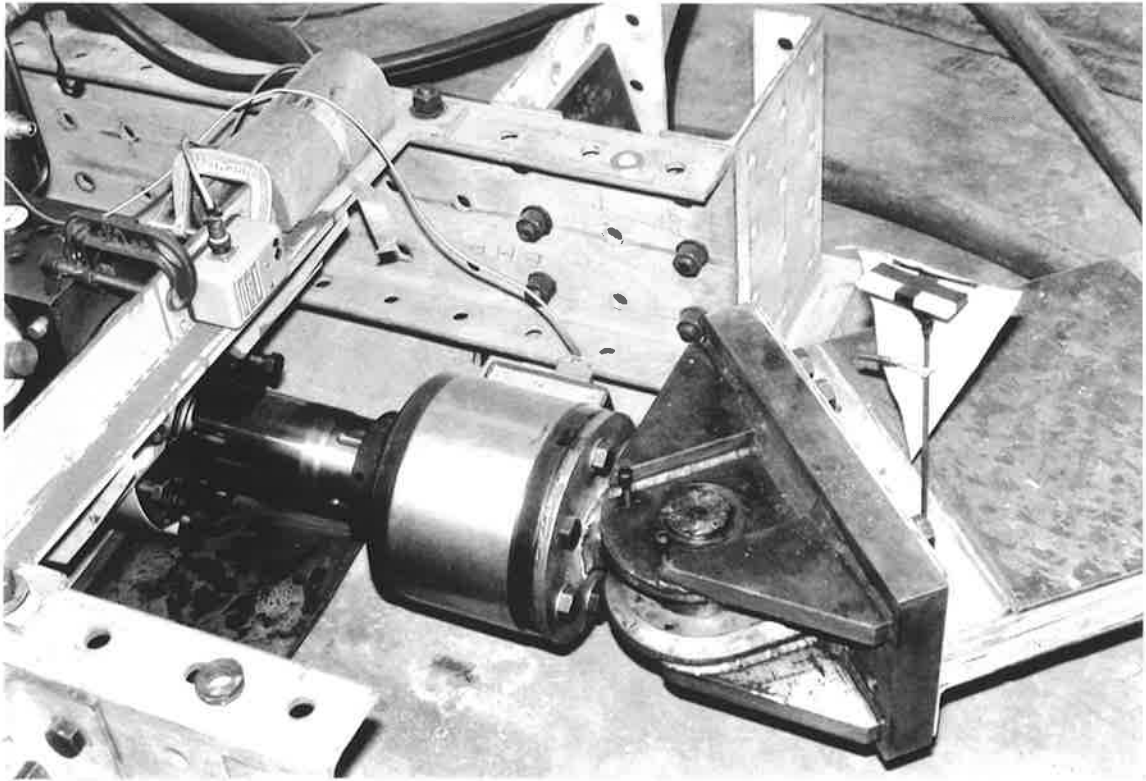


Figure 4.8 Connection at the column end

As both ends of the test specimen were supported (about 56mm off the ground from the LVL), a middle support was also required for stability and leveling of the specimen (see Figure 4.9). This also provided a stable support at the gusset joint to take up the self-weight of the specimen. To avoid restraining the specimen, the middle support required freedom of horizontal displacement in any direction while giving firm vertical support to the joint.

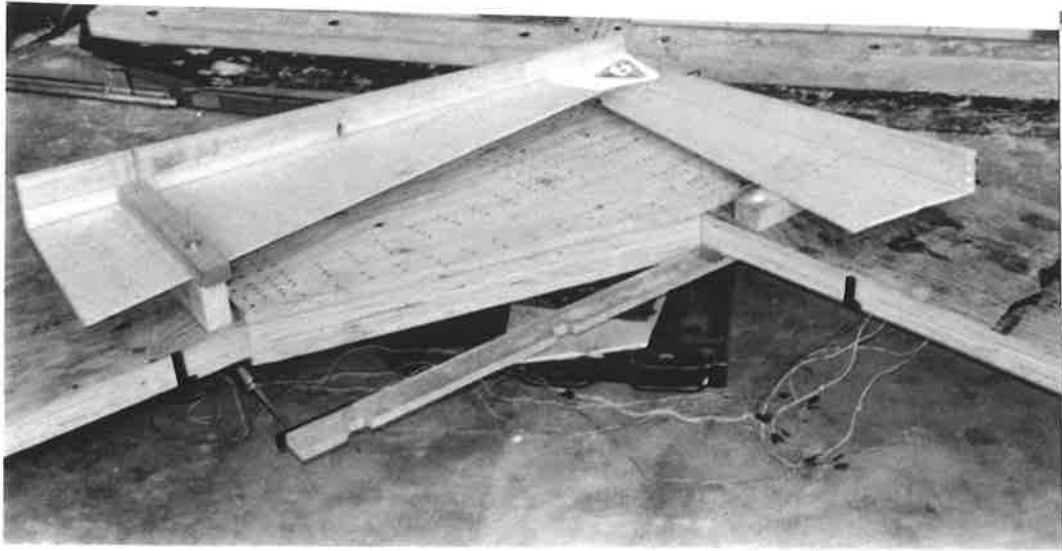


Figure 4.9 Middle support at the gusset plate

Figure 4.9 shows the middle support used for the test specimens. The system consisted of a cylindrical support that was supported on a thick steel plate which was then supported on a stack of steel packers. Grease was placed on the surface of the thick steel plate to minimize friction between the cylindrical support and this plate. This allowed the joint to slide with the support on the steel plate. Constant greasing was necessary to maintain a smooth sliding action.

It was also important to ensure that no moment was applied to the base of the rafter. Hence, the rafter base was connected to an anchorage which was allowed to rotate (see Figure 4.10).

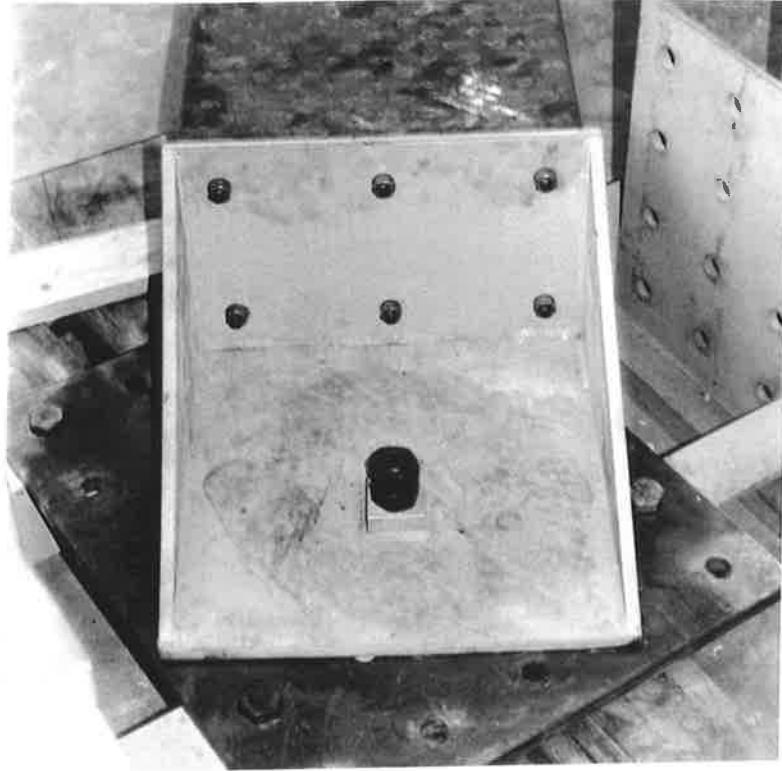


Figure 4.10 Pivot connection that connects to the rafter end & truss system

This pivot system provided the reaction forces for the rafter end and **eliminated any** moment transfer. Therefore, this zero moment support simulated the point of **contraflexure** along the rafter where only shear and axial forces would occur. The base angles of the rafter limb were bolted to the pivoting joint. This connection was designed to transfer any load from the LVL member through high tensile 24 mm bolts to a steel plate which was fixed to the ground studs by a steel truss system similar to the one used for the hydraulic jack. All the above connections were designed to withstand the ultimate load with a sufficient factor of safety to prevent fatigue failure of the steel connections.

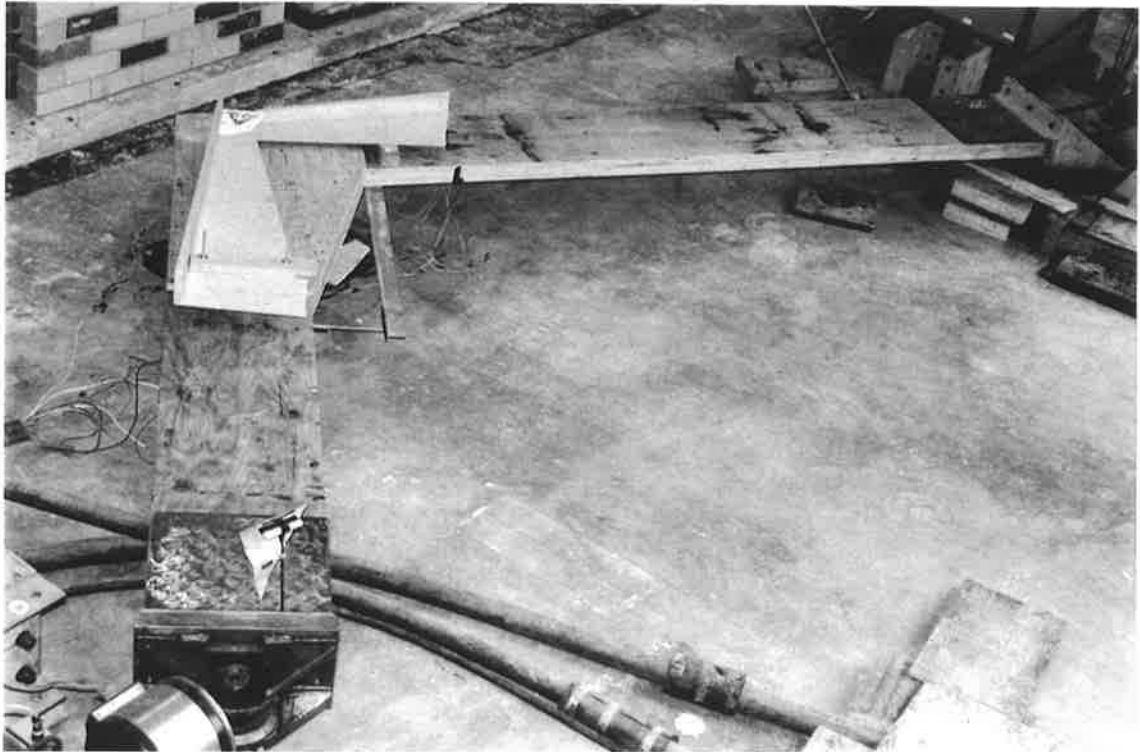


Figure 4.11 Top view of the set up of the specimen

The moment lever arm provided by this testing arrangement was estimated as being the shortest distance from the intersection of the LVL member centrelines to the line of loading action (see Figure 4.11). However, this moment arm was theoretical, since the exact centre of rotation was unknown (see section 4.3.3). Moreover, as the joint was pulled apart, the moment arm reduced in length slightly. As the **movement** of the joint was unknown, and was likely to be small compared to the **length** of the limb, the moment arm was assumed to be constant. Thus the theoretical moment experienced by the joint was always larger than or equal to the actual moment in tension mode. The change (approximately 0.1m) in moment arm (1.766m) was corresponded to an error of at most 5%.

Before engaging the joint into the test system, all the steel base plates were nailed to the bases of the LVL members. Afterwards, the angles on the rafter were bolted to the pivot joint and the specimen was leveled manually with a jack.

The column base connection was bolted to the knuckle joint connected to the hydraulic jack as the last step in the setting up. The joint was then loaded by means of a horizontally positioned Instron hydraulic ram with a controlling unit monitoring the load and the displacement of the ram (see Figure 4.12). The hydraulically powered loading device has a maximum static load capacity of 250kN. Dynamic loads of various patterns and magnitude can also be produced. As discussed earlier, dynamic cyclic loads with a sinusoidal variation of amplitude and a pre-set frequency were applied in addition to the static load.

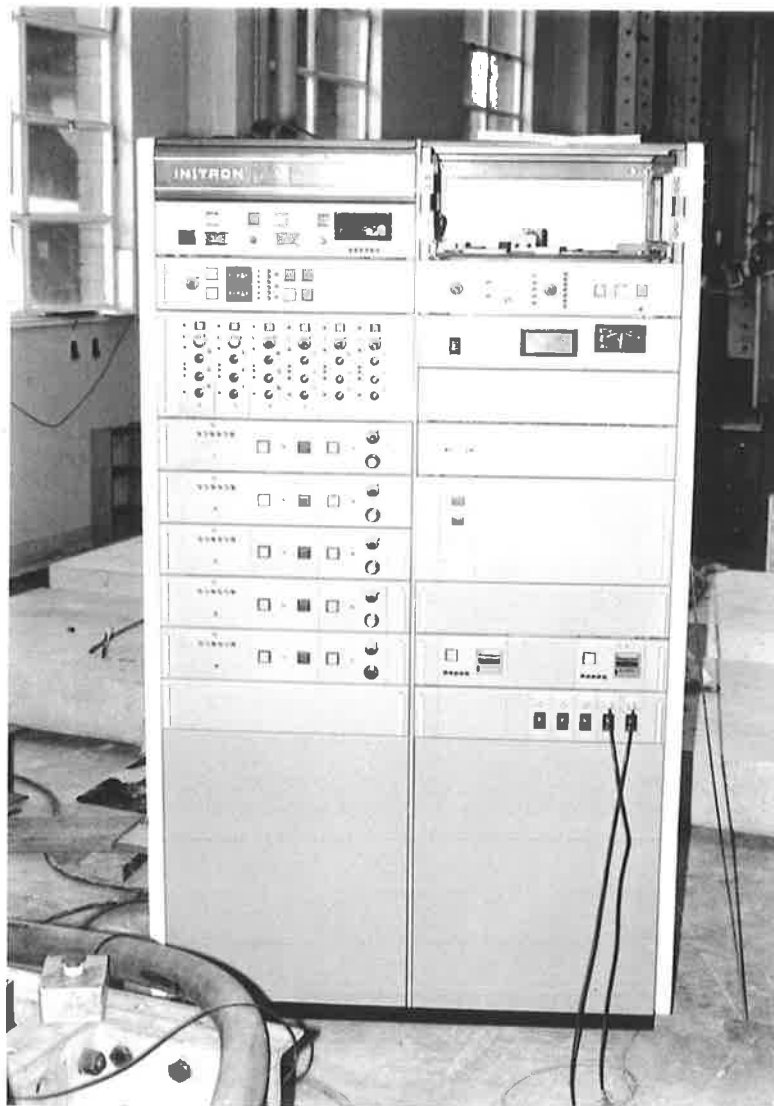


Figure 4.12 Control unit of the Instron machine

4.3.3 Instrumentation & Data acquisition

Section 2.3 gave an account of the multi-nailed joint research study by Batchelar (7) where he required a ram displacement of about 80mm for a smaller joint constructed with steel side plates to apply a load of 30kN. The load-displacement curve was linear. The ram displacement, Δ (see Figure 4.13), was a summation of displacement due to joint rotation plus bending, shear and axial deformation in the LVL members. The displacement due to joint rotation accounted for gusset plate bending while nail slips and wood deformation was formed around the nail site. Nail slips would be affected more by the dynamic loading than by those of bending, shear and axial load. Hence, by measuring the ram displacement and the joint rotation separately, the displacement due to bending, shear and axial load could be estimated. (see section 5.3.2)

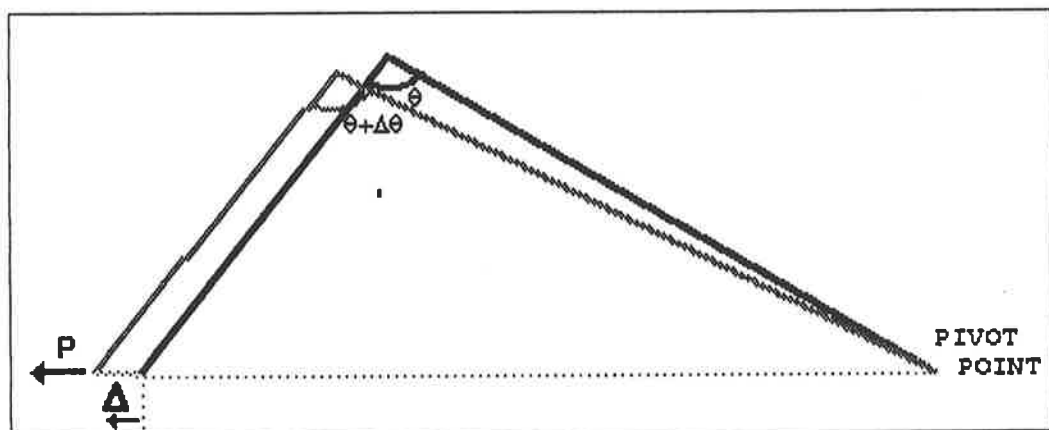


Figure 4.13 Specimen testing set up

In this experiment, ram displacement, rotation of the joint and strain across the LVL close to the gusset were measured by various instruments.

Another important parameter that would relate the joint rotation to the applied moment was the joint stiffness. Interestingly, Stevens (52) extrapolated the

results of Batchelar and Cavanagh (8) to the actual joint in the Wingfield building, taking into consideration the differences between the two joint designs. He estimated the stiffness of the joint to be between $14.7 \times 10^9 \text{ Nmm/radian}$ and $34 \times 10^9 \text{ Nmm/radian}$. He chose the value of $20 \times 10^9 \text{ Nmm/radian}$ as input for his computer analysis. The stiffness of the test specimen was expected to be more than four times smaller than this proposed value for the actual joint. This was because the applied moment in the $\frac{1}{2}$ -scale specimen was four times smaller than in the actual joint and the additional stiffening effect of bracing was not present at the laboratory testing. This stiffness value was important for load distribution in the portal frame; for a stiffer moment resisting joint inhibits rotation and more moment would be expected in the ridge at the centre of the portal frame.

It was necessary to define: performance requirements (stability, accuracy, reliability); measurement factors (duration, dynamic loading...); and environmental factors (temperature, vibration, moisture) in the experiment. Since the experiment was to be performed over a considerable period of time, stability and reliability were key factors in the choice of instrumentation. The choice was based primarily on what would give data which was free from excessive noise and drift, ease of calibration, instrument range and limitations.

Since the nature of this experiment was to investigate the long term effect of low magnitude cyclic loading superimposed on a constant load, a different approach for data collection was required than for a simple static test. In a simple static test, usually a relatively small amount of data is recorded. However, during long term dynamic testing, the amount of data and the rate of data logging is critical. Therefore, a sophisticated data acquisition system was necessary to cater for this requirement. In the following section, each type of electrical transducer is discussed with respect to its performance and limitations. The data collection system is also discussed.

a)Rotation:

One of the main aims of this experiment was to investigate the moment-rotation relationship of the gusset joint. This was achieved by measuring the relative rotation of the rafter and the column legs in the plane of the joint. The rotation between the rafter and the column was the relative rotation of those two legs at the positions just behind the gusset plate. In theory, for a known geometry, joint rotation can be deduced by simply measuring ram displacement. However, this was not possible because bending of the LVL members and rotation of the joint would occur simultaneously.

The relative rotation was induced by any relative rotation of the rafter and the column legs. This relative rotation was the result of a complex interaction between the gusset plates, the rafter and column which could be due to nail slip, plate displacement and relative movements between the two legs in the joint area.

Hence, three methods of rotation were devised and tested against each other during the experiment. Each has its own advantages but the DCDT (direct current differential transformer) method was found to be the most reliable.

LVDT method: This method was based on the simple geometry of the joint which visualized the timber joint as two simple members hinged at their junction. An imaginary triangle is formed by joining the point of intersection, to a point along the centreline of the rafter and another point along the centreline of the column as shown in Figure 4.14. Then, by measuring the X-Y displacement of those three points and hence determining the changes in the length of the sides of the imaginary triangle, it was possible to employ the cosine rule to compute the rotation of the joint. These displacement were measured by LVDT's (linear variable differential transformer).

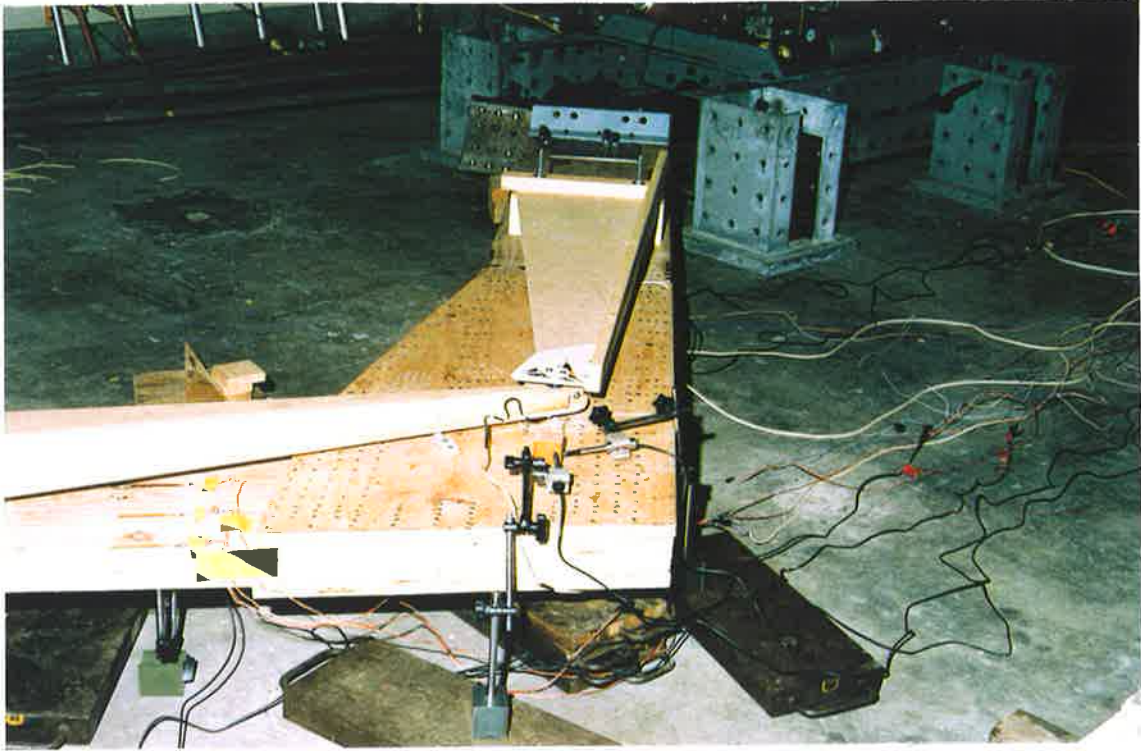


Figure 4.14 LVDT method by forming an imaginary triangle

For this method to work satisfactorily, the centre of rotation must be at the intersection of the member centrelines. Due to the complicated action between the LVL and the plywood gusset plate, there was no theoretical tool nor any indication from previous tests as to where the actual centre of rotation was located. Its position was assumed to be the meeting point of the centreline of the LVL legs. The other two points were chosen at convenient locations along the centrelines just off the gusset plates.

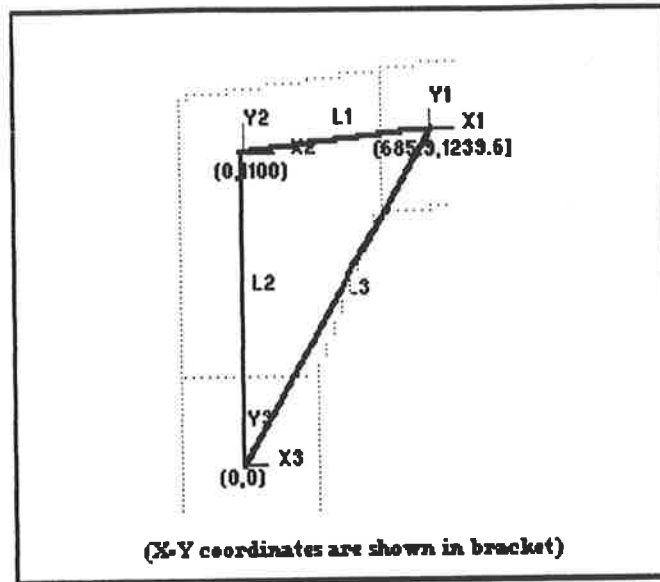


Figure 4.15 LVDT method

Joint rotations were calculated using the inputs of the X-Y displacements of the three points. From the new lengths of the sides of the imaginary triangle, the rigid displacement of the plate relative to the LVL members could be found.

From cosine rule: (referring to the Figure 4.15)

(where X1 and Y1 are X-Y coordinates of point 1 and likewise for X2, Y2, X3 and Y3)

$$L1 = [(685.9+X1-X2)^2 + (139.6+Y1-Y2)^2]^{1/2}$$

$$L2 = [(X2-X3)^2 + (Y2+1100-Y3)^2]^{1/2}$$

$$L3 = [(685.947+X1-X3)^2 + (1239.558+Y1-Y3)^2]^{1/2}$$

where L1, L2 & L3 are the lengths of the three sides of the imaginary triangle and α is the angle between L1 and L2

$$\text{angle} = \alpha = \cos^{-1} \{ [(-L3)^2 + (L1)^2 + (L2)^2] / (2 L1 L2) \}$$

$$\text{Rotation} = \theta = \alpha - 101.5^\circ$$

The actual measurement was made by means of attaching three 80x80x80mm timber cubes centred over the three corners of the triangle. Then each of the six 10mm LVDT's were mounted on an independent stand. They were placed to point perpendicular to the surface of these cubes in the direction opposite to the movement of the cubes. Dial gauges were used to measure the displacements for the initial static loading to compensate for the short range of the LVDT's. After readings from the dial gauges were taken, the LVDT's were set in their appropriate positions.

It should be noted that this method measures the absolute displacement of each point which includes the effects of axial, shear and bending deformation of the LVL members in addition to joint rotation. In practice, the LVDT's could not be positioned perfectly perpendicular to the surface of the cubes. Hence, errors were induced to the X-Y coordinates of the three points. Errors were also found in the calculations of the three lengths of the triangle, joint slip and joint rotation. Because this method was too complex in procedure and resulted in large human errors making the results unreliable, this method was abandoned after testing the first specimen.

RVDT Method: This method provided a direct measurement of the relative rotation of the rafter and column using a Rotary Variable Differential Transformer (RVDT). This device produces a voltage whose magnitude varies linearly with the angular rotation of its shaft. It works on a potentiometer principle similar to LVDT except there is a ferromagnetic rotor instead of a straight cylindrical core (see Figure 4.16).

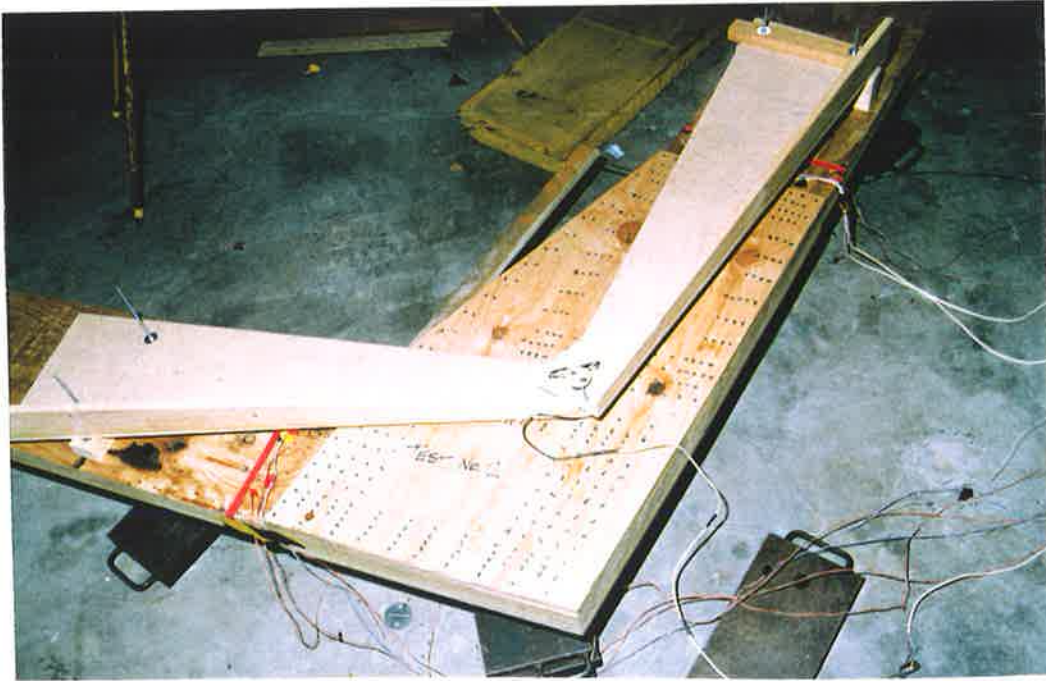


Figure 4.16 Rotary Variable Differential Transformer

Since the coupling between stationary windings and the rotor is electromagnetic, there is no mechanical friction or induced electrical noise. Within the range of 40 degrees, linearity is claimed to be better than $\pm 0.5\%$ of the full scale rotation. For the small angular rotations expected in this experiment, the linearity is improved. (e.g. for ± 5 degree rotation, the linearity is better than 0.1% of full scale). This instrument gave very small angle resolution and was precise enough for this experiment and relatively easy to install. A static calibration test on the RVDT unit was performed in 1991 by Stevens (52). The scale factor was found to be 122.6mV/degree with 15V input for rotation range of $+5.75^\circ/-8.36^\circ$ by utilizing a simple hinged board device.

Triangular mounting boards fixed to the LVL legs were designed to hold the RVDT and its shaft, thus the relative rotation between each LVL member was measured. The mounting board on the rafter side held the rotor body of the RVDT while the RVDT could rotate about a point on the rafter centreline (see Figure

4.17). The mounting board on the column side held the shaft of the RVDT, such that the RVDT could rotate about a point on the column centreline.

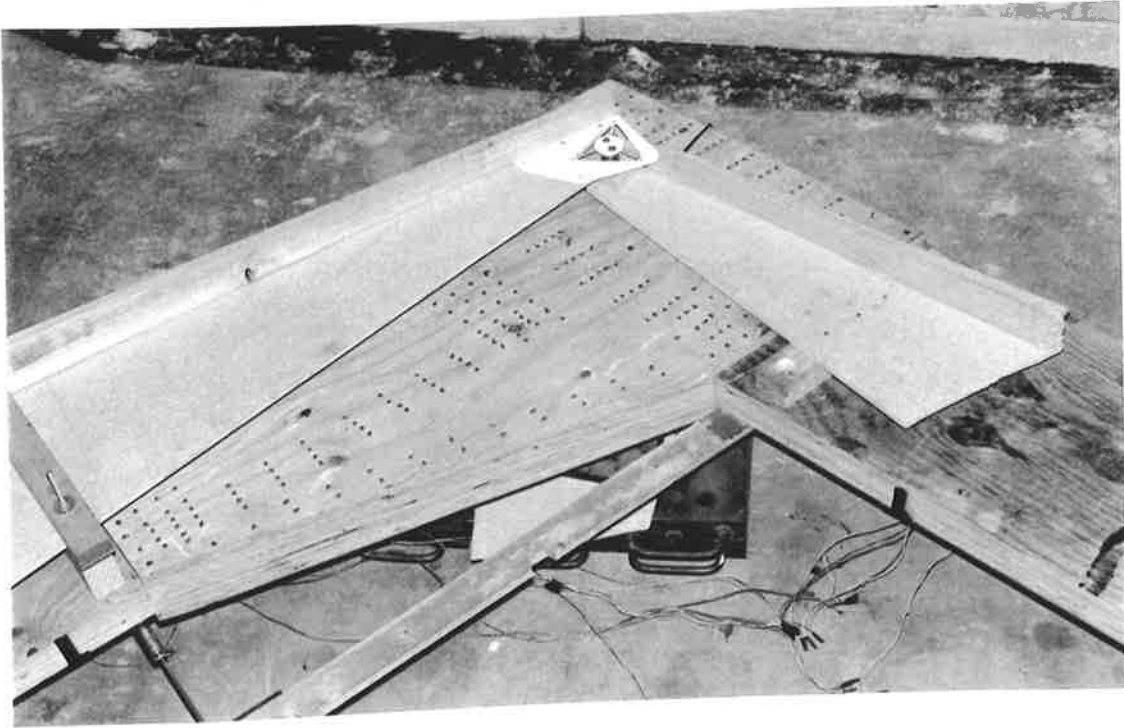


Figure 4.17 Mounting boards for the RVDT

These boards projected over the plywood gusset and allowed mounting of the RVDT at the assumed centre of rotation. They were fixed to the LVL members by screws and their triangular shape gave a stiff, securely fixed and yet light weight design. Being light weight timber boards, they had little inertia during cyclic loading and their fixing just beyond the gusset prevented them from taking up any bending displacement from the LVL member. However, to avoid any damage due to load transfer between the shaft and casing of the RVDT (Max. load = 3.63kg), a special connection was arranged for the RVDT. A pre-tensioned spring system was put between the mounting board tip and the shaft (see Figure 4.18). This in effect allowed the shaft of the RVDT to 'float'.

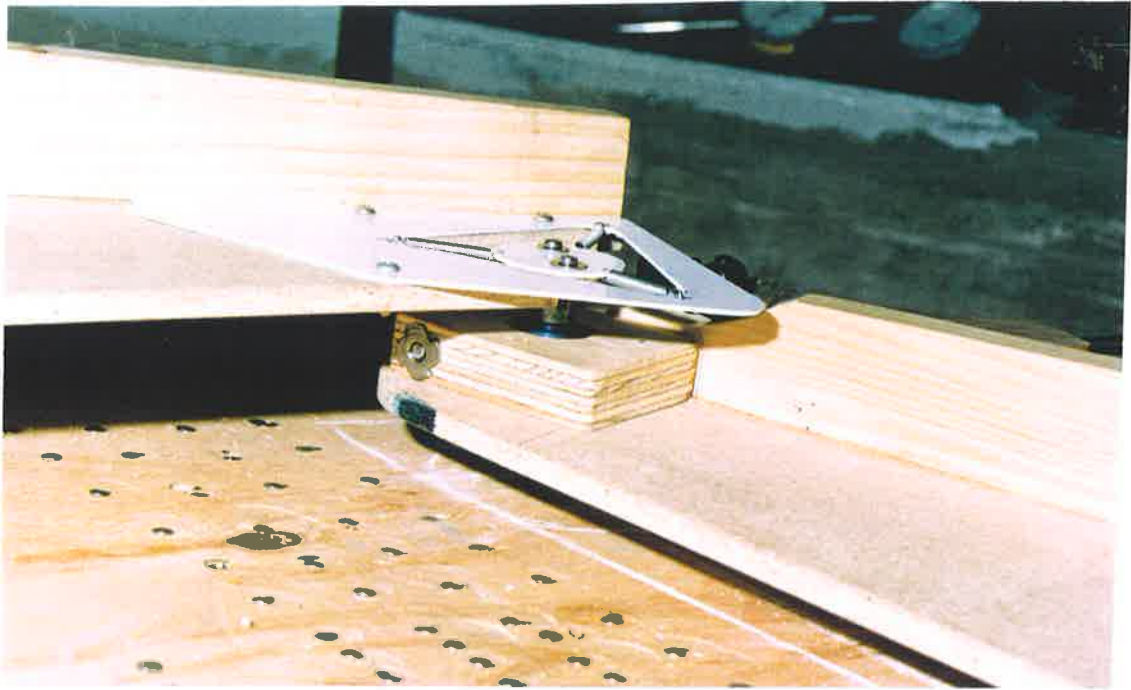


Figure 4.18 RVDT and the mounting system

The true centre of rotation of the joint was unknown due to the complex interaction between the LVL members and the plywood gusset plates. Initially, the RVDT was situated at the meeting point of the centreline of the column and the contact of the LVL members, i.e., position RVDT 2 as in Figure 4.19. However, visible relative movement of the RVDT to the mounting board occurred which **would not** exist if positioned at the centre of rotation. In an effort to locate the true **centre of rotation**, the position of the RVDT was shifted to the meeting points of the centrelines of the two LVL members, i.e., RVDT 1 in Figure 4.19. However, neither of the locations tried were satisfactory. Therefore, this method was also subsequently abandoned.

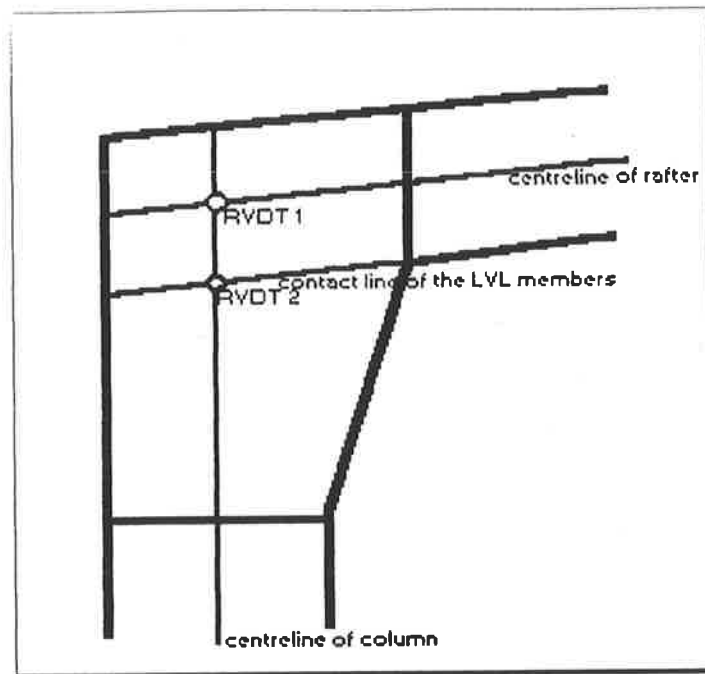


Figure 4.19 Locations of the RVDT

DCDT Method: This is a simple, indirect method. A stiff timber bar was nailed on the rafter just next to the gusset plate parallel to the gusset edge and with one end cantilevered to the column side and a long range DCDT was secured to the column along the edge of the gusset plate. The DCDT measured the relative movement between the timber bar and the column member (see Figure 4.20).

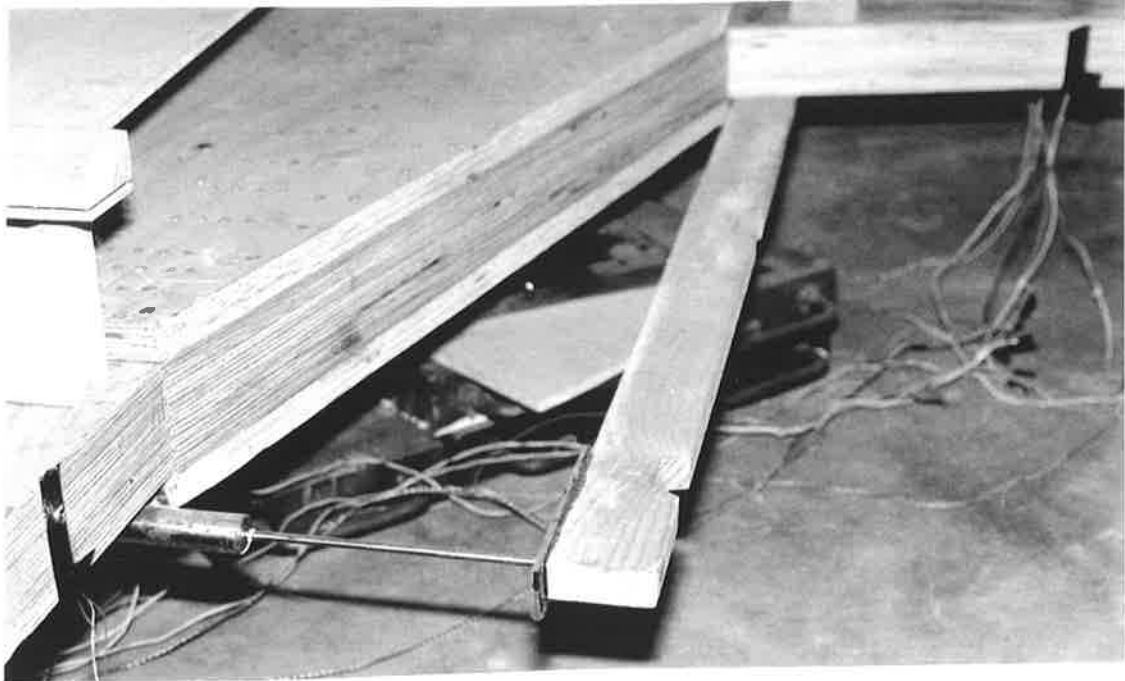


Figure 4.20 Arrangement of the DCDT method

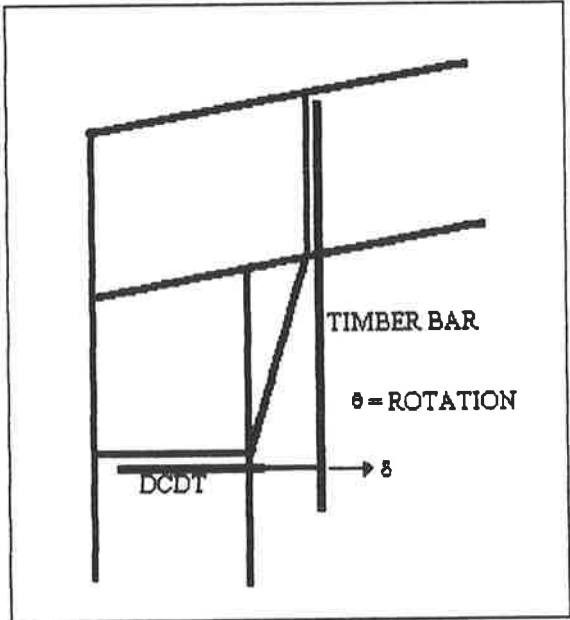


Figure 4.21 Geometry of the DCDT method

As shown by Figure 4.21, line CD denotes the inner edge of the timber bar while the DCDT is denoted by BC and the relative movement between the bar and the column is measured by the DCDT as δ (see Appendix B - a full mathematical explanation of the DCDT method). From the geometry of the DCDT arrangement, a relation between the rotation and the reading from DCDT (δ) was found to be $\theta = \tan^{-1}(\delta/AB)$ where θ is the rotation of the joint.

$$\delta = \tan\theta \cdot AB + (BC/\cos\theta) - BC$$

$$\cong \tan\theta \cdot AB \quad (\text{i.e. } \cos\theta \cong 1)$$

$$\theta \cong \tan^{-1}(\delta/AB)$$

where θ is the rotation of the joint

Since $AB=800\text{mm}$ and $BC=250\text{mm}$, for rotation of 1 degree ($\theta = 1^\circ$), the error from the approximation induced by using the DCDT method in δ was 0.27%; for $\theta = 0.5^\circ$, the error induced in δ was 0.17%. Therefore, the approximation was considered acceptable with less than 0.2% for rotation of 0.5 degree.

This procedure assumed that the joint went into pure rotation, therefore, any joint slip perpendicular to the DCDT would not be recorded and would induce error to the system. In all the tests, limited joint slip was observed. On the other hand, this procedure had the advantage that the method was very simple and straight forward, not only in setting up but also in data processing. Hence, while this was an indirect measurement in comparison to the RVDT method where angle changes were recorded directly, this method did not require the centre of rotation to be located exactly.

SPECIMEN	MEASUREMENT OF ROTATION
1	RVDT at the position 2*; LVDT; DCDT
2	RVDT at the position 2*,DCDT
3	RVDT at the position 1*,DCDT
4, 5, 6 & 7	DCDT

* RVDT position refers to Figure 4.19

Table 4.2 Measurement methods for rotation

The procedure used to measure rotations for each specimen is summarized in Table 4.2. The first specimen was tested using all three methods to measure the rotation of the joint. The RVDT was mounted at the meeting point of the column centreline and the LVL members contact line. The DCDT method and the RVDT method were in close agreement to each other. Due to the range of the DCDT used in the DCDT method for specimen 1, only two data points were recorded and gave insufficient evidence to conclude its accuracy. Inevitable human errors were contributed to the unreliable results by the complicated LVDT method. Therefore, for the next specimen, the LVDT method was dropped (see Figure 4.22).

The second specimen was tested using the RVDT and DCDT methods. Both sets of readings seemed to agree with each other for rotation less than 0.014 radian (0.8°). For larger rotations, the RVDT seemed to respond strangely to the rotation by recording almost constant joint rotation with increasing load. Thus, the RVDT method was considered to be less accurate with the unknown location of the centre of rotation. On the other hand, the plot of moment vs rotation (see Figure 4.23) showed that the DCDT method indicated a consistent pattern.

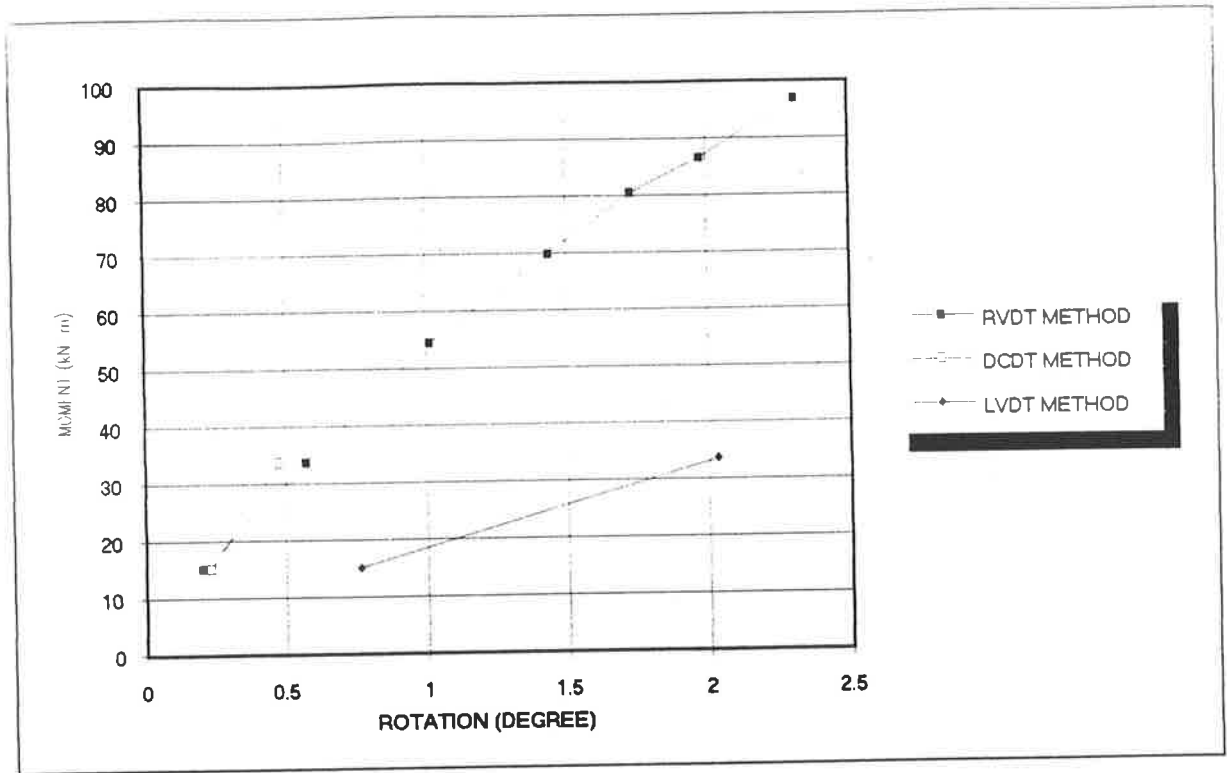


Figure 4.22 Moment vs rotation for specimen 1

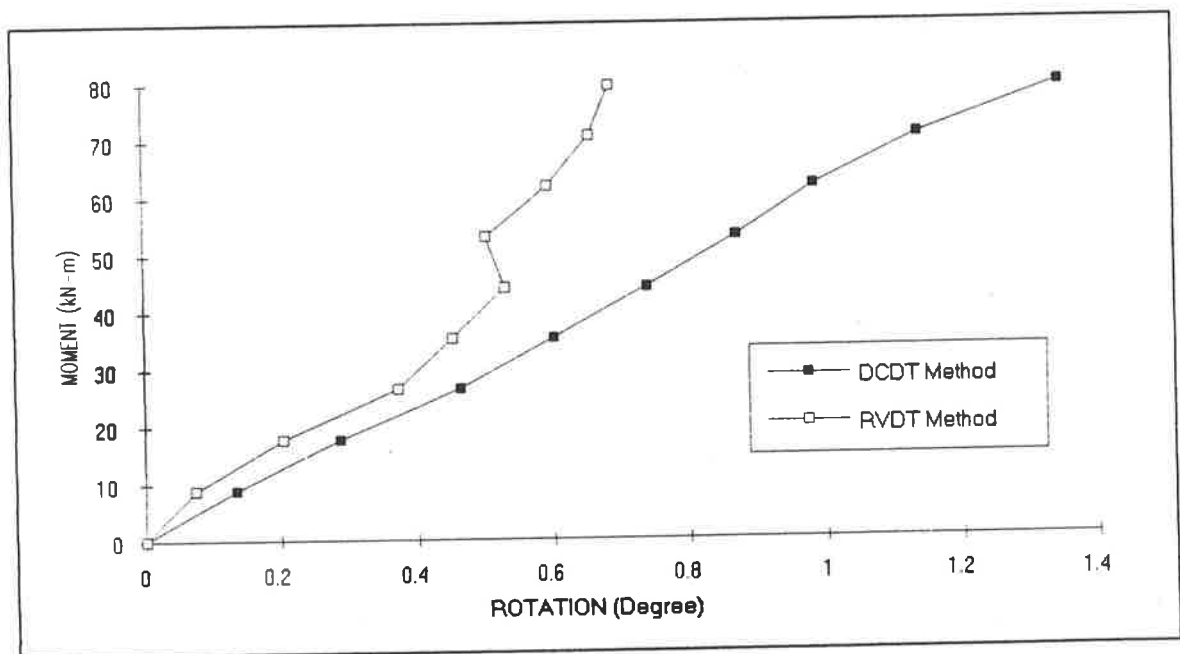


Figure 4.23 Moment vs rotation during the failure loading for specimen 2

The third specimen was also tested using the RVDT and DCDT methods to measure rotation. As for the second specimen, the DCDT method appeared to produce more reliable results. Translational movement was still observed during these tests at the meeting point of the two mounting boards for RVDT. Therefore, the meeting point of the two centrelines was still not the true centre of rotation. Rotational readings taken by the DCDT method were used.

Based on the test data for the first three specimens, it was concluded that the DCDT method was the most reliable method and was used in all subsequent tests to record the rotation.

(b) Strain:

The ram displacements imposed at the column base by the Instron hydraulic jack caused joint rotation. It also induced strains in all locations of the test specimen. Due to the complex interaction between the plywood gussets plates, nail groups and the LVL members, complex non-linear strain was expected on the surface of the plywood plates. Batchelar and Cavanagh (8) have previously put strain gauges along a line from the apex to the strut (see Figure 4.24).

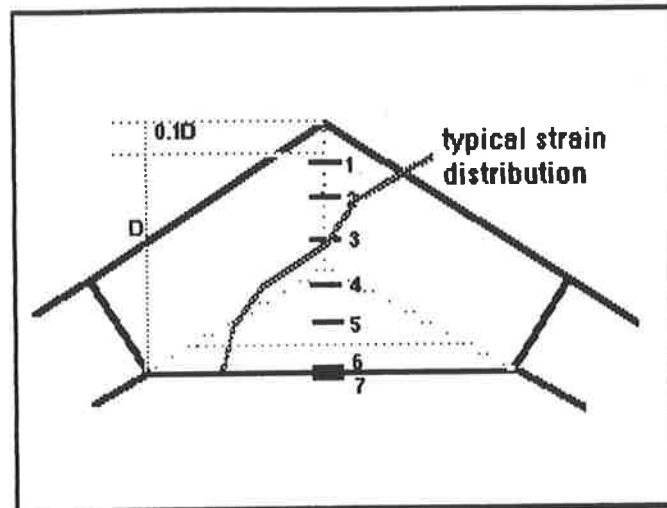


Figure 4.24 Gauge positions in the Batchelar and Cavanagh experiment

The strains found in the gusset plate were not linear with the point of zero strain being consistent at all load levels which was midway along the line. Similar strain measurement was later attempted by Batchelar and Hunt (9) with a line of strain gauges along the contact line between the rafter and column (see Figure 4.25). Again, non-linear strain distributions were observed.

The point of zero strain was found to be near the meeting point of this contact line and the centreline of the column (i.e. near point 3 of Figure 4.25). In the above experiments, no conclusive statement was made on the strain profile inside the gusset plate since the strain in the region of the gusset was non-linear and uncertain. In an experiment performed by Boulton (10), average timber strains at the extreme fibre of both members were monitored by electric resistance strain gauges. New Zealand practice currently recommends that the members be designed for the moments which occur a distance of $D/2$ from the edge of the plate. This allows for the stiffening effect of the joint itself and a stress raising effect observed at the extreme nails in the group.

Consequently, this experiment investigated the strain distribution along the above mentioned section of the column and rafter members adjacent to the plate.

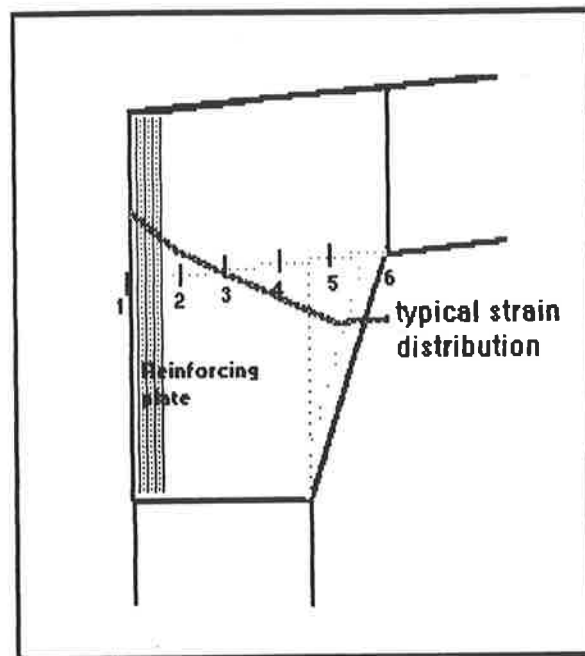


Figure 4.25 Gauge positions in the Batchelar and Hunt experiment

A preliminary study on the effectiveness of using strain gauges glued directly onto timber was carried out (Appendix B) in order to validate the use of strain gauges attached to LVL since the size of the strain gauge approaches the size of individual fibres in the cellular wood structure. From these findings, it was recommended that 68mm long electrical resistant strain gauges be used, mounted directly onto the LVL surface using "super glue paste" (water based glue might be absorbed into the timber before drying). The timber surface was properly prepared in accordance with "M-line Accessories" Instruction Bulletin B-129-6 to develop a chemically clean surface which had a roughness appropriate to the gauge installation requirements. 320 Grit abrasive paper was used to remove any loosely bonded adherents and level the surface

for suitable bonding. Then gauge location layout lines were drawn to locate the strain gauge before bonding the strain gauges (see Figure 4.26). For comparison, Batchelar utilized 60mm strain gauges mounted directly onto the plywood surface.

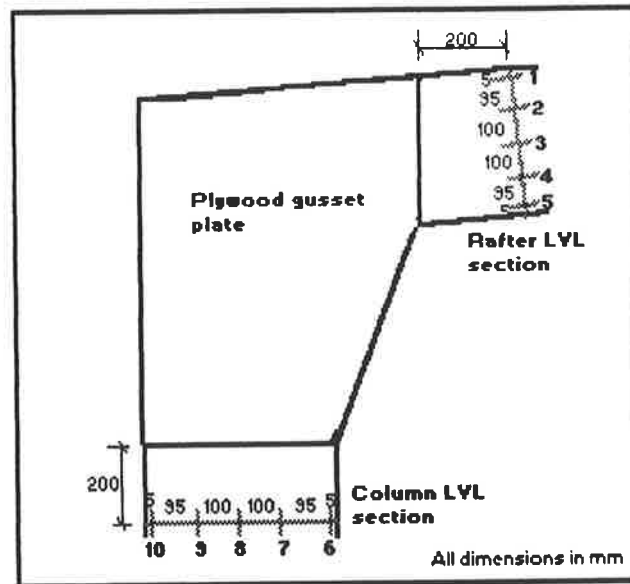


Figure 4.26 Locations of the strain gauges across the LVL members

The strain gauges were attached to the rafter and column LVL members at a distance of 200mm ($D/2$) away from the gusset plates as shown in Figure 4.26. Five strain gauges were mounted with approximately equal spacing along a line perpendicular to the LVL legs to give a strain distribution across the section on each LVL member. A low excitation voltage of 5 volts was used to avoid heating of the strain gauges which would in turn change the material properties and stresses of the strain gauges. Given a linear longitudinal strains, the average of the maximum tension and compression gave the axial strain while half the difference gave the bending strain (see section 5.3.2).

(c) Data logging:

The task of data logging was to accept signals from the instrumentation and amplify it before storing the data onto both a hard disk and a floppy disk. A flow chart describing the above data logging process is shown as in Figure 4.27.

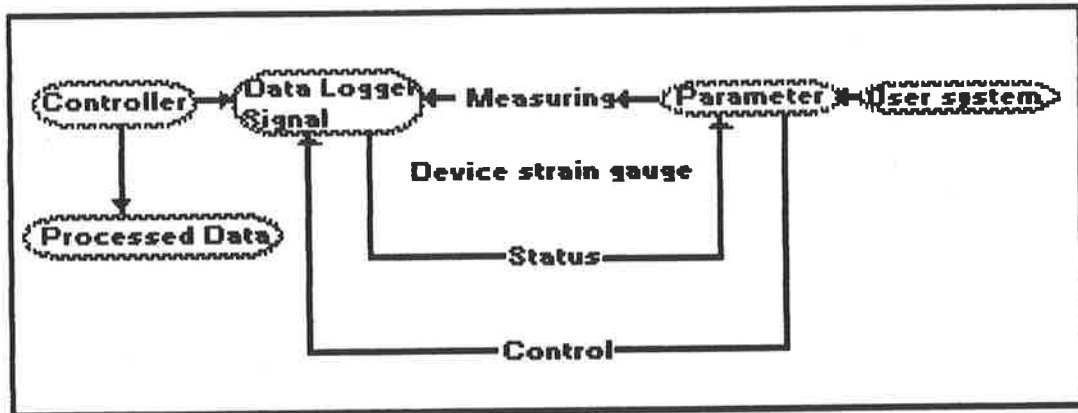


Figure 4.27 Flow chart for the data logging system

The data logger used for these tests was a Hewler Puckard HP3497A data acquisition / control unit with an IBM compatible laptop computer acting as a controller (see Figure 4.28). The 3497A performed the data acquisition task by inputting the signal (e.g. voltage) from the user system (moment-resisting joint). It then controlled the incoming signal by interrupting, switching and controlling source functions. This machine was adopted because it could take 50 readings per second to 5.5 digits accuracy with auto-ranging. This was important given input range from μV for strain gauges to mV for the DCDT. It has $1\mu\text{V}$ sensitivity, and a DC voltage measuring up to 119.9999V with an internal buffer memory capacity of 100 readings. An in-built 20 channel analog signal multiplexer (Option 010) was used to switch signals between the RVDT and

DCDT. Option 070 was installed in the 3497A to provide bridge completion ($\frac{1}{4}$ bridge configuration) for all the strain gauges. As mentioned before, the computer, through an IEEE card, was linked to the 3497A. A program in Basic Language was written to control the triggering and data collection of the 3497A (see appendix C). When the data was input in the computer, it was automatically scaled by the appropriate calibration factors for input into a conventional spreadsheet program for subsequent analysis. This process saved a great deal of time in sorting out the information and analyzing the data and was very beneficial for processing the large amount of data collected.

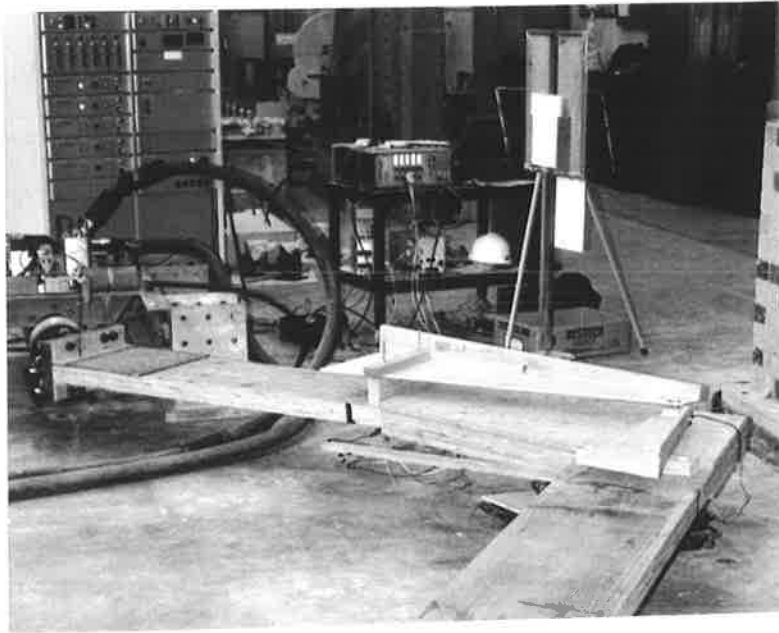


Figure 4.28 Data logger and the laptop computer as the controller

4.4 TESTING PROCEDURES

In section 4.2, the overall test program was outlined and the actual tests listed in Table 4.1. In single nail joint tests by Polensek (46), it was observed that a strict testing regime must be followed to ensure reliable results as testing conditions affect joint properties tremendously. For example, specimen assembly techniques, magnitude, rate of loading and theoretical assumptions, are all known to affect the behaviour of timber members. Since this research was very unique, previous laboratory works have either concentrated on fatigue testing on single nailed joint or static and seismic testing on multi-nailed joints, a new experimental set up was necessary. Prototypes were built for testing to failure to support the field testing of timber portal frames. In order to ensure that each of the seven moment-resisting joints was tested in the same manner, the following set of experimental procedures were strictly followed.

The testing involved first applying a standard loading calculated from AS1720 as 23kN (41kN-m) (25kN or 44kN-m was chosen for convenience - see section 3.4.2) for a working load moment which represented the dead load case. The cyclic loading superimposed on the static loading was chosen from the wind load code AS1170.2 as $\pm 9\text{kN}$ or $\pm 16\text{kN-m}$. Therefore, instead of having wind loading acting on the whole portal frame, a pair of loads acting opposite to each other was applied at the base of the specimen legs (see Figure 4.29).

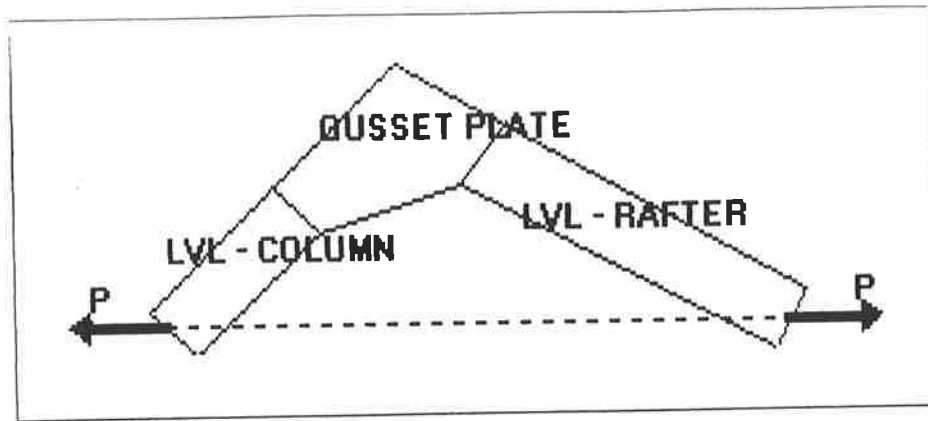


Figure 4.29 Load vector diagram for the specimen

This pair of loads induced axial and shear forces in each LVL member. The loading force was supplied by the Instron hydraulics jack at the base of the column leg. The Instron was operated in load control mode which meant that the loading forces were monitored by the controlling panel of the Instron machine. By using the load control option, apart from the advantage of simulating the real situation closely where wind load is applied irrespective of the joint displacement, it also gave constant stress amplitude. Displacement control was not used because the load necessary to apply a constant displacement would be lowered if the joint stiffness was to decrease.

In the investigation on the effects of testing variables on damping and stiffness of nailed wood to sheathing joints, Polensek (46) concluded that magnitude and rate of loading influence the joint damping and stiffness. Increasing loading rate increased damping and stiffness but increasing loading magnitude diminished both properties. In performing seismic tests with large load magnitudes and small numbers of cycles, Batchelar (7) adopted a loading rate of approximately 30mm per minute. The test loading was cyclic with peak loads applied for short periods of time (a few minutes or less). The time required to test these joints with large numbers of loading cycles was large and played an important part in determining the rate of cyclic loading of the joint.

Because of the large number of cycles to be applied, the fastest loading rate possible was used (i.e. 0.3-0.6Hz).

There were two specimens subjected to a simple static test to failure. The first test was aimed at determining the ultimate static strength of the joint for comparison with the code calculated static load capacity. In addition, it would give a good estimation of the joint's stiffness. The second such test was conducted to confirm the static test result and for comparison with the ultimate strengths obtained during the dynamic tests when the specimens were first subjected to fatigue loading. During the static tests, the Instron hydraulic jack was used to load the specimens continuously by manual control, stopping momentarily at 5kN (8.8kN-m) intervals to take readings. This process was carried out until the failure of the specimens occurred.

In each fatigue test, the specimen was loaded up to 44kN-m (45% of its experimental static strength) with data being collected at 5kN (8.8kN-m) increments. Then, a cyclic load with an amplitude of ± 16 kN-m (except ± 35 kN-m for the specimen 6 and ± 26 kN-m for specimen 7) was added for a predetermined number of cycles. In each test, the data was collected at regular time intervals in order to monitor changes in joint performance. For specimens 2, 3 & 4, the cyclic loading was interrupted twice everyday for data logging. A cyclic loading frequency of 0.6Hz was used for these tests while for specimens 6 and 7 where the load magnitudes were larger, smaller frequencies of 0.3Hz and 0.4Hz were used, respectively.



For data logging, the loading rate was slowed down during the cyclic loading phase. The method used to take all the readings at different parts of one loading cycle was to halt the automatic cyclic loading and adjust the load level at different points of the loading cycle manually. For each load point, a whole set of readings was obtained. In order to produce a smooth loading cycle, thirteen load levels were chosen (see Figure 4.30).

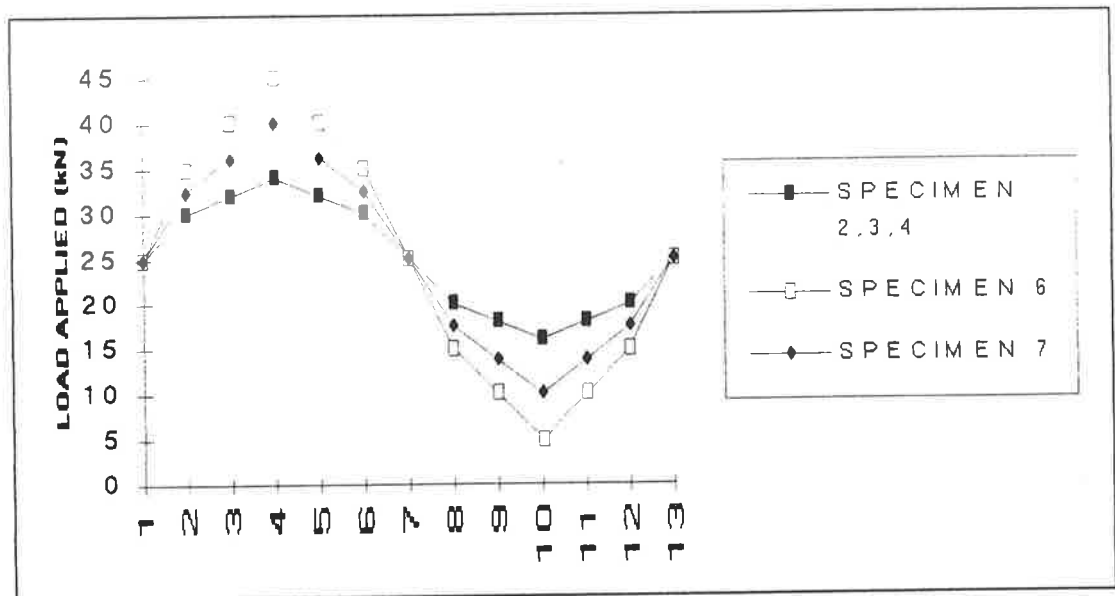


Figure 4.30 Points chosen for data logging within a complete load cycle

For each load level a set of data was recorded in the computer file. After the reading of all 13 points, the automatic cyclic loading was resumed. Once the required number of loading cycles were applied, the cyclic loading was stopped and the static load was removed. Immediately, the specimen was reloaded from zero at 5kN intervals until failure in order to determine the residual static strength of the joint after fatigue loading. In the final static loading tests, loading was applied using displacement control in order to prevent continual excessive displacement from the hydraulic ram after the joint failed.

The following chapter (Chapter 5) presents the experimental results and the discussion on the behaviour of the test joints.

CHAPTER 5

RESULTS AND DISCUSSION

5.1 INTRODUCTION

This chapter presents the results of tests conducted on seven 1/2-scale plywood gusset joints described in section 3.4. The testing program and key results, summarised in Table 5.1 (section 5.3), consisted of two static tests and five dynamic tests. The specimens which did not fail during the dynamic fatigue testing phase were also subsequently tested statically to failure in an effort to determine whether the fatigue loading had any effect on the residual static strength and stiffness of this type of joint. In all the experiments, the type of failure referred to here was loss of load carrying capacity. Excessive slip of the joint as is commonly used in AS1649(1) for determining basic working loads for metal fasteners was not considered as failure in these experiments.

Moment was plotted against rotation and ram displacement for each static test so that the static stiffness could be studied. Rotation as a function of ram displacement was also studied since the ram displacement was primarily a function of joint rotation and LVL member bending. Strain profile, joint stiffness and residual static

strength were investigated as functions of the number of cycles of fatigue loading for each dynamic test specimen. This chapter concludes with a comparison of the results from the seven tests and comments on the static and dynamic performance of the joints.

5.2 PRESENTATION OF TEST RESULTS

SPECIMEN 1

The first specimen was subjected to a simple static test to failure. The aim was to determine the static ultimate strength. This would not only provide a basis for comparison with the calculated strength from AS1720(2), but also formed a benchmark for comparison with the residual ultimate strengths obtained in subsequent tests where each specimen was first subjected to various amounts of fatigue loading. Moreover, this was an opportunity for testing the accuracy and reliability of the instrumentation.

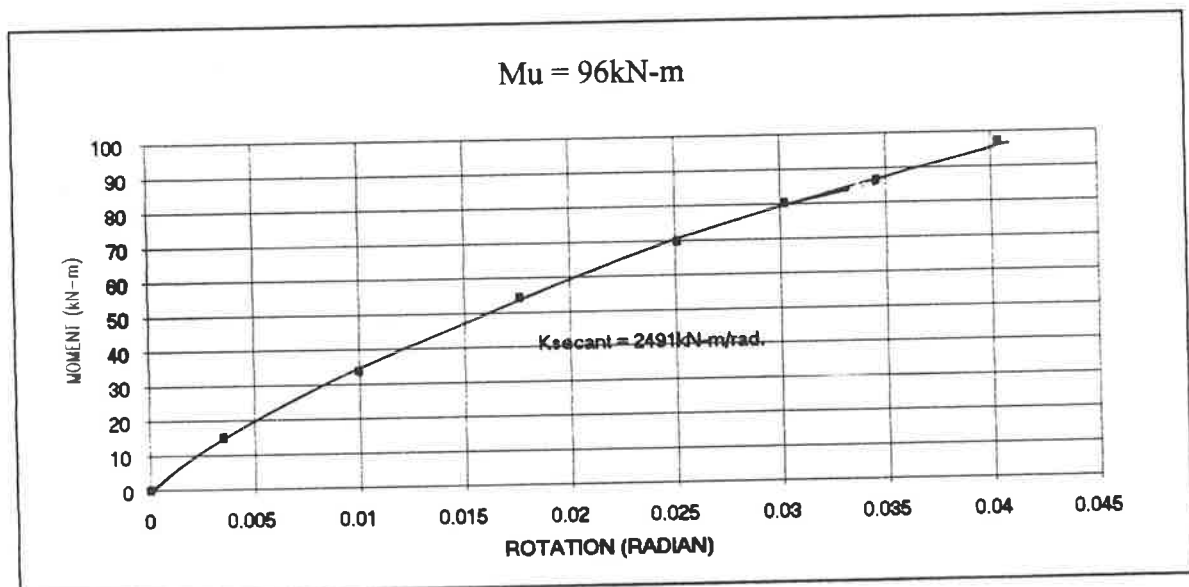


Figure 5.1 Moment vs rotation for specimen 1

From the graph (Figure 5.1) of joint moment, M , versus joint rotation, θ , one can see that the relationship was non-linear and that the joint softened slightly with increasing moments. The secant stiffness of the joint, obtained by dividing the maximum moment by the maximum rotation, was found to be 2491 kN-m/rad.

The strain profile across the LVL column section is shown in Figure 5.2 and was seen to be nearly linear with the neutral axis situated near the centreline of the member (12.5 mm from the centreline to the compression side). This implied that bending contributed the largest portion of stress. In all the strain plots, tension is positive and compression is negative.

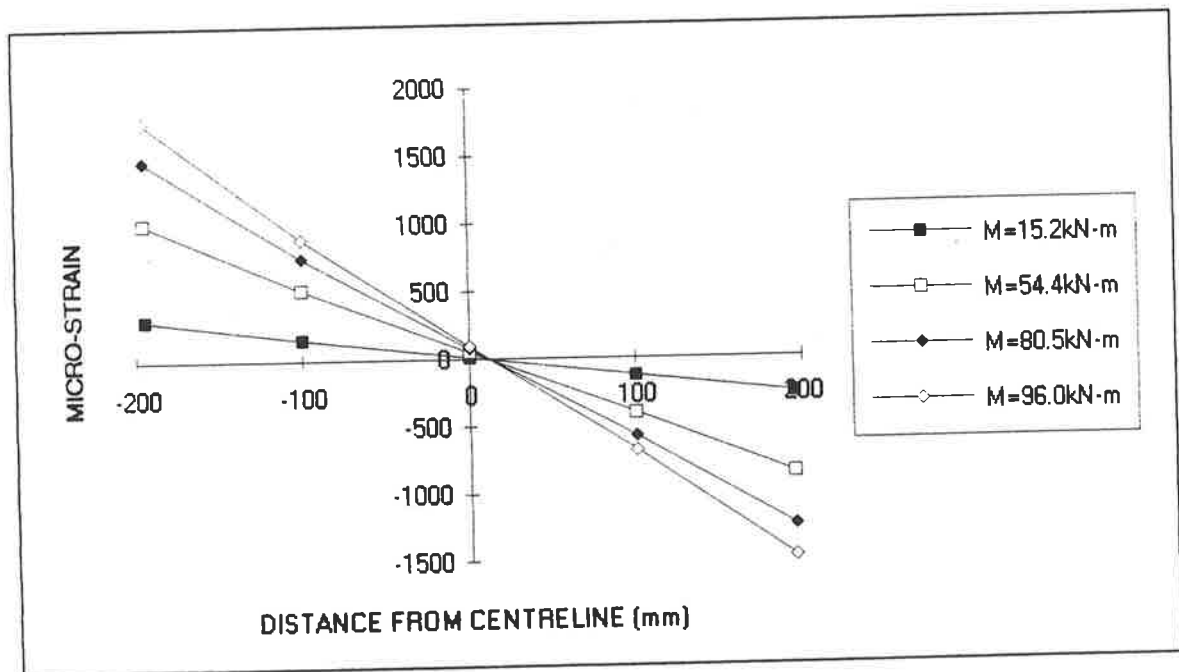


Figure 5.2 Strain across column for specimen 1

By integrating the strain profile, the axial load and bending moment at the location of the strain gauges could be evaluated from:

$$\sigma = E \times \varepsilon$$

$$P = \int \sigma \, dA \text{ and } M = \int \sigma y \, dA$$

where σ is stress, E is modulus of elasticity (13200MPa as stated in manufacturer literature see section 2.2.1), ε is strain, P is axial load, M is bending moment and A is area.

The accuracy of this calculation relies on the accuracy of the value for Young's modulus and strain values. Since there are only five strain values, there could be error induced. This is particularly true if the strain profile is non-linear. On the other hand, the bending moment and axial load could be confidently calculated by simple statics from the bending moment diagram and the axial load diagram in Figure 3.6. In this chapter, the axial load and bending moment calculated from the strain profile will be referred to as P_{strain} and M_{strain} whereas the axial load and bending moment calculated from statics will be referred to as P_{statics} and M_{statics} .

At the maximum load, P_{strain} and M_{strain} were calculated as 40.1kN (105% of P_{static}) and 36.9kN-m (70% of M_{static}) compared to the experimental values of 38.0kN and 52.4kN-m on the column. It should be noted that the values of moment computed here are for the strain gauge position on the LVL members. The maximum moment of 96.0kN-m given in Figure 5.1 applies at the intersection of the centrelines of the LVL members and is larger because the lever arm is greater at that location. The discrepancy between the results calculated from statics and strain could be due to the assumed value of modulus of elasticity of LVL.

The strain profile for the rafter member in Figure 5.3 is 50% higher than that in the column. This was because the rafter member was longer than the column member. However, it is of interest to note that the strain profile across the rafter was

non-linear and in close agreement with the strain profile reported by Batchelar(7). P_{strain} and M_{strain} were calculated as 41.6kN (90% of P_{static}) and 58.2kN-m (73% of M_{static}) respectively in contrast to P_{static} and M_{static} of 46.3kN and 79.2kN-m. The close correlation confirmed the reliability of the non-linear strain profile. This non-linearity could be due to initial stress which existed in the test specimen or deep beam bending action.

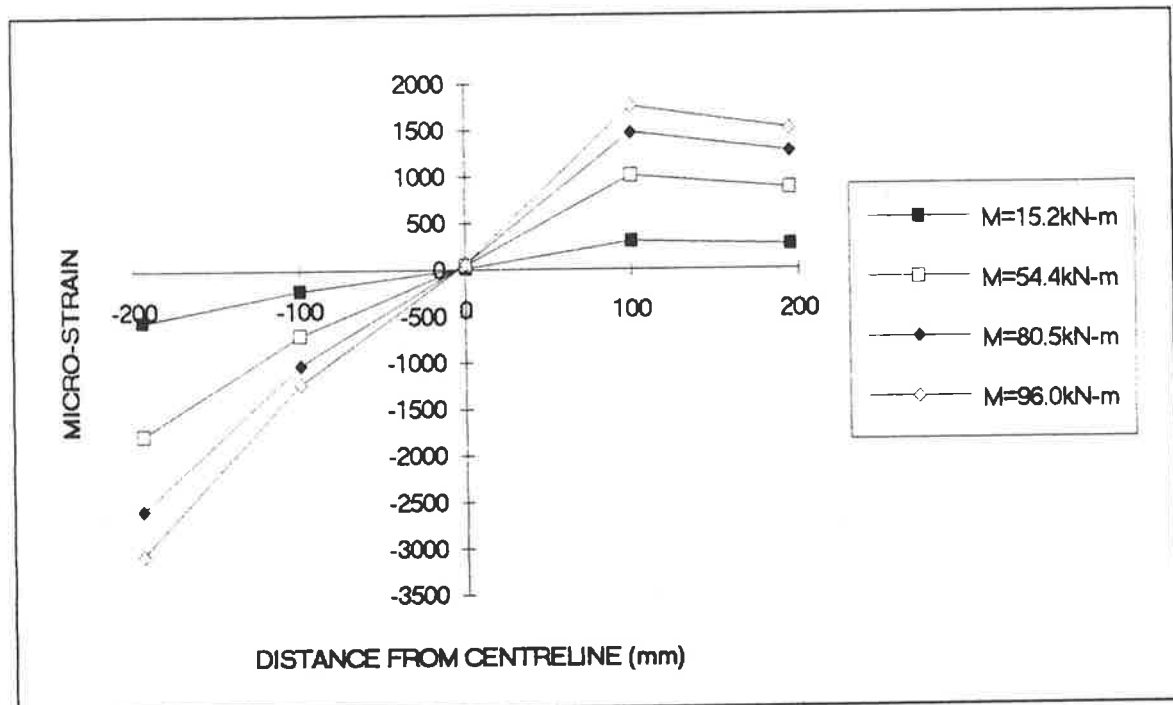


Figure 5.3 Strain across rafter for specimen 1

The static test concluded with the failure of the joint by a bending/tension failure of the LVL rafter member adjacent to the gusset plate. The failed specimen is shown below in Figure 5.4

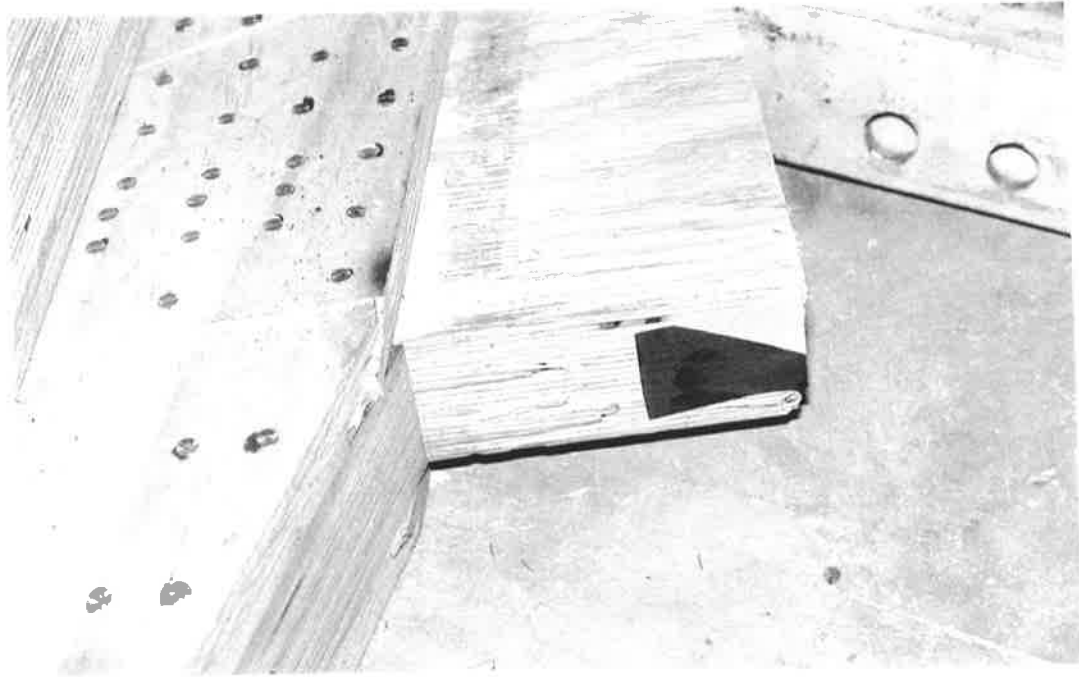


Figure 5.4 Failure mode of specimen 1

The ultimate ram load was 54.5kN and corresponded to a joint moment of 96kN-m (i.e. 230% of the design value of 44kN-m as calculated from AS1720). Although the failure of the specimen was sudden, some warning of that failure was given by the cracking noises which were heard at load levels of 80% of the failure load.

SPECIMEN 2

The second test specimen first underwent 250,000 cycles of fatigue loading. The fatigue loading consisted of 0.6Hz sinusoidal cycles having a joint moment amplitude of ± 16 kN-m which was superimposed onto a constant moment of 44kN-m. After the joint successfully withstood 250,000 cycles of fatigue loading, it was tested statically to failure to find the residual static strength of the joint.

The aim of the second test was to see whether the long term strength of the joint was affected by the fatigue loading. Besides, the test gave a visual impression of how the joint might react in a severe wind storm.

Figure 5.5 shows the joint rotation, always measured at a load of 44kN-m, for different numbers of cycles during the fatigue test. It was interesting to note that the general shape of the curve, including the initial jump in rotation and the gradual flattening out with increasing numbers of cycles, is typical of creep effects in timber. The question of creep will be discussed later in section 5.3.2.

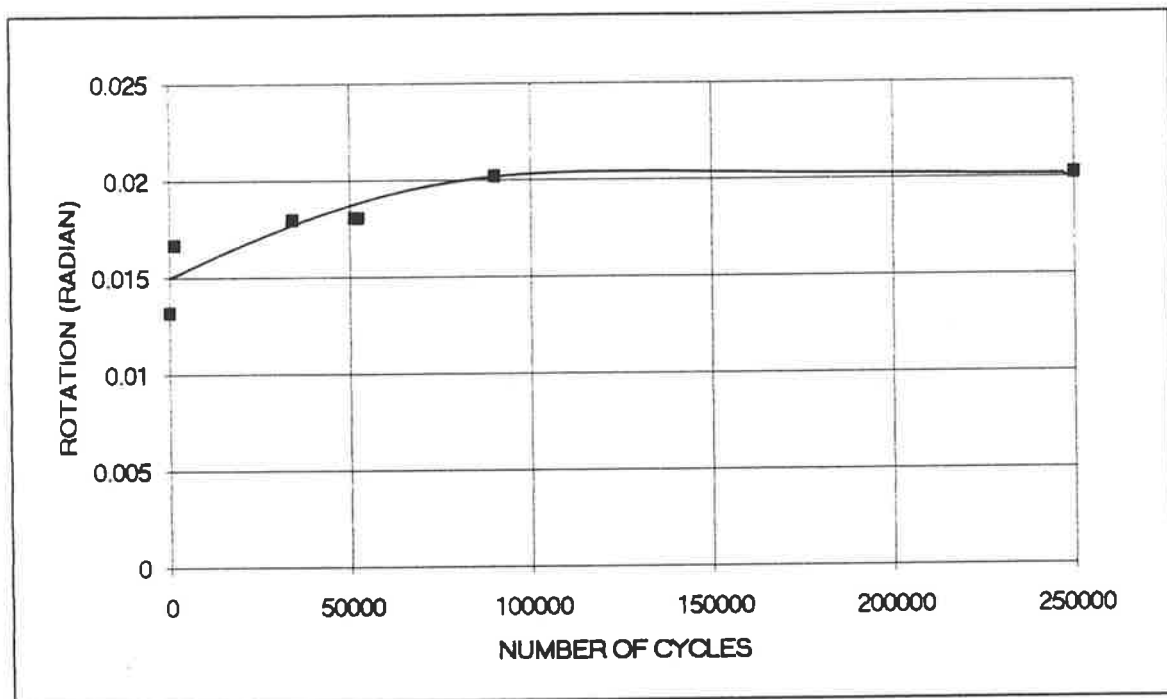


Figure 5.5 Rotation at 44kN-m vs number of cycles for specimen 2

Because of the possibility that creep could affect the amount of joint rotation, it was decided to investigate the difference between the maximum and minimum ($\theta_{\max} - \theta_{\min}$) rotation occurring within a single load cycle during the dynamic loading phase. It was felt that this parameter would better represent the instantaneous

rotation within a cycle and the dynamic stiffness of the joint. Thus, the change in rotation, $\Delta\theta = \theta_{\max} - \theta_{\min}$, was plotted versus the number of loading cycles, N , and is shown in Figure 5.6. The difference in the joint rotations, $\Delta\theta$, was seen to steadily increase.

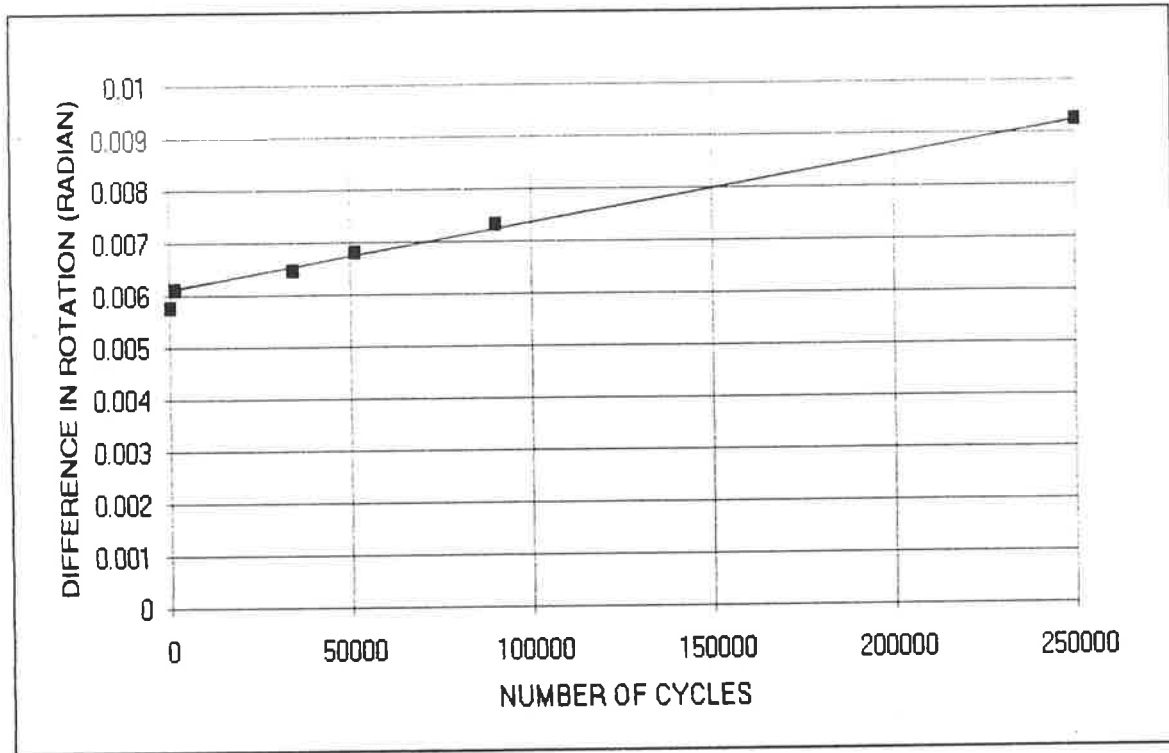


Figure 5.6 Difference in rotation vs number of cycles for specimen 2

Hence, although the total joint rotation appeared to become constant after about 100,000 cycles, there was an increase in the change of joint rotation, $\Delta\theta$, within each loading cycle. The joint stiffness ($K = \Delta M / \Delta\theta = (M_{\max} - M_{\min}) / (\theta_{\max} - \theta_{\min})$) within each cycle decreased with increasing number of loading cycles since the moment ΔM was held constant. This is illustrated more clearly in Figure 5.7 where the instantaneous joint stiffness K (normalized by the initial joint stiffness, K_i) is plotted against the number of loading cycles. For specimen 2, the joint stiffness after 250,000 cycles was approximately 63% of the initial stiffness. Since joint stiffness was a function

of instantaneous rotational difference, this dynamic joint stiffness was independent of creep.

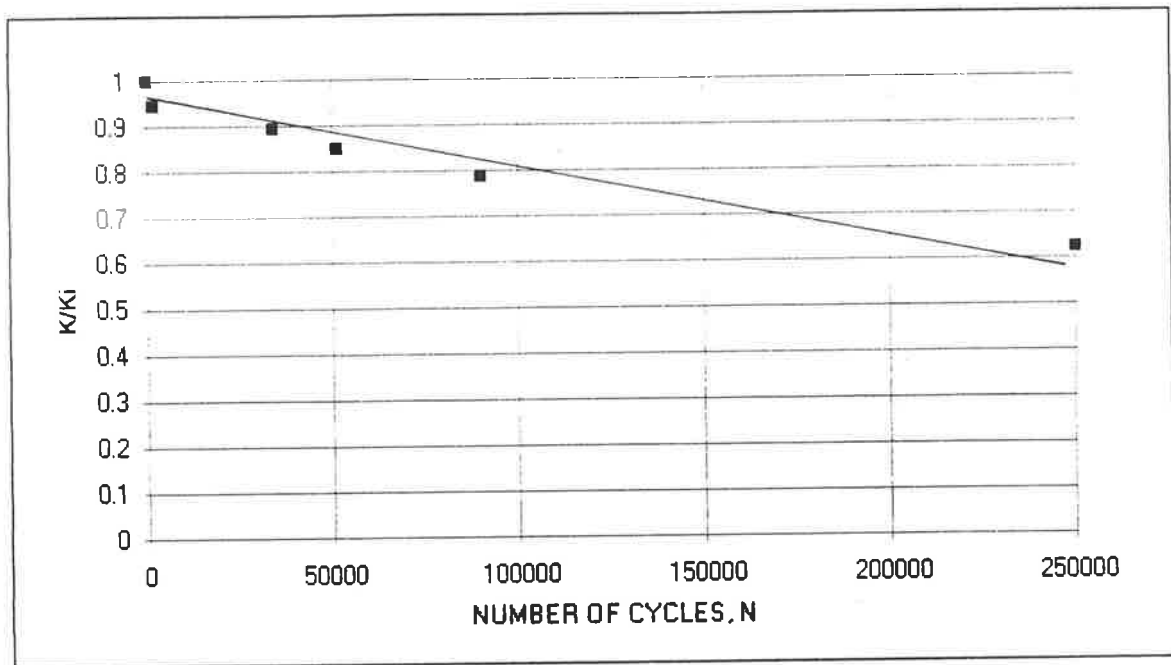


Figure 5.7 Stiffness vs number of cycles for specimen 2

The initial joint stiffness K_i was calculated by dividing the change in moment M by the change in rotation from the initial loading cycle. Thus, the results of Figure 5.7 indicate that the instantaneous joint stiffness varied between 3436kN-m/rad and 5519kN-m/rad.

Figure 5.8 shows the results of the static test conducted after the 250,000 cycles of fatigue loading had been applied and from this curve, the secant stiffness of the joint was estimated to be 3370kN-m/rad.

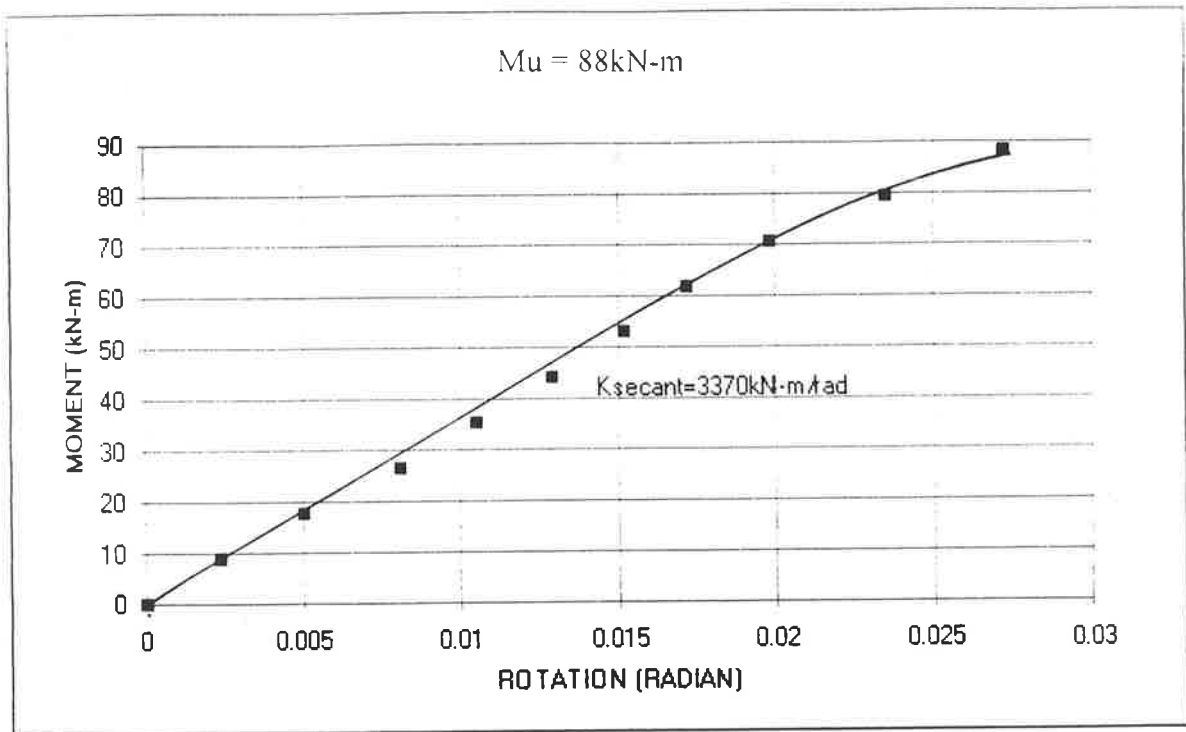


Figure 5.8 Moment vs rotation for specimen 2 (static test to failure)

The strain profile measured in the rafter and column sections during the static test are plotted in Figure 5.9 and Figure 5.10, respectively. Interestingly, the strain across the rafter appeared to be almost linear (Figure 5.9), with the neutral axis situated near the centreline of the rafter. This result is in contrast to the non-linear shape exhibited by the rafter during the static test of the first specimen. The only difference between the specimens was that the second specimen was "pre-loaded" with 250,000 cycles of fatigue loading. Hence, a possible reason for the linear strain profile was that the fatigue loading may have removed any initial stress which existed in the test specimen. The column member exhibited a nearly linear strain profile which was consistent with the results for the first specimen. At a recorded applied ram load of 45kN (79kN-m) during the static loading, the P_{strain} and M_{strain} for the rafter were 17.4kN (46% of P_{static}) and 48.5kN-m (75% of M_{static}), respectively, compared to the values calculated from statics of 38.0kN and 65.0kN-m. For the column member at the same

applied ram load, P_{strain} was 27.3kN (88% of P_{static}) and M_{strain} was 35.7kN-m (90% of M_{static}) in contrast to P_{static} of 31.2kN and M_{static} of 43.0kN-m.

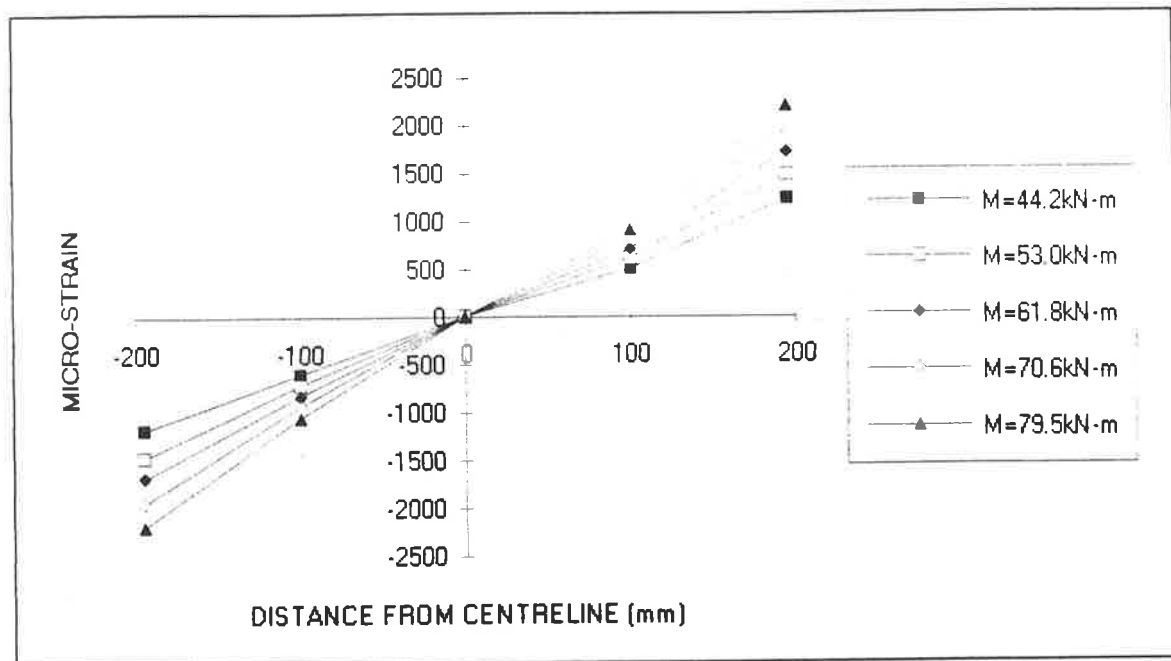


Figure 5.9 strain across rafter after 250000 cycles for specimen 2

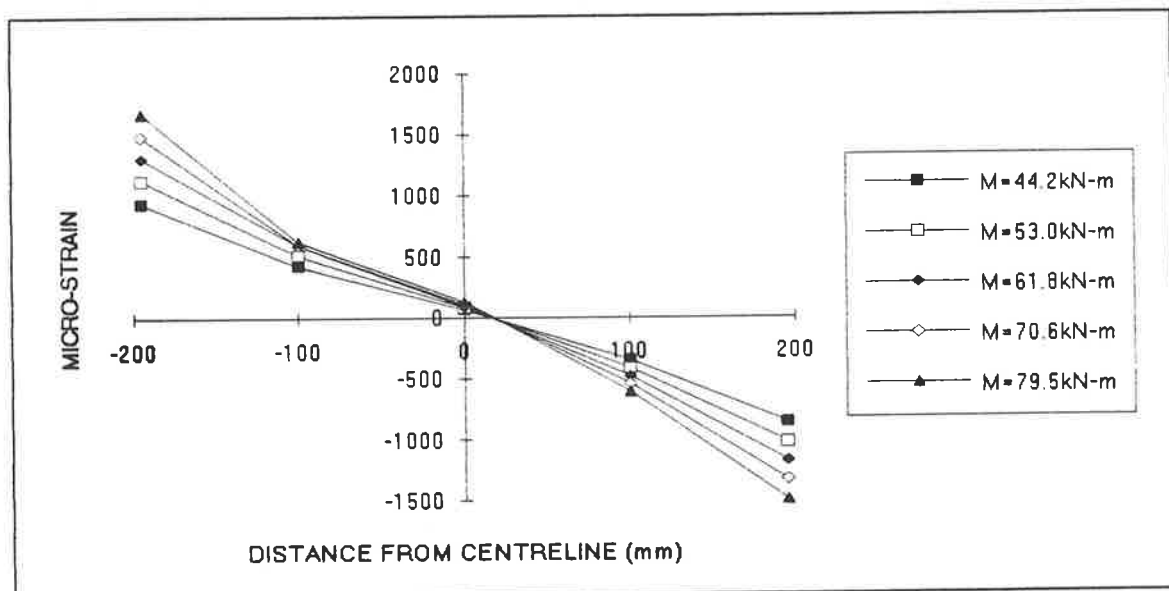


Figure 5.10 strain across column after 250000 cycles for specimen 2

The strain amplitude in the rafter was larger (about 30%) than that in the column and this is consistent with the test results from specimen 1. However, there is no obvious reason for a lower strain difference than specimen 1 between the rafter and the column in test specimen 2.

Testing of specimen 2 concluded with a static test to failure where ultimate load was found to be 88kN-m. This was approximately 92% of the static strength found in the first specimen. The failure mode for specimen 2 is shown in Figure 5.11 and consisted of a tension failure across the gusset plate between the column and rafter members.



Figure 5.11 Failure mode of the specimen 2

A final comment should be made regarding the response of specimen 2 during the cyclic testing. Obvious movement occurred between the LVL members and the gusset plate with a noticeable gap opening and closing at the contact line of the two LVL members during cyclic loading. In addition, movement was observed at each end of

the strut member, indicating relative movement of the two LVL legs. By monitoring lines drawn along the gusset plate edges on the LVL members, gusset slippage could be observed. After a number of cycles, the lines were no longer at the edges of the plate. This slippage was of the order of 5mm and was observed to be due mainly to slight movements of the nails. This implies that the gusset plates have moved relative to the LVL members and a gap between the LVL member has formed by the fatigue loading. Thus, the residual strength and stiffness were expected to drop.

SPECIMEN 3

The third specimen was loaded identically to the second (i.e., with a static moment of 44kN-m plus a cyclic moment of ± 16 kN-m). However, instead of 250,000 cycles of load, it was subjected to over one million cycles of load. The target of million cycles was set in order to attain a significant number of cycles, commonly used as a milestone in fatigue testing. The loading amplitude was not decreased since the second specimen survived the fatigue loading exceptionally well.

From the plot of rotation at 44kN-m of applied moment vs number of cycles (Figure 5.12), a definite increase in the rotation with increasing number of cycles can be seen. A steep increase in rotation was again observed in the early stage of testing with the increases in rotation gradually flattening out as in Figure 5.5.

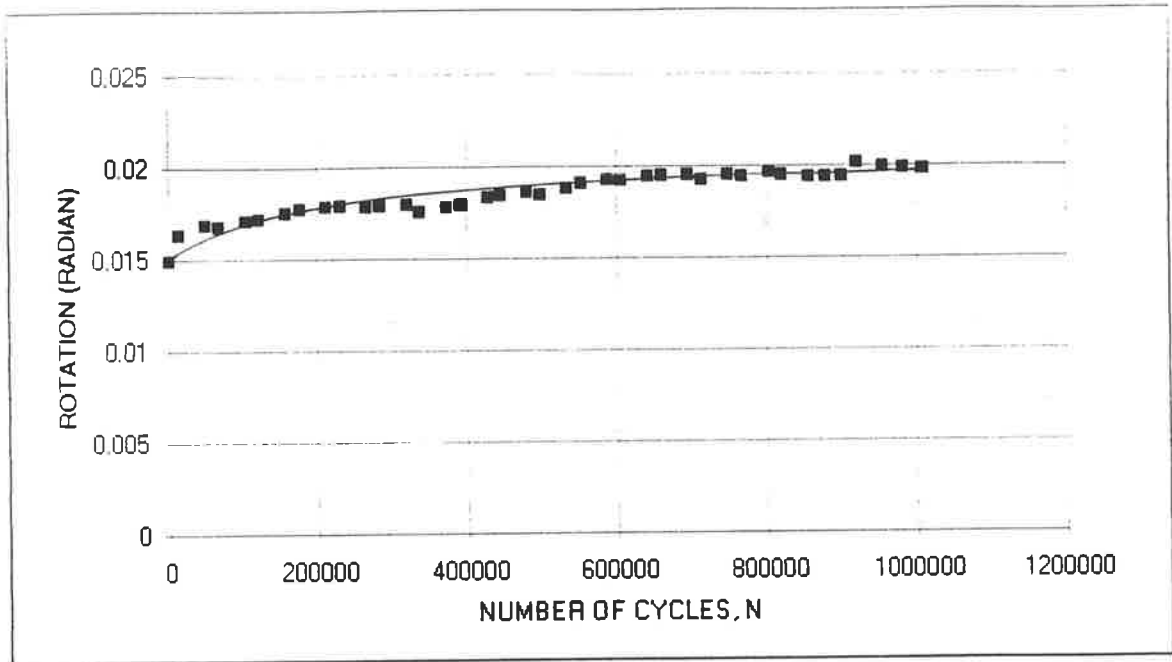


Figure 5.12 Rotation at 44kN-m vs number of cycles for specimen 3

In order to remove any creep effects from the analysis, $\Delta\theta$ vs number of cycles for specimen 3 is plotted in Figure 5.13. As for the second test specimen, there was a gradual increase in $\Delta\theta$ during the course of the experiment.

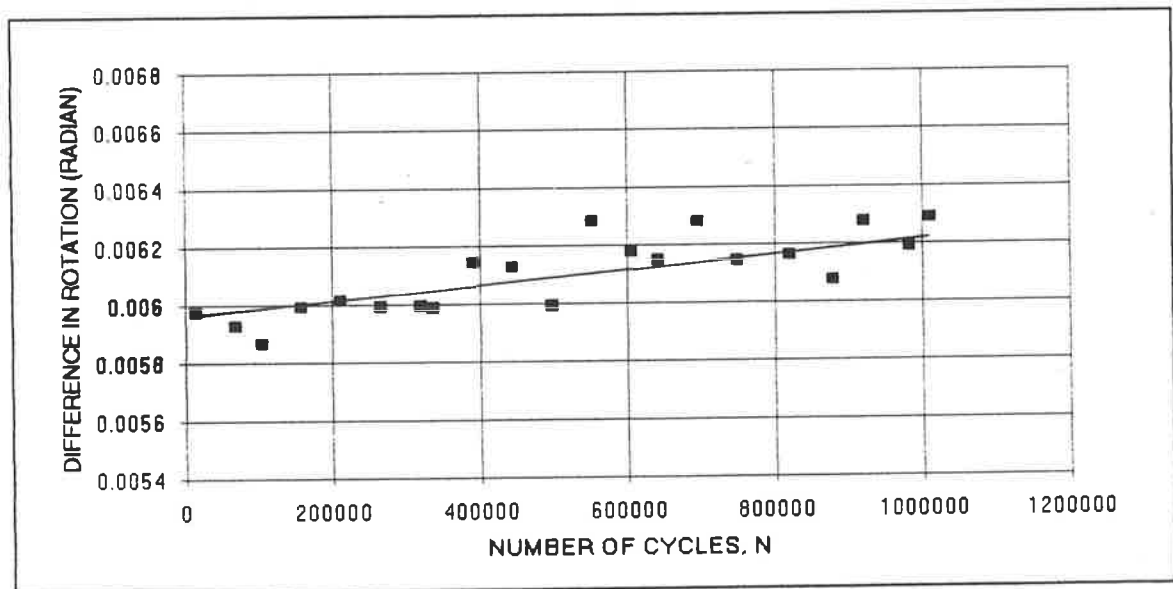


Figure 5.13 Difference in rotation vs number of cycles for specimen 3

As for specimen 2, the instantaneous joint stiffness K (normalized by K_i) was plotted against N (Figure 5.14). This plot also showed a gradual decrease in joint stiffness, of the order of 10% with $K_i = 5320\text{kN}\cdot\text{m}/\text{rad}$ and $K = 5055\text{kN}\cdot\text{m}/\text{rad}$ after million cycles. In specimen 2, the initial stiffness of $5519\text{kN}\cdot\text{m}/\text{rad}$ dropped to $3436\text{kN}\cdot\text{m}/\text{rad}$ after 250,000 cycles. Thus, a less significant stiffness depreciation was observed in specimen 3 despite a larger number of loading cycles.

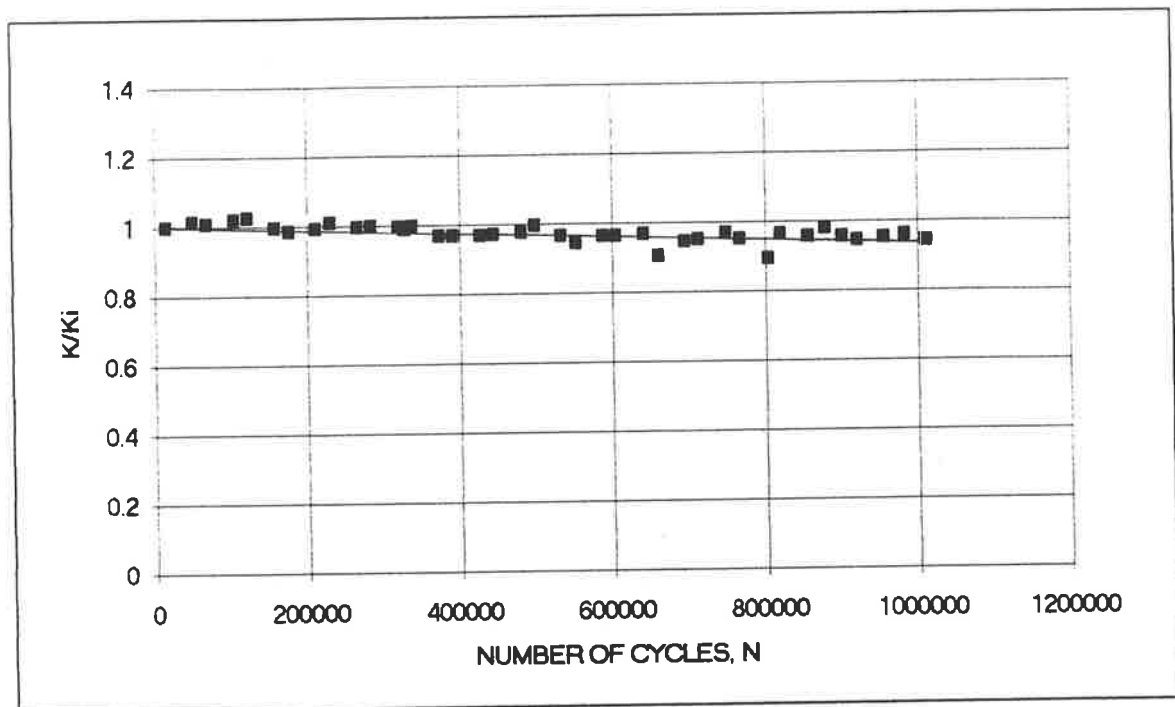


Figure 5.14 stiffness vs number of cycles for specimen 3

Specimen 3 was tested statically to failure after successfully withstanding one million cycles of cyclic loading. Figure 5.15 shows the moment vs rotation data collected from this test. An estimate of the joint secant stiffness from this joint plot was $3207\text{kN}\cdot\text{m}/\text{rad}$ and in good agreement with the joint stiffness for specimens 1 and 2.

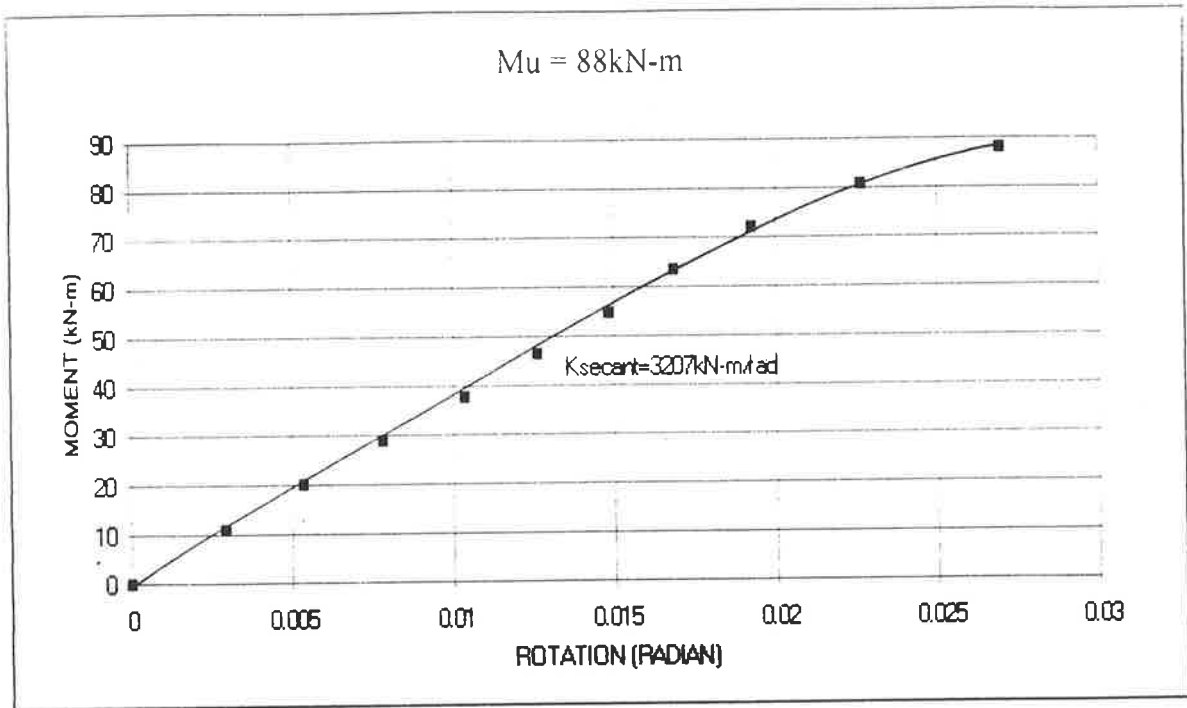


Figure 5.15 Moment vs rotation after 1,000,000 cycles for specimen 3 (static test to failure)

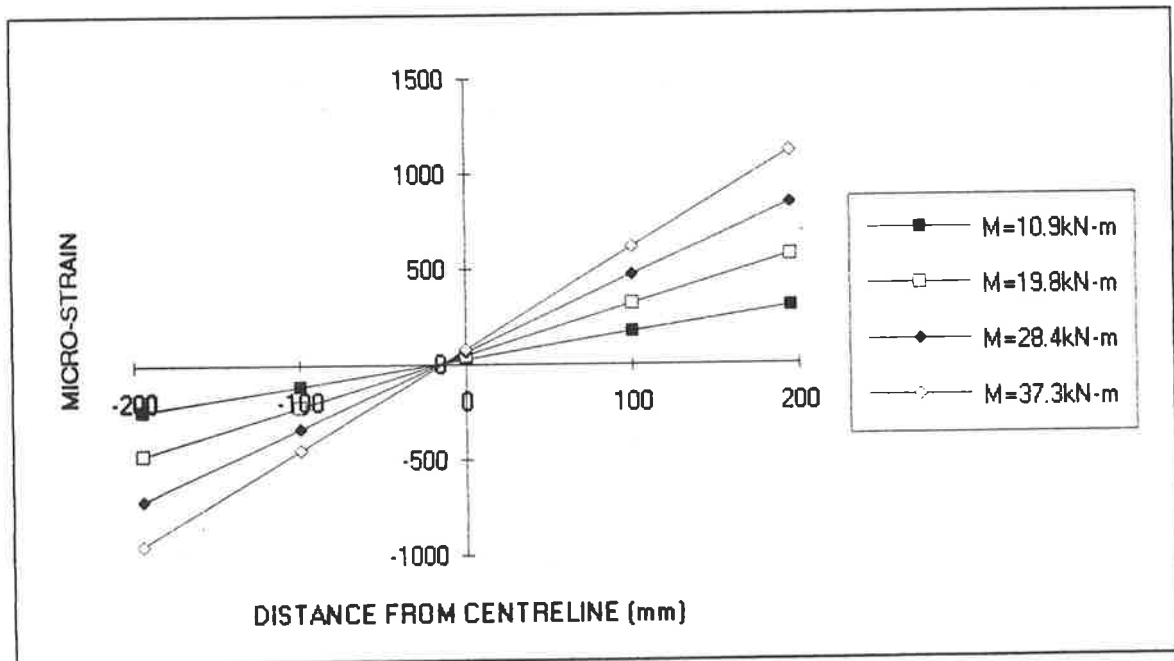


Figure 5.16 Strain across rafter during initial loading for specimen 3

In the early stages of the test while the specimen was being loaded initially upto the 44kN-m load, the rafter strain profile was essentially linear (see Figure 5.16). Slightly more tension than compression was observed and the neutral axis was very close to the centreline of the LVL member. These values apply before any cyclic loading.

The strain profiles were essentially linear for all readings taken during the periodic slow cycles before the half million cycle mark was reached. However, as the number of the cycles approached the 1 million mark, the linearity of the strain profile was lost and neutral axis shifted to a point between strain gauge 3 and strain gauge 4 (see Figure 5.17). Unlike the initial linear profile exhibited by the rafter in Figure 5.16, the member exhibited an inelastic strain profile which suggested yielding of the LVL might have occurred. More surprisingly, tension strain was observed in strain gauge 1 (i.e., -200mm from the centreline) at $M = 30.6\text{kN-m}$. This was probably due to the fact that the gauge was broken or the bonding became loose. In either case, gauge 1 readings were considered to be unreliable hereafter. At $M=62.0\text{kN-m}$, an estimate of the strain at position 1 was $-1504\mu\epsilon$ in order to achieve identical P_{strain} and P_{statics} at a value of 29.66kN. The respective M_{strain} was 42.0kN-m and M_{statics} was 50.7kN-m.

The strain profile at joint prior to failure during the final static loading test (Figure 5.18) was also highly irregular and was considered to be inaccurate for the same reasons as explained above.

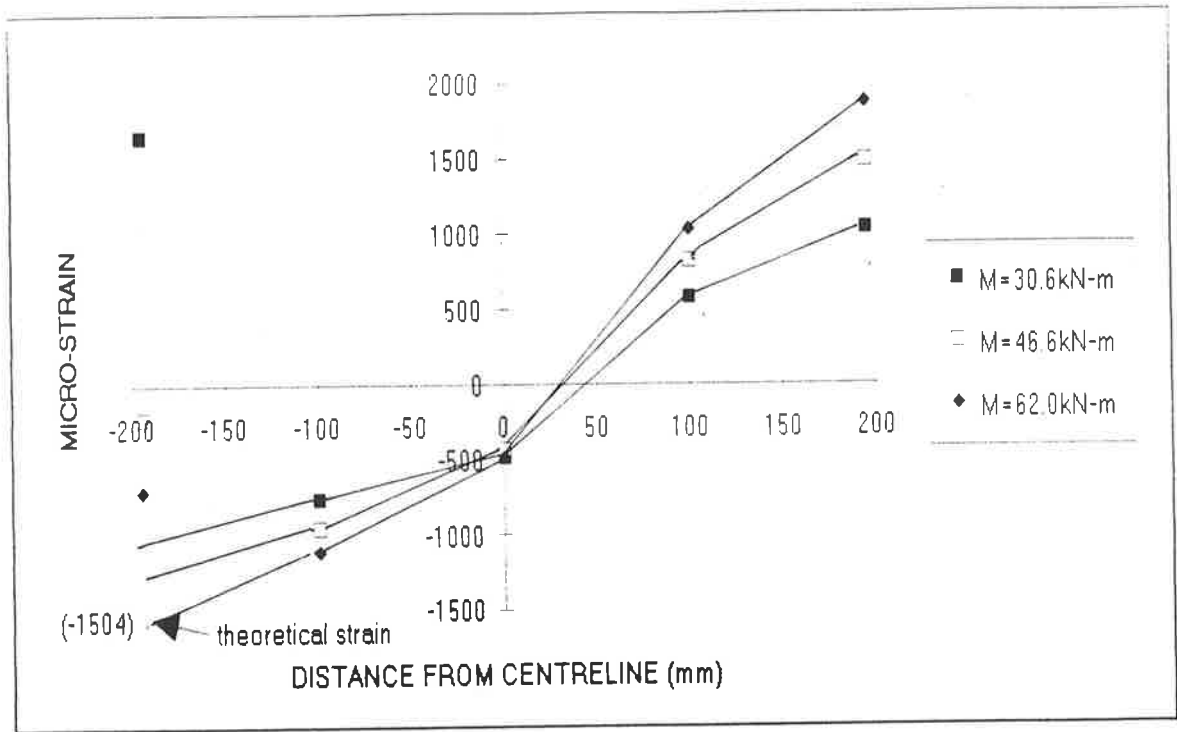


Figure 5.17 Strain across rafter at $N=1009752$ for specimen 3

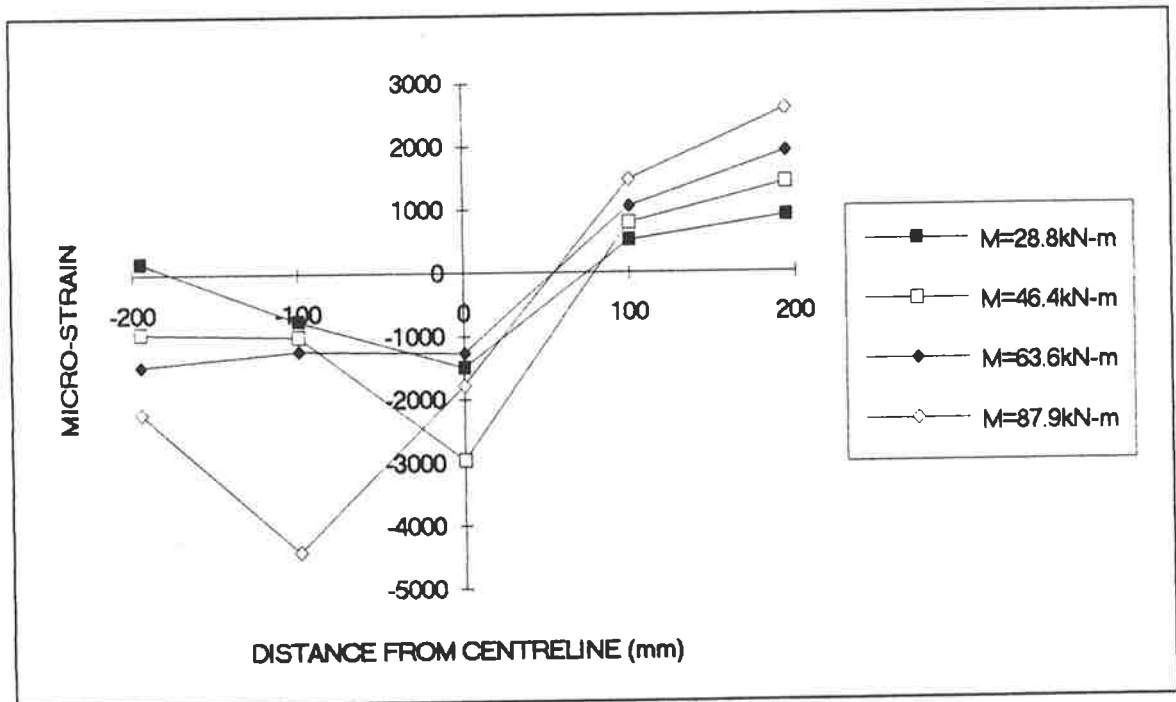


Figure 5.18 Strain across rafter during the final static test for specimen 3

About 50% less strain was experienced by the column since that leg has a shorter length (about 2/3 of the strain experienced by the rafter). The profile on the column was generally linear and the neutral axis was situated near the centreline for readings taken prior to the half million cycle mark (Figure 5.19).

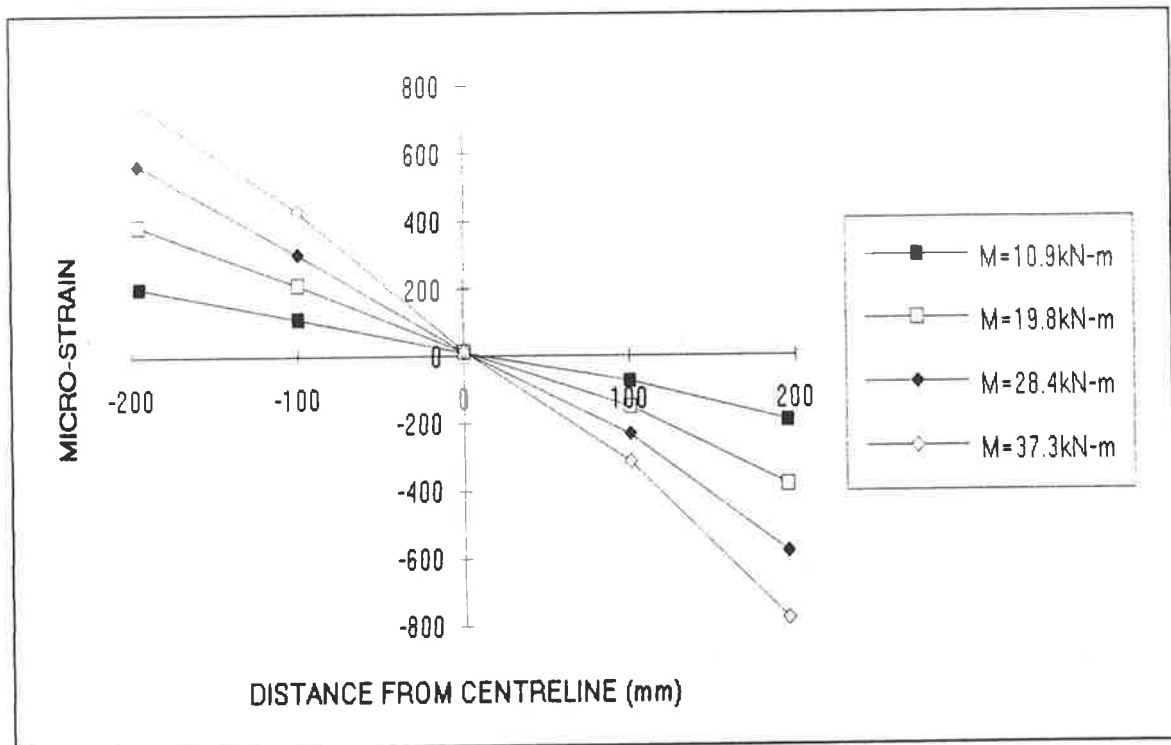


Figure 5.19 Strain across column at initial loading for specimen 3

However, after about 1 million cycles, the strain position next to the neutral axis (strain gauge 7) registered a higher than expected strain. This was due either to surface fibre failure or to yielding.

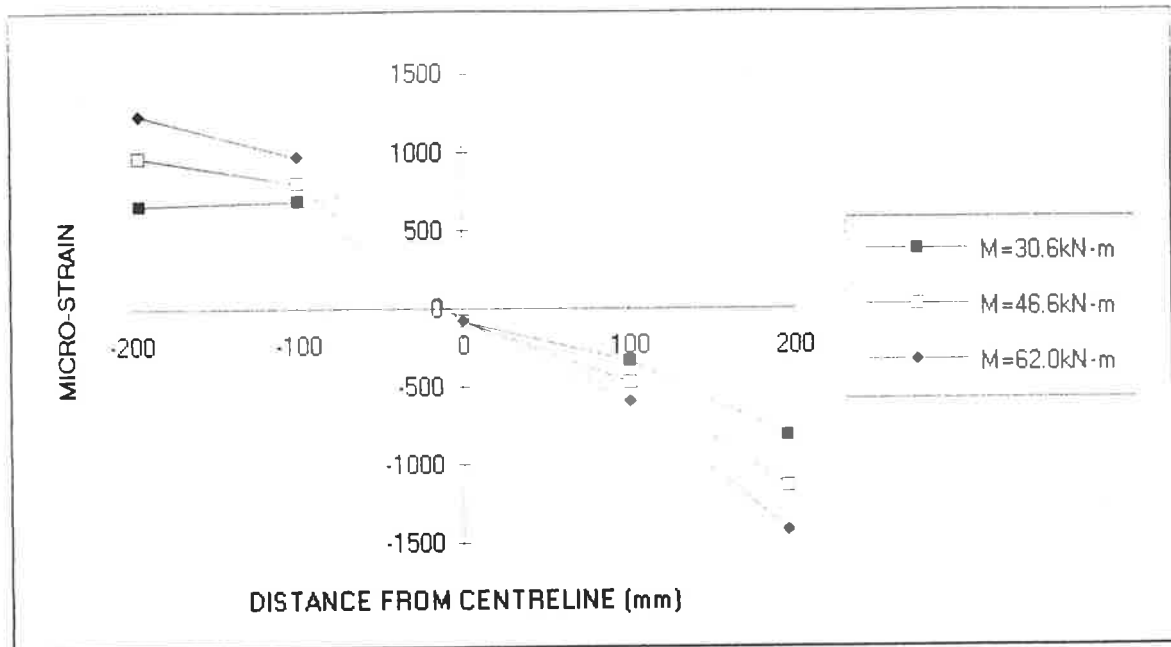


Figure 5.20 Strain across column at $N=1009752$ for specimen 3

Close correlation between P_{strain} and P_{statics} (24.9kN and 24.3kN respectively) and bending moments, at the section of the column 200mm from the gusset, (32.3kN-m and 33.5kN-m respectively) were observed at an applied moment of 62kN-m (from Figure 5.20). The strain profile at failure was non-linear and similar to that recorded after 1009752 cycles of loading.

Once the specimen had successfully withstood over one million cycles of dynamic loading, the specimen was tested to failure which gave an ultimate load of 50kN ($M_c=88\text{kN-m}$). The specimen suffered a bending/tension failure (Figure 5.21) at the LVL rafter leg along the cross section where the strain gauges were mounted at a moment of 88kN-m (same moment as specimen 2 and 92% that of specimen 1).

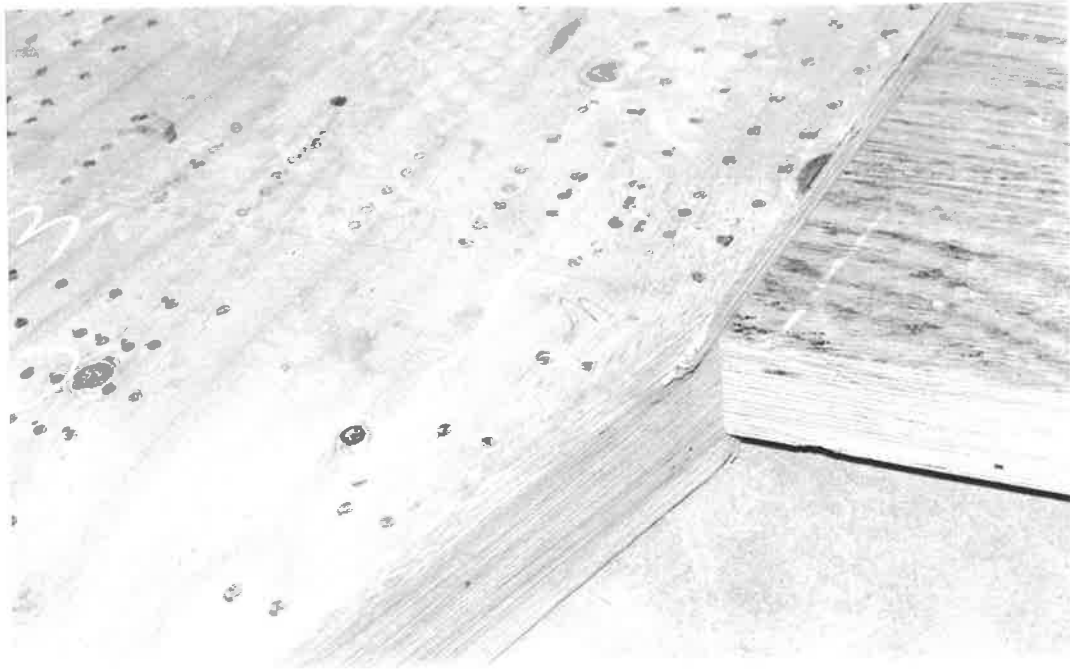


Figure 5.21 Failure mode for specimen 3

SPECIMEN 4

This specimen was subjected to 500,000 cycles of fatigue loading at the same load level as the previous test. With a cyclic frequency of 0.6Hz, the specimen was tested for 10 days with continual dynamic loading and then tested statically to failure in order to find the residual static strength.

Since test specimens 2 and 3 shared the same magnitude of residual strength of 88kN-m, irrespective of the number of cycles, the predetermined number of cycles for this joint specimen was between 250,000 and 1000,000 to complete the picture of fatigue behaviour.

The rotation at 44kN-m vs number of cycles curve in Figure 5.22 shows gradual increase in the rotation from 0.0136radian to 0.0178radian. (increase of 30% in rotation at 44kN-m).

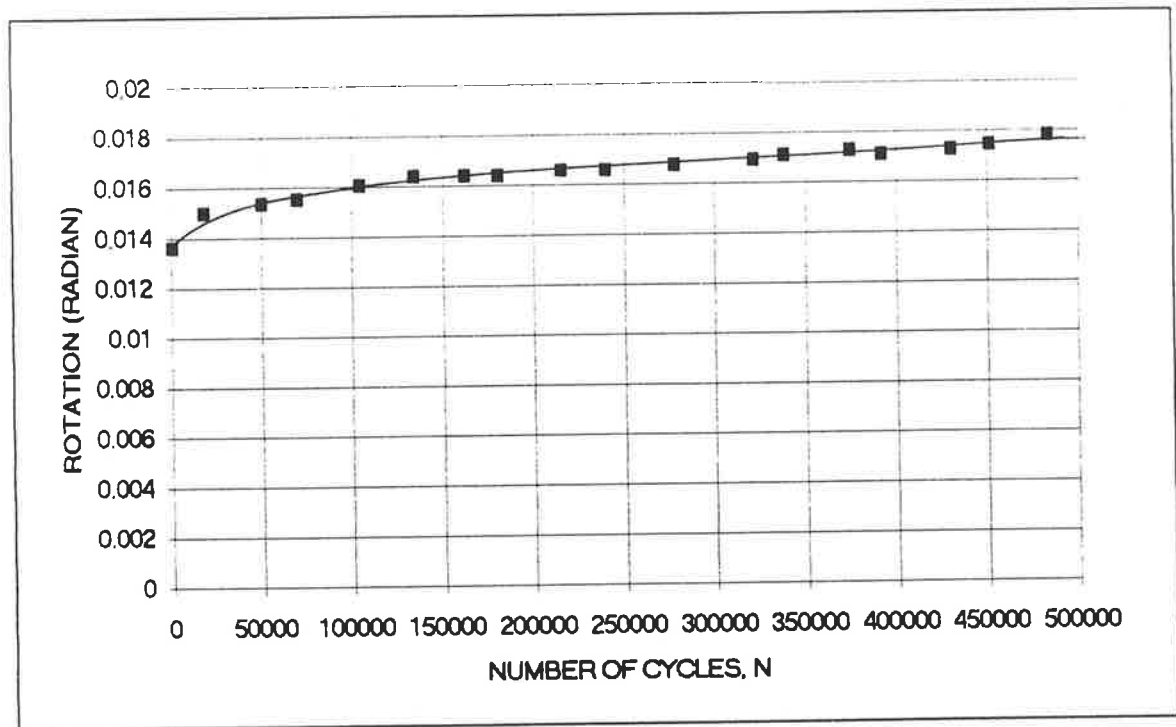


Figure 5.22 Rotation at 44kN-m vs number of cycles for specimen 4

As discussed earlier, this increase in rotation corresponds to a creep curve. However, a plot of the difference in rotation, $\Delta\theta$, vs number of cycles indicated an overall decrease as the number of cycle was increased (Figure 5.23).

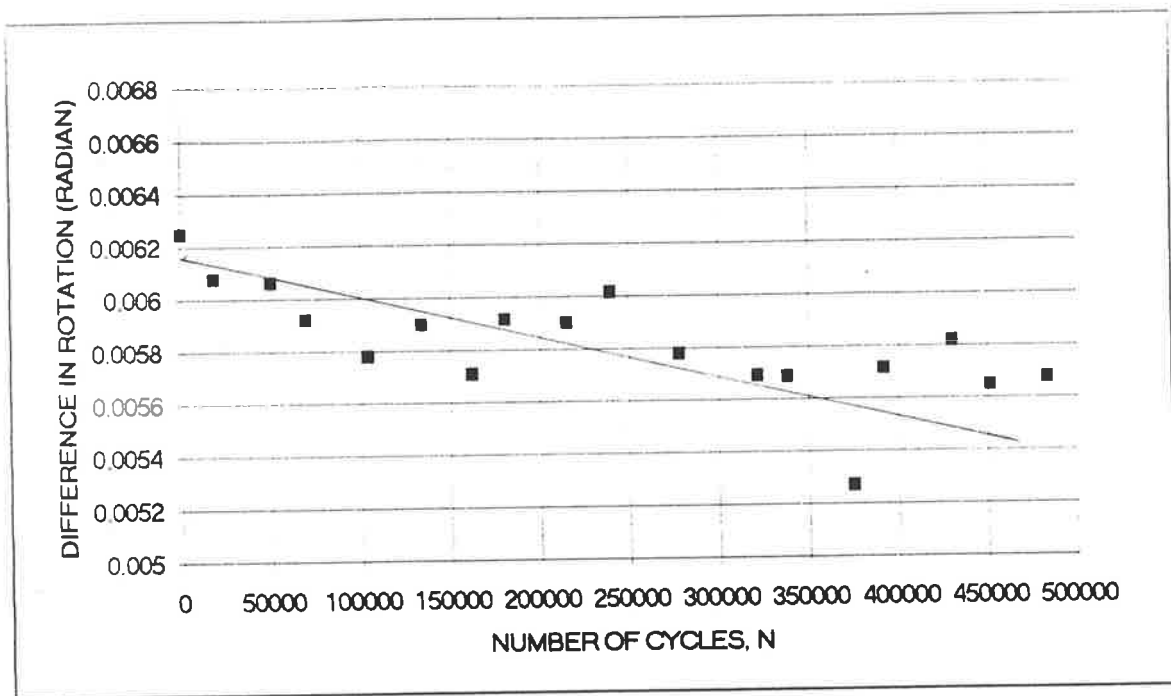


Figure 5.23 Difference in rotation vs number of cycles for specimen 4

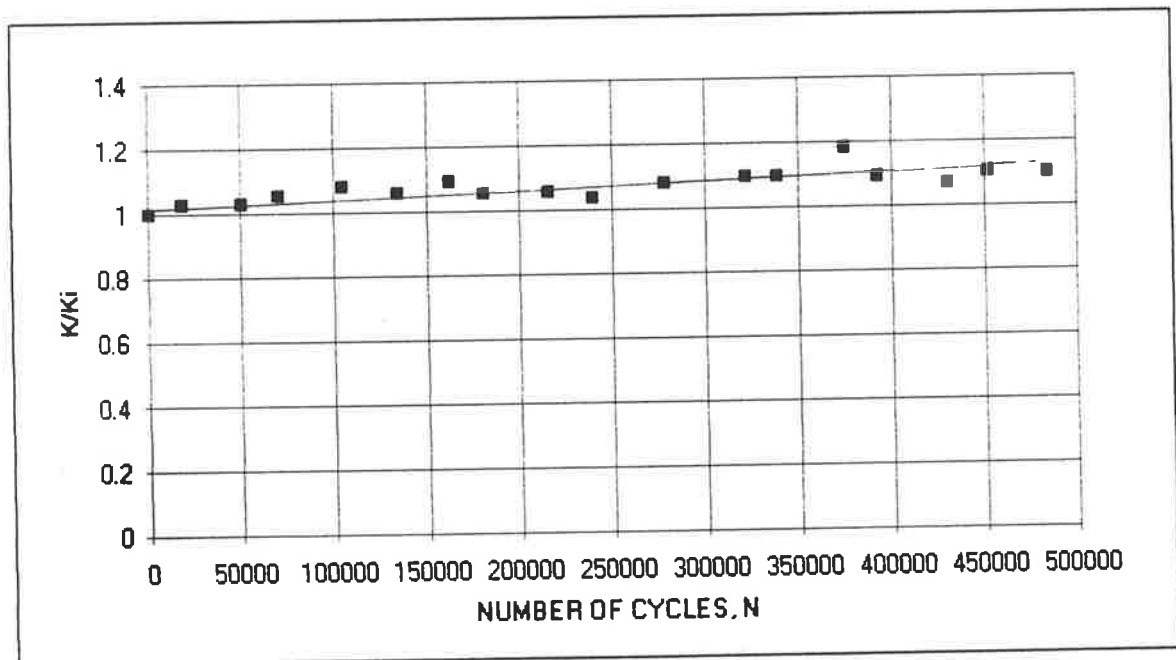


Figure 5.24 Stiffness vs number of cycles for specimen 4

The points in the graph did not form a smooth line but did show an overall drop in difference in rotation, $\Delta\theta$, within a single load cycle. This result disagreed with the previous tests where $\Delta\theta$ was seen to increase. The instantaneous stiffness normalised against K_i and plotted in Figure 5.24 showed a general increasing trend which was in contrast to previous results.

There was no obvious reason for the increase in stiffness. The final static secant stiffness was found to be 4372kN-m/rad from the results of the static test which are shown in Figure 5.25. This stiffness was 36% higher than that from the previous test.

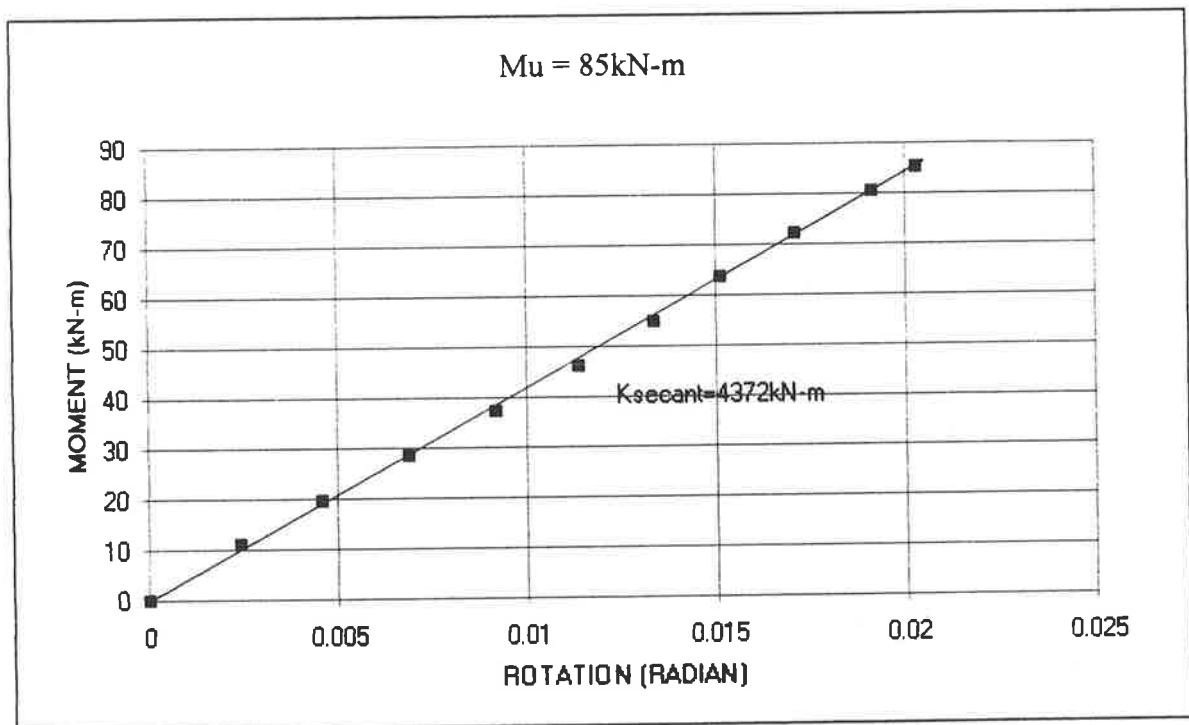


Figure 5.25 Moment vs rotation at failure loading for specimen 4
(static test to failure)

All the rafter member strain profiles were nearly linear with the zero strain point situated near the rafter centreline with compressive strain very similar to the tensile strain (see Figure 5.26).

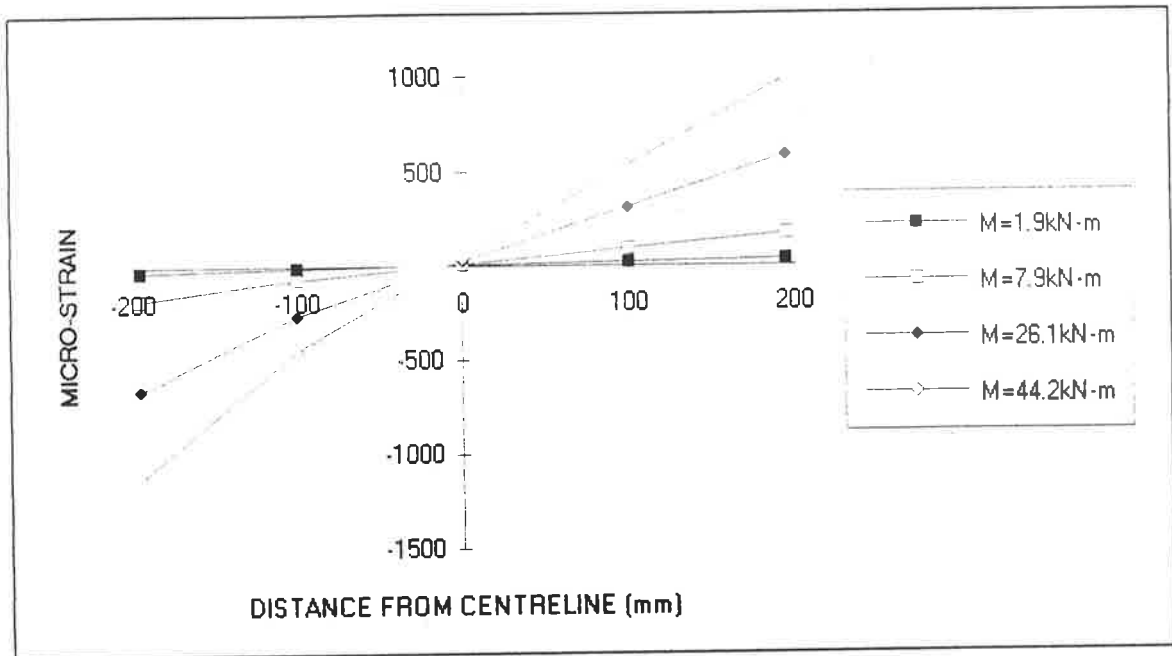


Figure 5.26 Strain across rafter at $N=206$ for specimen 4

With respect to the effect of fatigue loads, the strain profile shape did not alter significantly between cycle numbers $N=206$ and $N=483389$, and only resulted in a 10% increase in strain (see Figure 5.27). From Figure 5.27, P_{strain} was 15.4kN while M_{strain} was 30.7kN-m at the strain gauges location for an applied moment of 62.0kN-m. P_{statics} was 29.7kN and M_{statics} was 50.7kN-m calculated from simple statics.

On the other hand, the strain profile for the column section exhibited a very different pattern. It was never linear with the neutral axis shifting with increasing load and cycles (see Figures 5.28 and 5.29).

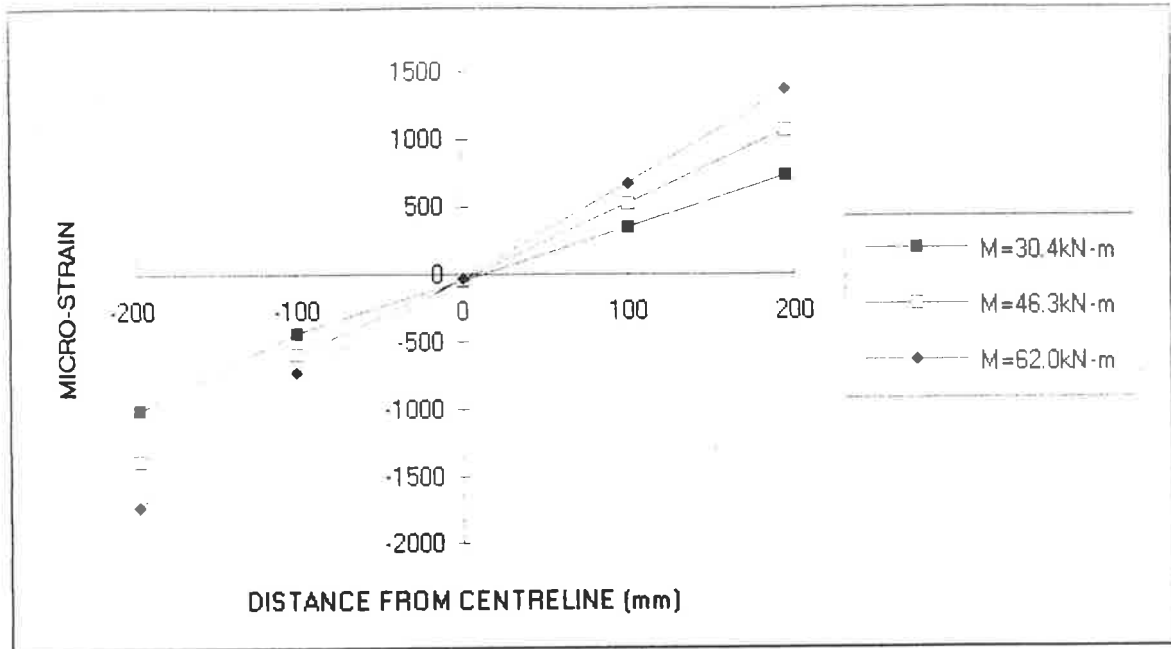


Figure 5.27 Strain across rafter at N=483389 for specimen 4

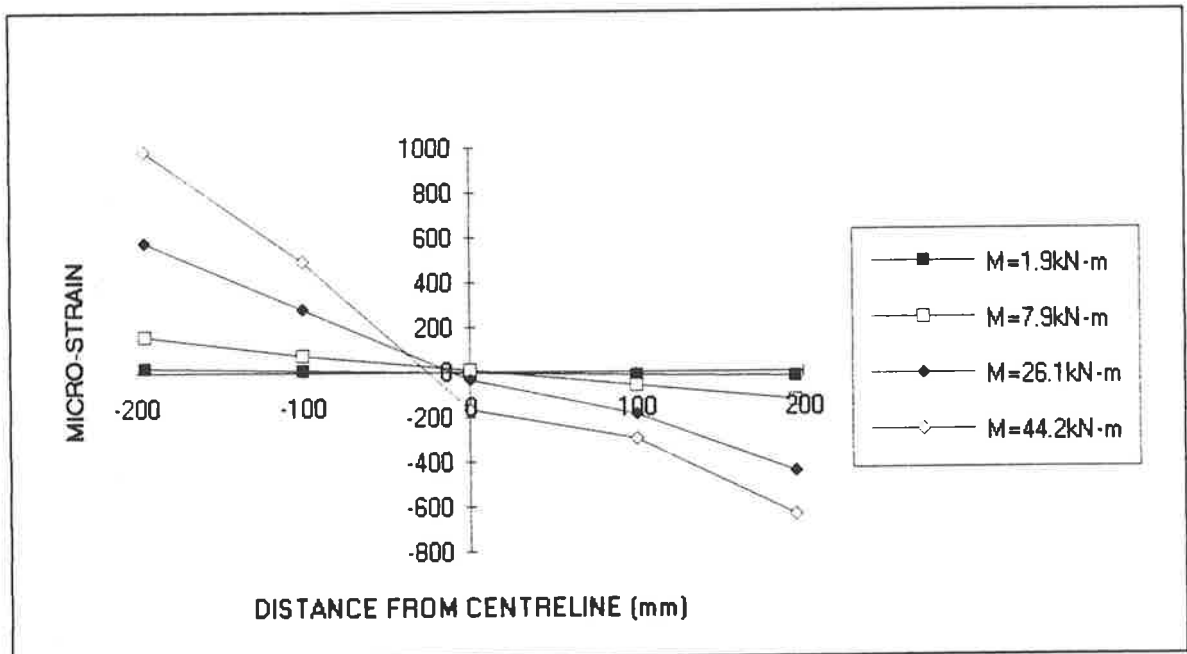


Figure 5.28 Strain across column at N=206 for specimen 4

When comparing the strain profile shapes at $N=206$ with that at $N=483389$ cycles, one can see that although the extreme strain magnitudes were similar (only about 10% increase), the neutral axis had shifted from the tension side to compression side as shown in Figure 5.29. This suggested inelastic behaviour in the column and associated permanent deformations in this leg. Even during the final static test to failure, the neutral axis was shifting with load change. Integrating the strain profile gave P_{strain} of 30.7kN and M_{strain} of 25.7kN-m as compared to P_{statics} of 24.3kN and M_{statics} of 33.5kN-m for an applied moment of 62kN-m.

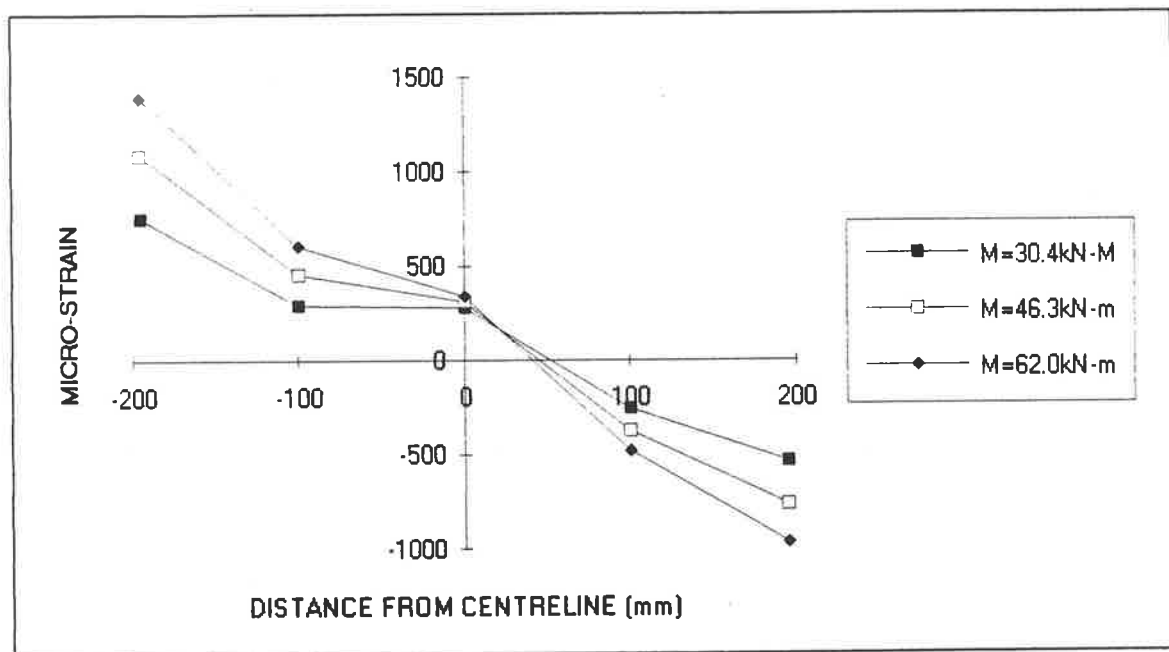


Figure 5.29 Strain across column at $N=483389$ for specimen 4

The ultimate load occurred at $M = 85\text{kN-m}$ with a tension failure of the plywood gusset plate section along the line between the LVL members (see Figure 5.30). This failure mode was identical to that of specimen 2.

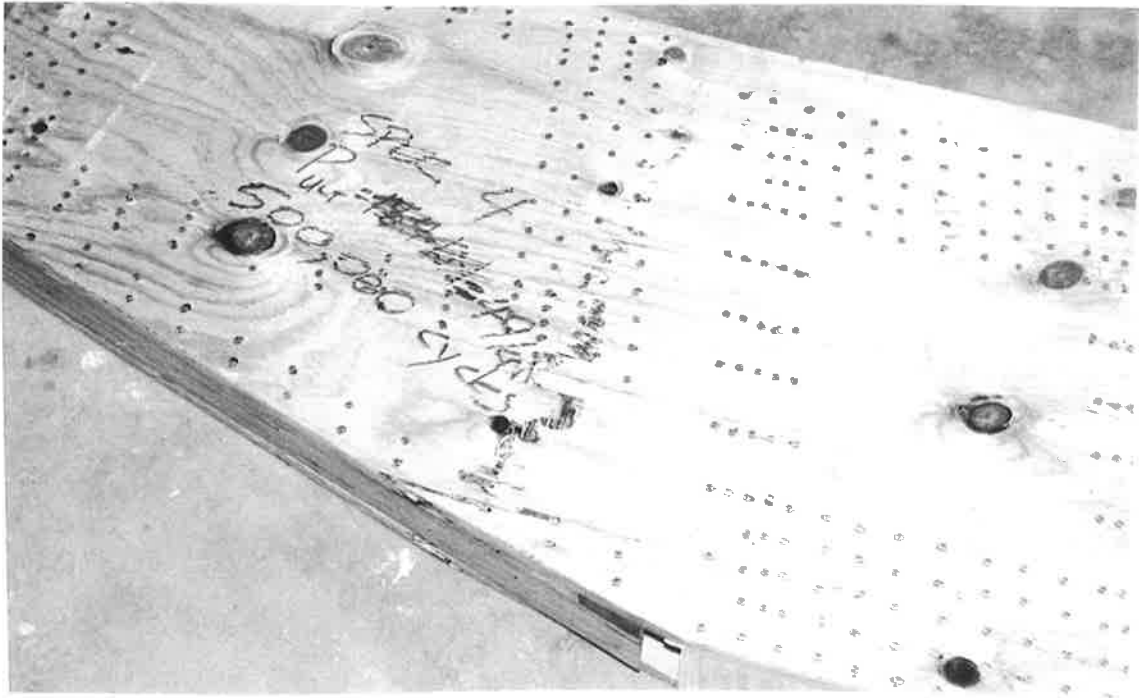


Figure 5.30 Failure mode of specimen 4

SPECIMEN 5

Specimen 5 was subjected to a simple static loading test to failure in order to confirm the experimental moment capacity of the joint determined by the same test on specimen 1. The reason for conducting a second static test was that in assessing the effect which fatigue loading has on the residual strength of this type of the joint, it was important to know accurately what the initial static strength of each specimen was. Since it was impossible to determine the initial static strength of a specimen before any cyclic loading, this test was aimed at establishing a better estimate of the typical strength. Furthermore, it gave an indication of whether the differences in residual static strength for the fatigue specimens were significant given the innate variation in specimen material properties..

The joint moment versus rotation is shown in Figure 5.31 for this test. The rate of increase in moment was less than that in rotation which indicated a softening joint as expected. This phenomenon was consistent with the previous static tests. The secant stiffness of this joint was estimated to be 3446kN-m/rad from this data. This value agreed with the static secant stiffnesses of specimens 2 and 3.

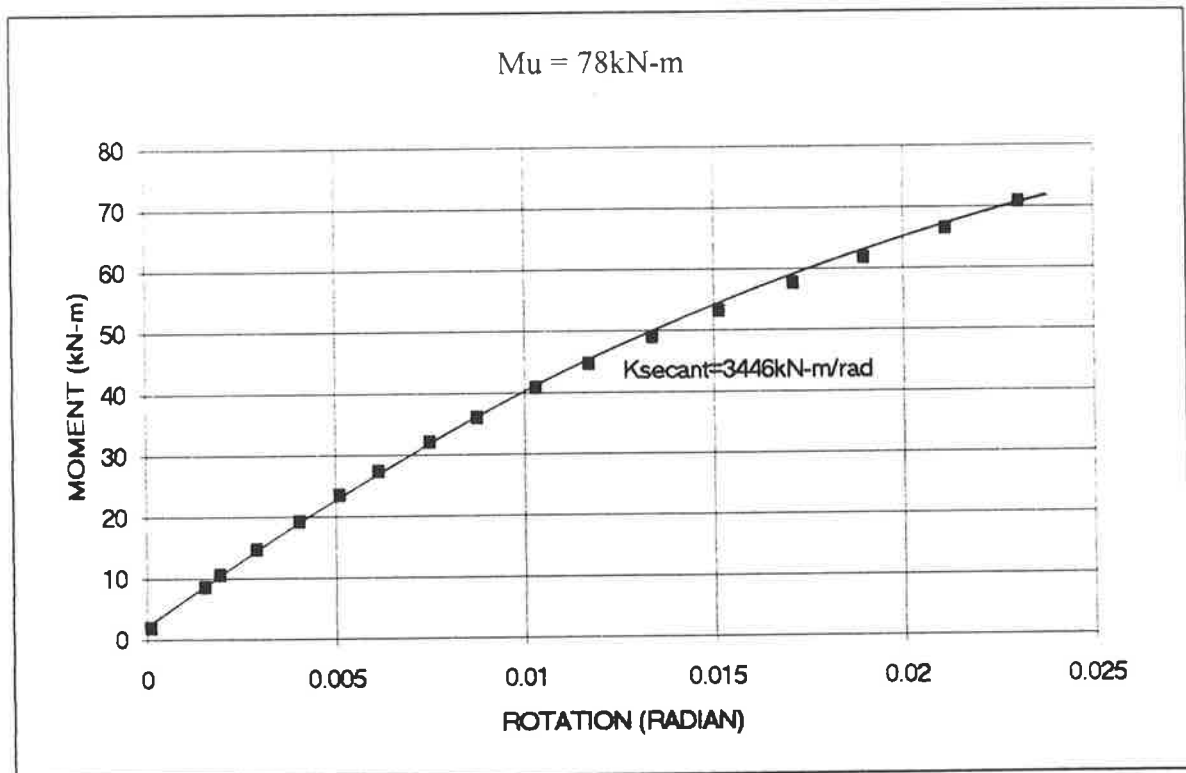


Figure 5.31 Moment vs rotation for specimen 5
(static test to failure)

The strain profile was linear in both LVL legs with the neutral axis located near the centreline (see Figures 5.32 and 5.33).

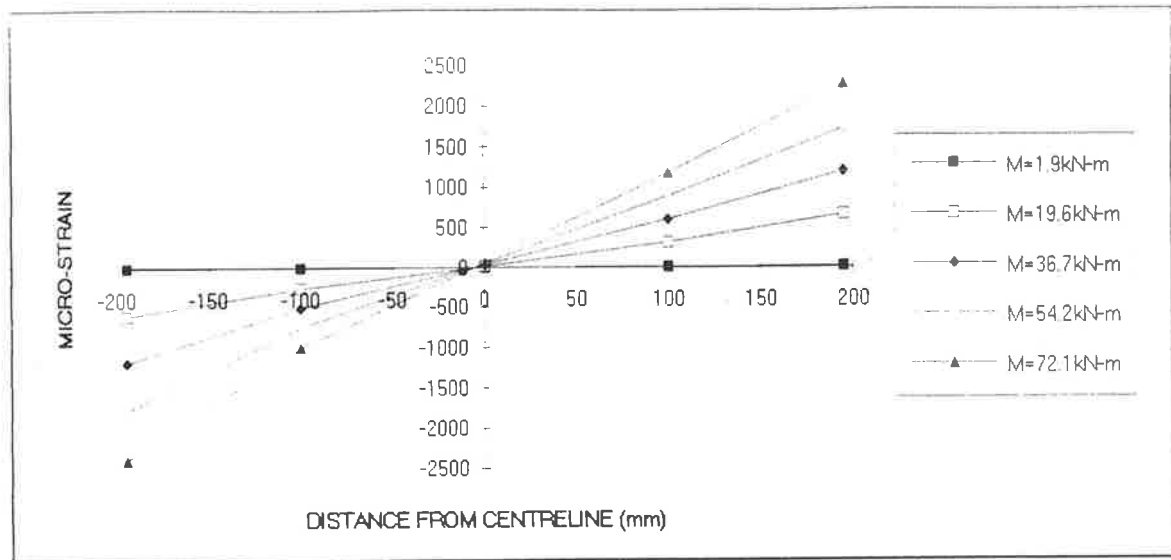


Figure 5.32 Strain across rafter for specimen 5

P_{strain} was 13.3kN (tension) which was surprisingly low as compared to P_{statics} of 34.5kN for the rafter member at an applied moment of 72.1kN-m, while M_{strain} was 51.2kN-m and M_{statics} was 58.9kN-m. With the same amplitude of load, the column member was found to have 34.4kN (tension) of P_{strain} and 28.3kN of P_{statics} while M_{strain} was 32.9kN-m and M_{statics} was 39.0kN-m.

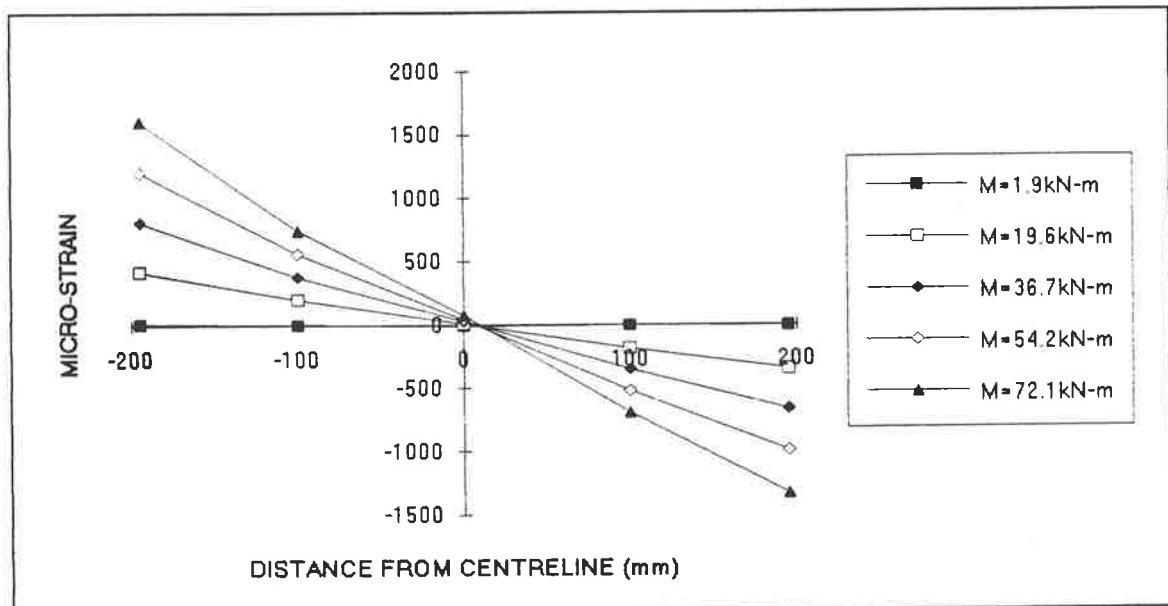


Figure 5.33 Strain across column for specimen 5

As with each of the previous static tests to failure, this specimen was loaded in 8.8kN-m increments until a fibre cracking sound was heard after the load level reached 53kN-m. Eventually, the failure occurred at a comparatively low ultimate moment capacity of 78kN-m (Ultimate moment for specimen 1 was 96kN-m). In the paper presented by Hunt and Bryant (23), it was reported that some moment resisting test specimens failed at embarrassingly low nominal timber stresses. These failures occurred as a consequence of tension fractures (perpendicular to the grain) in the outer laminates. In this experiment, a similar failure mode was observed in the gusset plate above the contact line of the LVL members (see Figure 5.34) and the corresponding bending stress, σ_b , was about 36.6MPa (where $\sigma_b = M/Z = 78 \times 10^6 / (2 \times 19 \times 580^2 + 6)$). This ultimate value was about twice the basic working stress of the plywood plates ($F'_b = 17\text{MPa}$).

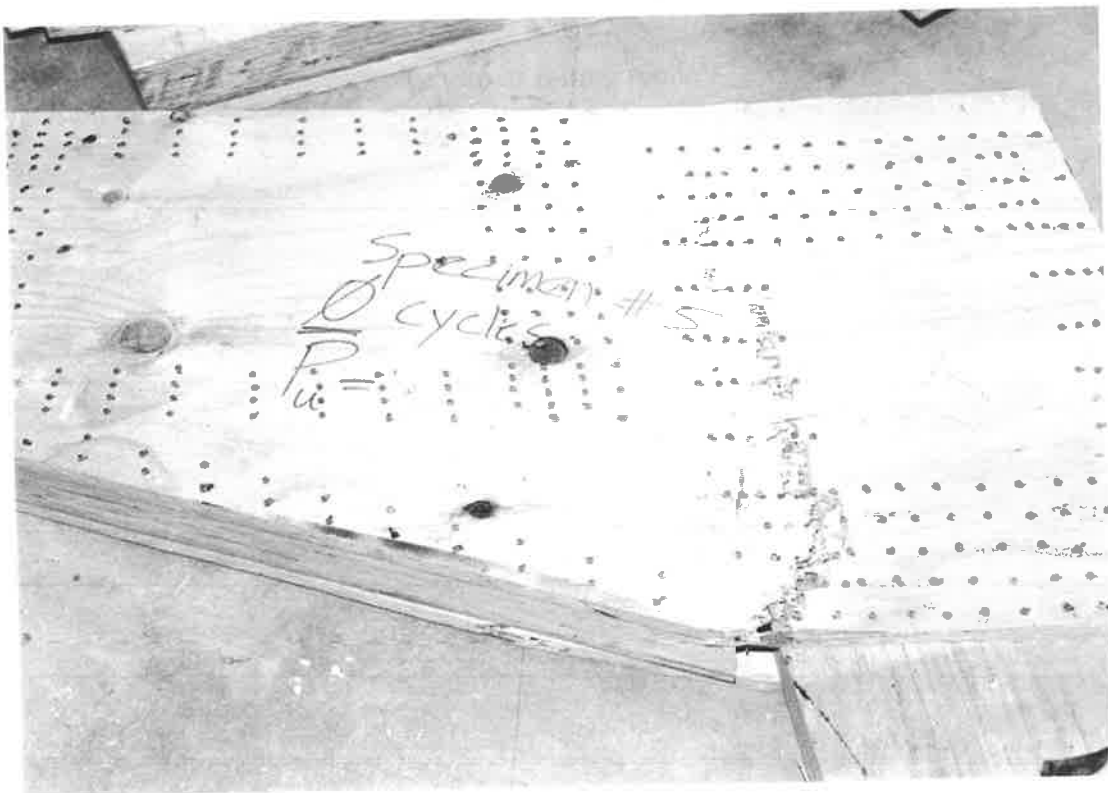


Figure 5.34 Failure mode for specimen 5

SPECIMEN 6

Specimen 6 was tested with a static moment of 44kN-m and a cyclic moment of ± 35 kN-m which gave a peak moment of 79kN-m. Early cyclic load behaviour was of special interest since it was thought that most of the decrease in strength occurred during the initial stages in the previous fatigue tests. The large amplitude of load was aimed at achieving a fatigue failure and thereby establishing the endurance limit for the joint.

Joint rotation at $M = 44$ kN-m is shown in Figure 5.35 as a function of the number of load cycles. It can be seen that there was a sharp increase in θ initially and a more gradual increase thereafter.

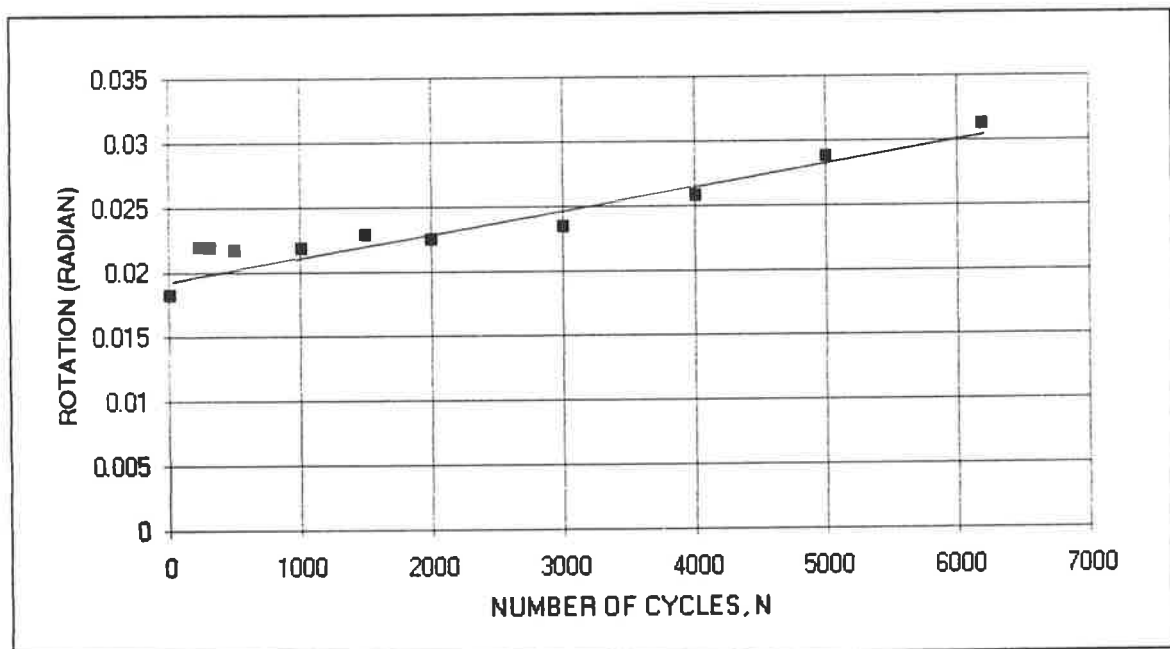


Figure 5.35 Rotation at 44kN-m vs number of cycles for specimen 6

The scatter in the data in the early stages of the test suggested there might be some nail bearing relocation and initial timber fibre failure. However, from 3,000 cycles onwards, the joint was well behaved and the plot shows a gradual increase in joint rotation.

The plot of the difference in rotation, $\Delta\theta$ (Figure 5.36) has an even more prominent initial jump during the first 500 cycles of loading. Likewise, the curve shows a clear trend of increasing rotations with continued cycling.

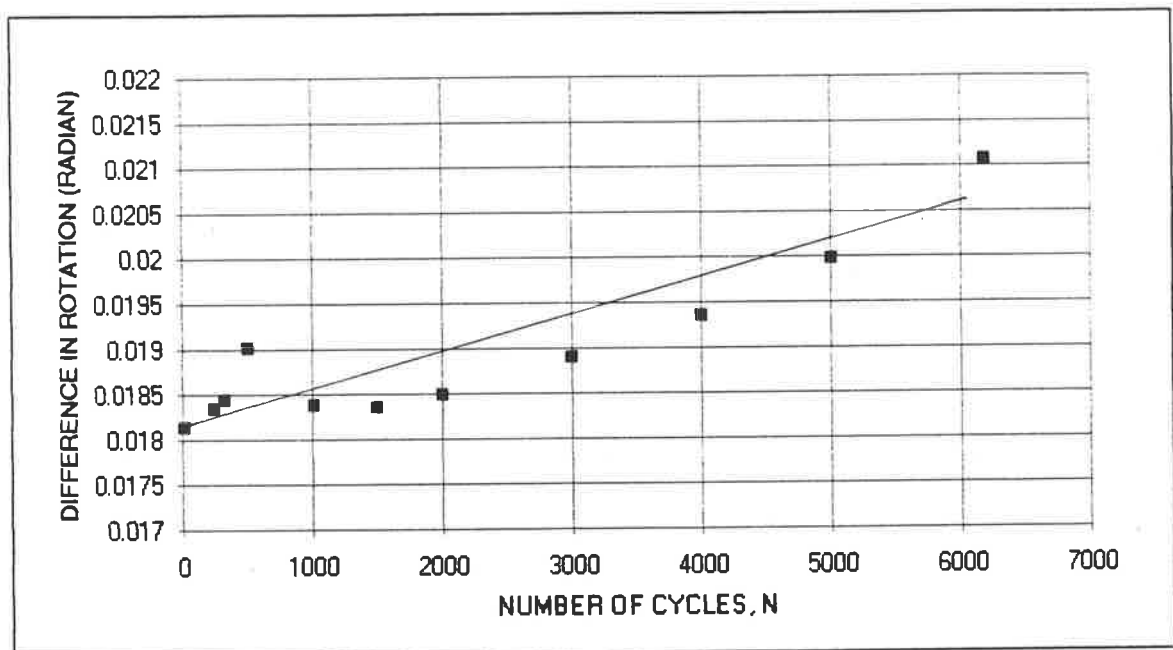


Figure 5.36 Difference in rotation vs number of cycles for specimen 6

Since the moment change, ΔM , was constant for each load cycle, the joint stiffness was seen to decrease (Figure 5.37) to a value of about 85% of the initial stiffness, K_i , just prior to failure.

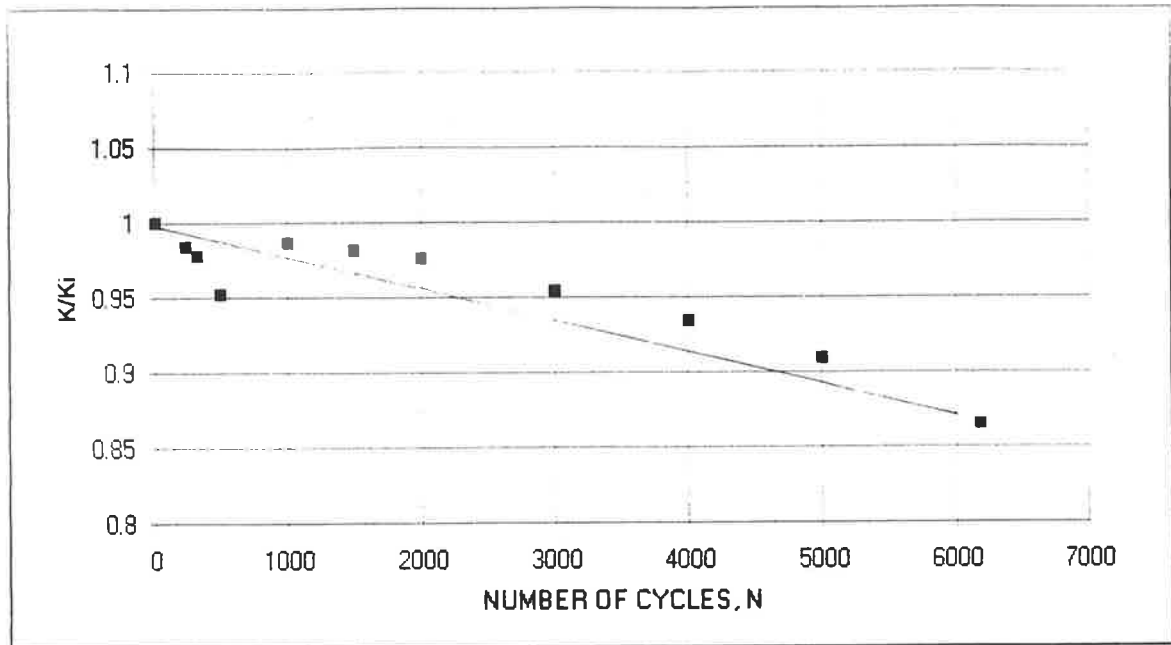


Figure 5.37 Stiffness vs number of cycles for specimen 6

Interestingly, the rafter strain profile was seen to be nearly linear at all load levels while the specimen was initially loaded before cycling was begun (Figure 5.38).

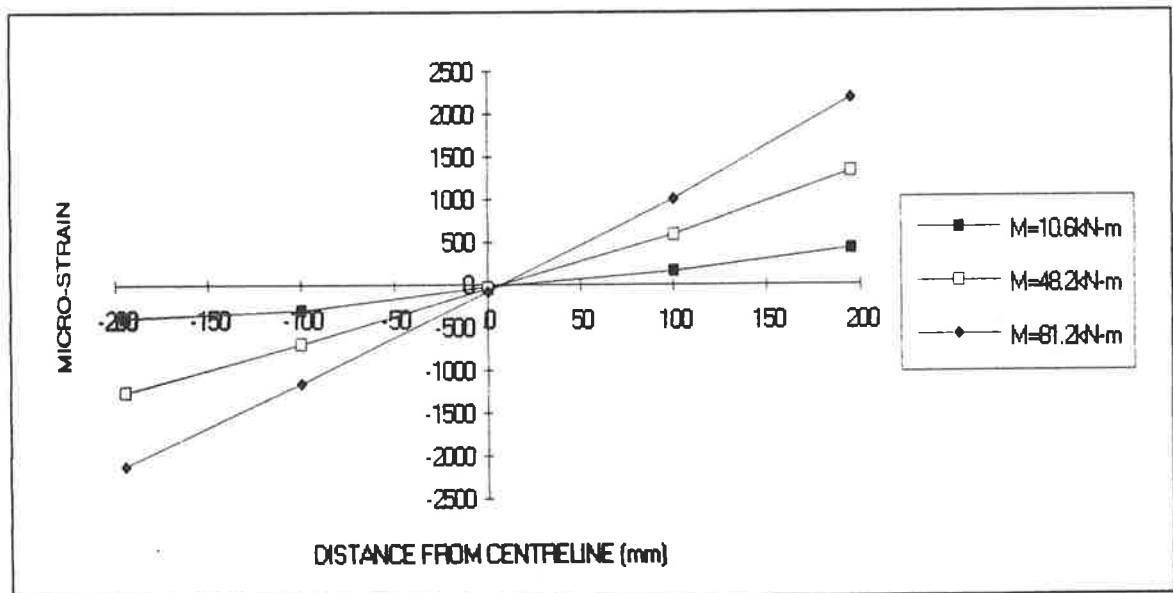


Figure 5.38 Strain across rafter at $N=10$ for specimen 6

However, as the number of cycles increased ($N=3000$, $N=6182$), the extreme fibre strains increased by 19% and the strain profile became non-linear when number of cycles, N , was 6182 (see Figure 5.39).

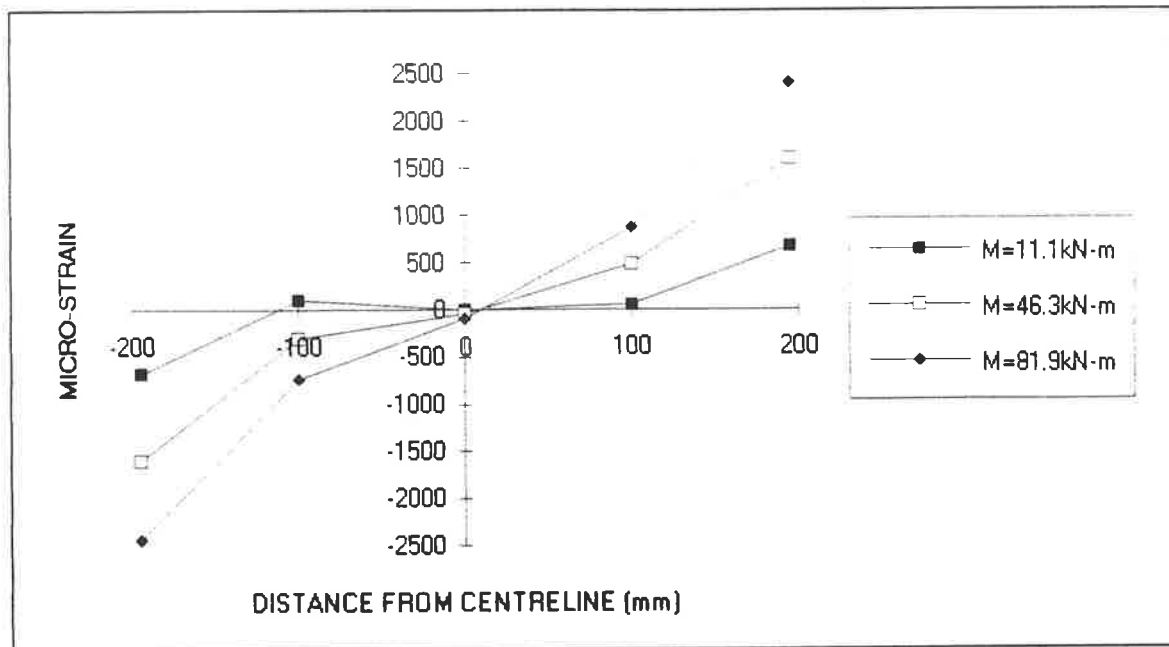


Figure 5.39 Strain across rafter at $N=6182$ for specimen 6

The strain profile of the rafter member gave surprisingly bad correlation between P_{strain} of -6.5kN and P_{statics} of 39.4kN and M_{strain} of 46.2kN-m and M_{statics} of 67.3kN-m at 81.9kN-m applied moment. These suggested unreliability of the strain gauges during such large cyclic loading. Although the maximum tensile strain limit for the strain gauges was 1.2% ($12000\mu\epsilon$), the cyclic loading induced a maximum strain of approximately $2500\mu\epsilon$ which could fail the gauge bonding or the strain gauges themselves due to fatigue.

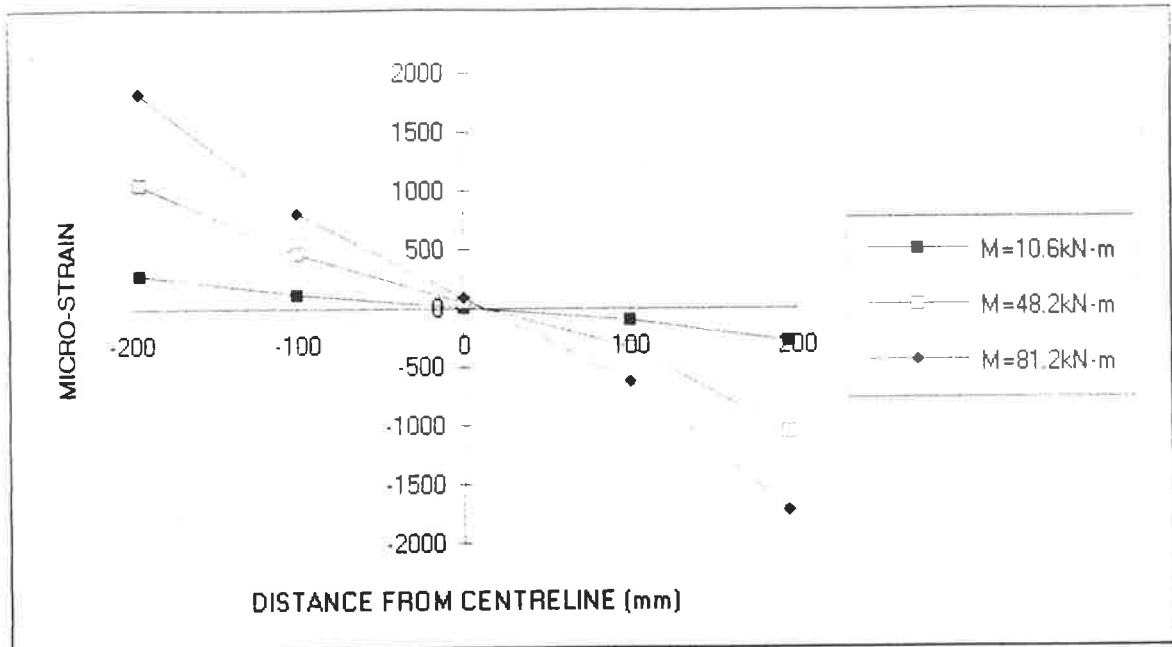


Figure 5.40 Strain across column at $N=10$ for specimen 6

While the column strain profile was never as linear as the strain profile for the rafter member (Figure 5.40), the profile become highly non-linear by cycle number $N=6182$ (see Figure 5.41).

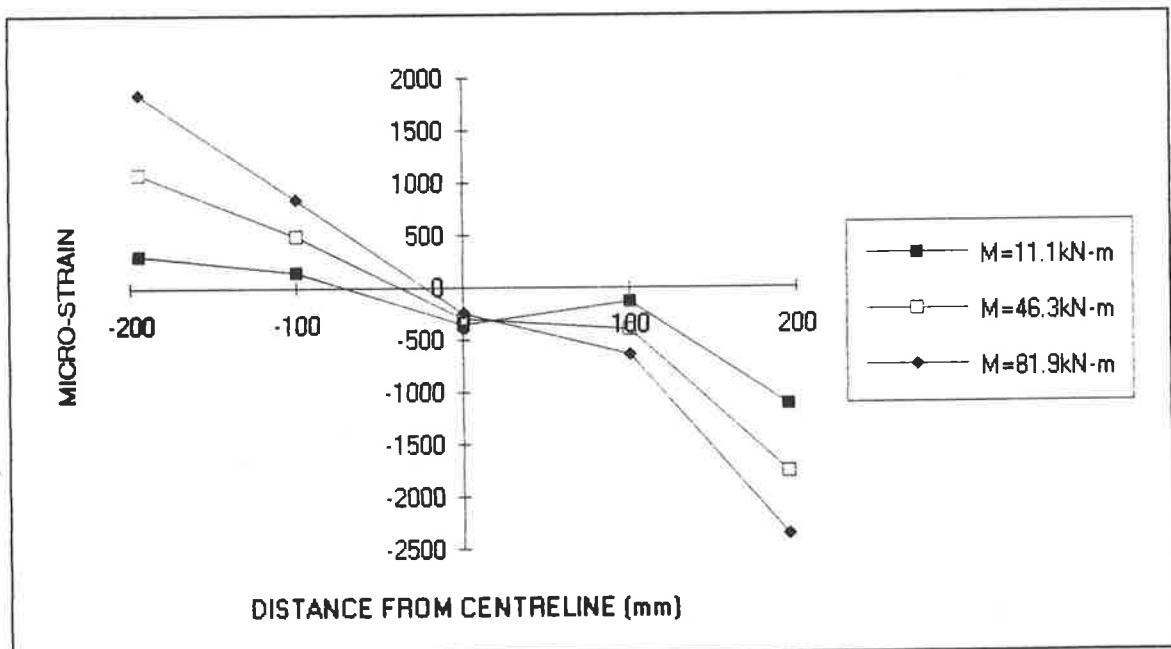


Figure 5.41 strain across column at $N=6182$ for specimen 6

In the comparison of the axial load (-26.0kN) and bending moment (41.9kN-m) from strain with the axial load (32.3kN) and bending moment (44.5kN-m) from statics, the large difference in axial loads suggested that the strain gauge readings were inaccurate.

In this test, significant gaps were observed between the LVL members and the gusset plate. The joint survived 6200 cycles of the loading before it failed in bending/tension across the rafter (see Figure 5.42).

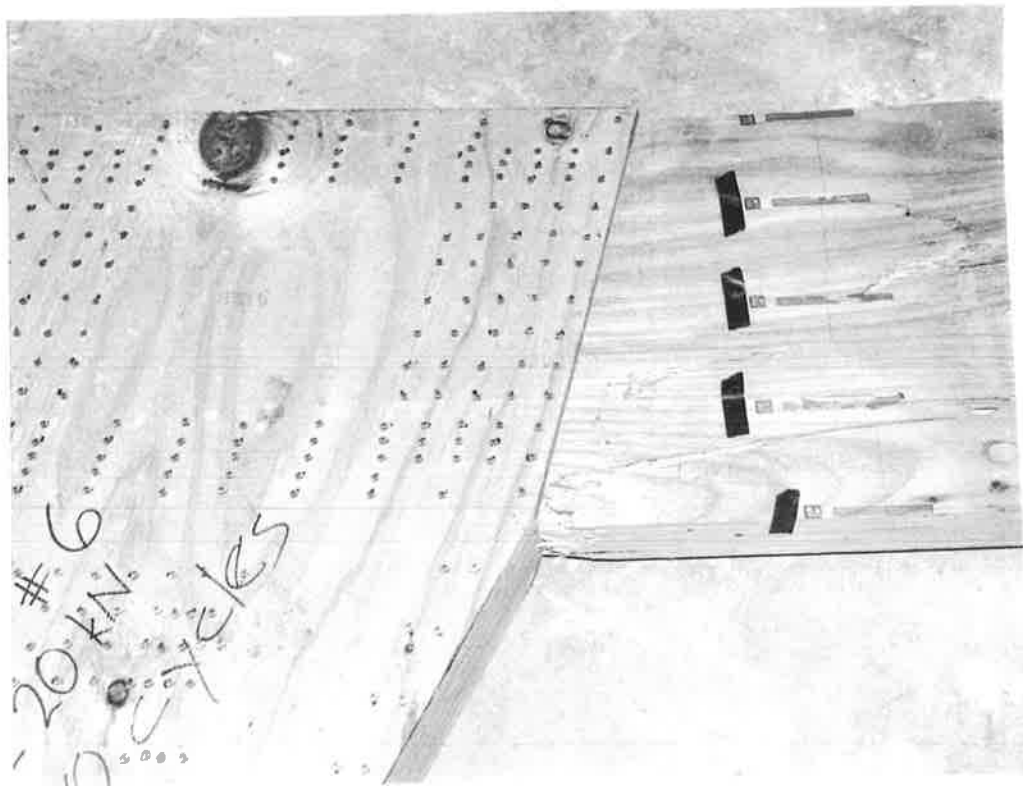


Figure 5.42 Failure mode of specimen 6

SPECIMEN 7

Specimen 7 was cycled with a constant moment of 44kN-m plus a dynamic moment of 26kN-m. Since specimen 6 failed during fatigue loading at $N=6200$, by lowering the cyclic load, it was expected that the endurance limit of this joint would be larger.

As for all previous tests, a rapid initial increase in rotation was observed, followed by a more gentle increase in rotation (Figure 5.43). After the first 10000 cycles, the increase was nearly linear.

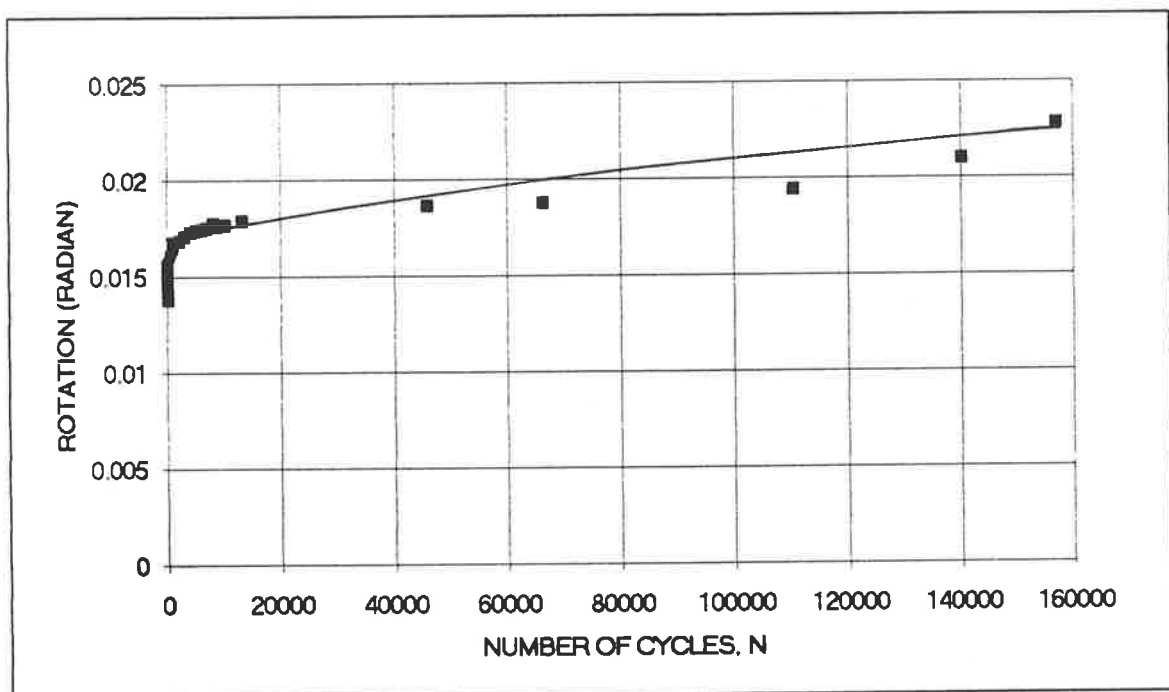


Figure 5.43 Rotation at 44kN-m vs number of cycles for specimen 7

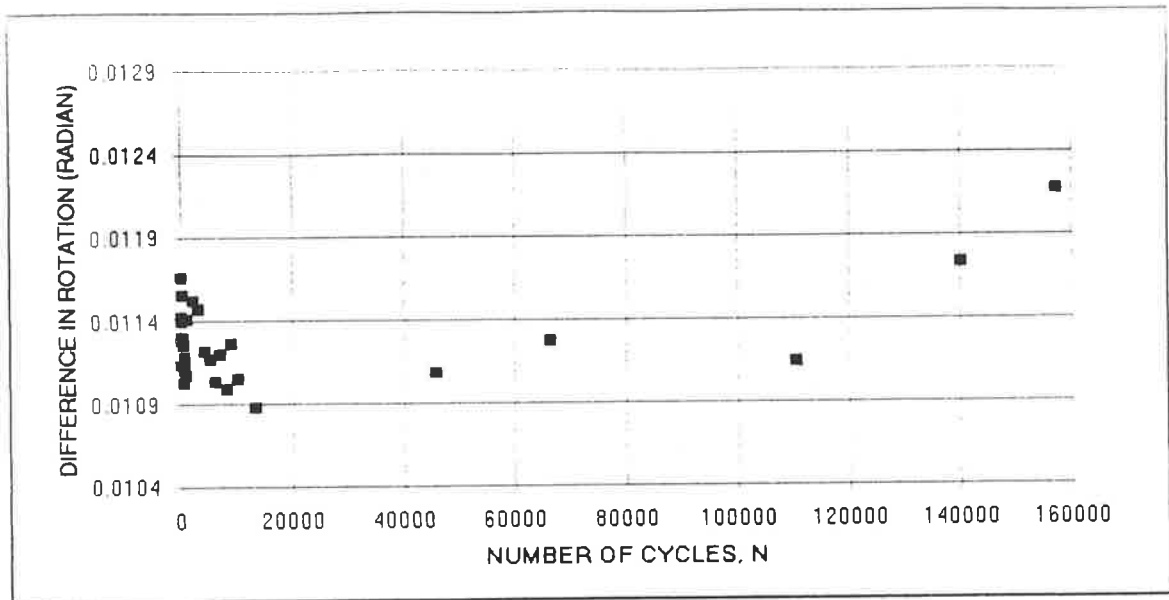


Figure 5.44 Difference in rotation vs number of cycles for specimen 7

Figure 5.44 shows the initial scattering of the rotation, $\Delta\theta$, before the difference in rotation dropped to the lowest point of 0.0109 radian at $N=13000$, then the difference in rotation increased steadily. However, the stiffness (Figure 5.45) also exhibited initial cyclic behaviour though in general it decreased as a whole.

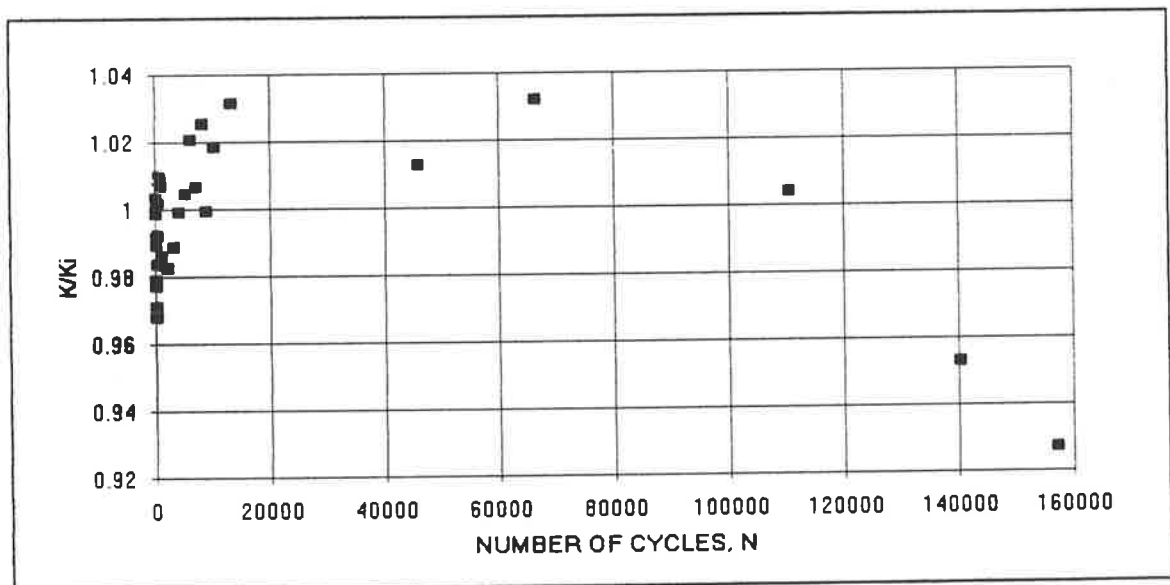


Figure 5.45 Stiffness vs number of cycles for specimen 7

There was inconsistency in S.G.5 reading (200mm from the centreline at $N=157028$ where higher strain was recorded for lower load level in the rafter section (see Figure 5.46). This could be a malfunction of that particular strain gauge. By equating P_{strain} and P_{statics} of 34.9kN at a recorded applied moment of 70kN-m, the strain at S.G.5 was calculated to be $1830\mu\epsilon$. The corresponding moment (from strain calculation) was 45.3kN-m compared to the moment (from statics calculation) of 59.7kN-m. Apart from that, the section was assumed to be a linear strain profile.

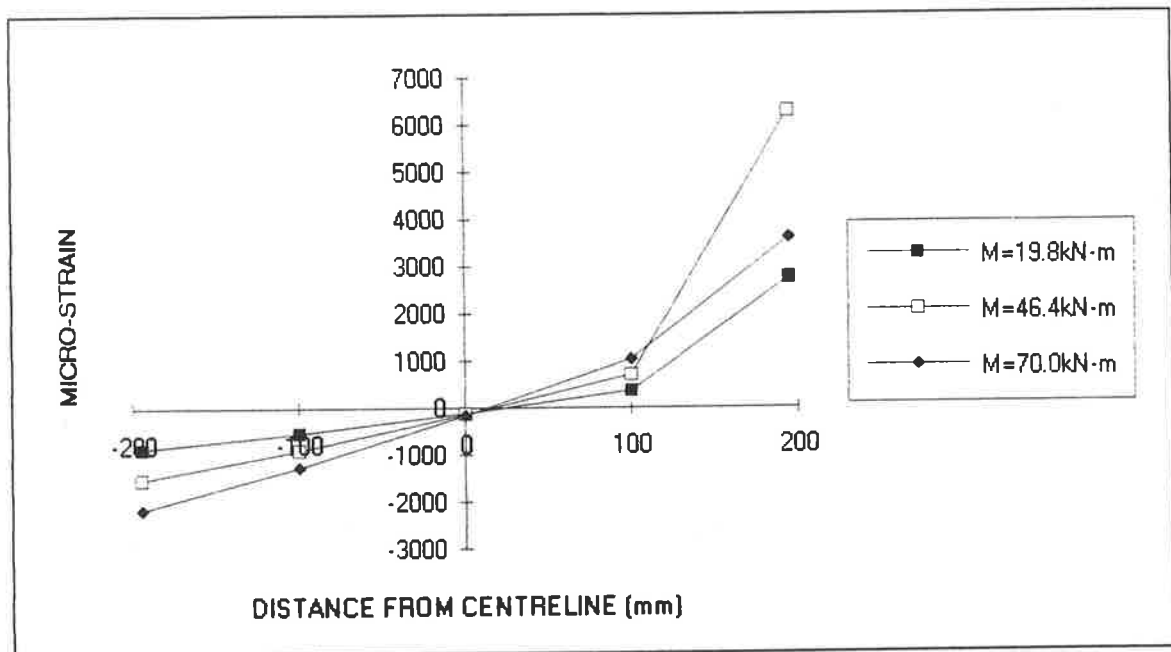


Figure 5.46 Strain across rafter at $N=157028$ for specimen 7

The strain profile in the column section was almost linear (see Figure 5.47). At an applied moment of 70.0kN-m, P_{strain} and M_{strain} were 20.5kN and 33.6kN-m while the corresponding P_{statics} and M_{statics} values were 28.6kN and 39.5kN-m.

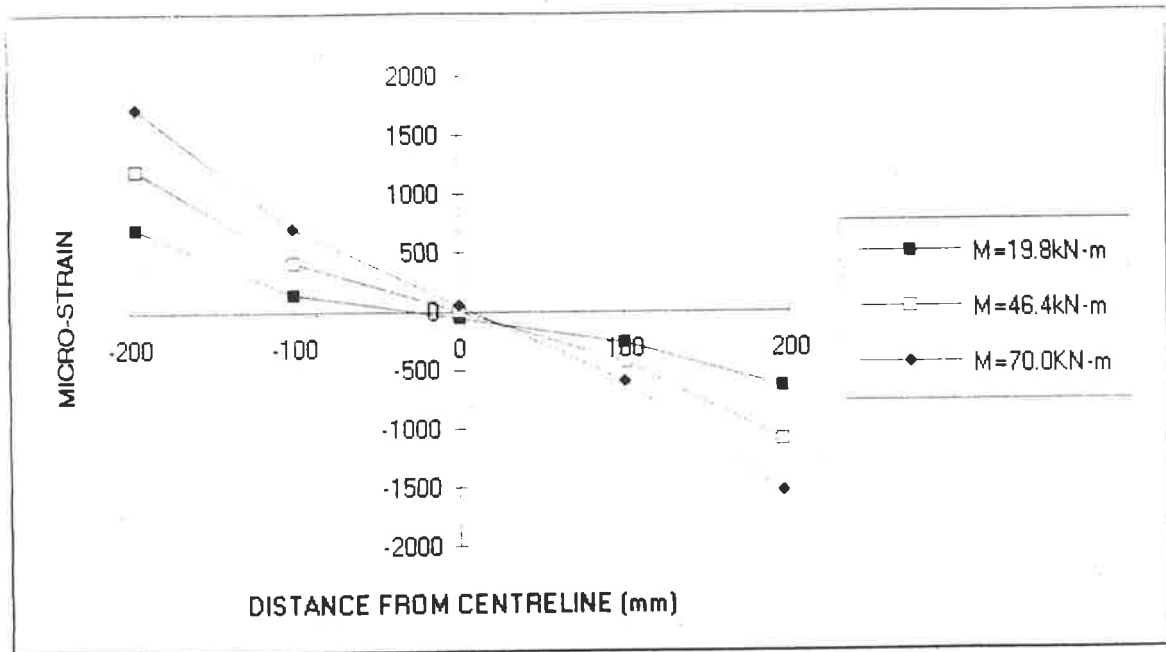


Figure 5.47 Strain across column at $N=157028$ for specimen 7

Specimen 7 survived 180290 cycles and it failed by partial gusset plate slippage and column fracture as shown in Figure 5.48.



Figure 5.48 Failure mode of specimen 7

5.3 COMPARISON OF THE RESULTS

Following the presentation of the experimental results for each specimen in section 5.2, this section provides an overview of the results, and highlights some of the key findings. First, theoretical predictions are compared to experimental results. Results from different specimens are also compared in order to gain a better understanding of the behaviour of the joint. This section is divided into two sub-sections for studying joint performance, namely, static and dynamic loading. In the static load section, special emphasis is placed on the residual strength, static strength, failure mode and the static stiffness. Thus, only specimens 1 to 5 are discussed in this section. On the other hand, the dynamic performance section pays special attention to the joint behaviour during cyclic loading. The creep, stiffness, endurance and strain profiles are discussed for specimens 2, 3, 4, 6 & 7. Key results are summarised in Table 5.1.

SPECIMEN	ROTATION	STRAIN	FAILURE MODE	REMARKS
1(static)	non-linear with moment increased at a lesser rate than θ ; $k_s=2491\text{kN-m/rad}$	linear at column but not rafter, 50% more strain on rafter	tension at rafter	reloading due to metal joint failure. $M_c=96\text{kN-m}$
2(250,000 cycles)	<i>creeping</i> , rotation increase at 25kN was steady after 100,000 cycles; <i>fatigue</i> , linear increasing; $(k/k_i)_d=-1.2 \cdot 10^{-6}$; $k_s=3370\text{kN-m/rad}$	linear at both column and rafter and NA at the c/l, 30% more strain on rafter, strain increase was small	tension along gusset	movement between LVL and gusset, bending of the steel angle at anchorage. $M_c=88\text{kN-m}$

SPECIMEN	ROTATION	STRAIN	FAILURE MODE	REMARKS
3(1000,000 cycles)	<i>creeping</i> , initial jump then continuous stepwise increase; <i>fatigue</i> , steadily increasing with initial drop; $(k/ki)_d = -1.2 \cdot 10^{-7}$; $k_s = 3207 \text{ kN-m/rad}$	linear upto 1000,000, 50 % more strain on rafter; strain increase was small; non-linear (inelastic) after 1000,000 at both	tension at rafter	as above. $M_c = 88 \text{ kN-m}$
4(500,000 cycles)	<i>creeping</i> : a gradual increase (30%); <i>fatigue</i> : scattered points but decrease overall! $(k/ki)_d = +1.44 \cdot 10^{-7}$; $k_s = 4372 \text{ kN-m/rad}$	rafter: linear, N.A. at c/l, 15% more on compression side, 15% more than column; column: nonlinear, N.A. changing, 36% more strain on tension side; strain increase was small (=10%)	tension along gusset	as above. $M_c = 85 \text{ kN-m}$
5(static)	non-linear with moment increased at a lesser rate than θ ; $k_s = 3446 \text{ kN-m/rad}$	rafter: linear, N.A. at c/l, more strain on compression side; 60% more than column; column: linear, N.A. at c/l, more strain on tension side.	tension along gusset	cracking sound heard after 53kN-m. $M_c = 78 \text{ kN-m}$
6(6182 cycles)	<i>creep</i> : initial jump at $N=250$, gradual increase after $N=3000$; <i>fatigue</i> : initial jump within 500 cycles, and then drop back to initial value before a steady increase after $N=2000$; $(k/ki)_d = -2.71 \cdot 10^{-5}$ after $N=2000$	rafter: linear initially, nonlinear and 19% increase when approaching failure; 20% more than column column: linear initially, nonlinear and 35% increase on the compression side at $N=6182$.	tension along rafter	bigger gaps were seen between LVL and gusset. $M_c = 80 \text{ kN-m}$
7(180290 cycles)	<i>creep</i> : mean increased cyclically at the initial 12 cycles, then the increase was linear; <i>fatigue</i> : cyclic behaviour before it dropped to the lowest point of 0.01rad at $N=13000$, then increase steadily; $(k/ki)_d = -8.5 \cdot 10^{-7}$	rafter: linear 25% more than column; column: linear	tension along column and nail slip	as above. $M_c = 71 \text{ kN-m}$

$(k_s = \text{static stiffness} \ \& \ (k/ki)_d = \text{slope of the dynamic normalized stiffness curve})$

Table 5.1 Key features of the experimental results

5.3.1 Static performance

As shown in Table 5.1, three specimens failed across the rafter section near the gusset; three others failed across the gusset plate, and one failed across the column section together with nail slip. This was different from the predictions by Lhuede's method (see section 2.2.3). The t/d ratio (the relationship of plate thickness and nail dimension) for the test joints was 6.6 which favoured nail yielding mode in the case of single nail joint. Lowe (32) commented that in most of the moment resisting joints designed and tested by Batchelar, the ultimate limit state of the joint was by some type of joint failure, such as tearing of the plywood side plate. This was partly consistent with the results presented here. Even though specimens 1 and 5 were built and tested identically, different failure locations were observed. Thus the failure mode and location were not consistently predictable. However, the plywood gusset plates were theoretically the weakest part of the joint (see section 3.5.4).

Tension fracture perpendicular to the grain of the outer laminates was found in all specimens. The location of the rafter LVL failure was found across the location where the strain gauges were mounted, i.e., around 200mm from the plywood gusset edge. This was the location of high bending stress without the strengthening effect of the plywood gusset plate. The basic working load of the LVL member was 42.84kN since the basic working shear stress of LVL was 1.7MPa. Therefore, it was not surprising to have failure at rafter section in specimen 1 and 3 where the experimental loads at that location (calculated by statics from Figure 3.6) were 54.5kN and 50kN respectively. On the other hand, the location of failure in the gusset plate was across the contact line of the LVL sections and this was the shortest distance across the plywood plate. Amongst the tests with final static loading to failure, all specimens that failed across the plywood gusset due to tension fracture contributed to the lowest ultimate moment (specimens 2, 4

and 5). This could be explained by the fact that the plywood was the weaker link in the joint design than the nail group and that the quality of the plywood is less consistent. This would draw attention to the significance in selecting high quality material in the regions of high stress, e.g. across the plywood and the LVL rafter.

One thing that was common to all specimen testing was the cracking sound preceding the final failure which gave warning as to when the specimen would fail. A review by Hunt and Bryant (22) of nail plate moment resisting joint tests at Auckland University showed that a significant number of joints failed as a result of brittle tension fracture of the outer timber laminates. In those tests, fracture perpendicular to the grain of the outer laminate was usually close to the edge of the joint plate and often through nail holes in clear grain laminates in most cases. Moreover, tension tests on a single lamination containing loaded nails showed that brittle, perpendicular to the grain, tension fracture could occur at stresses close to permissible design levels. The ultimate bending stresses for the first five specimens were 57.1MPa, 41.3MPa, 52.4MPa, 39.9MPa and 36.6MPa. These stresses were at least twice the working bending stresses of the plywood and LVL (17MPa & 16MPa respectively). The results of this project were similar to the above descriptions, especially the brittle behaviour at the failure, though the ultimate stresses were higher. Apart from the cracking sound heard before the failure, there was not much indication as to when the specimens would fail.

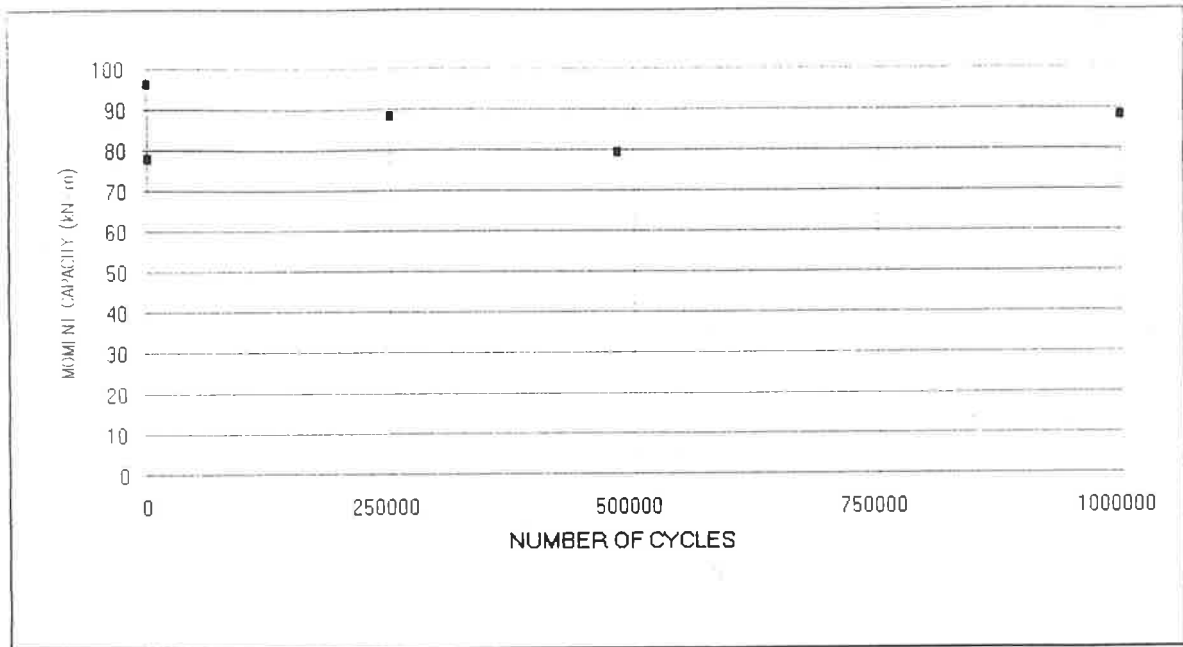


Figure 5.49 Residual strength vs number of cycles

The working moment of the nail group was 38.8kN-m while it was 25.6kN-m for the LVL member and 32.62kN-m for the plywood gusset plate (see Chapter 3). This showed that the failure of the nail group was the least likely mode of failure for the joint. This theoretical prediction was supported by the fact that every test specimen failed across either the plywood plate or the LVL. When comparing the experimental results to the calculated ultimate moment capacity of the nail group, the theoretical value was about one third that of the tested specimens. Thus the design was considered conservative and there was room for improvement in designing the joint (see Chapter 6).

The test results indicated that the fatigue loads do not cause a significant decrease in the residual strength of these joints as shown in Figure 5.49. This is most likely because the nail groups do not control the static strength. For specimens 2, 3 and 4, where the same fatigue loading was applied for 250,000 to 1,000,000 cycles, the ultimate moment was similar in magnitude, varying from 85kN-m to 88kN-m.

Moreover, specimen 3 survived over one million cycles, which was the maximum for fatigue test on this type of joint, coincidentally sharing the same ultimate moment with specimen 2 which had survived 250,000 cycles. This suggested that the ultimate static strength of the joint depends not on the loading duration but on the material strength. Furthermore, work by Stevens (52) has shown that in the full-scale joint in the timber portal frame there was an added factor of safety due to the stiffening effect of the cladding and bracing. Since the actual moment on the joint in the real portal frame differs theoretically from moments applied to the specimen by a factor of 4 due to scale effects (see section 3.4.1), the corresponding moment applied to the specimen would be higher than that experienced by the actual portal frame joint. Thus this joint type was expected to perform well and have minimal strength loss due to fatigue loading in the actual portal frame joints. All the specimens failed by tension fracture of the timber material, and the fatigue effect was not prominent in this research. On the contrary, the quality of the timber material influenced ultimate performance.

In specimens 1 and 5 where the joints were tested statically, the results gave two extreme ultimate static strengths of 96kN-m and 78kN-m and the residual strengths of the fatigue tests that failed by static loading fell in between the results of those two static tests. In addition, there was a 17kN-m difference between the two pure static tests. This illustrated that influence of the material variability, and of plywood in particular, since the specimens which had the lowest moment capacity experienced gusset failure. In assessing the effect that fatigue loading had on the residual strength of these types of joint, it was important to know accurately the initial static strength of each specimen. Ideally a large number of test specimens are needed in order to provide results from which reliable mean values can be drawn. In the research carried out by Hunt & Bryant, the paper described experimental tests on more than 5000 single nailed joints. However, because of the limited time and resources, only 7 specimens were tested and

this research must be considered as a preliminary study on the fatigue behaviour of the joint.

Apart from the material, there might be other reasons for this inconsistency in the results of the two pure static tests. Boulton (10) commented in his experiment that earlier tests performed better, with regards to the timber failure stress, which could be attributed to a greater conservatism at the time owing to the unknown factors associated with such joints. There might have been greater care in handling of the joints and data recording in the earlier specimens. Specimens were assumed to have nominal dimensions. However, quantitative terms always vary and thus give different results. The measurements might vary between different pieces of material e.g. some plywood plates have 20mm thickness and some 21mm; LVL members have varying cross section along their length; variability of material is always a disadvantage to timber even with the modern advanced processing of the material. Inconsistency could be found in other qualitative variables such as workmanship, testing conditions etc. Careful handling, fabrication and testing were ensured in order to give a high standard of workmanship quality control. After all seven joints were made, they were stored in a fashion that would give minimum initial stress to the specimens. Since the time required for the fabrication and testing of the joints spanned almost six months, and each test specimen typically took at least one week to manufacture, there were inevitably changes in the temperature and the moisture content of the timber. Although the laboratory has very good insulation by thick concrete walls and floor slab, there were still some noticeable temperature changes within a day. Therefore, extra caution was taken when interpreting the test data for changes due to testing conditions. Hansen et al (19) commented that the use of nail plates gave rise to special problems due to severe shrinkage cracks in the truss specimens which was due to difference in the moisture content at the time of assembly and testing. Furthermore, the loading rate was also a

factor that could alter the strength determination of the joints. As the rate of loading was increased, the stiffness in turn would increase and so would the ultimate strength. In this research, the loading rate of the cyclic component was different, 0.6Hz for specimen 2 to 4, 0.3Hz for specimen 6 and 0.45 Hz for specimen 7 (see sections 4.2 & 4.4). Manual control of static loading was adopted for all the static tests for it was difficult to make the loading rate identical. This could well introduce some undesirable inconsistencies in the experiment.

From the results, similar static stiffness was found before and after dynamic loading for specimens 2 and 3. This finding implied that the static stiffness seemed to be unaffected by cyclic loading. Moreover, this static stiffness varied from specimen 1 to specimen 5 without any obvious trend in regard to number of cycles and so this value was considered to be more dependent on the individual joint performance.

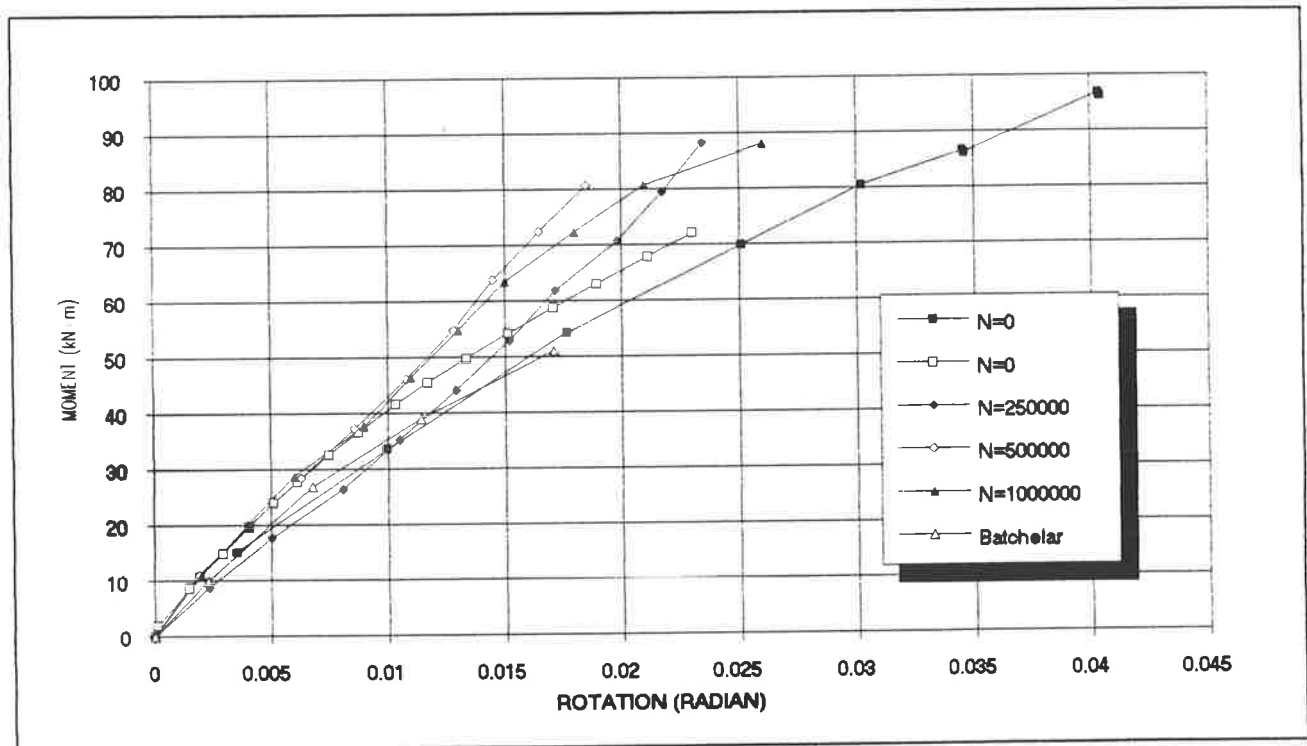


Figure 5.50 Moment vs rotation for all specimens

For the conventional static tests (specimens 1, 5 and the final static loading in the case of fatigue tests of specimens 2, 3 and 4), Figure 5.50 shows the relationship between the applied moment and joint rotation. As can be seen in this figure, the moment rotation characteristics of the joint are similar to those reported by Batchelar(7) (see Figure 5.50). There is little correlation between the number of cycles endured and the loss of static joint stiffness. In addition, an estimate of the static joint stiffness was given by the secant to the curves in Figure 5.50 between the origin and the last data point, and such static stiffness k_s was stated in Table 5.1. This value ranges from 2491kN-m/rad in specimen 1 to 4372kN-m/rad in specimen 4. The two static tests gave the lowest stiffness of $k_s=2491\text{kN-m/rad}$ and 3446kN-m/rad . The low stiffness values could be due to the fact that the specimens were tested for a bigger load range or that fatigue loading would increase the stiffness in the final static test. However, the experiment did not show higher stiffness with more cycles. On the other hand, for the specimens that have undergone fatigue loading before the static test, they shared very similar stiffness curves and the static stiffness were ranging from 3035kN-m/rad to 4372kN-m/rad. Hansen and Mortensen (19) found in their experiment that static load applied after the fatigue test showed an increased stiffness in two series of the portal frame tests. Polensek (46) (see section 2.3) in his simple nailed joint experiment explained that in tight joints, damping decreased as load increased for all cyclic magnitudes because partial gaps formed in contact interlayer as increasing shear load loosened and pulled out the nail. The reduction of joint tightness decreased interlayer friction and damping. Joints with gaps behaved differently; their damping changed little or even increased under increased load. The explanation is in the partial disappearance of the gap as the original size and shape of the gap changed under increasing loads; disconnected components came into partial contact, thus increasing interlayer friction and damping. This argument could be used to explain the increased stiffness after the fatigue loading in this research where gaps might have been present. This was because in

the joints with gaps, the interlayer friction was enhanced after the cyclic loading. Thus the stiffness was increased but the ultimate strength was lowered due to damage done to the timber during the fatigue loading.

5.3.2 Fatigue performance

When the endurance of the joint was considered, specimen 3 endured over one million cycles with $44\text{kN}\cdot\text{m} \pm 16\text{kN}\cdot\text{m}$ loading and specimens 6 and 7 for 6200 cycles and 180290 cycles respectively for loads that approached ultimate static strength (see Figure 5.51).

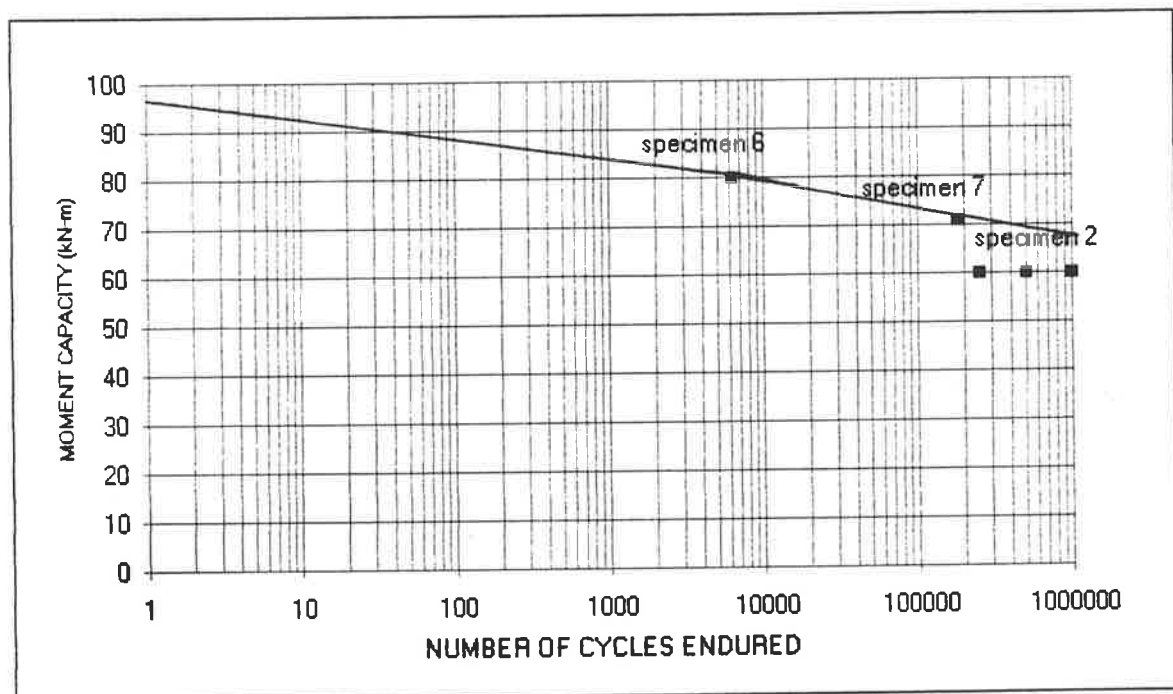


Figure 5.51 Endurance limit at different loading magnitude

Figure 5.51 shows the endurance limit of the joint, where specimen 6 was loaded with cyclic loading of $\pm 35\text{kN}\cdot\text{m}$ which failed after 6200 cycles and specimen 7

was loaded with $\pm 26\text{kN}\cdot\text{m}$ which endured 180290 cycles. However, specimen 2, 3 & 4 were loaded with dynamic component of $\pm 16\text{kN}\cdot\text{m}$ which were never failed during the fatigue loading and so would actually fall below the so-called endurance limit curve. Specimen 3 survived 1 million cycles before the static test to failure. This figure suggested that higher cyclic loads could lower the endurance limit as expected. In addition, the curve, with log scale on the x axis, showed a near linear relationship.

Plots of rotation vs number of cycles for each fatigue specimen were shown in section 5.2 where $44\text{kN}\cdot\text{m}$ was the average joint moment applied during the cyclic loading. The plots described the behaviour of the joint in terms of rotation under continual applied load of unchanged magnitude and could also be used to assess the creep effect on the specimens. Although creep was observed in all cases, the shapes of the rotation vs number of cycles curves and amount of rotation increase varied. Moreover, the rotations at 1 cycle were different and ranged from 0.013rad (0.76°) to 0.018rad (1.05°). Nonetheless, they all exhibited an initial jump at the early cycles. This initial jump was $3.5 \times 10^{-3}\text{rad}$ (0.2°) for specimens 2 and 6 and $1.7 \times 10^{-3}\text{rad}$ (0.1°) for specimens 3 and 7. In addition, there was no particular trend to when the jump occurred. In specimen 2, the jump was found in the first thousand cycles and specimen 6 has a shorter period of three hundred cycles for the jump. In specimen 7, continuous data logging was employed and close monitoring of the initial behaviour of the joint was made. There was a scattering of points on the plot during the first 12 cycles. Therefore, it is believed that the behaviour of the initial joint rotation was unpredictable but a general, rapid increase was likely. This behaviour could be explained by the fact that it might take certain number of cycles before all the nails were in load carrying mode. Afterwards, the increase in joint rotation would carry on with a lesser rate. Creep plots are usually smooth curves with decreasing rates of displacement with time and the rate depends on environmental factors and the stress levels. It is common in timber and in

this experiment, creep is a material characteristic. For all the tests, typical smooth curves were obtained after the initial jump. The total creep were 4×10^{-3} rad (0.23°) to 7×10^{-3} (0.4°) for specimens 2 to 4 while for bigger cyclic loading, the creep were 0.013rad (0.75°) for specimen 6 and 8.9×10^{-3} rad (0.51°). The large dynamic loading component enhanced the creep effect for those specimens.

The difference in rotational displacement between the highest and lowest loads within a complete cycle gave the instantaneous rotational difference. These values were plotted against the number of cycles to give an indication of the fatigue behaviour during the cyclic loading. The plots were shown in section 5.2. There were very close rotational difference at 0 cycle of 5.8×10^{-3} rad (0.33°) to 6.3×10^{-3} rad (0.36°) for specimens of +/- 16kN-m cyclic load while 18.2×10^{-3} rad (1.04°) and 11.3×10^{-3} rad (0.65°) for specimen 6 and specimen 7 respectively. However, the initial behaviour of the specimens was not so clear. Tests 3 and 7 have an initial drop of rotational difference, and this could be due to the fact that as the load increased, gaps between the LVL members disappeared and thus frictional forces limited the extent of rotation. On the other hand, results of specimens 4 and 6 gave scattered points in the early part of the curves. This scattering could be due to the complex interaction between the nails, plywood and the LVL members. There were overall increases in rotational difference in all specimens except test 4. No apparent reason was able to explain this exceptional case except that there were probably some errors. All the increase in rotational differences were small and specimen 6 had the largest increase of 3×10^{-3} rad (0.17°).

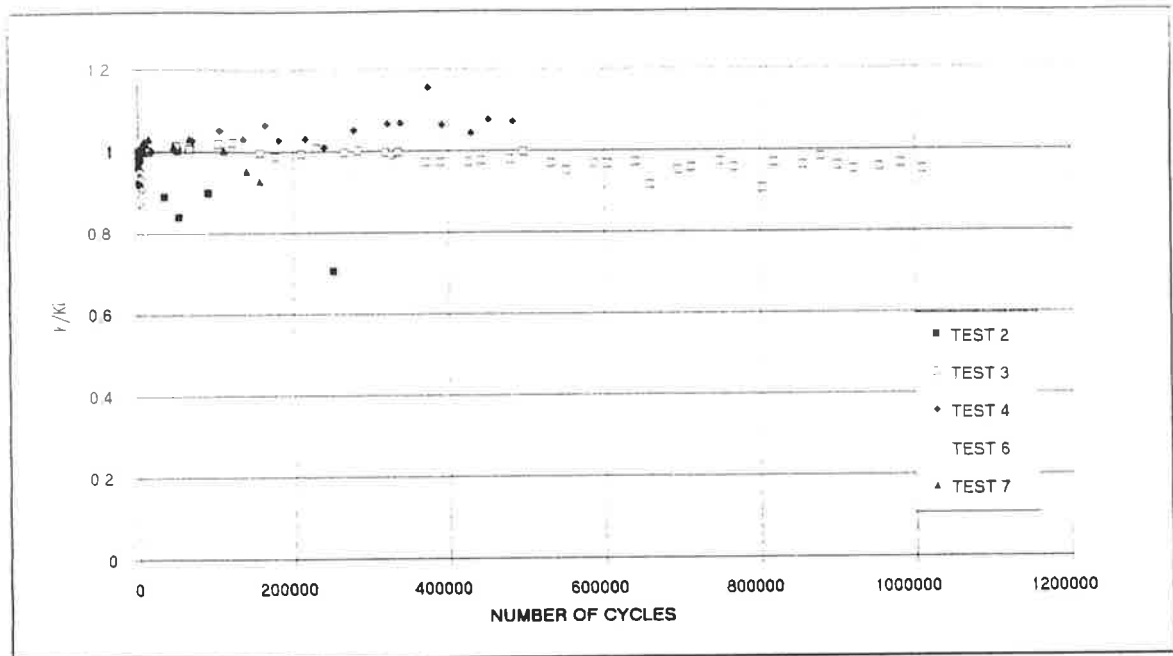


Figure 5.52 Stiffness vs number of cycles for all specimens

Figure 5.52 shows the stiffness plot for all specimens with the stiffness normalised by the initial stiffness to give a dimensionless parameter. Care should be taken to interpret the results since the initial stiffness might not be totally reliable due to the reasons explained earlier in this section. The stiffness term was calculated by dividing the change in moment by rotational difference. All the curves showed overall steady decrease except specimen 4. In tests 2, 3 and 4, although the applied loading was identical, the stiffness plots were quite different in shape and slope. Specimens 2, 3 and 4 shared similar initial stiffness (ranged from 5519 to 4965kN-m/rad) while at higher cyclic loads, the initial stiffnesses were 3892kN-m/rad (specimen 6) and 4759kN-m/rad (specimen 7). In Table 5.1, the approximate slopes of these normalised curves were calculated as $(k/ki)_d$, the values for tests 2, 3 and 4 were -1.2×10^{-6} , -1.2×10^{-7} and $+1.44 \times 10^{-7}$ respectively. These results showed that there was no particular trend for the stiffness of this type of joint but material variability and complex interaction within the joint would dominate the stiffness behaviour of a particular joint. For the last two tests

where the cyclic loading was increased, the slope of normalised stiffness curve was -2.71×10^{-5} for specimen 6 and -8.5×10^{-7} for specimen 7. We could conclude from this stiffness plot that for joint under higher magnitude of dynamic loading, there would be a faster depreciation of stiffness as expected. Moreover, there was no correlation between the moment capacity of the joint and its stiffness, therefore a stiffer joint was not necessarily a stronger joint.

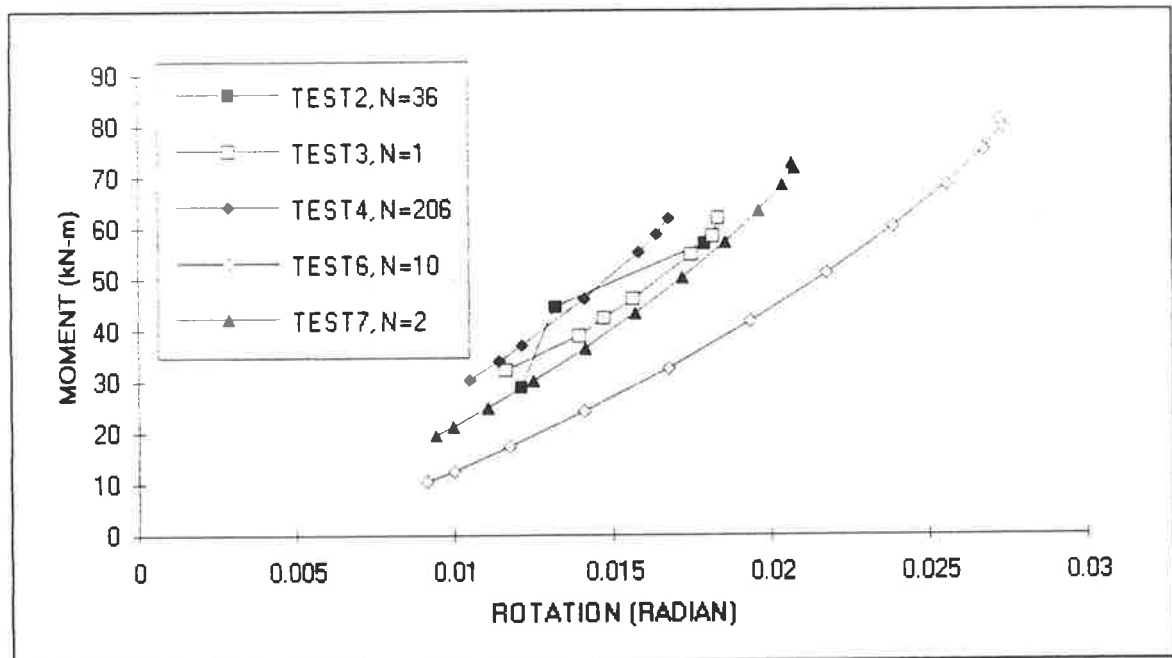


Figure 5.53 Moment vs rotation at initial cycles

Because of the rapid increase in joint rotation observed in the previous tests, it was decided to study the moment-rotation relationship for all specimens during the early stage of loading as seen in Figure 5.53. Each curve shows a half load cycle. Tests 2 to 4 had the same loading pattern and the respective curves exhibited similar behaviour. For specimen 7 where the cycle load was ranged from 18kN-m to 71kN-m within a cycle, the slope resembled that for the previous curves but the curve was shifted to the right of the previous ones. This corresponded to more rotation for the same

applied moment. This was even more obvious for specimen 6 where the maximum applied moment was 79kN-m. Not only was the range of the curve lengthened, but it was also pushed even further to the right of the other curves. Even for the same applied moment, the rotation was larger than for the other loading cycles. Moreover, the curve for specimen 6 seemed to have a smaller slope, implying a less stiff joint. For the large cyclic loads applied to specimens 6 and 7, it was logical to expect more damage to the joint, i.e. more joint slip, nail loosening, wood crushing and LVL bending even after just a few cycles. All of these factors would contribute to more joint rotation and less load resistance.

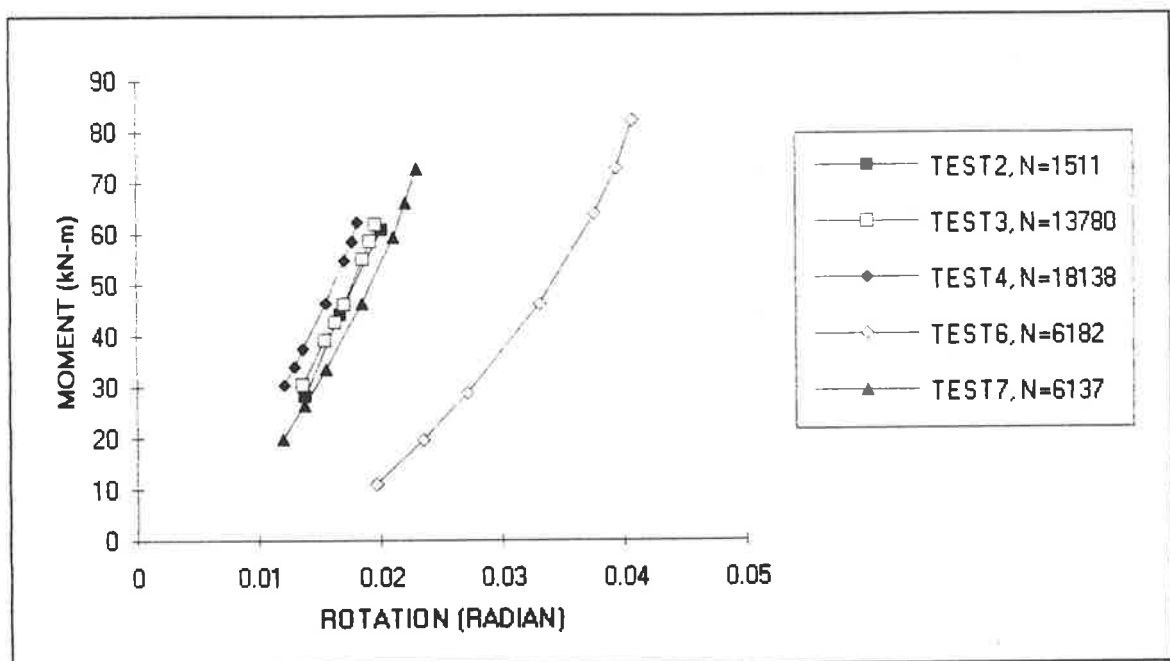


Figure 5.54 Moment vs rotation at certain number of cycles

The above described situation became even prominent after a number of cycles (Figure 5.54). The number of cycles chosen for comparison was as close as possible to 6200 at which specimen 6 failed due to fatigue (Since readings were taken at certain time intervals, the number of cycles chosen for comparison were not exactly

6200). Again, the curves for specimens 2, 3 and 4 were nearly identical to each other and the specimens having higher cyclic loading were positioned to the right of these curves. All the curves shifted to the right meant that the specimens rotated more for the same load level. This phenomenon was most evident in specimen 6 where the rotation after 6200 cycles was about 60% larger than the initial rotation. In addition, the stiffness of specimen 6 at 6200 cycles was approximately 11% lower than the initial joint stiffness. Therefore, it was seen that this type of timber joint is more susceptible to higher cyclic load producing less resistance to rotation and lower stiffness.

From the instrumentation, ram displacement and joint rotation were recorded. There were several factors contributing to the ram displacement, one is the joint rotation and the other is the bending and length change in the LVL limbs and any flexure in the metal angles in both of the anchorages. All these could give extra ram displacement. Assuming that all the ram displacement was due to joint rotation, the rotation (θ) can be calculated as a function of ram displacement (D) utilising the cosine rule (see Figure 5.55).

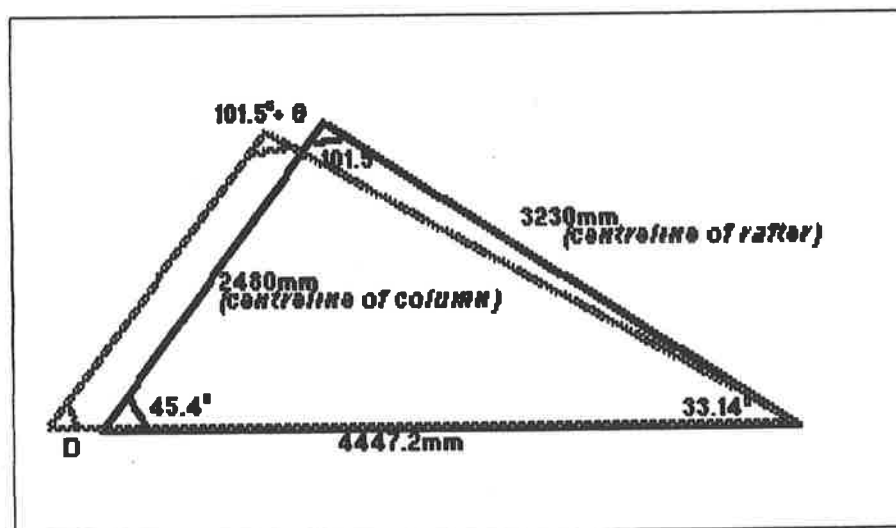


Figure 5.55 Diagram for calculating rotation as a function of ram displacement

$$3230^2 + 2480^2 - 2(3230)(2480) \cos(101.5^\circ + \theta) = (4447.2 + D)^2$$

$$\vdots$$

$$\theta = (0.033) D$$

(D in mm and θ is in degree)

This relationship is given as $\theta = (0.0005762) D$ where D is the ram displacement in mm and θ is the joint rotation in radian. Theoretically, rotation was linearly related to ram displacement with a scaling factor of 0.0005762. This value is compared to the relationship between rotation and ram displacement calculated during each test and a typical curve for specimen 1 is shown in Figure 5.56.

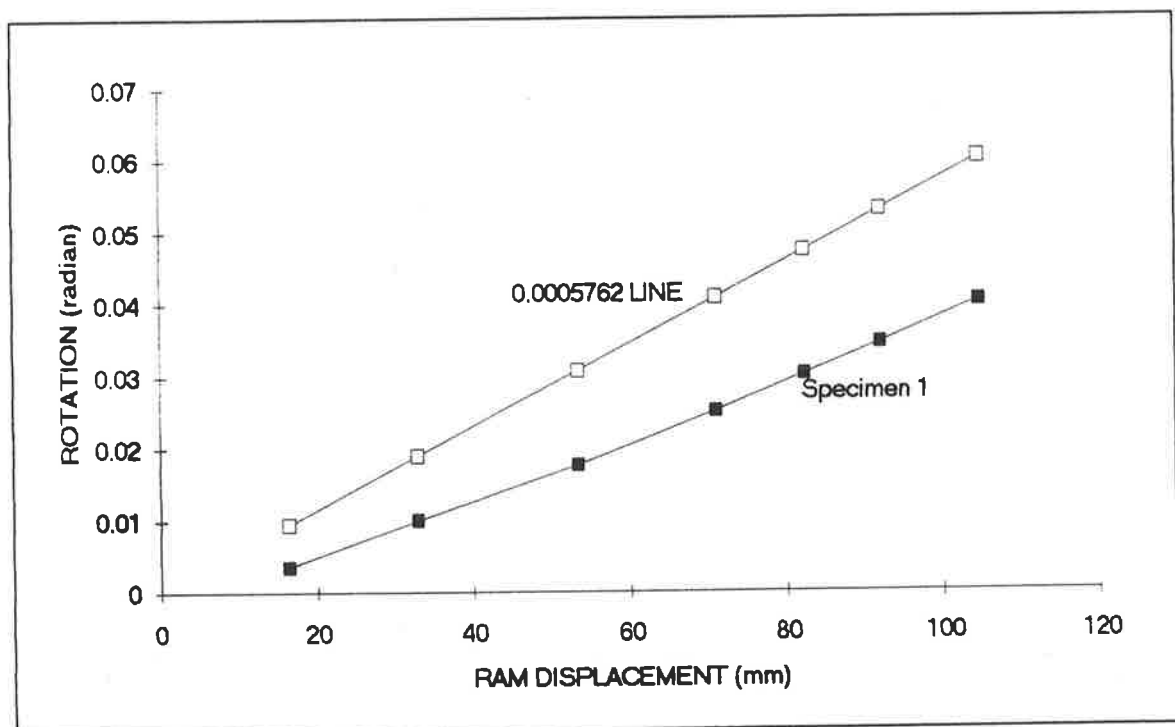


Figure 5.56 Rotation vs ram displacement for specimen 1

The equations for each of the seven specimens are as follow:

Specimen 1	:	$\theta = 0.000419 D$
Specimen 2	:	$\theta = 0.000349 D$
Specimen 3	:	$\theta = 0.000402 D$
Specimen 4	:	$\theta = 0.000314 D$
Specimen 5	:	$\theta = 0.000332 D$
Specimen 6	:	$\theta = 0.000349 D$
Specimen 7	:	$\theta = 0.000297 D$

where θ is the joint rotation in radian and D is the ram displacement in mm

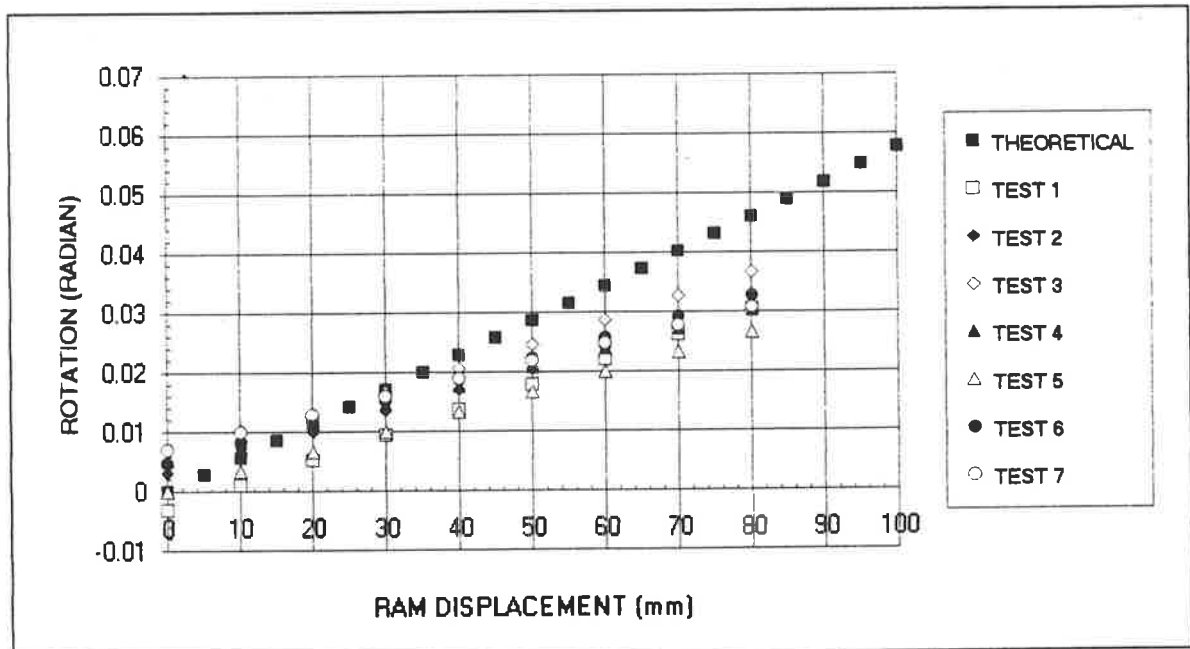


Figure 5.57 Rotation vs ram displacement for all specimens

Figure 5.57 shows the theoretical relationship between rotation and ram displacement together with the results for all specimens. The proportion of ram displacement due to true joint rotation in the tests was from 51% to 72% of the

theoretical prediction. The average slope for all the specimens was 0.000348 which was 60.4% of the theoretical value of 0.0005762. Therefore, we could conclude that approximately 60.4% of the ram displacement was caused by pure joint rotation and the remaining 39.6% of ram displacement went to bending, axial deformation of LVL and other losses.

The strain of LVL members was influenced by the alignment of the joint, thus special care was taken to ensure the leveling of the specimen in order to prevent any torsion stress. There was a general trend for strain profile across the LVL members, the strain on the rafter was always higher than the strain profile on the column by 15% to 60%. It was because of the longer length of the rafter that created higher moment at that rafter section. This higher moment in turn induced bending to cause more strain experienced by the rafter section. Hunt and Bryant (23) studied the stresses in the region of this type of joint and they observed that the highest fibre stresses occurred next to the gusset plate where the strain gauges were mounted in this study. This result was borne out here where three of the specimens failed at that location. Figure 3.6 shows that the axial load and bending moment at the strain gauges locations for both column and rafter members derived from statics. For the column member, the axial load was $0.633P$ and bending moment was $0.721Px$ while for the rafter member, the axial load was $0.845P$ and bending moment was $1.766P-0.536Px$ (P was the applied ram load & x was the distance along the LVL member). Strain profiles for each specimen were integrated to calculate the axial load and bending moment. In Table 5.2, the calculated values are listed where $P(\text{strain})$ and $M(\text{strain})$ denote axial load and bending moment calculated from strain profiles and $P(\text{statics})$ and $M(\text{statics})$ denote axial load and bending moment calculated from statics.

STRAIN GAUGE READINGS FOR <i>COLUMN</i>							
Figure number	Applied Moment (kN-m)	Total area	Total moment area	P(theo) (kN)	M(theo) (kN-m)	P(exp) (kN)	M(exp) (kN-m)
5.2 +	96	0.048	44.4135	40.0914	36.93432	37.9764	52.35181
5.10 +	79	0.032	42.9483	27.2765	35.71582	31.185	42.989625
5.20	62	0.03	38.8337	24.948	32.29418	24.3243	33.531908
5.29 *	62	0.036	30.9175	30.686	25.71106	24.3243	33.531908
5.33 +	72	0.041	39.5604	34.3991	32.89845	28.2744	38.97726
5.41	81.9	-0.03	50.4309	-25.995	41.93840	32.285	44.4895
5.47	70	0.024	40.3757	20.4574	33.57646	28.62	39.513
STRAIN GAUGE READINGS FOR <i>RAFTER</i>							
Figure number	Applied Moment (kN-m)	Total area	Total moment area	P(theo) (kN)	M(theo) (kN-m)	P(exp) (kN)	M(exp) (kN-m)
5.3	96	0.05	69.9997	41.58	58.21181	46.306	79.15312
5.9 +	79	0.020	58.3452	17.3804	48.51987	38.025	64.998
5.17 *	62	0.035	50.5301	29.6632	42.02083	29.6595	50.69844
5.27 +	62	0.018	36.9062	15.3846	30.69122	29.6595	50.69844
5.32 +	72	0.016	61.5984	13.3056	51.22527	34.476	58.93152
5.39	81.9	-0.01	55.5676	-6.4864	46.21006	39.425	67.298
5.46 *	70	0.042	54.4667	34.90	45.29457	34.90	59.65372

+ denotes linear strain profile
* denotes rectified strain profile

Table 5.2 Axial load and bending moment derived from strain profiles

Comparison between the axial loads and bending moments by the two different methods were made in the previous section. Generally the two sets of values did not agree too well especially in specimen 6 where compressive (negative) axial loads were found. The high applied load in specimen 6 might have prevented the proper functioning of the strain gauges. It was interesting to note that for all linear strain profiles across the rafter sections (specimens 2, 4 & 6), comparatively small $P(\text{strain})$'s were found which linked to gusset failure eventually. In the case of linear strain profile in the rafter section, a relatively higher proportion of the applied ram load was transferred to the gusset instead of the rafter members which induced failure at the gusset plate.

From the strain profile diagrams in section 5.2, when the strain gauge readings at the edge were compared at different number of cycles, we noticed that the strain increase due to cyclic loading was small. As described before in section 5.2, not all the strain profiles were nearly linear. In fact, there were three cases (test specimens 1, 3 & 6) where the strain profiles were highly nonlinear in the rafter after a large number of cycles (approaching the final number of cycles). This inelastic strain behaviour of the rafter section was in close agreement with the strain profile reported by Batchelar (7) for earthquake loading. The non-linear strain profile could be caused by yielding of the timber fibre and excess LVL bending and axial load contributed to inelastic behaviour. On the other hand, this could be due to local fibre cracks in the LVL section where yielding occurred and gave this inelastic behaviour. Gusset plate stiffening could also affect strain distribution which could cause failure in the rafter member instead of the plywood. Moreover, all the specimens that had non-linear strain profiles failed by tension fracture of the rafter at the section where the strain gauges were mounted. The non-linear strain profile resembled the elastic distribution of strain across a section of a

deep beam in which the strain distribution is far from linear and that the maximum compression strain occurs some distance from the edge.

In test 2, 4 & 5 where the specimens failed by tension fracture of the plywood gusset, the strain profiles were either both linear or at worst, only non-linear across the column section. The strain profile was also seen to be linear in specimen 7 where the joint was failed by nail slip and tension fracture across the column.

An attempt was made to understand the behaviour of the LVL members under strain as the number of loading cycles increased. Data for strain gauge 1 (195mm from the centre line of the rafter) at 44kN-m is shown in Figure 5.58 for all specimens that have undergone cyclic loading.

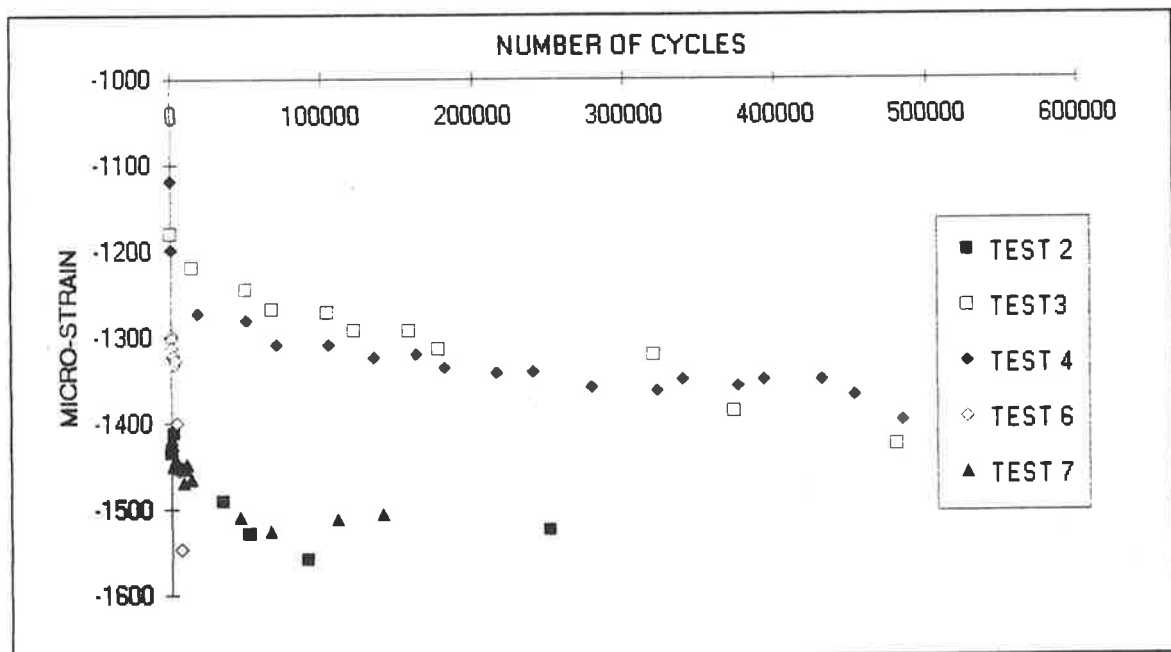


Figure 5.58 Strain vs number of cycles for all specimens

All tests had steep initial slope and then gentle slope after a certain point except specimen 6. This implied that the LVL section was sensitive to applied moment in the early loading stage and this behaviour resembles creep behaviour for constant loaded joints. However, there was a large scatter of strain data in the early stage of loading; the initial strains ranged from $-1100\mu\epsilon$ to $-1420\mu\epsilon$ even though tests 2, 3 and 4 had an identical loading pattern and magnitude. This implied scatter of Young's Modulus (material inconsistency) or just local strain effect. In addition, tests 6 and 7 clearly had a generally higher strain amplitude and the slope of the strain curves were steeper (see Figure 5.59). Nonetheless, tests 3 and 4 produced similar strain curves which were expected while test 2 had 20% higher strain. The performance of specimen 2 may be due to a previous loading which was caused by a metal base connections failure during static loading. This preloading may have induced some minor cracks in the timber fibre. When restarting the second test, damage may have been caused to the specimen. Furthermore, this strain data relied very much on the local fibre behaviour during the tests.

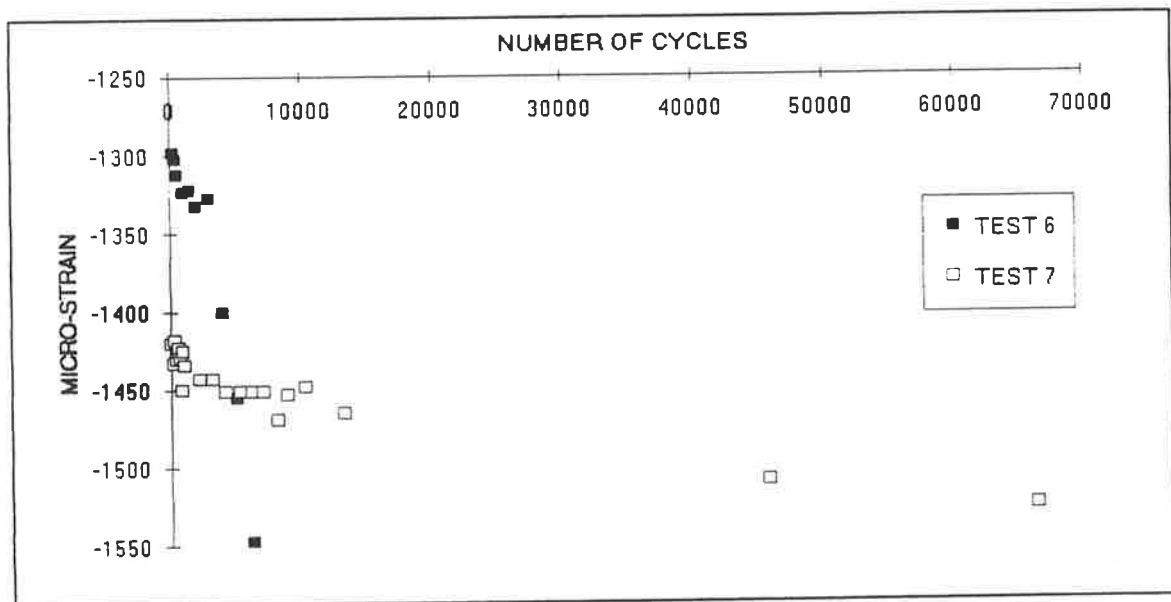


Figure 5.59 Strain vs number of cycles for specimens 6 & 7

Figure 5.59 illustrated the behaviour of the specimens 6 and 7 where the peak cyclic loading approached the ultimate strength. When the cyclic magnitude was 66% higher than the previous loading, the strain curve still shared similar shape and slope and the specimen failed by nail slip and column tension fracture. In contrast, specimen 6 gave almost a straight strain curve indicating that strain increased steadily until failure. This was caused by the high cyclic loading amplitude of $\pm 35\text{kN-m}$ which probably induced more prominent fibre cracking and the specimen eventually failed along the rafter section. The strain vs number of cycles plots once again showed the material variability (Young's Modulus) since the difference in the plots were obvious under identical situation.

CHAPTER 6

CONCLUSION

6.1 SUMMARY AND GENERAL CONCLUSIONS

In this study of the fatigue behaviour of timber moment resisting joints, no drastic change was observed in the joint properties of: residual strength, stiffness and strain across the LVL members under the influence of long period of cyclic loading of magnitude of 44 ± 16 kN-m. Up to one million continuous cycles were applied to one test specimen. Based on the results of this experiment, a conservative conclusion for this type of moment resisting timber joint is that the joint could be expected to behave very well under fatigue loading due to wind.

From this investigation, the failure of three specimens was by bending/tension fracture along the LVL rafter section near the location of the strain gauges. Another three failed by tension fracture across the gusset plywood plate along the contact line of the LVL members, and the last specimen by the joint slip and column fracture. Material failure rather than nail failure was the dominating factor in this research in both static and dynamic tests. It could be explained by the fact that material

strength (especially plywood gussets) was the weaker link and the nail group was the strongest part of the joint design. It was concluded that the residual moment capacities were dependent on the residual timber strength rather than on the nail groups for this type of joint.

Testing specimen 5 for pure static loading was intended to confirm the static strength of the joint. Nevertheless, before this second static loading test, the results (specimens 1 to 4) suggested that a reasonable estimation of the reduction of strength which could be expected in a joint subject to fatigue loading was about 10% of the initial strength. The residual strength after cyclic loading of ± 16 kN-m ranged from 85 kN-m to 88 kN-m (122% & 135% of the theoretical ultimate strength by thin walled analogy in Table 3.2). However, test 5 gave a surprisingly low static strength of 79 kN-m (82% of the static strength of test 1); this value was even lower than the residual strength of each of the previous test specimens. Since the residual strength of identical specimens after enduring a set number of fatigue cycles should have a lower residual static strength, the results strongly pointed to the fact that timber material variability plays an important role in ultimate strength. Moreover, gusset plate failure was associated with the lowest observed ultimate moment capacities in specimens 2, 3 and 5 even though this type of plywood gusset plate survived a static moment of 96 kN-m in specimen 1 and failed at 79 kN-m in specimen 5. This further supports the suggestion that strength variation of timber, especially plywood, controls the joint performance.

The number of cycles endured by the joint seemed not to be a key factor in determining the residual strength which was evident from the results in specimens 2, 3 and 4 where the specimens cycled for 1/4 million and 1 million cycles shared the same residual strength and it was lower in the case of 1/2 million cycles. However, three results are not statistically sufficient to draw a firm conclusion on the relation between

number of cycles and residual strength. However, it was strongly suspected that any loss in residual strength occurred in the early stages of dynamic loading was most likely due to creep. This was supported by the fact that most of the stiffness drop was observed during the initial cycles with changes afterwards being more gradual.

Creep effect is an important consideration in the design of timber structures, because timber is more susceptible to creep effects than other materials such as concrete or steel. Moreover, timber is more responsive to environmental changes, and so strict manufacturing and handling standards are necessary. In this research, where time was an important consideration in this long term cyclic loading, specimens were exposed to different environmental changes. There was a gradual increase in rotation at the same applied moment level (44kN-m) of each cycle in all tests. In addition, this increase was non-uniform. Most of the increase in rotation was found in early cycles of the test before a more steady and slower increase was observed. This suggested a response of typical timber creep where there was permanent bending induced in the LVL members and also some minor joint slip. The unpredictable initial behaviour was investigated in specimens 6 and 7. Nonetheless, there was no particular trend of joint performance in the initial cyclic loading. Precambering members in actual timber portal frames is often employed to counter this effect.

No conclusive trend for changes in stiffness for the initial few thousand cycles was found even with close monitoring in tests 6 and 7. The overall stiffness decreased in all specimens (except specimen 4) which demonstrated the fatigue effect of the dynamic load on the joint though the decrease was small (the reduction in joint stiffness was about 5% for specimen 3). It was noted that the difference in stiffness from specimen to specimen was greater than the change in stiffness for any specimen. There were slightly steeper stiffness plots for specimens with higher cyclic loading amplitude.

It was expected that the fatigue effect would be magnified by higher cyclic load. However, the slope of the stiffness plots (Figure 5.52) for specimens 2, 3 and 4, though sharing identical loading pattern, were quite different and pointed to the fact that material variability again contributed to this uncertainty.

The strain profile across the LVL members in four specimens (2, 4, 5 & 7) was linear as expected from the applied axial and bending stress along the members. In addition, more strain was expected across the rafter section since it has a higher constant axial stress due to the angle of the applied load and a higher bending stress at the location nearer to the meeting point of the centrelines of the limbs. Three out of four of these specimens failed along the gusset by tension fracture. On the other hand, the rest of the specimens that gave non-linear strain profiles across the rafter section and failed across the rafter members.

6.2 RECOMMENDATIONS AND SUGGESTIONS FOR FUTURE WORK

It is recognised that this project is limited in scope, and that it is perhaps inappropriate to make too many conclusive statements regarding the behaviour of this type of joint under cyclic loading. However, based on the results, it is suggested that working stress levels of cyclic fatigue loading does not appear to result in massive reductions in residual strength and stiffness of large multi-nail plywood gusseted joints where the timber strength, and not the nail groups strength, is the limiting factor for the joint. Moreover, these conclusions are thought to be relevant to any other similar multi-nail plywood gusseted joint, whether in timber portal frames or in other types of structures. Notably this type of pure timber nailed moment resisting joint behaved exceptionally well under cyclic loading. Should further testing confirm these

conclusions, this type of joint could be expected to perform satisfactorily under very large wind and earthquake load. Moreover, future portal frame structures could be designed according to the existing design practice without any special fatigue provision. This type of joint is expected to perform satisfactorily in areas where dynamic loading is common, e.g. in timber bridges.

As explained in the previous section, variability in the results of identical tests and unexpected outcomes among the specimens make it difficult to draw definite conclusions about the experiment and the true performance of the joint. This was especially evident in the conventional static tests where the moment capacity of the joint was found before any previous loading was applied. The static test was vital to set a basis for comparison with the fatigue test results. However, the two static tests resulted in two extreme values. Without one of the two data, entirely different conclusions could be drawn. Therefore, future tests on these type of moment resisting joints, each specimen type should be repeated with a sufficient number of tests at each load level to establish a statistical bound for the results. In simple timber joint experiments(21)(22)(39)(51), where requirements of resources and time for a specimen were much less, hundreds or even thousands of tests were performed to cater for the material variability characteristic of timber. From a larger population sample, more statistically significant results can be obtained. Moreover, in respect of the complexity of the moment resisting joints as compared with the simple nailed joints, it is highly recommended to repeat tests several times to confirm the reliability of the results, although much time and effort would have to be spent on each specimen.

The static tests for the first five specimens failed by tension fracture across either the plywood gusset plate or the LVL rafter member. This confirmed the results of theoretical calculations that the nail group was not the weakest part of the joint.

The theoretical calculations, according to AS 1720(2), gave the working moment capacity of nail group to be 39 kN-m while the LVL members and plywood gusset had working moment capacities of 26 kN-m and 33 kN-m, respectively. On the basis that the whole joint is only as strong as its weakest component, it would seem logical to design the joint with nail group strength which is as strong as the timber material. Thus the nails and the surrounding timber are stressed at the same level, and the fatigue loading could then have more noticeable effects. This would be in slight contrast to the joint designed in this experiment and that of Boults(10). He suggested that by concentrating on the ultimate timber strength and stiffness as the only design criteria, coupled with the use of permissible nail values, the number of nails per joint tended to be high. In addition, a lower nailing density, within the requirement of strength and stiffness, would improve ductility and seismic performance. In a more recent investigation in Japan(27), the current permissible nail load assigned in the timber design code is thought too conservative for use in the design of timber moment resisting joints. This conservatism leads to an excessive use of nails which also invites a high initial stiffness but less ductility at the final stage. For future research, it is recommended to use a nail pattern design that is less conservative than the one in this project which was adopted from an existing timber portal frame structure. In this way, the jointing system could be investigated on its efficiency and improvements in joint design may be made.

Classical fatigue experiments have consisted of the applications of cyclic loading to a component until failure which places the emphasis on predicting the endurance of a structural component. For multi-nailed timber joints where the joint performed very well under fatigue loads as reported here, engineers are probably less concerned with the number of load cycles endured. Moreover, this approach might be adequate in design mode but not in the analysis mode where problems might arise in deciding what to do with a component part way through its design life. Oehlers(40)

suggested that the designer is more concerned with predicting the static strength of a structure after a period of cyclic loading which is exactly the opposite of the present fatigue design techniques. Therefore, for the experiment reported here and future research, interaction between the strength of a structure and the applied cyclic loads must be allowed for. In this way, the approach could be adopted at the design stage where extra allowance could be made for fatigue damage and at the analysis stage where existing structures could be assessed for their residual strength. To this end, it is recommended that in future, there should be a theoretical study on the residual strength (after dynamic loading) of this type of joint to complete the picture of the residual strength and residual endurance of the joint. On the other hand, suggestions on the improved gussets for timber portal frames by Batchelar(7) lead to more economical designs which change the orientation of the plywood gusset and utilize mild steel reinforcing strip. Since this type of moment resisting joints have been widely used, further practical ways for strengthening the weak points in the joint would be another valuable area for future research to assist designers.

Although the results in this preliminary research require further testing to support the findings, they do appear to indicate that multi-nailed plywood gusseted joints are not adversely affected by the fatigue loads and no substantial losses were found at serviceability levels. If considerations for design such as durability, construction and maintenance could be addressed, and with increased confidence in the fatigue behaviour of this type of joint, this jointing technique could be employed in other areas apart from timber portal frames where cost-efficiency, strength, ease of construction and fire resistance are points of concern in the design. One of the areas that is recommended for consideration is timber bridges since this type of timber joint appears to give superior fatigue behaviour. Future research is highly recommended to fully assess the potential of multi-nail joints.

APPENDIX A

Preliminary study on mounting strain gauges

Due to the non-homogeneity, cellular structure and anisotropy of timber, measuring surface strain of timber materials may not be as simple as with steel or concrete materials. A surface fibre on a timber surface may experience different strain to its neighbouring fibre. Therefore, it is a possibility that strain gauges approaching the size of the surface fibres would only provide the strain of particular fibres rather than the overall surface strain of the timber. In view of this problem, six different strain gauge settings were investigated to check their accuracy and reliability. Based on the idea of averaging fibre strain on the surface of the timber, five settings utilised thin pieces of plastic bonded between the timber and strain gauges. These thin plastic sheets served as a membrane bonded onto the more irregular surface of timber and provided a smooth homogeneous surface for mounting 10mm long strain gauges. Five different thicknesses and textures of plastic were studied. In addition, a 68mm long strain gauge was utilised which was mounted directly onto the timber surface (see Figures A.1 & A.2). A high strength gluing gel was used to bond the strain gauges.

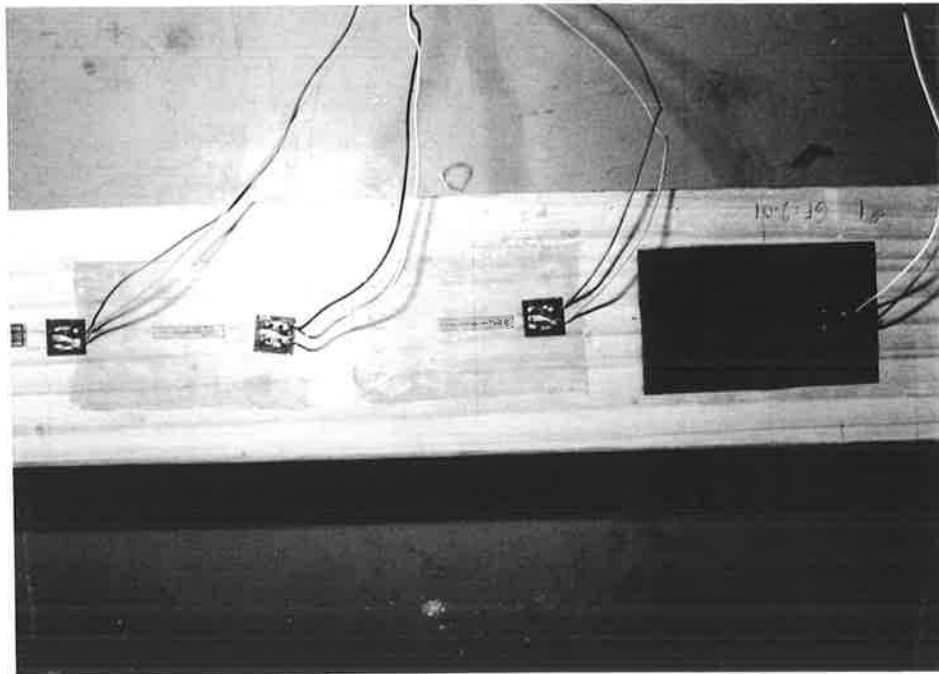


Figure A.1 10mm strain gauge bonded onto a plastic sheet covering the timber surface

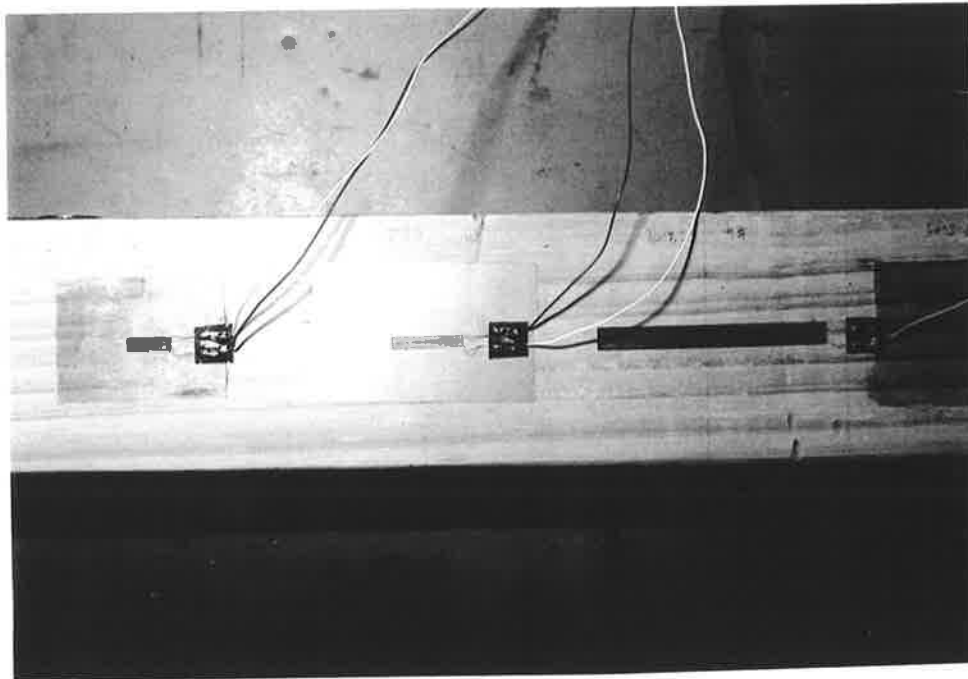


Figure A.2 68mm strain gauge mounted directly onto the timber surface

A timber beam was used to perform a simple test where the six strain gauge settings were mounted on as shown in Figure A.3. Two identical loads P , were applied at both ends of the beam and two supports were placed $L/4$ from each applied load where L was the total length of the beam. Two dial gauges were placed at the middle of the beam to find the maximum bending due to the applied loads.

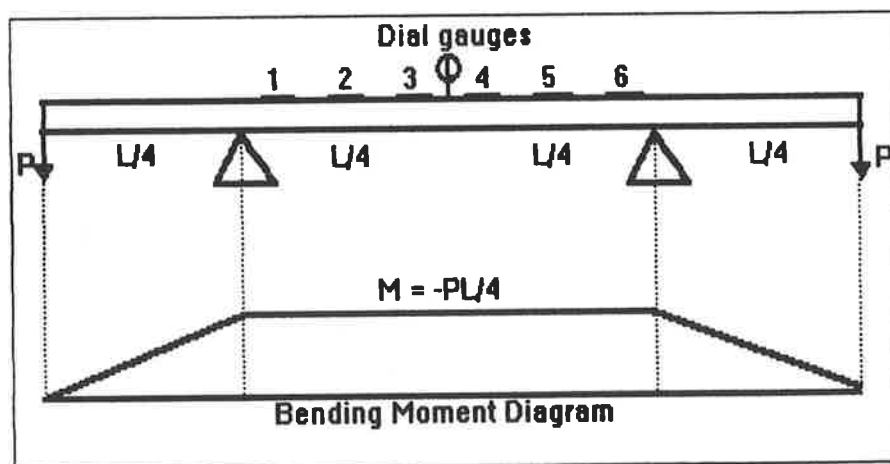


Figure A.3 Experimental set-up for strain gauge test

The six settings were located between the two supports where there was a constant bending moment of $PL/4$. Thus, in theory, all settings would experience the same strain induced by the end loads. The six settings are summarised in Table A.1.

SETTING	1	2	3	4	5	6
PLASTIC SHEET	50x80 x2.1mm	50x80 x0.45mm	50x80 x1.1mm	No plastic	50x80 x1.55mm	45x60 x2.05mm
STRAIN GAUGE	10mm	10mm	10mm	68mm	10mm	10mm

Table A.1 Summary of the six strain gauge settings

From linear elastic theory, the deflection of the beam is $V = (PL/8EI)(x^2-Lx+3L^2/16)$

Since $d^2V/dx^2=1/R$ where R is the curvature of the beam,

$$d^2V/dx^2 = PL/4EI = 1/R \dots (1)$$

$$V_{max} = -PL/128EI, \therefore EI = -PL/128V_{max} \dots (2)$$

Since strain = $\epsilon = y_{max}/R$ (where y_{max} denotes half the thickness of the beam),

Using (1) & (2),

$$\text{Strain derived from dial gauge reading} = \epsilon_d = 32V_{max}y_{max}/L^2$$

Given $y_{max} = 23.02\text{mm}$ and $L = 1200\text{mm}$ by measurement,

$$\epsilon_d = 5.115 \times 10^{-3} V_{max}$$

Different applied loads were added to the beam and the results for different settings were tabulated in Table A.2 while the data were plotted in Figure A.4 with strain vs the applied load. From this figure, if 'STRAIN', calculated from dial gauges' readings, gave the actual strain, then S.G.5 gave the most unreliable results; probably due to improper bonding of the plastic sheet to the timber. S.G.1, 2 and 4 were reasonably accurate, different from theory by less than an 4%. Eventually, the 68mm strain gauge (S.G.4) system, mounted directly onto the timber, was chosen for measuring strain on the test specimens due to its accuracy and convenience.

LOAD (N)	D.G.1	D.G.2	V1	V2	AVER.V	STRAIN ($\mu\epsilon$)	S.G.1 ($\mu\epsilon$)	S.G.2 ($\mu\epsilon$)	S.G.3 ($\mu\epsilon$)	S.G.4 ($\mu\epsilon$)	S.G.5 ($\mu\epsilon$)	S.G.6 ($\mu\epsilon$)
0	3.448	3.495	0	0	0	0	0	0	0	0	0	0
20	3.518	3.505	0.07	0.01	0.04	20.4624	13	12	13	14	1	10
60	3.577	3.518	0.129	0.023	0.076	38.8786	36	35	33	38	5	31
80	3.598	3.537	0.15	0.042	0.096	49.1098	48	48	44	51	5	40
100	3.623	3.57	0.175	0.075	0.125	63.945	61	61	55	64	9	50
120	3.648	3.589	0.2	0.094	0.147	75.1993	74	74	66	76	8	58
140	3.67	3.61	0.222	0.115	0.1685	86.1979	85	86	77	89	10	68
160	3.698	3.63	0.25	0.135	0.1925	98.4753	98	98	88	101	9	79
180	3.7	3.651	0.252	0.156	0.204	104.358	110	110	99	114	8	89
200	3.731	3.675	0.283	0.18	0.2315	118.426	121	123	110	127	9	97
220	3.751	3.705	0.303	0.21	0.2565	131.215	134	135	121	140	12	107
236	3.77	3.73	0.322	0.235	0.2785	142.469	144	145	130	149	12	115
252	3.785	3.75	0.337	0.255	0.296	151.422	153	155	137	159	12	122
268	3.8	3.765	0.352	0.27	0.311	159.095	163	164	147	171	13	130
288	3.823	3.805	0.375	0.31	0.3425	175.209	175	176	157	182	13	139
308	3.849	3.821	0.401	0.336	0.3685	188.51	187	188	167	196	13	148
288	3.829	3.818	0.391	0.323	0.357	182.627	175	177	158	184	11	139
268	3.812	3.79	0.364	0.295	0.3295	168.559	164	165	146	173	10	129
236	3.771	3.748	0.323	0.253	0.288	147.329	145	146	129	152	7	116
220	3.751	3.732	0.303	0.237	0.27	138.121	134	137	120	143	5	107
180	3.7	3.68	0.252	0.185	0.2185	111.776	111	112	98	118	2	87
140	3.65	3.625	0.202	0.13	0.166	84.919	86	88	75	93	0	67
100	3.57	3.608	0.122	0.113	0.1175	60.1093	61	62	52	66	0	46
60	3.55	3.529	0.102	0.034	0.068	34.7861	36	37	30	40	-1	25
20	3.5	3.49	0.052	-0.005	0.0235	12.0217	11	12	7	14	-2	1
0	3.445	3.49	-0.003	-0.005	-0.004	-2.0462	0	0	-4	-1	-1	-1

where D.G. stands for dial gauge, V stands for vertical deflection
 Strain is calculated from dial gauge readings and S.G. stands for strain gauge

Table A.2 Results of the preliminary test on different strain gauge settings

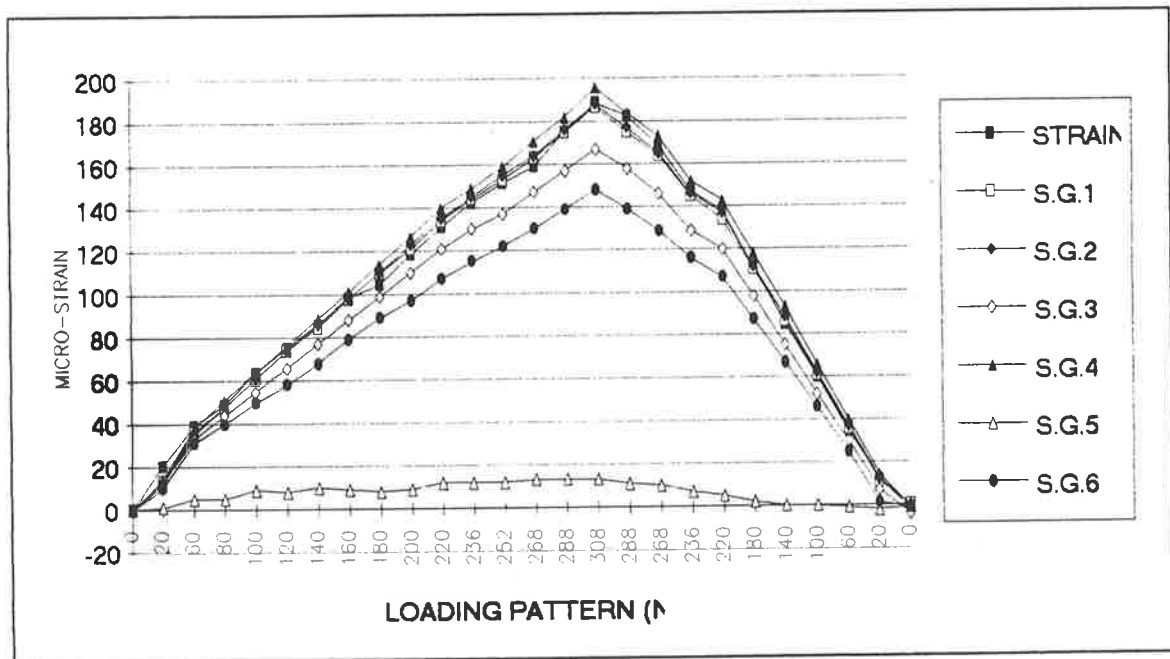


Figure A.4 Comparison between different strain gauge settings

APPENDIX B

DCDT Method

Figure 4.20 shows the geometry of the DCDT method where CD forms the length of the timber bar and BC is the length of the part of DCDT that protrudes from the LVL member. Figure B.1 is used to aid the formulation of the variable δ (change in length of DCDT) in terms of θ (change in joint rotation).

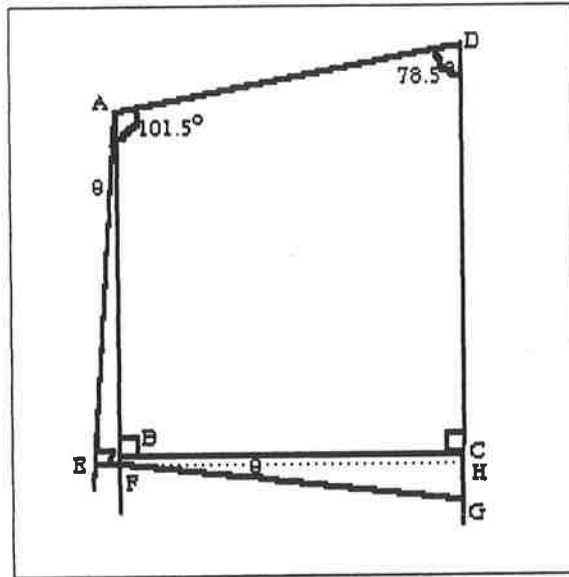


Figure B.1 DCDT method

Letters (e.g. FG) denote lengths as shown in Figure C.1

$$\angle HFG = \theta \text{ and } FG = FH/\cos\theta = BC/\cos\theta$$

$$\text{In } \triangle AEF, EF = \tan\theta \times AE = \tan\theta \times AB$$

$$\begin{aligned} \text{Change in length of DCDT} = \delta &= EG - BC \\ &= (EF + FG) - BC \\ &= \tan\theta \times AB + BC/\cos\theta - BC \end{aligned}$$

Since θ is small, $\cos\theta \cong 1$,

$$\text{Thus } \delta \cong \tan\theta \times AB$$

$$\& \text{ Change in joint rotation} = \theta \cong \tan^{-1}(\delta/AB)$$

APPENDIX C

Basic Program for controlling the data logger through the laptop computer

This program is written for the computer to command the data logger to take readings at a set time interval using an IEEE card in the computer. The drivers for this card were provided by the manufacturer. Then, these readings are calculated into useful information (strain, rotation, load and displacement) by appropriate equations in the program. Finally, the information is stored into a spreadsheet readable file in comma separate variable (CSV) format.

```
10 REM JOINT3.bas 14/7/92.
11 REM joint.bas modified to include strain gauges, DCDT's & RVDT
20 CLEAR ,50000! ' BASIC Declarations
30 DIM INIT0(9),INIT1(9), VOLTS0(9), VOLTS1(9),STRAIN(9),LVDT(5)
40 IBINIT1 = 50000!
50 IBINIT2 = IBINIT1 + 3 ' Lines 1 through 6 MUST be included in your program.
60 BLOAD "\gpib-pc\bib.m",IBINIT1
65 REM Initialise IEEE Card
70 CALL
IBINIT1(IBFIND,IBTRG,IBCLR,IBPCT,IBSIC,IBLOC,IBPPC,IBBNA,IBONL,IBRSC,IBSRE,IBRSV,IB
PAD,IBSAD,IBIST,IBDMA,IBEOS,IBTMO,IBEOT,IBRDF,IBWRTF)
80 CALL
IBINIT2(IBGTS,IBCAC,IBWAIT,IBPOKE,IBWRT,IBWRTA,IBCMD,IBCMDA,IBRD,IBRDA,IBSTOP,
IBRPP,IBRSP,IBDIAG,IBXTRC,IBRDI,IBWRTI,IBRDIA,IBWRTIA,IBSTA%,IBERR%,IBCNT%)
90 REM BASIC Example Program - Device
100 REM You MUST merge this code with DECL.BAS.
110 REM
120 REM Assign a unique identifier to device and
130 REM store in variable DVM%.
140 REM
150 BDNAMES$ = "dev9"
160 CALL IBFIND(BDNAMES$, DVM%)
170 REM The IEEE card is ready for operation
180 REM The next step is to set up the computer and output files
190 CLS
200 PRINT "SILO DATA LOGGING SYSTEM FOR MOMENT-RESISTING JOINT"
210 PRINT ""
220 PRINT "PLEASE PUT A FORMATTED DISK IN DRIVE A,"
230 PRINT ""
240 INPUT "TYPE IN THE NAME OF THE OUTPUT FILE (LESS THAN 6 CHARS)"; N$
290 PRINT ""
300 PRINT "THE OUTPUT FILES ARE NOW SET UP ON DRIVES A: AND C:"
310 REM The next step is to initialise the logger and take all the zero readings
320 PRINT ""
330 PRINT "AN INITIAL SET OF READINGS WILL NOW BE TAKEN FROM THE LOGGER"
340 REM Initialising the logger
```



```

350 WRT$ = "SISO1SD1VT4VD5VA1" : CALL IBWRT(DVM%, WRT$)
360 REM Reading the I excitation voltage for the card and print for reference
370 WRT$="AI50SE1": CALL IBWRT(DVM%,WRT$)
375 MASK%=&H4800:CALL IBWAIT(DVM%,MASK%)
380 R$=SPACES(14): CALL IBRD(DVM%,R$)
390 EV0=VAL(R$)
460 PRINT ""
470 PRINT "EXCITATION VOLTAGE IS "; EV0
500 PRINT ""
550 REM Read the initial value of all active gauges
560 FOR I=40 TO 49
570 WRT$= "AI" + STR$(I) + "SE1" : CALL IBWRT(DVM%,WRT$)
575 MASK%=&H4800:CALL IBWAIT(DVM%,MASK%)
580 R$=SPACES(14): CALL IBRD(DVM%,R$)
590 INIT0(I-40)=VAL(R$)
600 NEXT I
601 REM Read the initial values for all DCDT's
603 WRT$= "AI60SE1" : CALL IBWRT(DVM%,WRT$)
604 MASK%=&H4800:CALL IBWAIT(DVM%,MASK%)
605 R$=SPACES(14): CALL IBRD(DVM%,R$)
606 INIT1=VAL(R$)
620 REM Read the initial values for RVDT
625 WRT$= "AI66SE1" : CALL IBWRT(DVM%,WRT$)
630 MASK%=&H4800:CALL IBWAIT(DVM%,MASK%)
635 R$=SPACES(14): CALL IBRD(DVM%,R$)
636 RVDTI=VAL(R$)
638 PRINT " INITIAL READINGS TAKEN - OK TO BEGIN STATIC LOADING"
675 REM This next section control the logging.
680 REM When function key F1 is pressed logging continuous
690 REM When function key F2 is pressed logging every 10 minutes
700 REM When function key F3 is pressed logging every hour
710 REM When function key F5 is pressed the system closes down
720 ON KEY (1) GOSUB 890 : KEY (1) ON
730 ON KEY (2) GOSUB 940 : KEY (2) ON
740 ON KEY (3) GOSUB 990 : KEY (3) ON
750 ON KEY (5) GOSUB 780 : KEY (5) ON
760 REM Idle loop for program to execute while waiting for function keys to be pressed
770 GOTO 770
780 REM Shut down sequence at end of test
790 TIMER OFF : KEY (1) OFF : KEY (2) OFF : KEY (3) OFF : KEY (5) OFF
800 CLOSE #1 :CLOSE #2
810 WRT$ = "SI": CALL IBWRT(DVM%, WRT$)
820 CLS
830 PRINT " SHUT DOWN COMPLETE REMOVE DISK FROM DRIVE A:"
840 PRINT "SWITCH OFF EQUIPMENT"
850 END
860 REM
870 REM
880 REM
890 REM Logging as fast as possible
900 TIMER OFF
905 LOGTIME =.3
910 ON TIMER (5) GOSUB 1070
920 TIMER ON

```

```

930 RETURN
940 REM logging every 10 minutes
950 TIMER OFF
955 PRINT"LOGGING EVERY 10 MINUTES"
956 LOGTIME = 10
960 ON TIMER (600) GOSUB 1070
970 TIMER ON
980 RETURN
990 REM logging every hour
1000 TIMER OFF
1005 PRINT"LOGGING EVERY 60 MINUTES"
1006 LOGTIME =60
1010 ON TIMER (3600) GOSUB 1070
1020 TIMER ON
1030 RETURN
1040 REM
1050 REM
1060 REM
1070 REM This is the section that takes a set of readings from the logger.
1080 REM Works out the strains and print them to disk and to the screen
1090 REM Take a set of readings
1140 REM Read the value of all active gauges
1150 FOR I=40 TO 49
1160 WRT$= "VT4VT3AI" + STR$(I) + "SE1" : CALL IBWRT(DVM%,WRT$)
1165 MASK%=&H4800:CALL IBWAIT(DVM%,MASK%)
1170 R$=SPACES$(14): CALL IBRD(DVM%,R$)
1180 VOLTS0(I-40)=VAL(R$)
1190 NEXT I
1200 REM Read the value of DCDT's
1210 WRT$= "VT4VT3AI60SE1" : CALL IBWRT(DVM%,WRT$)
1215 MASK%=&H4800:CALL IBWAIT(DVM%,MASK%)
1220 R$=SPACES$(14): CALL IBRD(DVM%,R$)
1225 VOLTS1=VAL(R$)
1235 REM Read the value of RVDT
1241 WRT$= "VT4VT3AI66SE1" : CALL IBWRT(DVM%,WRT$)
1242 MASK%=&H4800:CALL IBWAIT(DVM%,MASK%)
1243 R$=SPACES$(14): CALL IBRD(DVM%,R$)
1244 RVDT=VAL(R$)
1245 REM Read the value of load & displacement
1246 WRT$= "VT4VT3AI67SE1 " : CALL IBWRT(DVM%,WRT$)
1247 MASK%=&H4800:CALL IBWAIT(DVM%,MASK%)
1248 R$=SPACES$(14): CALL IBRD(DVM%,R$)
1249 LOAD1=VAL(R$)
1250 WRT$= "VT4VT3AI68SE1 " : CALL IBWRT(DVM%,WRT$)
1251 MASK%=&H4800:CALL IBWAIT(DVM%,MASK%)
1252 R$=SPACES$(14): CALL IBRD(DVM%,R$)
1253 MOVE=VAL(R$)
1260 REM Work out strain values
1265 FOR I =0 TO 9
1270 VOLTS0(I) = (VOLTS0(I) -INIT0(I))/EVO
1280 STRAIN(I) = -(4000000!*VOLTS0(I)/(2.08*(1+2*VOLTS0(I))))
1290 NEXT I
1300 REM Work out displacement from DCDT's
1302 DISPL = (VOLTS1-INIT1)/0.0669

```

```

1303 ROT = ((ATN(DISPL/780))*630/11)
1315 REM Work out the rotation from RVDT, load & displacement
1316 ROT = (RVDT-RVDTI)/0.1126
1317 LOAD2 = LOAD1*25
1318 MOVE1 = MOVE*12.5
1322 REM Now print the strains to the screen
1330 CLS
1340 PRINT "THE STRAINS AT THE VARIOUS GAUGE POSITIONS"
1350 PRINT ""
1355 PRINT TIMES$
1360 PRINT ""
1365 PRINT "LOGGING TIME = ";LOGTIME;" Minutes"
1367 PRINT ""
1370 FOR I=0 TO 9
1380 PRINT "GAUGE"; I;
1385 PRINT USING "#####";STRAIN(I);
1386 PRINT " Micro Strain"
1388 NEXT I
1389 PRINT " "
1390 PRINT "THE ROTATION BY THE DCDT METHOD"
1408 PRINT "ROTATION1";ROTA;
1409 PRINT " "
1410 PRINT "THE ROTATION BY THE RVDT METHOD"
1411 PRINT "ROTATION"; ROT;
1412 PRINT " "
1413 PRINT "LOAD (KN) ";LOAD2;
1414 PRINT " "
1415 PRINT "DISPLACEMENT OF LOAD CELL (mm)";MOVE1;
1500 REM Now make up the output string ready for CSV format on the disks
1510 A$=TIMES$+" "+STR$(STRAIN(0))+"," +STR$(STRAIN(1))+"," +STR$(STRAIN(2))
1520 A$=A$+" "+STR$(STRAIN(3))+"," +STR$(STRAIN(4))+"," +STR$(STRAIN(5))
1530 A$=A$+" "+STR$(STRAIN(6))+"," +STR$(STRAIN(7))+"," +STR$(STRAIN(8))
1534 A$=A$+" "+STR$(STRAIN(9))+"," +STR$(DISPL)+"," +STR$(ROTA)
1535 A$=A$+" "+STR$(ROT)+"," +STR$(LOAD2)+"," +STR$(MOVE1)
1539 NCS=NS +".CSV"
1540 NAS="A." + NS + ".CSV"
1541 OPEN "A",#1,NCS
1542 OPEN "A",#2,NAS
1543 PRINT #1, A$
1544 PRINT #2, A$
1545 CLOSE #1 :CLOSE #2
1560 RETURN
□

```

Note : Slight variations were made for some tests to cater for other methods (LVDT & RVDT) of joint rotational measurement.

APPENDIX D

Calculations of joint strengths

(A) Determination of nail yield load by Yield Theory

By using Yield Theory, F_u for a single nail can be found: (6)

Given: t_1	=	thickness of plywood gusset plate
t_2	=	thickness of LVL member
$f_{e(1,2)}$	=	wood embedding strength _(ply,LVL)
M_y	=	nail yield moment
d	=	nail diameter
f_s	=	nail strength
F_u	=	nail yield load

$$f_s = 1500 \text{MPa} \quad (39)$$

$$M_y = (d/6)f_s = 2.87/6 \times 1500 = 5910 \text{Nmm}^2$$

$$\gamma = M_y/f_e = 5910/85 = 69.5 \text{mm}^{-1}$$

$$\beta = f_{e1}/f_{e2} = 85/93.5 = 0.91 \quad (39)$$

$$\alpha = t_2/t_1 = 63/19 = 3.3$$

$$t_1/(\gamma)^{0.5} = 2.28 > \{2\beta/(1+\beta)\} = 0.98$$

$$2-2\{\beta/(1+\beta)\}^{0.5} = 0.62 < t_1/(\gamma)^{0.5} = 2.28 < 2+2\{\beta/(1+\beta)\}^{0.5} = 3.38$$

$$\{[2(1+\beta)t_1^2/\beta(2+\beta)^2]+[4\gamma/\beta^2(2+\beta)]\}^{0.5} - t_1/(2+\beta) + 2(\gamma)^{0.5}/(\beta)^{0.5} = 28.1 \leq t_2 = 63$$

\therefore Mode 1.3

$$\begin{aligned} F_u &= f_{e1} [2\beta(1+\beta)t_1^2/(2+\beta)^2 + [4\beta\gamma/(2+\beta)]]^{0.5} - \beta t_1/(2+\beta) \\ &= 85 [148.2 + 86.9]^{0.5} - 5.94 = 798.4 \text{N} \end{aligned}$$

(B) Moment capacity of actual joint

(i) Thin walled tube analogy:

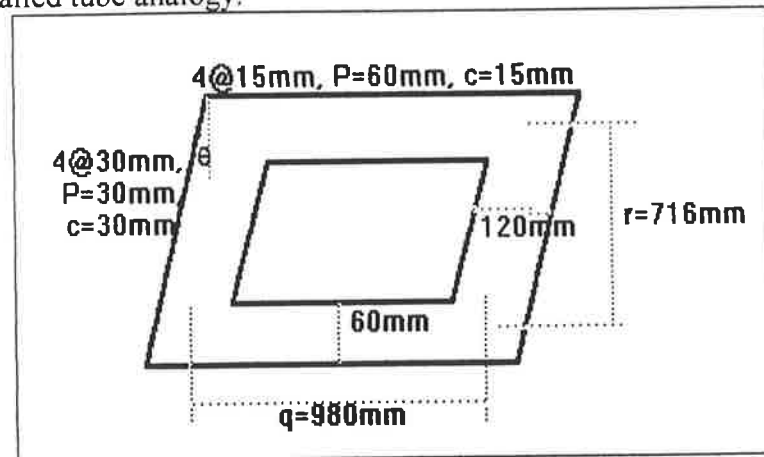


Figure D.1 Nail rings in actual joint

- Given: c = Nail spacing
 p = Nail pitch
 s = Nail ring width
 n = Number of nail rows
 F_u = Nail yield load
 f = Nail stress
 r, q = Dimensions of the nail pattern (see Figure E.1)
 M_c = Moment Capacity

Weight spacing $c = 716 \times 30 / (716 + 980) + 980 \times 15 / (716 + 980) = 21.3 \text{ mm}$

Weight nail pitch $p = 716 \times 30 / (716 + 980) + 980 \times 60 / (716 + 980) = 47.3 \text{ mm}$

Weight nail ring width $s = c(n-1) = 84 \text{ mm}$

$F_u = 798.4 \text{ N}$ (by yield theory)

$f = F_u / cp = 798.4 / (21 \times 47.3) = 0.8 \text{ MPa}$

Moment capacity $M_c = 4 f s r q \cos \theta = 4(0.8)(84)(716)(980) \cos 11.5^\circ$

$M_c = 184.8 \text{ kN-m}$

Therefore, for two sides of the joint, the Moment Capacity M_c

$M_c = 2 \times 184.8 = \underline{\underline{370 \text{ kN-m}}}$

(ii) Shared rivet group analogy:

Given: I = Polar moment of inertia of plane area
r,q = Dimensions of the nail pattern (see Figure E.1)
s = Nail ring width
Z_o = Distance between the furthest nail and the centroid
F_u = Nail yield load
c = Nail spacing
p = Nail pitch
M_c = Moment Capacity

$$I = s/6 (r+q)^3 = 84/6 (716+980)^3 = 6.83 \times 10^{10} \text{mm}^4$$

$$\begin{aligned} Z_o &= 0.5 [r^2+q^2+2rq\sin\theta]^{0.5} \\ &= 0.5 [716^2+980^2+2(716)(980)\sin 11.5^\circ]^{0.5} \\ &= 661.97 \end{aligned}$$

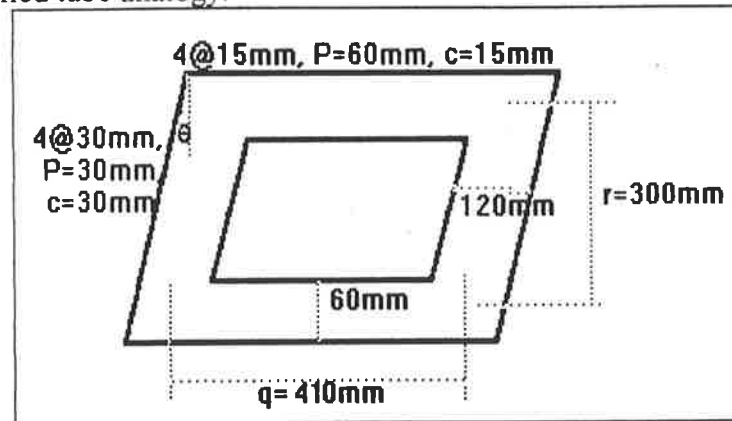
$$M_c = 2 I F_u / c p Z_o = (2)(6.83 \times 10^{10})(798.4)/(21)(47.3)(661.97) = 163.99 \text{kN-m}$$

Therefore, for two sides of the joint, the Moment Capacity M_c

$$M_c = 2 \times 163.99 = \underline{\underline{328 \text{kN-m}}}$$

(C) Moment capacity of test specimen

(i) Thin walled tube analogy:



Given: c	=	Nail spacing
p	=	Nail pitch
s	=	Nail ring width
n	=	Number of nail rows
F _u	=	Nail yield load
f	=	Nail stress
r, q	=	Dimensions of the nail pattern (see Figure D.1)
M _c	=	Moment Capacity

Weight nail spacing $c = 300 \times 30 / (300 + 410) + 410 \times 15 / (300 + 410) = 21 \text{mm}$

Weight nail pitch $p = 300 \times 30 / (300 + 410) + 410 \times 60 / (300 + 410) = 47.3 \text{mm}$

Weight nail ring width $s = c(n-1) = 84 \text{mm}$

$F_u = 798.4 \text{N}$ (by yield theory)

$f = F_u / cp = 798.4 / (21 \times 47.3) = 0.8 \text{MPa}$

Moment capacity $M_c = 4 f s r q \cos \theta = 4(0.8)(84)(300)(410) \cos 11.5^\circ$

$M_c = 32.55 \text{kN-m}$

Therefore, for two sides of the joint, the Moment Capacity M_c

$M_c = 2 \times 32.55 = \underline{\underline{65 \text{kN-m}}}$

(ii) Shared rivet group analogy:

Given: I = Polar moment of inertia of plane area
 r, q = Dimensions of the nail pattern (see Figure E.1)
 s = Nail ring width
 Z_o = Distance between the furthest nail and the centroid
 F_u = Nail yield load
 c = Nail spacing
 p = Nail pitch
 M_c = Moment Capacity

$$I = s/6 (r+q)^3 = 84/6 (300+410)^3 = 5.01 \times 10^9 \text{mm}^4$$

$$Z_o = 0.5 [r^2+q^2+2rq\sin\theta]^{0.5}$$
$$= 0.5 [300^2+410^2+2(300)(410)\sin 11.5^\circ]^{0.5}$$
$$= 277.1$$

$$M_c = 2 I F_u / c p Z_o = (2)(5.01 \times 10^9)(798.4)/(21)(47.3)(277.1) = 29.1 \text{kN-m}$$

Therefore, for two sides of the joint, the Moment Capacity M_c

$$M_c = 2 \times 29.1 = \underline{\underline{58.1 \text{kN-m}}}$$

BIBLIOGRAPHY

1. Australian Standard 1649-1974, "Methods for the determination of Basic Working Loads for Metal Fasteners for Timbers".
2. Australian Standard 1170.2-1989, "SAA Loading Code, Part 2: Wind Loads", Sydney, 1988.
3. Australian Standard 1720.1-1988, "SAA Timber Structures Code, Part 1: Design Methods".
4. AUSTRALIAN GOVERNMENT PUBLISHING SERVICE, (1987). "Timber technology - Wood properties", Training Manual 22-1.
5. ATHERTON, G.H., ROWE, K.E., BASTENDORFF, K.M. (1980). "Damping and slip of nailed joints", *Wood Science*, 12(4), 218-226.
6. AUNE, P., PATTON-MALLORY, M. (1986). "Lateral load-bearing capacity of nailed joints based on the yield theory (a) theoretical development & (b) experimental verifications", *US Department of Agriculture, Forest Service, Forest Products Laboratory Research Paper FPL*.
7. BATCHELAR, M.K. (1984). "Improved plywood gusset joints for timber portal frames", *Proceedings, Pacific Timber Engineering Conference, Auckland, May 1984, Vol. 2, 655-666*.
8. BATCHELAR, M.K., CAVANAGH, G.J. (1984). "Nailed plywood gusset joints for timber portal frames", *Proceedings, Pacific Timber Engineering Conference, Auckland, May 1984, Vol. 2, 631-642*.
9. BATCHELAR, M.L., HUNT, R.D. (1991). "Composite plywood and steel plates for moment-resisting joints in timber frames", *Proceedings, International Timber Engineering Conference, London, UK, Vol. 3, 3.104-110*.
10. BOULT, B.F. (1987). "Moment resisting joints", *New Zealand journal of Timber Construction*, 3(2), 265-276.
11. BUCHANAN, A.H., CHINNIAH, R., MOSS, P.J. (1989). "Behaviour of nailed gusset connections under simulated fire exposure", *Proceedings, Second Pacific Timber Engineering Conference, Auckland, Vol. 2, 125-129*.
12. CREWS, K. (1991). "Joints and connections: Timber engineered structures", *Australian Forest Industries Journal, November 1991, 32-37*.
13. CREWS, K. (1992). "Research and development trends in structural applications of timber for expansion of the non-residential market for forest products in Australia - 1990 Gottstein Fellowship Report", *National Educational Trust of the Australian Forest Products industry*.
14. CRUZ, H.M.P., HILSON, B.O., WHALE, L.R.J. (1991). "Dynamic behaviour of nailed timber joints - embedment tests under cyclic load", *Proceedings, International Timber Engineering Conference, London, UK, Vol. 3, 3.11-19*.
15. FOSCHI, R.O., LONGWORTH, J. (1975). "Analysis and design of griplam nailed connections", *Journal of Structural Engineering, ASCE*, 101(12), 2537-2600.
16. GIBSON, J.A. (1984). "Timber moment frames and their use", *Proceedings, Pacific Timber Engineering Conference, Auckland, May 1984, Vol. 2, Paper 224, 127-133*.

17. GIRHAMMAR, U.A., ANDERSSON, H. (1988). "Effect of loading rate on nailed timber joint capacity", *Journal of structural Engineering, ASCE*, 114(11), 2439-2456.
18. GRIFFITH, M.C., HIRST, M.J.S., LEE, D.S.C. (1993). "Experimental study of fatigue effects on plywood gusseted timber joints", *paper accepted for 13th Australasian conference on The Mechanics of Structures and Materials, Wollongong*.
19. HANSEN, F.T., MORTENSEN, N.L. (1991). "Full-scale testing of prefabricated timber frames subjected to dynamic load", *Proceedings, International timber Conference, London, UK, Vol. 3*, 3.97-103.
20. HUANG, S.Y., YU, P.M., HONG, J.Y. (1989). "The reliability of bolted joints in timber structures", *Proceedings, Second Pacific Timber Engineering Conference, Auckland, Vol. 2*, 57-60.
21. HUNT, R.D., BRYANT, A.H. (1990). "Laterally loaded nail joints in wood", *Journal of structural Engineering, ASCE*, 116(1), 111-124.
22. HUNT, R.D., BRYANT, A.H. (1984). "Nailed joints for timber structures", *Proceedings, Pacific Timber Engineering Conference, Auckland, May 1984, Vol. 2, Paper 091*, 616-620.
- 22A. HUNT, R.D., BRYANT, A.H. (1993). "Stress concentration and stress intensity factor for timber members", *13th Australasian conference on Mechanic of structures and materials, University of Wollongong, July 1993*.
23. HUNT, R.D., BRYANT, A.H. (1988). "Stresses in region of moment resisting joints in timber structures", *Eleventh Australasian Conference on the Mechanics of Structures and Materials, Auckland, August 1988*, 115-120.
24. HUNT, R.D., BRYANT, A.H. (1989). "Strength of timber members in joint regions", *Proceedings, Second Pacific Timber Engineering Conference, Auckland, Vol. 2*, 77-81.
25. KARACABEYLI, E., FOSCHI, R.O. (1987). "Glulam rivet connections under eccentric loading", *Canadian Journal of Civil Engineering*, 14(5), 621-630.
26. KOMATSU, K. (1989). "Behaviour of nailed timber joints with steel side plates", *Proceedings, Second Pacific Timber Engineering Conference, Auckland, Vol. 2*, 89-94.
27. KOMATSU, K. (1989). "Performance of timber moment-resisting joints", *Proceedings, Second Pacific Timber Engineering Conference, Auckland, Vol. 2*, 25-30.
28. KOMATSU, K., KAMIYA, F., HIRASHIMA, Y. (1988). "Two storey Glualm portal frames", *New Zealand Journal of Timber Construction*, 4(2), 9-12.
29. LHEUDE, E.P. (1990). "A reappraisal of nailed timber joint design loads", *Proceedings, Second National Structural Engineering Conference, Adelaide, October 1990, Vol. 11*, 361-365.
30. LHEUDE, E.P., BREITINGER, H.O. (1989). "Load capacities of punched nail plates in wood defects", *Proceedings, Second Pacific Timber Engineering Conference, Auckland, Vol. 2*, 83-87.
31. LHEUDE, E.P., GERRARD, C.M., MACINDOE, L. (1989). "Comparison of finite element analyses and experimental tests of bolted timber connections loaded perpendicular to the grain", *Proceedings, Second Pacific Timber Engineering Conference, Auckland, Vol. 1*, 315-321.

32. LOWE, P.G. (1989). "Timber engineering research in a university environment", *Proceedings, Second Pacific Timber Engineering Conference, Auckland, Vol. 3*, 99-102.
33. LOWE, P.G., EDWARDS, M.R. (1984). "Aspects of ductility in nailed timber connections", *Proceedings, Pacific Timber Engineering Conference, Auckland, May 1984, Vol. 2*, 622-630.
34. MACK, J.J. (1981). "Intermittent loading of nailed joints", *CSIRO Australia, Division of Building Research Technical Paper (Second series) No. 40*.
35. MACK, J.J. (1960). "Repetitive loading of nailed timber joints", *CSIRO Australia, Division of Forest Products Technology Paper No. 10*.
36. MACK, J.J. (1966). "The strength and stiffness of nailed joints under short duration loading", *CSIRO Australia, Division of Forest Products Technology Paper No. 40*.
37. MOSS, P.J., CARR, A.J., BUCHANAN, A.H. (1986). "Seismic response of low rise buildings", *Bulletin of the New Zealand Society for Earthquake Engineering*, 19(3), 180-199.
38. NATIONAL ASSOCIATION OF FOREST INDUSTRIES. (1988). "Timber Datafile SSI - Timber Portal Frames".
39. NICHOLLS, K. (1990). "Nail Plated Timber Connections", *Final Year Research Project submitted in partial fulfilment of B.E., Department of Civil Engineering, The University of Adelaide*.
40. OEHLERS, D.J. (1991). "Residual strength of structural components subjected to cyclic loads", *paper accepted for publication in Journal of Structural Engineering, ASCE, revised December 1991*.
41. OEHLERS, D.J., FOLEY, L. (1985). "The fatigue strength of stud shear connections in composite beams", *Proceedings, Institution of Civil Engineers, Part 2, 1985, Paper 8890, 79, June*, 349-364.
42. OEHLERS, D.J., COUGHLAN, C.G. (1986). "The shear stiffness of stud shear connections in composite beams", *Journal of Construction, Steel Research* 6, 273-284.
43. OHASHI, Y., SAKAMOTO, I. (1989). "Study on laminated timber moment-resisting joint", *Proceedings, Second Pacific Timber Engineering Conference, Auckland, Vol. 2*, 37-42.
44. PARAMESWAR, H.C., MANSELL, M.G. (1989). "Limit state design of nail plate joints in timber trusses", *Proceedings, Second Pacific Timber Engineering Conference, Auckland, Vol. 1*, 151-154.
45. PELLICANE, P.J., BODIG, J., MUTUKU, R.N. (1989). "Modelling the moment rotation behaviour of bolted joints subject to rotational loading", *Proceedings, Second Pacific Timber Engineering Conference, Auckland, Vol. 2*, 43-47.
46. POLENSEK, A. (1988). "Effects of testing variables on damping and stiffness of nailed wood-to-sheathing joints", *Journal of Testing and Evaluation*, 16(5), 474-480.
47. PURKISS, J.A. (1987). "Load-deflection behaviour of timber portal frames under sway", *Journal of Construction and Building Materials, Vol. 1, No. 2, June 1987*, 76-82.

48. ROWLEY, R.B., KROONENBERG, J. (1989). "LVL - an introduction and case study", *Proceedings, Second Pacific Timber Engineering Conference, Auckland, Vol. 1, 1-3.*
49. SIGRIST, C. (1989). "Nailed joints in timber construction", *Proceedings, Second Pacific Timber Engineering Conference, Auckland, Vol. 2, 71-76.*
50. SOLTIS, L.A., MTENGA, P.V.A. (1985). "Strength of nailed wood joints subjected to dynamic load", *Forest products Journal, 35(11 12), 14-18.*
51. SOLTIS, L.A., NELSON, N., HILLIS, J.L. (1989). "Effect of loading mode on duration-of-load factors", *Proceedings, Second Pacific Timber Engineering Conference, Auckland, Vol. 1, 213-218.*
52. STEVENS, W.B. (1993). "Dynamic loadings on timber portal frame buildings", *M.Eng. Sci. Thesis, Department of Civil and Environmental Engineering, The University of Adelaide.*
53. THOMAS, B., MALHOTRA, S.K. (1985). "Behaviour of timber joints with multiple nails", *Journal of Structural Engineering, ASCE, 111 (5), 973-991.*
54. TSUJINO, T. (1988). "Deformation analysis of wooden frames assembled with nailed plywood gusset-plates", *Mokuzai Gakkaishi, Journal of the Japan Wood Research Society, 34(5), 395-400.*
55. WALFORD, G.B. (1988). "Analysis of timber portal frame gusset joints", *Proceedings, 1988 International Conference on Timber Engineering, Seattle, Washington USA, September 1988, Vol. 1, 428-431.*
56. WILLIAMS, R.L. (1984). "Design of timber structures to resist high wind and earthquake", *Proceedings, Pacific Timber Engineering Conference, Auckland, May 1984, Vol. 2, 439-445.*
57. YTTRUP, P.J. (1989). "Construction techniques for timber portal framed buildings using on-ground assembly", *Proceedings, Second Pacific Timber Engineering Conference, Auckland, Vol. 3, 59-63.*
58. YTTRUP, P.J. (1989). "The Scrimber International Buildings, Mt Gambier, Australia", *Proceedings, Second Pacific Timber Engineering Conference, Auckland, Vol. 3, 35-39.*